pISSN 2765-2203
eISSN 2765-2211

PNIE

PROCEEDINGS OF THE

NATIONAL INSTITUTE OF ECOLOGY OF THE REPUBLIC OF KOREA

Volume 7 Issue 4 November 2026



PROCEEDINGS OF THE NATIONAL INSTITUTE OF ECOLOGY OF THE REPUBLIC OF KOREA
Volume 7 Issue 4, November 2026
National Institute of Ecology

PNIE PROCEEDINGS OF THE NATIONAL INSTITUTE OF ECOLOGY OF THE REPUBLIC OF KOREA

pISSN 2765-2203
eISSN 2765-2211

Volume 7, Issue 4, November 2026

Aims and Scope

Proceedings of the National Institute of Ecology of the Republic of Korea (PNIE) is an open access and online journal aimed at promoting outcomes of basic ecological researches carried out in Korea and abroad. The journal focuses on not only basic ecological research on terrestrial and aquatic populations, communities, ecosystems and landscapes but also applied issues such as data science and climate change based on ecological research.

About the Journal

PNIE is the official English language journal of the National Institute of Ecology of the Republic of Korea. PNIE started its first issue in November 1, 2020. PNIE is published quarterly in a year (February 1, May 1, August 1, November 1). The journal publishes research papers, invited reviews and data papers. This multidisciplinary journal is a showcase of original researches being conducted by the ecologists in Korea and abroad. And PNIE is committed to represent ecological research from Asia-Pacific region. Worldwide cooperative research initiatives are also welcome.
PNIE is an Open Access journal. It means that all articles published by PNIE are made freely and permanently accessible online immediately upon publication, without subscription charges or registration barriers.

Contacts

For subscription and all other information visit our website available from: https://acoms.accesson.kr/pnie/oprs/main/jrnlMain.do. To subscribe to this journal or renew your current subscription, please contact us through Tel (+82-41-950-5421) or E-mail (pnie@nie.re.kr).

Disclaimer

The publisher, editors, and reviewers do not assume any legal responsibility for errors, omissions, or claims, nor do they provide any warranty expressed or implied, with respect to information published in Proceedings of the National Institute of Ecology of the Republic of Korea.

Copyright © National Institute of Ecology.

Proceedings of the National Institute of Ecology of the Republic of Korea

Printed on October 25, 2026
Published on November 1, 2026

Publisher: National Institute of Ecology
Editor-in-Chief: Ohseok Kwon

Published by National Institute of Ecology (NIE)
1210 Geumgang-ro, Maseo-myeon, Seocheon-gun, Chungcheongnam-do, 33657, Korea
Tel: +82-41-950-5421, E-mail: pnie@nie.re.kr
Homepage: http://www.nie.re.kr

Printed by MEDrang Inc.
2nd Floor, Hyoryeong Building, 32 Mugyo-ro, Jung-gu, Seoul 04521, Korea
Tel: +82-2-325-2093, Fax: +82-2-325-2095, E-mail: info@medrang.co.kr
Homepage: http://www.medrang.co.kr

This is an Open Access article distributed under the terms of the Creative Commons Attribution Non-Commercial License (http://creativecommons.org/licenses/by-nc/4.0) which permits unrestricted non-commercial use, distribution, and reproduction in any medium, provided the original work is properly cited.

PNIE PROCEEDINGS OF THE NATIONAL INSTITUTE OF ECOLOGY OF THE REPUBLIC OF KOREA

pISSN 2765-2203
eISSN 2765-2211

Publisher

National Institute of Ecology

Editor-in-Chief

Ohseok KWON (*Kyungpook National University, Korea*)

Deputy Editor-in-Chief

Sun Hee HONG (*Hankyong National University, Korea*)
Youngho CHO (*National Institute of Ecology, Korea*)

Editorial board

Climate Change

Josu González ALDAY (*Universitat de Lleida, Spain*)
Lillian Jennifer V. RODRIGUEZ (*Univeristy of Philippines-Diliman, Philippines*)

Conservation Assessment

Baek-Jun KIM (*National Institute of Ecology, Korea*)
Chulgoo KIM (*National Institute of Ecology, Korea*)
Hye Kwon KIM (*Chungbuk National University, Korea*)
Ji Young JUNG (*Korea Polar Research Institute, Korea*)
Ki-Jung NAM (*Gyeongsang National University, Korea*)
Ohseok KWON (*Kyungpook National University, Korea*)
Vivi NOVIANTI (*State University of Malang, Indonesia*)

Information and Technology

Biswajeet Pradhan (*Distinguished Professor Biswajeet Pradhan, Australia*)
Hamid Reza Pourghasemi (*Shiraz University, Iran*)
Hyeong Cheol PARK (*National Institute of Ecology, Korea*)
Kidong KIM (*National Institute of Ecology, Korea*)
Saro LEE (*Korea institute of Geoscience and Mineral Resources, Korea*)
Suntae KIM (*Jeonbuk National University, Korea*)

Risk Assessment

Jung Ro LEE (*National Institute of Ecology, Korea*)
Moon Bo CHOI (*Kyungpook National University, Korea*)
Sun Hee HONG (*Hankyong National University, Korea*)
Youngho CHO (*National Institute of Ecology, Korea*)
Yuno DO (*Kongju National University, Korea*)

Environmental Policy

Hyun-Woo LEE (*Korea Environment Institute, Korea*)
Wooyeong JOO (*National Institute of Ecology, Korea*)

Managing Editor

Min-Ho CHANG (*National Institute of Ecology, Korea*)
Younmi RYU (*National Institute of Ecology, Korea*)

Manuscript Editor

Yuseong JO (*MEDrang Inc., Korea*)

PNIE PROCEEDINGS OF THE NATIONAL INSTITUTE OF ECOLOGY OF THE REPUBLIC OF KOREA

pISSN 2765-2203
eISSN 2765-2211

Volume 7, Issue 4, November 2026

CONTENTS

Original Articles

Conservation Assessment

143 Nationwide Habitat Suitability of the Amur Hedgehog (*Erinaceus amurensis*) in the Republic of Korea
Kyungmin Kim

155 Potential Hillslope Soil-Loss Pressure in the Catchments of South Korea's Inland Protected Wetlands: Contrasting a Land-Cover Trend with Rainfall Variability over 35 Years
Sunmin Lee, Jeong-Cheol Kim

173 Habitat Use of Sympatric *Onychodactylus sillanus* and *Hynobius* spp. Larvae in a Mountain Stream on the Southeastern Korean Peninsula
June Kim, Min-Woo Park, Jia Lee, Daesik Park

181 Functional Traits and Competitor-Stress-Tolerator-Ruderal Strategies of *Phragmites australis* in Southwestern Korean Estuaries
Dong-Ho Son, Seok Yeoul Ko, Kyoung Hoon Yang, Min Jae Kim, Jong-Wook Kim, Hyeon-Ho Myeong

Information and Technology

190 Time-Series Analysis of Spatial Cluster Changes in Grade 1 Zones of the Ecological and Nature Map: 2007-2025
Ha-Eun Lee, Hye-Yeon Yoon

200 Long-Term Tidal Flat Area Variation at the Nakdong River Estuary Measured from Multi-Temporal Sentinel-1 with Tidal and Seasonal Correction
Won-Kyung Baek, Moung-Jin Lee, Jun-Ho Lee, Keunyong Kim, Sung-Hwan Park, Joo-Hyung Ryu

213 U-Net Semantic Segmentation of Quadrat Underwater Imagery for Automated Benthic Cover Classification
Sung-Hwan Park, Nam-Hoon Kim, Won-Kyung Baek, Soonyoung Choi, Jong-Seok Lee, Euiyoung Jeong

Case Report

225 A Checklist of the Subfamily Epipaschiinae (Lepidoptera, Pyralidae) from Korea, with Two Newly Recorded Species
Hanul Kim, Jae-Ho Ko, Ulziijargal Bayarsaikhan

PNIE PROCEEDINGS OF THE NATIONAL INSTITUTE OF ECOLOGY OF THE REPUBLIC OF KOREA

Original Article

PNIE 2026;7(4):143-154
https://doi.org/10.22920/PNIE.2026.7.4.143
pISSN 2765-2203, eISSN 2765-2211

Nationwide Habitat Suitability of the Amur Hedgehog (*Erinaceus amurensis*) in the Republic of Korea

Kyungmin Kim*

Research Institute of EcoScience, Ewha Womans University, Seoul, Korea

ABSTRACT

The habitat characteristics of small mammals with low detectability remain poorly documented. The Amur hedgehog (*Erinaceus amurensis*) is widely distributed across Northeast Asia, but its habitat associations have rarely been quantified at a national scale. This study developed the first nationwide habitat suitability model for the species in the Republic of Korea using occurrence records from the National Ecosystem Survey (NES), a systematic national biodiversity monitoring framework. To account for spatial sampling bias, a target-group background approach used records of other sympatric mammals collected under the same NES protocol to approximate survey effort. Using MaxEnt with 93 spatially unique records and an initial set of 12 environmental predictors, the model showed moderate predictive performance (mean area under the receiver operating characteristic curve=0.778±0.034; mean true skill statistic=0.380±0.055). Elevation (46.6%) and land cover (19.8%) were the most influential predictors of suitability. High-suitability areas were concentrated in upland regions and heterogeneous landscapes, where forests and grasslands were interspersed. These results indicate that the Amur hedgehog is associated with structurally complex environments and lower levels of urbanization. This study provides an ecological baseline for understanding the broad-scale habitat associations of this species in the Republic of Korea. The resulting habitat suitability map can guide future field surveys and provide a basis for species-specific monitoring and conservation planning.

Keywords: Conservation, *Erinaceus amurensis*, Habitat suitability, Small mammal, Species distribution modeling

Introduction

Understanding the habitat associations of wildlife is fundamental for identifying ecological requirements and predicting species distributions across heterogeneous landscapes (Elith & Leathwick, 2009; Guisan & Thuiller, 2005). Such information directly contributes to biodiversity conservation and informs spatial planning by revealing environmental features that promote species persistence under ongoing land-use changes. Small mammals play important functional roles in ecosystems, contributing to processes such as nutrient cycling, seed dispersal, and the maintenance of trophic dynamics across diverse landscapes (Paniccia *et al.*, 2022). Despite their ecological importance, ecological knowledge of many small-bodied or inconspicuous mammals remains limited, and broad-scale quantitative information on their habitat associations is particularly scarce (Caldwell *et al.*, 2024; Fisher & Owens, 2004). This imbalance in available knowledge is evident across geographic regions and taxonomic groups and reflects long-standing differences in research attention and sampling intensity among taxa (Hortal *et al.*, 2015; Trimble & Van Aarde, 2010). Therefore, substantial

Received May 11, 2026; **Revised** July 23, 2026; **Accepted** July 27, 2026

***Corresponding author:** Kyungmin Kim
e-mail kyungminkim0829@gmail.com
https://orcid.org/0000-0003-3138-7511

This is an Open Access article distributed under the terms of the Creative Commons Attribution Non-Commercial License (http://creativecommons.org/licenses/by-nc/4.0), which permits unrestricted non-commercial use, distribution, and reproduction in any medium, provided the original work is properly cited.

Copyright © National Institute of Ecology.

knowledge gaps persist for many small mammalian species, constraining broad-scale biodiversity assessments and hindering their explicit inclusion in conservation planning (Hortal *et al.*, 2015).

Small insectivorous mammals play important ecological roles in regulating invertebrate populations and contributing to nutrient cycling across diverse habitats (Gago *et al.*, 2023; Williams *et al.*, 2018). Within this functional group, the Amur hedgehog (*Erinaceus amurensis*) is distributed across parts of Northeast Asia. However, ecological knowledge of this species remains scarce throughout its range. Existing studies have largely focused on taxonomy, genetic structure, species occurrence records, or responses to habitat fragmentation (Bannikova *et al.*, 2014; Kim *et al.*, 2017; Kim *et al.*, 2026), and the nationwide habitat suitability and landscape-level distribution of the species remain poorly understood. Furthermore, its population status and ecological role remain poorly documented. This information gap is particularly relevant in the Republic of Korea, where the Amur hedgehog is the only native hedgehog species. Therefore, it is necessary to establish baseline ecological knowledge, including landscape-scale habitat use, to understand its ecological significance and to inform future conservation and management efforts.

The distribution of wildlife species can be influenced by multiple environmental factors, including climatic conditions, land cover, topography, anthropogenic disturbances, and resource availability. Climatic factors, including temperature and precipitation, shape the energetic costs of thermoregulation and reproduction and often define the broad geographic limits of species ranges (Araújo & Guisan, 2006; Sunday *et al.*, 2012). Land cover determines the quantity and quality of suitable habitats by providing shelter and nesting sites and by influencing habitat connectivity and movement opportunities (Betts *et al.*, 2017). Topographic variables, such as elevation and slope, modify microclimatic conditions and water availability and mediate local habitat suitability and dispersal pathways (Moore *et al.*, 1993). Anthropogenic elements, including urban areas and road networks, contribute to habitat loss, fragmentation, and increased mortality risk (Ibisch *et al.*, 2016; Trombulak & Frissell, 2000). Resource availability, particularly the abundance of invertebrates, directly affects foraging success and energetic intake and is thus a critical determinant of habitat quality for insectivorous mammals (Mazerolle & Villard, 1999). This full range of environmental gradients is necessary for accurately characterizing habitat associations at the landscape scale and for developing robust models to predict species distributions across varying environmental conditions (Peterson *et al.*, 2011).

Although multiple environmental factors influence wildlife distribution, the ecological determinants of Amur hedgehog occurrence have not been evaluated using a spatially explicit analytical framework. Presence-only modeling approaches, such as MaxEnt, offer a practical means of examining habitat associations when detailed ecological information is limited, as they incorporate environmental gradients without requiring systematic absence data (Elith *et al.*, 2006; Phillips *et al.*, 2006). Applying such an approach enables a structured assessment of how climatic, land cover, topographic, and anthropogenic variables correspond to the observed occurrence patterns across broad spatial extents. Establishing this ecological context is essential for interpreting the distribution of the Amur hedgehog within rapidly changing landscapes in the Republic of Korea and for identifying the environmental conditions that are most likely to support its presence. Therefore, landscape-scale modeling represents a necessary foundation for filling longstanding ecological knowledge gaps and guiding future investigations into the spatial ecology and conservation needs of this understudied species.

This study aimed to provide the first quantitative nationwide assessment of the habitat associations of the Amur hedgehog in the Republic of Korea. Verified occurrence records were integrated with a set of ecologically relevant environmental variables to identify broad-scale factors associated with species distribution. Using the MaxEnt algorithm, key variables associated with the occurrence of the Amur hedgehog were identified, and a nationwide habitat suitability map depicting its potential distribution at the landscape scale was generated. By linking species occurrence with nationwide environmental gradients across the country, this study provides nationwide evidence addressing a longstanding knowledge gap for this data-deficient mammal. These results provide a context for guiding future ecological investigations of this species and serve as a reference point for discussions related to its conservation in the Republic of Korea.

Materials and Methods

Study area

This study was conducted in the Republic of Korea, located in the southern part of the Korean Peninsula in Northeast Asia, covering an area of approximately 100,412 km^2 (Fig. 1). The country has a temperate climate with four distinct seasons. According to the 1991-2020 climatological normal values, the nationwide annual mean temperature is approximately 12.8°C and the mean annual precipitation is approximately 1,418 mm (Korea Meteorological Administration, 2025). January is the coldest month, with mean minimum temperatures ranging from –6.9 to 3.6°C; August is the warmest, with mean maximum temperatures ranging from 19.7 to 26.7°C. Precipitation is highly seasonal, with approximately 60% of the annual rainfall occurring during the summer.



Fig. 1. Map of the Republic of Korea showing the Baekdudaegan mountain range, which forms the principal mountainous axis of the Korean Peninsula. Administrative boundaries are shown for spatial reference.

The topography of the country is dominated by mountains in the east and lower plains in the west and southwest, producing pronounced elevation gradients and regional climate variations. The Baekdudaegan mountain range forms the primary orographic backbone of the Korean Peninsula, extending from the northeast to the south. The elevation generally decreases from the eastern highlands to the western lowlands, with the highest elevation in the inland region of the Republic of Korea, reaching 1,915 m on Jiri Mountain. Jeju Island, located off the southern coast of the Korean Peninsula, where the presence of the Amur hedgehog remains uncertain, was excluded from the study area.

Species occurrence data and preprocessing

Species occurrence data for the Amur hedgehog were obtained from the National Ecosystem Survey (NES) conducted by the Ministry of Environment of the Republic of Korea. This nationwide government-led program is implemented every five years and systematically monitors biodiversity using standardized field protocols across the country (National Institute of Ecology, 2019). This study used records from the two most recent survey periods, the fourth and fifth NES, conducted between 2014 and 2023. Field surveys were conducted by teams of two professionally trained surveyors, and each detection method was applied in accordance with the NES guidelines. Direct observations were performed along transects during daytime surveys, camera traps were installed to monitor wildlife within each sampling unit, and field signs, such as droppings or tracks, were searched during ground inspections. Given that the NES is conducted repeatedly across multiple seasons within each five-year cycle, the compiled dataset represents observations accumulated over an extended temporal coverage rather than a single-year snapshot.

To reduce spatial redundancy in the occurrence dataset, duplicate records located within the same sampling location were removed so that each remaining point represented a unique occurrence location. However, as the NES does not provide quantitative information on survey effort or detection probability, it is not possible to explicitly model variations in detectability across space or fully correct for heterogeneous sampling intensity using traditional effort-based approaches. As an initial diagnostic step, the spatial distribution of hedgehog occurrence was evaluated using Global Moran's I to assess the presence of strong spatial clustering. This analysis was conducted at a 1-km resolution, which was selected based on established spatial ecology principles recommending that spatial autocorrelation be assessed at a scale broader than both the positional uncertainty of field-collected GPS coordinates and the unknown fine-scale structure of the underlying ecological processes (Dale & Fortin, 2014; Legendre & Fortin, 1989). This choice reduced the influence of location errors and minimized the detection of artificial clustering patterns arising from overly fine analytical grids.

As removing duplicate records alone cannot fully address spatial sampling bias in presence-only data, a target-group background approach was adopted to account for heterogeneous survey effort in species distribution modeling, as recommended for correcting sample selection bias in MaxEnt models (Kramer-Schadt *et al*., 2013; Phillips *et al*., 2009). Occurrence records of other mammalian species surveyed under the same NES framework were used as a proxy for the spatial structure of the survey effort, under the assumption that these records share similar survey designs, accessibility constraints, and detection processes. Specifically, occurrence records of 10 mammalian species surveyed during the same periods as the Amur hedgehog were compiled, including the water deer (*Hydropotes inermis*), raccoon dog (*Nyctereutes procyonoides*), roe deer (*Capreolus pygargus*), Siberian chipmunk (*Eutamias sibiricus*), Eurasian red squirrel (*Sciurus vulgaris*), Siberian weasel (*Mustela sibirica*), wild boar (*Sus scrofa*), Korean hare (*Lepus coreanus*), Ussuri mole (*Mogera robusta*), and Asian badger (*Meles leucurus*). A total of 97,027 occurrence records of these species were used to characterize the spatial distribution of the survey effort.

To standardize the sampling units and reduce the overrepresentation of repeatedly surveyed locations, target group occurrence records were aggregated using a 1×1 km grid. Each grid cell containing at least one mammalian record was treated as a single sampling unit, resulting in 24,412 grid-based effort points. This aggregation

does not reduce spatial coverage but instead collapses repeated observations within the same survey area into a single representation of the survey effort, thereby providing a more stable approximation of survey intensity across space (Phillips *et al.*, 2009). Kernel density estimation (KDE) was then applied to these grid-based effort points to generate a continuous surface representing the relative survey intensity across the study area. The kernel density was calculated using a cell size of 1 km and a search radius of 10 km, reflecting the national spatial extent of the NES and ensuring a smooth approximation of the spatial variation in the sampling effort. The resulting density surface was normalized to a range of 0-1, and a small minimum value was assigned to all cells to avoid the complete exclusion of unsampled areas during background selection. This bias surface was subsequently supplied to MaxEnt as a bias file to weight the background point selection toward areas with higher inferred survey effort, following established recommendations for bias correction in presence-only species distribution models (Kramer-Schadt *et al.*, 2013). By incorporating this bias file while keeping all other model settings unchanged, the background sampling was constrained to reflect the spatial structure of the survey effort, rather than assuming uniform sampling across the landscape.

Environmental variables

To model habitat suitability for the Amur hedgehog, a set of environmental variables representing climate, topography, land cover, anthropogenic disturbances, and resources likely to influence species distribution was selected. All 12 environmental predictors were resampled to a 100-m resolution to ensure a consistent spatial scale across variables (Table 1). A grid size of 100 m is widely used in species distribution modeling because it avoids over-precision relative to typical field-collected occurrence coordinates and aligns with the general recommendations that environmental layers should not exceed the effective spatial accuracy of the presence data (Elith *et al*., 2011; Fourcade *et al*., 2014; Guisan & Zimmermann, 2000).

The climatic variables, including annual mean temperature and annual precipitation, were obtained from WorldClim v2.1 (Fick & Hijmans, 2017). Topographic variables were derived from the Digital Elevation Model provided by the U.S. Geological Survey (USGS, 2014). Three terrain-related predictors were considered: elevation, slope, and aspect. These variables influence microclimatic conditions, vegetation structure, and species movement patterns and are often associated with habitat selection in small mammals (Tattersall *et al.*, 2001). Land cover data were derived from the ESA WorldCover 2020 product, which classifies the global land surface into discrete categories at a 10-m resolution (Zanaga *et al.*, 2021). Eight land-cover classes were included in the analysis and represented by the following numerical codes: forest (10), shrubland (20), grassland (30), cropland (40), built-up area (50), bare vegeta-

Table 1. Environmental predictors used to model habitat suitability for the Amur hedgehog (*Erinaceus amurensis*) in the Republic of Korea, grouped by thematic category

Classification	Variable	Source
Climate	Annual mean temperature	WorldClim v2.1 (Fick & Hijmans, 2017)
	Annual precipitation	WorldClim v2.1 (Fick & Hijmans, 2017)
Topography	Elevation	Digital Elevation Model (DEM), USGS
	Slope	Derived from DEM, USGS
	Aspect	Derived from DEM, USGS
Land cover	Land cover (categorical)	ESA WorldCover 2020
	Distance to forest	Euclidean distance to forest land cover class, ESA WorldCover 2020
	Distance to shrubland	Euclidean distance to shrubland land cover class, ESA WorldCover 2020
	Distance to grassland	Euclidean distance to grassland land cover class, ESA WorldCover 2020
Anthropogenic disturbance	Distance to road	Euclidean distance to roads, National Transport Information Center
	Proportion of built-up area	Calculated from the ESA WorldCover 2020 built-up area
Resources	Arthropod abundance	Kernel density estimation of insect occurrences, 4th and 5th National Ecosystem Survey

The data sources for all predictors are specified within the table.
DEM, Digital Elevation Model; USGS, U.S. Geological Survey.

tion (60), water bodies (80), and wetlands (90). Euclidean distance layers were generated for all three natural land cover groups (forest, shrubland, and grassland) to capture the proximity effects that might influence the movement and habitat use of the Amur hedgehog. The anthropogenic disturbance variables included the proportion of built-up area within each raster cell and the distance to the nearest road. The proportion of built-up area was used to quantify local urbanization intensity and evaluate associations with human-modified environments. The distance to roads, derived from the national road network provided by the National Transport Information Center, was included as an indicator of direct mortality risk and fragmentation pressure for small terrestrial mammals (Benítez-López *et al.*, 2010).

The resource category included a single variable representing the abundance of arthropods. Hedgehogs consume various invertebrates, including insects, earthworms, and beetles (Jia *et al*., 2024; Plazi TreatmentBank, 2023), making the spatial distribution of potential prey an important component of habitat suitability. Given that the NES primarily detects flying or surface-active insects, this variable does not represent true prey availability but serves as a proxy for general arthropod abundance. Although a variety of invertebrates constitute the diet of hedgehogs, the detailed dietary composition of this species in the Republic of Korea has not yet been empirically established. Therefore, this layer was intended to reflect the landscape-scale distribution of potential prey availability rather than a definitive prey composition. To generate this layer, KDE was applied to insect occurrence records from the fourth and fifth NES, thereby matching the temporal range of hedgehog occurrence data. The KDE was selected because it provides a continuous spatial surface for arthropod occurrence and minimizes sampling irregularities across survey locations. It also allowed gradual changes in arthropod density to be represented without imposing artificial spatial boundaries, thereby facilitating the interpretation of landscape-level patterns in potential prey availability. Over 510,000 insect records were processed, and bandwidths of 1, 5, 10, and 30 km were compared to identify an appropriate spatial scale. Preliminary comparisons indicated that bandwidths ≥10 km substantially reduced spatial variance in arthropod density, whereas the 1-km bandwidth maintained finer-scale patterns relevant to resource distribution. Based on these comparisons, a 1-km bandwidth was selected to retain fine-scale spatial variation in arthropod occurrence while limiting excessive smoothing at broader scales, consistent with the importance of considering spatial scale in habitat and species distribution modeling (Elith & Leathwick, 2009; Wintle *et al*., 2005). The KDE surface was then normalized to a 0-1 range to allow the resulting arthropod abundance layer to be interpreted on a standardized scale and to ensure compatibility with other environmental predictors.

All environmental variables were examined for multicollinearity to reduce redundancy and ensure the stability of the model. Pearson's correlation coefficients (r) were calculated for all pairwise combinations of continuous variables. When strong correlations were identified ($|r|>0.7$), one of the correlated variables was excluded based on ecological interpretability and relative contributions in the preliminary models. All layers were clipped to the national boundary of the Republic of Korea and processed using ArcGIS Pro 3.4.0 (ESRI, Redlands, CA, USA) to ensure alignment and compatibility for MaxEnt modeling.

MaxEnt modeling

Species distribution models were developed in MaxEnt v3.4.4 (Phillips *et al.*, 2020) using the occurrence records of the Amur hedgehog and selected environmental variables as predictors. In total, 10,000 background points were sampled using the bias surface described above, thereby weighting the background selection according to the inferred spatial distribution of the survey effort. This number is widely used because it sufficiently samples the environmental space while avoiding unnecessary computation, and increasing it further yields little improvement in model performance (Barbet-Massin *et al*., 2012; Phillips *et al*., 2006; Phillips & Dudik, 2008). The regularization multiplier was fixed at a default value of 1 to control model complexity and avoid overfitting, whereas feature classes were automatically selected by MaxEnt based on the number of presence records, allowing the model to flexibly capture nonlinear species–environment relationships (Merow *et al.*, 2013). Five replicate models were run using a cross-validation approach to assess model robustness. The model performance was evaluated using the area under the receiver operating characteristic curve (AUC) and true skill statistic (TSS). The AUC provides a threshold-independent measure of discrimination, whereas the TSS combines sensitivity and specificity at an optimal threshold, complementing the AUC by accounting for potential prevalence effects (Allouche *et al.*, 2006; Liu *et al.*, 2011). The 10% cumulative threshold was applied to assess the training omission rates. This threshold excluded the lowest 10% of suitability scores among known presence locations, and omission rates were calculated by comparing the observed presence with predictions at this threshold, following the procedure described by Phillips *et al.* (2006).

Following the initial model calibration with all predictors, variable contributions were assessed using permutation importance scores, which measured the decrease in model performance when the variable values were randomly permuted. Predictors with a permutation importance of <5% were excluded because such variables are unlikely to meaningfully improve predictive power and

may introduce noise (Gogol-Prokurat, 2011). The model was rerun using the reduced predictor set. This iterative selection process produced a more parsimonious model with comparable or improved predictive performance relative to the full model, which is consistent with the recommended best practices for species distribution modeling (Elith *et al.*, 2011).

Results

Species occurrence data preprocessing

During the study period, a total of 109 Amur hedgehog occurrence records were identified, representing only a very small fraction (approximately 0.1%) of the total mammal observations in the NES (Fig. 2). Sixteen duplicate records with identical coordinates were removed from the initial dataset, resulting in 93 spatially unique presence points of the Amur hedgehog used for modeling. Amur hedgehog occurrence points were sparsely distributed across the country. Spatial autocorrelation analysis using Global Moran's I indicated that the occurrence distribution was not significantly clustered on the 1-km grid scale (Moran's I=0.042, P=0.129).

To evaluate the spatial structure of the survey effort underlying the presence-only data, mammal occurrence records from the same survey framework were compiled and aggregated into a 1×1 km grid. This procedure resulted in 24,412 grid-based effort locations, representing the spatial footprint of the mammalian survey coverage across the study area. The resulting effort distribution showed strong spatial heterogeneity, with higher concentrations of survey effort in accessible regions and comparatively sparse coverage in other areas. This spatial pattern was subsequently reflected in the bias surface used during species distribution modeling, allowing model predictions to account for uneven survey coverage rather than assuming spatially uniform sampling.

MaxEnt modeling

In the environmental variable set, the annual mean temperature was removed because it showed high collin-

Table 2. Permutation importance of environmental variables used in the MaxEnt model for *Erinaceus amurensis*

Classification	Variable	Permutation importance (%)
Topography	Elevation	46.6
Land cover	Land cover	19.8
	Distance to forest	5.0
	Distance to grassland	6.7
Anthropogenic disturbance	Proportion of built-up area	17.1
Resources	Arthropod abundance	4.8

Higher values indicate a greater influence on model performance when the variable was randomly permuted.



Fig. 2. Spatial distribution records of the Amur hedgehog (*Erinaceus amurensis*) across the Republic of Korea obtained from the fourth and fifth National Ecosystem Surveys (2014-2023). Duplicate locations were removed to minimize spatial redundancy before habitat suitability modeling.

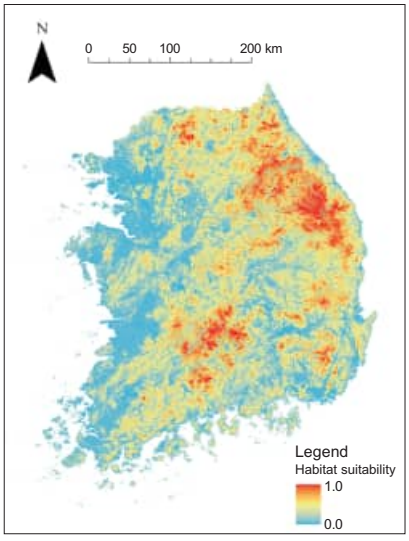

Fig. 3. Predicted habitat suitability map for the Amur hedgehog (*Erinaceus amurensis*) generated by the MaxEnt model using 93 occurrence records and environmental predictors. Warmer colors indicate areas of higher predicted suitability, whereas cooler colors indicate lower suitability.

earity with elevation, which was retained as a representative topographic variable. The final model retained elevation, land cover, proportion of built-up area, distance to grassland, distance to forest, and arthropod abundance as key predictors (Table 2) and yielded an average AUC of 0.778±0.034 and a mean TSS of 0.380±0.055. In general, the predicted habitat suitability of the Amur hedgehog in the Republic of Korea was highest in mountainous regions characterized by higher elevations, whereas low-lying western areas exhibited low suitability (Fig. 3).

Habitat suitability varied markedly across the gradients of key environmental predictors. The MaxEnt model indicated that environmental variables related to topography and land cover structure played a dominant role in shaping the predicted habitat suitability for the Amur hedgehog (Table 2). Among all predictors, elevation showed the highest contribution to the model, accounting for 46.6% of the permutation importance. Habitat suitability increased monotonically with elevation and gradually approached a plateau at higher elevations, indicating a stronger association with upland than with lowland areas (Fig. 4). Land cover was the second most important variable (19.8%), highlighting the role of broad habitat types in shaping hedgehog distribution. Among the land cover categories, forests exhibited the highest predicted suitability, followed by grasslands, whereas other land cover types showed consistently lower suitability.

The proportion of built-up areas also showed a relatively high permutation importance (17.1%). The response curve revealed a clear negative relationship, with habitat suitability declining substantially as the proportion of built-up areas increased, approaching near-zero values at high proportions. Landscape proximity variables exhibited moderate effects, with distance to grassland (6.7%) and distance to forest (5.0%) contributing to model performance. In both cases, the predicted suitability decreased with increasing distance, indicating that the occurrence of the Amur hedgehog was more strongly associated with

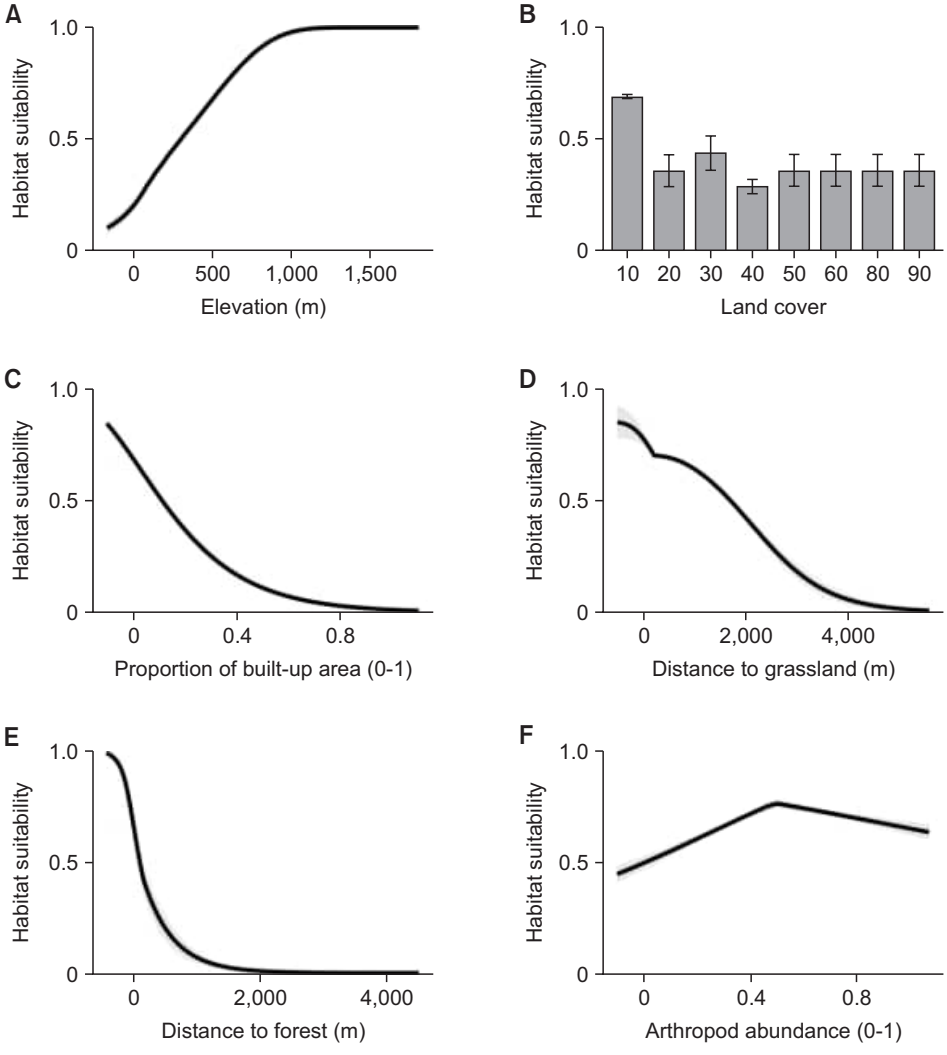

Fig. 4. Response curves showing the relationships between habitat suitability for the Amur hedgehog (*Erinaceus amurensis*) and the six environmental predictors retained in the final MaxEnt model: (A) elevation, (B) land cover, (C) proportion of built-up area, (D) distance to grassland, (E) distance to forest, and (F) arthropod abundance. Solid lines represent the mean predicted suitability, and gray bands (and error bars for land cover) represent the standard errors around the mean based on five cross-validation replicates. Land cover classes were labeled using ESA WorldCover category codes (forest 10, shrubland 20, grassland 30, cropland 40, built-up area 50, bare ground 60, water 80, and wetlands 90).

areas near grasslands and forests. Arthropod abundance showed a lower permutation importance (4.8%), with suitability increasing up to intermediate values and slightly declining at higher values. Overall, the response curves were smooth, monotonic, or weakly unimodal, indicating gradual changes in predicted suitability across environmental gradients.

Discussion

To date, this is the first nationwide assessment of habitat suitability for the Amur hedgehog in the Republic of Korea by integrating presence-only occurrence records from a long-term national monitoring program with landscape-scale environmental predictors. The final model identified elevation, land cover, and proportion of built-up areas as the most influential variables shaping habitat suitability, indicating that the broad topographic context, dominant habitat type, and landscape-scale urbanization jointly structure the distribution of the Amur hedgehog. Habitat suitability exhibited gradual and spatially structured responses across these predictors, suggesting that Amur hedgehog occurrence is associated with multiple components of landscape configuration and anthropogenic modification. Despite moderate discriminatory performance, the model revealed consistent associations with major environmental gradients at the national scale. This suggests that the broad-scale habitat associations of the Amur hedgehog can be inferred even under data-limited conditions when dominant environmental gradients are explicitly considered.

Topographic context emerged as the strongest predictor of habitat suitability, with elevation showing a clear positive association. The predicted suitability increased from low-lying areas to higher elevations and gradually stabilized in the upper elevation ranges, indicating a stronger association between Amur hedgehog occurrence and upland environments. Elevation is widely recognized as an integrative environmental gradient that co-varies with multiple ecological factors, including temperature regimes, vegetation structure, and habitat heterogeneity, all of which can influence the distribution of small terrestrial mammals (McCain, 2005). In the Republic of Korea, elevational gradients coincide with pronounced changes in landscape composition and configuration, with higher elevations generally characterized by more continuous forest cover and distinct habitat structures than those in lowland areas. From this perspective, the positive response to elevation likely reflects broader environmental conditions associated with upland landscapes rather than altitude alone. Similar studies have shown that elevation can effectively capture constraints on species occurrence through its association with landscape structure and environmental conditions, even in the absence of strict elevational specialization (Foster *et al.*, 2022). Accordingly, elevation in this study should be interpreted as a spatially integrative predictor summarizing the correlated environmental gradients relevant to the habitat suitability of the Amur hedgehog.

Land cover was the second most influential predictor, with forests exhibiting the highest predicted suitability, followed by grasslands. The other land cover categories consistently showed lower-suitability values. This pattern indicated that Amur hedgehog occurrence was more strongly associated with forested and semi-natural open habitats than with intensively modified land cover types. Previous studies on hedgehogs have emphasized the importance of habitat structure and ground-level complexity for shelter and movement, rather than relying on a single habitat type (Hof *et al.*, 2012). Forests are likely to provide favorable microhabitats, including leaf litter, coarse woody debris, and understory structures that support shelter and foraging opportunities. Such structurally complex environments have been shown to facilitate hedgehog movement and persistence, particularly by providing daytime refuge and protection from predation and disturbance (Rasmussen *et al.*, 2019). Grasslands located near forests may further increase habitat suitability by providing open foraging areas and potential access to invertebrate prey while maintaining proximity to cover. Similar habitat associations have been reported in European hedgehog studies, where landscapes composed of wooded elements interspersed with open or semi-natural habitats have been associated with higher hedgehog occurrence (Gazzard *et al.*, 2022). Consistent with these findings, the results of the present study suggest that Amur hedgehog occurrence on a broad spatial scale may be associated with landscapes where forests and grasslands occur in close proximity, highlighting the role of land cover composition rather than individual habitat classes alone.

In addition to land cover variables, distance-based predictors provide further insights into the spatial configuration of suitable habitats. Habitat suitability declined sharply with increasing distance from the forest, indicating that proximity to forested environments is closely associated with the conditions under which Amur hedgehogs are more frequently observed. Distance to grassland showed a similar monotonic response, with suitability highest near grasslands and progressively decreasing with distance. Together, these patterns suggest that suitable habitats are concentrated in landscapes where forests and grasslands are spatially proximate rather than being independently distributed across the landscape. These proximity relationships indicate that habitat suitability may be influenced not only by the presence of favorable land cover but also by its spatial arrangement. These patterns suggest a stronger association with landscapes where forest cover and open habitats occur in close proximity.

Urbanization showed a strong negative influence on habitat suitability, as indicated by the high permutation importance of the proportion of built-up areas and the rapid decline in suitability with increasing urban cover. Predicted suitability was highest at very low levels of urbanization and approached near-zero values in highly urbanized landscapes, indicating a strong negative association between habitat suitability and landscape-scale urbanization in the Republic of Korea. This pattern contrasts with the findings of several studies that have reported frequent occurrence or increased use of urban environments by hedgehogs, particularly in systems characterized by residential green spaces and fine-scale habitat heterogeneity (Hof *et al*., 2012; Li *et al*., 2023; Pettett *et al*., 2017). For example, Li *et al.* (2023) reported a higher occurrence probability of hedgehogs in densely urbanized landscapes, suggesting that urban tolerance may vary with environmental and infrastructure conditions. The contrasting responses observed in this study may reflect regional differences in urban forms and spatial configurations of green spaces. Urban development in the Republic of Korea is often concentrated in lowland areas in the western part of the country, where densely built-up areas may reduce habitat continuity and ground-level structural complexity. This interpretation is consistent with that of a recent nationwide study in which the Amur hedgehog showed a relatively high sensitivity to habitat fragmentation (Kim *et al.*, 2026). Therefore, these results suggest that hedgehog responses to urbanization are context-dependent and that patterns reported in other regions may not be directly transferable to the Korean landscape.

Habitat suitability showed a nonlinear response to arthropod abundance, increasing at low to intermediate values and declining slightly at higher values. Given that this variable functions as an indirect proxy rather than a direct measure of prey biomass, the observed patterns should be interpreted with caution. Nonlinear responses to indirect predictors are common in species distribution models and often arise from spatial covariation with other environmental features, rather than from direct biological thresholds (Austin, 2007). Therefore, the modest decline at higher values may reflect the association between arthropod-rich areas and landscape contexts that are otherwise less suitable for hedgehog occurrence. Similar deviations from monotonic resource responses have been documented in empirical studies of habitat selection, in which increased resource availability does not necessarily translate into proportional increases in space use (Boyce *et al.*, 2002). Accordingly, the arthropod abundance in this study should be regarded as a broad index of potential food availability rather than a definitive driver of habitat suitability.

Overall, the spatial patterns identified in this study indicate that suitable habitats for the Amur hedgehog in the Republic of Korea are concentrated in upland landscapes characterized by forest-dominated land cover, adjacent semi-natural open habitats, and low levels of urbanization. These results highlight the importance of landscape-scale environmental gradients in shaping the predicted distribution of the Amur hedgehog. By emphasizing broad environmental gradients, the model provides a coherent framework for interpreting how topography, habitat composition, and urban expansion interact to shape habitat suitability for the Amur hedgehog across the national landscape.

Despite the nationwide scope of this assessment, some limitations should be acknowledged. As a correlative presence-only model, MaxEnt identifies associations between environmental conditions and species occurrence rather than causal habitat preferences, and the resulting predictions should therefore be interpreted as relative habitat suitability rather than occurrence probability or occupancy. Additionally, several predictors represent indirect proxies for ecological processes and may not fully capture the conditions directly experienced by the Amur hedgehog. Finally, model performance was evaluated through internal cross-validation, and the predicted habitat suitability has not yet been validated using an independent dataset. Independent field validation would therefore be valuable for evaluating the robustness of the spatial patterns identified in this study.

Conclusion

This study provides an initial ecological framework for understanding the broad-scale spatial associations of the Amur hedgehog in heterogeneous landscapes across the Republic of Korea. Although the model is exploratory in nature, it consistently identifies upland and mountainous areas as regions of higher habitat suitability, particularly where forest-dominated land cover is prevalent and landscape-scale urbanization is low. These results indicate that the spatial distribution of suitable habitats is strongly associated with topographic context, dominant habitat type, and the extent of urban development.

The model further revealed that Amur hedgehog occurrence is associated with forested environments and adjacent semi-natural open habitats, while suitability declines sharply with increasing built-up land cover. This pattern suggests that this species is associated with relatively less-modified landscapes, where extensive urbanization corresponds to lower predicted suitability at broader spatial scales. In Korea, the concentration of predicted suitable habitats in upland regions may arise from the combined influence of environmental conditions associated with higher elevations and lower suitability in heavily urbanized lowland areas. Consequently, these patterns suggest

that further expansion of urban development into currently less-modified upland areas could reduce suitable habitat.

The Amur hedgehog remains a poorly documented component of mammalian fauna in the Republic of Korea, with limited species-specific ecological information available at the national scale. The spatial outputs generated in this study provide a practical reference for identifying areas of higher predicted suitability and can be used to guide future monitoring efforts, support hypothesis-driven field surveys, and inform preliminary conservation planning. This study establishes a baseline for integrating the Amur hedgehog into broader biodiversity assessments and improving the understanding of habitat associations in data-limited small mammals across complex landscapes.

Conflict of Interest

The author declares that he has no competing interests.

Acknowledgments

I am grateful to the National Institute of Ecology for providing access to species occurrence data derived from the National Ecosystem Survey of Korea.

Funding

None.

References

Allouche, O., Tsoar, A., and Kadmon, R. (2006). Assessing the accuracy of species distribution models: prevalence, kappa and the true skill statistic (TSS). *Journal of Applied Ecology*, 43, 1223-1232. https://doi.org/10.1111/j.1365-2664.2006.01214.x

Araújo, M.B., and Guisan, A. (2006). Five (or so) challenges for species distribution modelling. *Journal of Biogeography*, 33, 1677-1688. https://doi.org/10.1111/j.1365-2699.2006.01584.x

Austin, M. (2007). Species distribution models and ecological theory: a critical assessment and some possible new approaches. *Ecological Modelling*, 200, 1-19. https://doi.org/10.1016/j.ecolmodel.2006.07.005

Bannikova, A.A., Lebedev, V.S., Abramov, A.V., and Rozhnov, V.V. (2014). Contrasting evolutionary history of hedgehogs and gymnures (Mammalia: Erinaceomorpha) as inferred from a multigene study. *Biological Journal of the Linnean Society*, 112, 499-519. https://doi.org/10.1111/bij.12299

Barbet-Massin, M., Jiguet, F., Albert, C.H., and Thuiller, W. (2012). Selecting pseudo-absences for species distribution models: how, where and how many? *Methods in Ecology and Evolution*, 3, 327-338. https://doi.org/10.1111/j.2041-210x.2011.00172.x

Benítez-López, A., Alkemade, R., and Verweij, P.A. (2010). The impacts of roads and other infrastructure on mammal and bird populations: a meta-analysis. *Biological Conservation*, 143, 1307-1316. https://doi.org/10.1016/j.biocon.2010.02.009

Betts, M.G., Wolf, C., Ripple, W.J., Phalan, B., Millers, K.A., Duarte, A., *et al*. (2017). Global forest loss disproportionately erodes biodiversity in intact landscapes. *Nature*, 547, 441-444. https://doi.org/10.1038/nature23285

Boyce, M.S., Vernier, P.R., Nielsen, S.E., and Schmiegelow, F.K.A. (2002). Evaluating resource selection functions. *Ecological Modelling*, 157, 281-300. https://doi.org/10.1016/s0304-3800(02)00200-4

Caldwell, I.R., Hobbs, J.P.A., Bowen, B.W., Cowman, P.F., DiBattista, J.D., Whitney, J.L., *et al*. (2024). Global trends and biases in biodiversity conservation research. *Cell Reports Sustainability*, 1, 100082. https://doi.org/10.1016/j.crsus.2024.100082

Dale, M.R.T., and Fortin, M.J. (2014). *Spatial analysis: a guide for ecologists*. 2nd ed. Cambridge University Press.

Elith, J., Graham, C.H., Anderson, R.P., Dudík, M., Ferrier, S., Guisan, A., *et al*. (2006). Novel methods improve prediction of species' distributions from occurrence data. *Ecography*, 29, 129-151. https://doi.org/10.1111/j.2006.0906-7590.04596.x

Elith, J., and Leathwick, J.R. (2009). Species distribution models: ecological explanation and prediction across space and time. *Annual Review of Ecology, Evolution, and Systematics*, 40, 677-697. https://doi.org/10.1146/annurev.ecolsys.110308.120159

Elith, J., Phillips, S.J., Hastie, T., Dudík, M., Chee, Y.E., and Yates, C.J. (2011). A statistical explanation of MaxEnt for ecologists. *Diversity and Distributions*, 17, 43-57. https://doi.org/10.1111/j.1472-4642.2010.00725.x

Fick, S.E., and Hijmans, R.J. (2017). WorldClim 2: new 1-km spatial resolution climate surfaces for global land areas. *International Journal of Climatology*, 37, 4302-4315. https://doi.org/10.1002/joc.5086

Fisher, D.O., and Owens, I.P. (2004). The comparative method in conservation biology. *Trends in Ecology & Evolution*, 19, 391-398. https://doi.org/10.1016/j.tree.2004.05.004

Foster, N.J., Maloney, R.F., Seddon, P.J., Rodríguez-Recio, M., and van Heezik, Y. (2022). High-elevation landforms limit the movement of invasive small mammal species. *Landscape Ecology*, 37, 2651-2670. https://doi.org/10.1007/s10980-022-01496-8

Fourcade, Y., Engler, J.O., Rödder, D., and Secondi, J. (2014). Mapping species distributions with MAXENT using a geographically biased sample of presence data: a performance assessment of methods for correcting sampling bias. *PLoS One*, 9, e97122. https://doi.org/10.1371/journal.pone.0097122

Gago, H., Drechsler, R.M., and Monrós, J.S. (2023). Algerian and European hedgehogs cohabiting in periurban environments: spatial behaviour and habitat use. *European Journal of Wildlife Research*, 69, 19. https://doi.org/10.1007/s10344-023-01644-8

Gazzard, A., Yarnell, R.W., and Baker, P.J. (2022). Fine-scale habitat selection of a small mammalian urban adapter: the West European hedgehog (*Erinaceus europaeus*). *Mammalian Biology*, 102, 387-403. https://doi.org/10.1007/s42991-022-00251-5

Gogol-Prokurat, M. (2011). Predicting habitat suitability for rare plants at local spatial scales using a species distribution model. *Ecological Applications*, 21, 33-47. https://doi.

org/10.1890/09-1190.1

Guisan, A., and Thuiller, W. (2005). Predicting species distribution: offering more than simple habitat models. *Ecology Letters*, 8, 993-1009. https://doi.org/10.1111/j.1461-0248.2005.00792.x

Guisan, A., and Zimmermann, N.E. (2000). Predictive habitat distribution models in ecology. *Ecological Modelling*, 135, 147-186. https://doi.org/10.1016/s0304-3800(00)00354-9

Hof, A.R., Snellenberg, J., and Bright, P.W. (2012). Food or fear? Predation risk mediates edge refuging in an insectivorous mammal. *Animal Behaviour*, 83, 1099-1106. https://doi.org/10.1016/j.anbehav.2012.01.042

Hortal, J., de Bello, F., Diniz-Filho, J.A.F., Lewinsohn, T.M., Lobo, J.M., and Ladle, R.J. (2015). Seven shortfalls that beset large-scale knowledge of biodiversity. *Annual Review of Ecology, Evolution, and Systematics*, 46, 523-549. https://doi.org/10.1146/annurev-ecolsys-112414-054400

Ibisch, P.L., Hoffmann, M.T., Kreft, S., Pe'er, G., Kati, V., Biber-Freudenberger, L., *et al*. (2016). A global map of roadless areas and their conservation status. *Science (New York, N.Y.)*, 354, 1423-1427. https://doi.org/10.1126/science.aaf7166

Jia, X., Li, Q., Yang, X., Li, D., and Jin, Z. (2024). Comparative analysis of the gut microbiota composition and diversity in *Erinaceus amurensis* from the Wandashan Mountain range area based on metagenomics. *Frontiers in Microbiology*, 15, 1479352. https://doi.org/10.3389/fmicb.2024.1479352

Kim, K., Kim, K., and Jang, Y. (2026). Trait-based ecological indices for evaluating mammalian species responses to habitat fragmentation. *Ecological Indicators*, 182, 114498. https://doi.org/10.1016/j.ecolind.2025.114498

Kim, N.H., Lim, S.J., Chae, H.M., and Park, Y.C. (2017). Complete mitochondrial genome of the Amur hedgehog *Erinaceus amurensis* (Erinaceidae) and higher phylogeny of the family Erinaceidae. *Genetics and Molecular Research*, 16.

Korea Meteorological Administration. (2025). *Korea Meteorological Administration web site*. Retrieved Sep 23, 2025 from https://www.weather.go.kr.

Kramer-Schadt, S., Niedballa, J., Pilgrim, J.D., Schröder, B., Lindenborn, J., Reinfelder, V., *et al*. (2013). The importance of correcting for sampling bias in MaxEnt species distribution models. *Diversity and Distributions*, 19, 1366-1379. https://doi.org/10.1111/ddi.12096

Legendre, P., and Fortin, M.J. (1989). Spatial pattern and ecological analysis. *Vegetatio*, 80, 107-138. https://doi.org/10.1007/bf00048036

Li, Z., Shi, X., Lu, J., Fu, X., Fu, Y., Cui, Y., *et al*. (2023). Assessing mammal population densities in response to urbanization using camera trap distance sampling. *Ecology and Evolution*, 13, e10634. https://doi.org/10.1002/ece3.10634

Liu, C., White, M., and Newell, G. (2011). Measuring and comparing the accuracy of species distribution models with presence–absence data. *Ecography*, 34, 232-243. https://doi.org/10.1111/j.1600-0587.2010.06354.x

Mazerolle, M.J., and Villard, M.A. (1999). Patch characteristics and landscape context as predictors of species presence and abundance: a review1. *Écoscience*, 6, 117-124. https://doi.org/10.1080/11956860.1999.11952204

McCain, C.M. (2005). Elevational gradients in diversity of small mammals. *Ecology*, 86, 366-372. https://doi.org/10.1890/03-3147

Merow, C., Smith, M.J., and Silander Jr, J.A. (2013). A practical guide to MaxEnt for modeling species' distributions: what it does, and why inputs and settings matter. *Ecography*, 36, 1058-1069. https://doi.org/10.1111/j.1600-0587.2013.07872.x

Moore, I.D., Lewis, A., and Gallant, J.C. (1993). Terrain attributes: estimation methods and scale effects. In A.J. Jakeman, M.B. Beck, M.J. McAleer (Eds.), *Modelling change in environmental systems* (pp. 189-214). John Wiley & Sons.

National Institute of Ecology (NIE). (2019). *The 5th national ecosystem survey guidelines*. NIE.

Paniccia, C., Laura Carranza, M., Frate, L., Di Febbraro, M., Rocchini, D., and Loy, A. (2022). Distribution and functional traits of small mammals across the Mediterranean area: landscape composition and structure definitively matter. *Ecological Indicators*, 135, 108550. https://doi.org/10.1016/j.ecolind.2022.108550

Peterson, A.T., Soberón, J., Pearson, R.G., Anderson, R.P., Martínez-Meyer, E., Nakamura, M., *et al*. (2011). *Ecological niches and geographic distributions*. Princeton University Press.

Pettett, C.E., Moorhouse, T.P., Johnson, P.J., and Macdonald, D.W. (2017). Factors affecting hedgehog (*Erinaceus europaeus*) attraction to rural villages in arable landscapes. *European Journal of Wildlife Research*, 63, 54. https://doi.org/10.1007/s10344-017-1113-6

Phillips, S.J., Anderson, R.P., and Schapire, R.E. (2006). Maximum entropy modeling of species geographic distributions. *Ecological Modelling*, 190, 231-259. https://doi.org/10.1016/j.ecolmodel.2005.03.026

Phillips, S.J., and Dudík, M. (2008). Modeling of species distributions with Maxent: new extensions and a comprehensive evaluation. *Ecography*, 31, 161-175. https://doi.org/10.1111/j.0906-7590.2008.5203.x

Phillips, S.J., Dudík, M., Elith, J., Graham, C.H., Lehmann, A., Leathwick, J., *et al*. (2009). Sample selection bias and presence-only distribution models: implications for background and pseudo-absence data. *Ecological Applications*, 19, 181-197. https://doi.org/10.1890/07-2153.1

Phillips, S.J., Dudík, M., and Schapire, R.E. (2020). Maxent software for modeling species niches and distributions (version 3.4.4). *American Museum of Natural History*. Retrieved May 16, 2025 from https://biodiversityinformatics.amnh.org/open_source/maxent/.

Plazi TreatmentBank. (2023). *Erinaceus amurensis, Schrenck, 1859: food and feeding section*. Plazi TreatmentBank. Retrieved Sep 23, 2025 from https://treatment.plazi.org/GgServer/xhtml/038787D0FFD3FFC2FA68F711FAC578A9.

Rasmussen, S.L., Berg, T.B., Dabelsteen, T., and Jones, O.R. (2019). The ecology of suburban juvenile European hedgehogs (*Erinaceus europaeus*) in Denmark. *Ecology and Evolution*, 9, 13174-13187. https://doi.org/10.1002/ece3.5764

Sunday, J.M., Bates, A.E., and Dulvy, N.K. (2012). Thermal tolerance and the global redistribution of animals. *Nature Climate Change*, 2, 686-690. https://doi.org/10.1038/nclimate1539

Tattersall, F.H., Macdonald, D.W., Hart, B.J., Manley, W.J., and Feber, R.E. (2001). Habitat use by wood mice (*Apodemus sylvaticus*) in a changeable arable landscape. *Journal of Zoology*, 255, 487-494. https://doi.org/10.1017/s095283690100156x

Trimble, M.J., and Van Aarde, R.J. (2010). Species inequality in scientific study. *Conservation Biology*, 24, 886-890. https://doi.org/10.1111/j.1523-1739.2010.01453.x

Trombulak, S.C., and Frissell, C.A. (2000). Review of ecological effects of roads on terrestrial and aquatic communities. *Conservation Biology*, 14, 18-30. https://doi.org/10.1046/j.1523-1739.2000.99084.x

U.S. Geological Survey (USGS). (2014). *USGS digital elevation model (DEM).* USGS. Retrieved Sep 7, 2022 from https://www.usgs.gov/faqs/what-a-digital-elevation-model-dem.

Williams, B.M., Baker, P.J., Thomas, E., Wilson, G., Judge, J., and Yarnell, R.W. (2018). Reduced occupancy of hedgehogs (*Erinaceus europaeus*) in rural England and Wales: the influence of habitat and an asymmetric intra-guild predator. *Scientific Reports*, 8, 12156. https://doi.org/10.1038/s41598-018-30130-4

Wintle, B.A., Elith, J.A.N.E., and Potts, J.M. (2005). Fauna habitat modelling and mapping: a review and case study in the Lower Hunter Central Coast region of NSW. *Austral Ecology*, 30, 719-738. https://doi.org/10.1111/j.1442-9993.2005.01514.x

Zanaga, D., Van De Kerchove, R., De Keersmaecker, W., Souverijns, N., Brockmann, C., Quast, R., *et al*. (2021). *WorldCover 10 m 2020 v100*. European Space Agency. Retrieved Jun 15, 2025 from https://zenodo.org/records/5571936.

PNIE PROCEEDINGS OF THE NATIONAL INSTITUTE OF ECOLOGY OF THE REPUBLIC OF KOREA

Original Article

PNIE 2026;7(4):155-172
https://doi.org/10.22920/PNIE.2026.7.4.155
pISSN 2765-2203, eISSN 2765-2211

Potential Hillslope Soil-Loss Pressure in the Catchments of South Korea's Inland Protected Wetlands: Contrasting a Land-Cover Trend with Rainfall Variability over 35 Years

Sunmin Lee[1], Jeong-Cheol Kim[2]*

[1]Climate Adaptation Cooperation Division, Korea Adaptation Center for Climate Change (KACCC), Korea Environment Institute, Sejong, Korea
[2]Ecological Big Data Team, Division of AI for Ecological Information, National Institute of Ecology, Seocheon, Korea

ABSTRACT

Inland wetlands lie at the base of their catchments; therefore, upstream hillslope erosion is a potential sediment-source pressure. Whether this pressure has changed over recent decades, and what drives it, has rarely been quantified for South Korea's protected inland wetlands. We delineated the catchments of 28 of the 33 inland Wetland Protected Areas from a 30 m digital elevation model and estimated potential hillslope soil loss with the Revised Universal Soil Loss Equation (RUSLE) across seven 5-year epochs (1986-2020), with land cover and event-based rainfall erosivity from 66 hourly gauges. Recent (2013-2020) mean soil loss spanned an order of magnitude among 18 local wetlands (3.6-79 t ha^{-1} yr^{-1}; median 22), was highest below cultivated hillslopes and lowest at intact montane bogs, and increased in 14 of the 18. Factorial attribution showed that rainfall erosivity governed inter-epoch variation and was the more precisely resolved driver (median share 0.51; bootstrap interval 0.39-0.68). Land cover determined the direction of change where cover shifted, but seven epochs leave this separation wide (median 0.44; 0.20-0.67); the share reached 0.69-0.94 at only five small, strongly changed catchments and was zero at four catchments with unchanged cover. The ranking was robust to cover, slope-length, and gauge-network inputs, and higher soil loss was associated with lower vegetation-index levels (ρ=−0.57); however, it was sensitive to the support-practice factor. The results provide a catchment screening list, not a ranking of delivered sediment, and indicate that protecting a wetland requires managing its catchment, not only its boundary.

Keywords: Conservation of natural resources, Rain, Remote sensing technology, Soil erosion, Wetlands

Introduction

Inland wetlands deliver a disproportionate share of freshwater ecosystem services, including water storage, nutrient processing, and habitats for exceptional biodiversity, relative to their small areas (Mitsch & Gosselink, 2015). Because they occupy topographic low points, they are also the potential receiving end of what their catchments shed. Soil eroded on hillslopes and routed

Received July 20, 2026; **Revised** August 20, 2026; **Accepted** August 21, 2026

***Corresponding author:** Jeong-Cheol Kim
e-mail jckim@nie.re.kr
https://orcid.org/0000-0003-2271-5691

This is an Open Access article distributed under the terms of the Creative Commons Attribution Non-Commercial License (http://creativecommons.org/licenses/by-nc/4.0), which permits unrestricted non-commercial use, distribution, and reproduction in any medium, provided the original work is properly cited.

Copyright © National Institute of Ecology.

downslope can, where sufficiently delivered and retained, accumulate in the wetland basin and, over decades, raise turbidity, bury substrate, and contribute to infilling. Hillslope erosion within the catchment is, therefore, a potential cumulative sediment source pressure on a protected wetland—an upstream hazard that warrants monitoring and management, whether or not the delivered fraction can be quantified. Whether that pressure truly reaches the wetland and translates into in-wetland harm at a given site depends on delivery, retention, and the wetland's own resilience, which are beyond the focus of this study. In this study, we quantify catchment-scale potential soil loss as a screening measure of this pressure, not as delivered sediment load or measured ecological impact.

The magnitude of this potential sediment-source pressure is determined by erosion processes within the upstream catchment. According to the Universal Soil Loss Equation (USLE) and its revised form, the Revised Universal Soil Loss Equation (RUSLE), hillslope soil loss is a product of rainfall erosivity, soil erodibility, topography, cover, and support practices (Renard *et al*., 1997; Wischmeier & Smith, 1978). Of these factors, land-use change acts mainly through the cover and management factor. Land-cover change has been shown to reorganize erosion intensity at the basin scale (Ozsahin *et al*., 2018), whereas rainfall erosivity carries the imprint of climate variability. Thus, a catchment's potential soil loss pressure depends on how the catchment is used and how hard the rain falls, both of which have changed in recent decades.

Previous studies have established a wetland-infilling problem and rainfall-versus-landscape decomposition. Skagen *et al*. (2016) modeled sediment accumulation in prairie-pothole wetlands with RUSLE coupled with sediment routing and explicitly separated the relative roles of precipitation and landscape, projecting that a substantial fraction of prairie wetlands could be filled within the century, and Zarrinabadi *et al*. (2023) quantified agricultural sediment infilling of Canadian prairie wetlandscapes. Given this lineage, we cannot claim that the underlying idea is novel. What remains open is the different settings and evidentiary bases. The prairie-pothole system is a semiarid, depressional, dryland–agriculture landscape, whereas the temperate East Asian monsoon, with its summer-concentrated erosivity and paddy-dominated valleys, is a distinct regime hydrologically and land-use-wise. Previous wetland-sediment studies have also leaned on scenarios or static land-cover snapshots rather than observed multi-decadal cover changes and have treated individual wetlands or landscapes rather than a national set of legally protected sites.

Korea offers components to close this gap. A continuous, 30 m, seven-epoch satellite land-cover series (1986-2020) recorded the actual trajectory of the catchment cover, a national wetland inventory delineated the protected sites, and a detailed soil map, together with a dense hourly rain-gauge network, supplied the remaining RUSLE factors. Two methodological points should be emphasized. First, rainfall erosivity, the factor that most directly governs how intensely sediment is mobilized, is usually approximated in Korean applications from annual precipitation, which cannot capture storm intensity. Following evidence that such regressions lose the intensity signal (Lee & Heo, 2011; Panagos *et al*., 2017), we therefore computed erosivity directly as event EI_{30} (the product of storm kinetic energy and maximum 30-minute intensity) from hourly gauge data (Renard *et al*., 1997; Wischmeier & Smith, 1978). Second, we framed soil loss as a relative, comparative measure across wetlands and epochs rather than as absolute tonnage, in line with standard RUSLE practice.

In our previous studies, RUSLE applications in Korea were confined to river riparian zones, single basins, and before-and-after comparisons at two time points (Kim *et al*., 2018; 2019; 2020). The present study differs in target, unit, and time; it covers the national set of inland protected wetlands, works at the scale of each wetland's delineated catchment, and resolves a 35-year seven-epoch trajectory. This study aimed to (i) quantify and rank the soil-loss pressure on protected wetland catchments; (ii) characterize how that pressure has moved from 1986 to 2020; (iii) separate the land-cover and rainfall contributions to that change, distinguishing the directional trend from the inter-epoch variability; and (iv) identify the wetlands where catchment management could most plausibly reduce the pressure.

Materials and Methods

Study area and target wetlands

We analyzed the catchments of South Korea's inland Wetland Protected Areas (designated under the Wetland Conservation Act; list from the National Institute of Ecology, as of 2024) (Fig. 1). Because the designations are a finite, legally fixed population, and we analyze all that can be analyzed, the study represents a census, not a sample. Of the 33 designated inland sites, three (Daejeon Gapcheon, Cheorwon Igil-ri, and Yeongyang Janggumegi) postdate the 2022 National Wetland Inventory used for boundaries and have no mapped polygons, leaving 30. "Inland" is the administrative category and includes river estuaries; coastal tidal flats are designated separately and fall outside this study.

Wetland polygons were obtained from the 2022 National Wetland Spatial Information dataset (2,704 inland wetlands). That file was declared EPSG:4326 but contained coordinates in Korea 2000 Central Belt (EPSG:5186) projected meters. We verified this by matching polygon centroids to the per-record latitude/longitude fields (me-

dian offset≈20 m) and reassigned the coordinate reference system (CRS) accordingly. Designations were named and not keyed to the inventory; therefore, we matched each by name—exact match first, then a substring match, with two sites (Jeonnam-Gwangju Jangrok, Suncheon Waryong) resolved by hand against location because the inventory names them differently. Where a name returned several candidates, we selected the polygon closest in area to the gazetted figure.

The analysis unit is the wetland polygon, the body that receives the sediment, and not the larger gazetted area, which includes the surrounding forest at many sites. The gap can be wide: Waryong is a 2.1 ha polygon against an 89.9 ha designation; the inventory there maps only the wetland core, and that designation is larger than the 0.62 km^2 catchment we delineate. Our unit was a mapped wetland body that was not interchangeable with the protected area.

Catchments were classified into three groups by hydrological setting:

- Local (n=18): bogs, crater (oreum) wetlands, and lacustrine wetlands whose catchment is the wetland's own sediment-shed. Headline group.
- River-reach (n=7): riverine (Korean type R*) wetlands whose catchment is a whole upstream river basin (catchment area>50 km^2); their "catchment" is basin-scale yield rather than local pressure. Thus, they are reported separately.
- Estuarine (n=3): tidal/estuary wetlands where RUSLE is not meaningful.

The river-reach rule is conjunctive (riverine type and >50 km^2). Thus, the local group is not uniformly small: it spans 0.12 km^2 (Duung) to 144 km^2 (Upo), and Upo (144 km^2) exceeds the smallest river-reach basin (96 km^2), and Madongho (92 km^2) is close to it. Size governs how the group behaves and sediment connectivity (Section "Catchment sediment-source screening and robustness"); therefore, Table 1 lists the catchment area per site.

One estuarine site (Han Estuary) could not be delineated within the maximum digital elevation model (DEM) window, and one island bog (Jangdo) fell outside the soil map and land-cover coverage; both were dropped, resulting in 28 analyzed catchments.

A 30 m DEM resolves the delineation of the smallest local catchments (down to 0.12 km^2, ≈130 cells, at Duung) less precisely than the larger basins: the D8 (eight-direction flow) boundary of a catchment only a few dozen cells across is more sensitive to pit-filling and flat-resolution choices than a catchment spanning thousands of cells, even though every catchment passed the same three delineation gates (Section "Data and catchment delineation"). This is not tested against a finer DEM here; the slope length and steepness (LS) cap sensitivity (50-200 m, Section "Robustness and corroboration") bounds a related but not identical source of uncertainty (the flow-path length within the catchment, not its outer boundary).

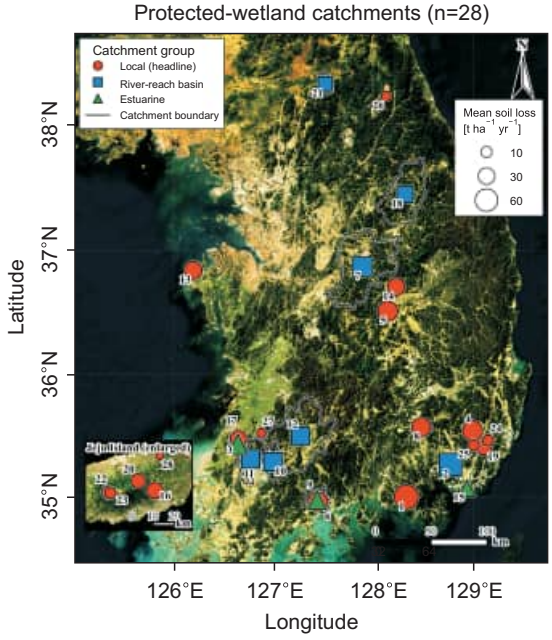

Fig. 1. Study area: 28 protected-wetland catchments across South Korea over Esri World Imagery. Symbols mark catchment group (circle, local; square, river-reach; triangle, estuarine); symbol area is proportional to mean soil loss, and numerals give the rank in Fig. 4. Inset, Jeju Island enlarged.

Data and catchment delineation

The five inputs and their sources are listed in Table 2.

The cover factor was derived from the published continuous time-series land cover maps for South Korea using Google Earth Engine, distributed through Eco-Bank, the National Institute of Ecology's ecological data platform (National Institute of Ecology, 2023; dataset DOI 10.22756/GEO.20230000000838). It is delivered as seven 5-year majority composites (not annual): 1986-1990, 1991-1995, 1996-2000, 2001-2005, 2006-2010, 2013-2015 and 2016-2020, with 2011-2012 absent. The 5-year majority compositing suppressed inter-annual and residual-cloud noise, and it incidentally diluted the effect of Landsat-7 Enhanced Thematic Mapper Plus (ETM+) scan-line corrector failure (SLC-off, post-2003) gaps in the later composites, as a class was assigned from the most frequent valid observation over 5 years. We used a distributed product and did not reassess its classification accuracy. Our inference rests on the cover-driven ranking and its 35-year change rather than on single-pixel labels, and the cover signal is cross-checked against a separately processed normalized difference vegetation index (NDVI)

Table 1. Soil-loss results by protected-wetland catchment (n=28)

Wetland	Group	Catchment (km^2)	A (mean)	A (recent, 2013-2020 mean)	Change (%)	LC trend share	Rain var. share	Interaction resid.
Madongho (Goseong)	Local	92.24	69.67	78.63	75.10	0.41	0.75	4.88
Hwapocheon (Gimhae)	River-reach	96.04	59.65	65.63	100.50	0.61	0.41	5.70
Waryong (Suncheon)	Local	0.62	44.95	45.79	43.50	0.94	0.30	−3.25
Dongcheon Estuary (Suncheon)	Estuarine	482.82	40.94	45.52	67.20	0.98	0.46	0.58
Incheongang Estuary	Estuarine	280.42	47.24	43.53	11.00	0.28	0.75	−0.39
Jangrok (Jeonnam-Gwangju)	River-reach	715.20	38.29	39.87	31.80	0.59	0.67	−0.03
Nakdong Estuary	Estuarine	70.98	31.06	39.35	107.70	0.41	0.62	4.09
Chimsil (Seomjin River)	River-reach	2,971.04	36.57	39.11	48.20	0.71	0.65	0.96
Damyang River	River-reach	507.36	38.58	38.98	28.60	0.50	0.73	0.17
Gonggeomji (Sangju)	Local	30.78	46.08	36.20	1.70	0.48	0.51	−1.77
Binaeseom (Chungju)	River-reach	3,121.70	41.76	36.07	−18.70	0.39	0.54	−4.29
Upo	Local	144.40	40.97	34.24	−3.40	0.51	0.69	−0.56
Hwaeomneup	Local	0.16	25.15	33.62	166.40	0.79	0.24	3.03
Ungok (Gochang)	Local	15.77	28.90	32.44	40.00	0.59	0.44	−0.55
Mulyeongari (Jeju)	Local	0.38	28.98	31.42	16.00	0.00	1.00	0.00
Hanbando (Yeongwol)	River-reach	1,887.88	28.42	23.82	−5.40	0.63	0.58	−1.94
Muljangori (Jeju)	Local	0.77	22.19	23.54	10.30	0.00	1.00	0.00
Duung	Local	0.12	35.23	21.58	−46.40	0.77	0.36	0.02
Doline (Mungyeong)	Local	0.64	33.88	21.58	−27.00	0.76	0.30	−4.39
Jaeyaksan (Miryang)	Local	2.17	46.61	19.18	−35.70	0.69	0.16	−0.66
Yongyangbo (Cheorwon)	River-reach	206.63	20.61	16.71	−15.10	0.75	0.93	−0.06
Sumeunmulbaengdui (Jeju)	Local	1.46	14.19	16.58	26.80	0.39	0.76	0.24
1100 Highland (Jeju)	Local	0.50	11.29	12.97	15.60	0.37	0.50	−0.09
Mujechineup	Local	0.26	10.81	12.92	59.30	0.47	0.38	1.33
Sinbulsan	Local	0.38	10.33	8.44	26.20	0.01	0.33	0.36
Yongneup (Daeamsan)	Local	1.88	7.50	6.18	1.90	0.01	0.77	−0.03
Wolyeong (Jeongeup)	Local	0.52	5.74	5.10	1.30	0.00	1.00	0.00
Dongbaekdongsan (Jeju)	Local	0.85	3.51	3.63	10.20	0.00	1.00	0.00

A is soil loss (t ha^{-1} yr^{-1}). A (recent) is the mean of the last two epochs (2013-2015 and 2016-2020), the endpoint of the change statistic, not the 2016-2020 epoch alone. Change is first-two vs. last-two epoch means. Land-cover trend share, rainfall variability share, and the interaction residual ($\Delta A - \Delta A_{land} - \Delta A_{clim}$, t ha^{-1} yr^{-1}) are from the factorial decomposition; the bounds on the two shares are given in Supplementary Table 1. Catchment area is listed because the local group spans three orders of magnitude and size governs sediment connectivity (Section "Catchment sediment-source screening and robustness").
LC, land cover; resid., residual.

series (Section "Robustness and corroboration"); therefore, the analysis is buffered against per-pixel classification error, and the reliance on the provider's product is nonetheless stated as a limitation (Section "Limitations and conclusion"). Therefore, the temporal analysis is an epoch-change analysis rather than an annual trend. Rainfall erosivity uses the 66 Automated Synoptic Observing System (ASOS) stations with ≥30-year continuous hourly records (of 81 installed; 15 were excluded for short records). The land-cover time series and national wetland spatial information for 2022 are openly available through EcoBank (National Institute of Ecology; land-cover dataset DOI 10.22756/GEO.20230000000838). The ASOS hourly precipitation data are available from the Korea Meteorological Administration open data portal, the SRTM DEM via Google Earth Engine, and a detailed soil map

Table 2. Data sources for the RUSLE factors and the catchment delineation

Factor/input	Source	Resolution/period
Land cover (C)	Continuous time-series land cover maps for South Korea (National Institute of Ecology, 2023)	30 m, 7 classes; seven 5-year epochs, 1986-2020 (no 2011-2012)
Wetland polygons	National Wetland Spatial Information	Polygons; 2022
Soil (K)	Detailed soil map, Rural Development Administration (Jung *et al*., 2004)	1:25,000
Rainfall (R)	ASOS hourly precipitation, Korea Meteorological Administration	66 stations; 1986-2020
Terrain (LS, delineation)	SRTM DEM via Google Earth Engine (Gorelick *et al*., 2017)	30 m

ASOS, Automated Synoptic Observing System; DEM, digital elevation model; SRTM, Shuttle Radar Topography Mission.

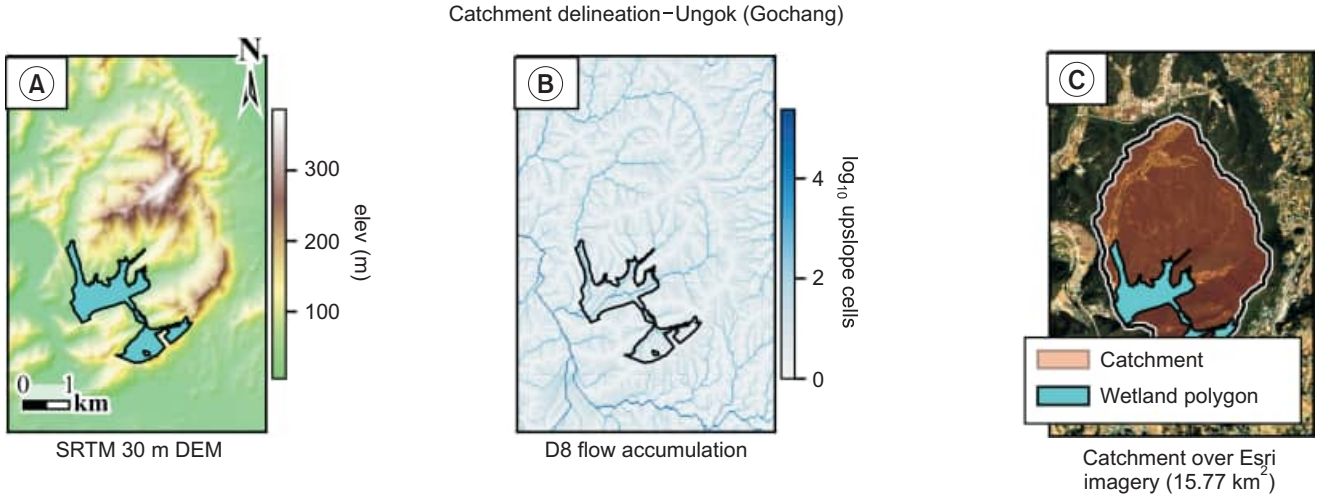

Fig. 2. Catchment delineation for Ungok (Gochang): (A) 30 m DEM with hillshade and the wetland polygon; (B) log-scaled D8 flow accumulation; (C) the upslope contributing area taken as the catchment, over Esri World Imagery. Contributing area is used because pour-point routing mis-sizes crater and ridge-line wetlands. DEM, digital elevation model; D8, eight-direction; SRTM, Shuttle Radar Topography Mission.

from the Rural Development Administration. The derived catchment results are provided in Table 1 and Supplementary Tables 1 and 2, and further derived data are available from the corresponding author upon request.

Catchment delineation

Catchments were delineated from the 30 m DEM with D8 flow routing in Pysheds (Fig. 2) in the following sequence: fill pits→fill depressions→resolve flats→flow direction→the set of cells draining into the wetland body (upstream breadth-first search over the D8 graph). An upstream contributing-area definition was used because pour-point routing missizes craters and ridge-line wetlands. HydroBASINS level-12 sub-basins were tested first and rejected as they overestimated small mountain bog catchments by 6- to 79-fold and omitted islands. Each catchment had to pass through three gates: it could not touch the DEM window edge (otherwise, the window was enlarged), it had to contain the wetland, and it had to exceed the wetland area.

RUSLE factors

Annual soil loss follows RUSLE (t ha^{-1} yr^{-1}); all factors are in SI units:

$$A=R\cdot K\cdot LS\cdot C\cdot P$$

The coefficients follow established Korean applications (Kim *et al*., 2018; 2019; 2020) except where noted.

Rainfall erosivity (R; EI_{30}): Rather than a rainfall-depth regression of the kind commonly substituted when high-resolution records are unavailable (Renard & Freimund, 1994), R was computed directly as event EI_{30} from ASOS hourly data: events separated by ≥6 hours dry gaps (<1.27 mm), erosive if ≥12.7 mm; unit energy.

$$e_r=0.29[1-0.72\ \exp(-0.05\ i_r)];\ E=\Sigma\ e_r\ v_r$$

where I_{30} is the maximum 30-minute intensity within the storm. ASOS reports rainfall at fixed 60-minute resolution, from which true 30-minute intensity cannot be recovered; I_{30} was therefore approximated by the storm's peak 1-hour intensity, and both the resulting apparent intensity and the storm energy computed from it understate the breakpoint-derived (true sub-hourly) EI_{30}. Following the fixed-interval conversion factors of Yin *et al*. (2007), who related 5- to 60-minute fixed-interval EI_{30} to breakpoint EI_{30} over 456 storms at five Chinese stations, we applied a single factor of 1.73 to the per-storm EI_{30} product ($E \times I_{30}$), rather than compounding Yin *et al*. (2007)'s separate E (×1.105) and I_{30} (×1.668) sub-factors, since 1.105×1.668≈1.84 already diverges from their reported combined 1.73 and the two sub-corrections are not independent. The factor is climate-dependent (reported range 1.40-1.90, tested as a sensitivity, Section "Robustness and corroboration") and was applied as a per-catchment, per-epoch scalar to R. Therefore, it changes the absolute value of A but leaves the ranking and all attribution fractions unchanged. Missing hourly values within an otherwise used station year were treated as zero rainfall, a conservative choice that can only under-count, not over-count, a storm. Station R was validated against Shin *et al*. (2019), who computed R for 46 Korean stations from 5-minute data: national median≈4,900, monsoon (Jun-Sep) share≈79%, a significant long-term trend at only a small minority of stations (3 of the 27 long-record stations available when the check was made), and extreme years coinciding with typhoons (e.g., Rusa 2002)—an annual-scale feature that does not survive the 5-year epoch means used here (Section "Thirty-five-year trajectories"). Epoch-mean station R was interpolated by inverse-distance weighting (power 2, in projected meters) to a single representative point per catchment (its polygon centroid), not averaged over a gridded rainfall surface; because the ≥30-year completeness criterion (above) requires every one of the 66 stations to have a valid record in each of the seven epochs, the interpolating network is the same 66 stations in every epoch. Therefore, epoch-to-epoch differences in R reflect rainfall, not a changing gauge count (the separate 27→66 network upgrade is tested in sensitivity, Section "Robustness and corroboration").

Soil erodibility (K): Wischmeier soil-series K values from the detailed soil map (Jung *et al*., 2004) were rasterized to the land-cover grid following the Korean national practice. Non-erodible map units (rock, water, tidal flat, and levee) were set to K=0, soil complexes to the mean K of their components, and a few series absent from the look-up table to the median K of the tabulated series.

Slope length and steepness (LS): Desmet and Govers (1996) and Moore and Burch (1986) used the real upslope contributing area from DEM flow accumulation as follows:

$$LS=(A_s/22.13)^m (\sin\theta/0.0896)^{1.3}$$

with A_s the specific catchment area and

$$m=\beta/(1+\beta);\ \beta=(\sin\theta/0.0896)/(2.96\sin^{0.79}\theta+0.56)$$

The specific catchment area was capped at 100 m slope length. In RUSLE, L is the hillslope length up to where flow concentrates into channels; therefore, using raw flow accumulation inflates LS along valley cells, and the cap (RUSLE guidance max≈122 m) removes this artifact (tested at 50 and 200 m in sensitivity).

Cover management (C): The 7-class land cover was mapped to USDA-based C values (settlement 0.001, cropland 0.27, forest 0.007, grass 0.05, wetland 0, barren 1.0, and water 0). The coarse scheme prevents splitting paddy/field/orchard and conifer/broadleaf; the two lumped classes were varied by ±20% in sensitivity.

Support practice (P): P=1.0 (the seven-class land-cover scheme cannot separate paddy from upland field; a slope-based variant was retained as the sensitivity option).

Soil loss, trajectory, and attribution

Relative framing

All factors are in SI. Therefore, the absolute A value was ~15-fold higher than the values reported in earlier Korean studies that combined a customary-unit Toxopeus R (~490) with SI K/LS/C; this difference is a unit correction, not a physical discrepancy. R and K, the two factors most often mismatched in the Korean literature, are dimensionally consistent as used here: R carries units MJ mm ha^{-1} h^{-1} yr^{-1} and K the conventional RUSLE SI unit t ha h ha^{-1} MJ^{-1} mm^{-1} (Renard *et al*., 1997); their product cancels MJ, mm, and h, leaving t ha^{-1} yr^{-1} once multiplied by the dimensionless LS, C, and P, matching the reported units of A. We confirmed this cancellation explicitly rather than inheriting it from previous unit-mixed applications. Following long-standing guidance on what the equation can and cannot support (Wischmeier, 1976), we treated A as a relative measure whose inferences rest on ranking, trajectory, and attribution, all of which are unit-invariant, rather than on absolute tonnage or fixed 5-class thresholds.

Trajectory and attribution

For each catchment, we computed the R-independent product S=mean(K·LS·C·P) per epoch on the catchment grid, and A(t)=R(t)·S(t). The epoch trend was summarized by Kendall's τ and Sen's slope (7 points; low power, consistent with Shin *et al*. [2019]'s no-trend finding). This change was attributed to a factorial experiment holding one driver at the initial (first two-epoch mean) level:

- land-cover series $A_{land}(t)=R_0 \cdot S(t)$ (rainfall fixed)

- rainfall series $A_{clim}(t)=R(t) \cdot S_0$ (land cover fixed)

These were decomposed in two ways: The directional trend compares the size of each series' Sen's slope, sen_land and sen_clim (both signed and computed over the seven mid-year epochs), as a share of their combined magnitude:

$$land_trend_frac=|sen_land| \div (|sen_land|+|sen_clim|)$$

Therefore, the land-cover share reflects how much of the combined magnitude of drift each driver contributes to, irrespective of whether the two slopes point in the same way or oppose each other (the sign is discarded only in this ratio; opposing slopes are not netted against one another; they are both counted as drift to be attributed). The inter-epoch variability compares each series's standard deviation (SD) across seven epochs:

$$clim_var_frac=sd(A_clim) \div [sd(A_land)+sd(A_clim)]$$

Both ratios are undefined (reported as missing) when their denominator is zero, that is, when neither driver shows any resolvable slope or spread at all. This did not occur because every catchment has non-zero rainfall variability. This occurs by construction in the four catchments whose land-cover map never changes (sen_land=0 exactly), where land_trend_frac is reported as zero rather than absent because the numerator, not the denominator, vanishes there. Neither ratio nor the underlying Sen's slope and standard-deviation estimators apply any explicit weight for epoch duration: the 3-year 2013-2015 epoch enters the seven-point series as one value like every 5-year epoch, and Sen's slope uses the actual calendar mid-year of each epoch (1988, ..., 2014, and 2018) as its time axis rather than an epoch index. Therefore, unequal spacing is reflected in the slope's time scale, but the shorter epoch is not down-weighted in either estimator. Section "Limitations and conclusion" (ii) discusses the resulting low power of any formal trend test on seven unequally-spaced points. The interaction residual $\Delta A-\Delta A_{land}-\Delta A_{clim}$ is reported. Land-cover change was further described by the 1986-1990→2016-2020 transition matrix over the local catchments.

Robustness and corroboration

Sensitivity

The wetland ranking was tested on the 2016-2020 epoch against the discretionary choices: cropland and forest C±20%, LS slope-length cap 50/100/200 m, and the EI_{30} correction factor 1.40-1.90. Individual catchment A changed by up to ~28%, but the ranking was stable (Spearman ρ=0.990-0.997, Kendall's τ=0.952-0.974, top-8 overlap 7 or 8 of 8); the EI_{30} factor is a per-catchment scalar and leaves ranking and attribution fractions unchanged. The sensitivity set consisted of the 28 analyzed catchments; Jangdo, which lies outside the soil and land cover coverage, was excluded.

The support-practice factor was swept separately because setting P=1 everywhere (Section "RUSLE factors") is the assumption most likely to bias the ranking rather than blur it: a terraced paddy carries a P well below 1, and the highest-ranked catchments are paddy-dominated valley catchments. Therefore, we recomputed A with P=0.5, 0.3, and 0.15 applied to the cropland class, deliberately a worst case rather than an estimate, since the 7-class scheme lumps upland fields and orchards (true P near 1) together with paddy. If the ranking holds under this condition, then it also holds for any realistic paddy fraction (Table 3).

Vegetation-index corroboration

Because the cover management factor was assigned from a discrete seven-class land-cover series, we cross-checked the cover signal against a continuous vegetation index that was processed independently. Growing-season (May-September) NDVI (Tucker, 1979) was computed for each catchment in each of the seven epochs from Landsat surface reflectance (Collection 2, Level 2): Landsat 5 Thematic Mapper (TM) and Landsat 7 ETM+ for 1986-2010, and Landsat 8 Operational Land Imager (OLI) for 2013-2020. Clouds and cloud shadows were masked using the QA_PIXEL band. NDVI=(NIR−red)/(NIR+red), where NIR is near-infrared reflectance, was evaluated on the per-epoch median-reflectance composite and reduced to the catchment mean at 100 m in Google Earth Engine (Gorelick *et al*., 2017). Catchment NDVI change (last two minus the first two epoch means) was compared with the C-factor change, soil loss change, and mean soil loss by Spearman rank correlation, for the full set and for the headline local group alone. Because the TM/ETM+ and OLI red and near-infrared bands have slightly different spectral response functions, a small cross-sensor offset (of order 0.02; Roy *et al*., 2016) can accompany the 2013 transition from TM to OLI; therefore, the absolute 1986-2020 greening magnitude is treated as indicative only, and the results serve solely as an ordinal, within-set corroboration, which is insensitive to a constant offset. These correlations cross-check a signal that the study derives elsewhere; therefore, we report point estimates with 95% bootstrap intervals (10,000 resamples of catchments) and no *P*-values. Six coefficients across two groupings would invite a multiple-comparison correction that these data cannot support, and the intervals show what 18 to 28 catchments support. We used the local group (n=18) as

Table 3. Sensitivity of the catchment ranking to discretionary factor choices, evaluated on the 2016-2020 epoch

Scenario	Spearman	Kendall	Top-8 overlap	Max ΔA (%)
Base	1.000	1.000	8/8	0.00
C_crop+20	0.995	0.968	8/8	16.60
C_forest+20	0.997	0.974	8/8	20.00
C_crop-20	0.997	0.968	8/8	16.60
C_forest-20	0.993	0.958	8/8	20.00
LS_cap50	0.990	0.952	7/8	27.70
LS_cap200	0.994	0.952	8/8	28.40
P_crop0.5	0.952	0.857	7/8	41.50
P_crop0.3	0.888	0.751	6/8	58.00
P_crop0.15	0.794	0.656	6/8	70.50

Spearman and Kendall rank correlation of A against the baseline, top-8 overlap, and maximum individual change. The P_crop rows apply a paddy-like support-practice factor to the whole cropland class, which also contains upland field and orchard whose true P is near 1; they are therefore a worst case for the P=1 assumption, not an estimate of it (Section "Robustness and corroboration").
C, cover management factor; LS, slope length and steepness factor; P, support practice factor; A, soil loss.

the primary comparison because RUSLE is not meaningful for the tidal flats of estuarine catchments (Section "Study area and target wetlands"), and those sites are dominated by open water; the all-catchment coefficient is reported alongside it.

Attribution uncertainty

As the attribution fractions were estimated from only seven epochs, the sampling uncertainty was bounded by a case (epoch) bootstrap. The seven epochs were resampled with replacement 2,000 times; each resample was re-sorted by year, and every quantity (the stabilized baseline [first-two-epoch mean], the Sen's-slope trend components, and the standard-deviation variability components) was recomputed exactly as for the point estimate, yielding 95% percentile intervals for the land-cover trend share and the rainfall variability share per catchment. A group-level statistic (median share across local catchments) was bootstrapped with a single shared epoch resampling applied to all catchments.

These intervals were heuristic bounds, not formal confidence intervals. A case bootstrap assumes exchangeable observations, but epochs are ordered in time: resampling with replacement breaks that order, and pairs in duplicated years contribute no slope; therefore, the number of pairwise slopes entering each Sen estimate varies between resamples. A block bootstrap respects the ordering, but is not meaningful in a series of seven. Therefore, we used the intervals only to determine whether a share sits on one side of an equal split, and not as a calibrated probability.

Sediment-connectivity robustness

RUSLE estimates hillslope soil loss, not the fraction of soil actually delivered to the wetland; cells far from the wetland or buffered by intervening low-gradient ground deliver less. To test whether this changed the priority ranking, we weighted the soil loss of each final epoch cell using a flow-distance sediment delivery ratio:

$$SDR(cell)=\exp(-d/L)$$

where d is the D8 downslope flow path distance from the cell to the wetland body, and L is the characteristic delivery length (Borselli *et al*., 2008). The connectivity-weighted catchment soil loss is then:

$$A_{conn}=R\cdot\Sigma(K\cdot LS\cdot C\cdot SDR)/\Sigma(SDR)$$

compared with the unweighted A by Spearman rank correlation, sweeping L over 500/1,000/2,000 m.

Results

Soil loss and catchment typology

Range and ordering

The estimated soil losses in the 28 delineated catchments spanned more than one order of magnitude. We report the 2013-2020 mean (hereafter, recent A), the endpoint of the change statistic used throughout (Section "Soil loss, trajectory, and attribution"), which is steadier than any single epoch. Recent A ranged from 3.6 to 79 t ha^{-1} yr^{-1} (Table 1, Fig. 3A). Within the headline local group (n=18), the median was 22 t ha^{-1} yr^{-1} and the

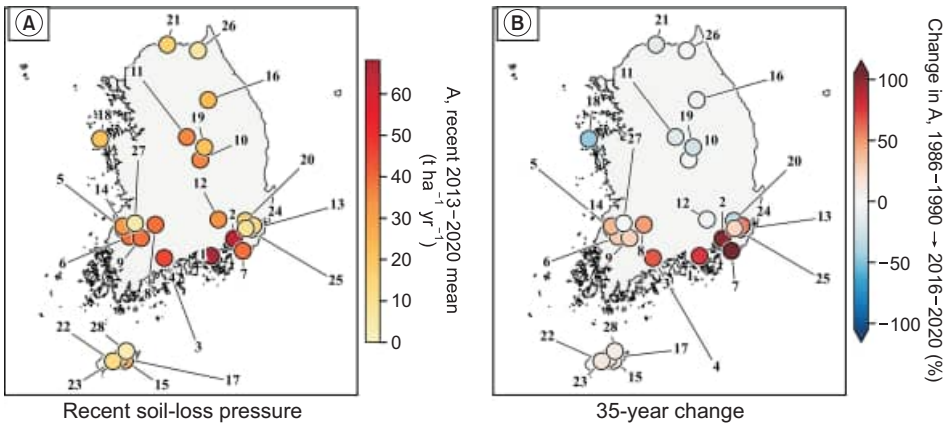

Fig. 3. Potential hillslope soil-loss pressure across the wetland catchments. (A) Recent soil loss (2013-2020 mean), (B) change from 1986-1990 to 2016-2020 on a diverging scale (red, rising; blue, falling). Numerals give the rank by recent A. A, soil loss.

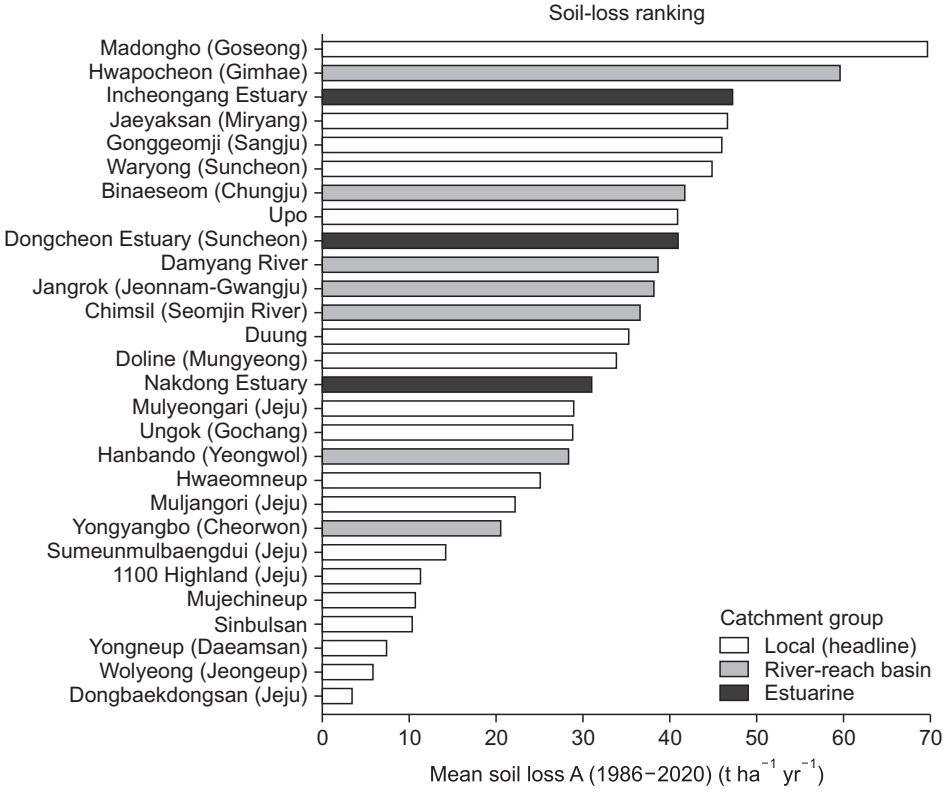

Fig. 4. Wetland-catchment soil-loss ranking by mean A (1986-2020). Bars are keyed to catchment group by color. A, soil loss.

maximum is Madongho (Goseong), 79 t ha^{-1} yr^{-1}. The ordering was governed by relief and cover rather than by catchment size, and the 35-year mean-A ranking (Fig. 4) tracked recent A closely (Spearman ρ=0.85, local group) without being identical. The lowest-loss catchments were the intact montane and Jeju crater bogs (Dongbaekdongsan 3.6, Wolyeong 5.1, Daeamsan Yongneup 6.2, Sinbulsan 8.4), whose catchments are small, forested, and near-pristine. The highest-loss local catchments (Madongho 79, Waryong 46, Gonggeomji 36, Upo 34, and Hwaeomneup 34) were situated below cultivated or peri-urban hillslopes. In the factor maps (Fig. 5), the hotspots were on steep-LS, high-C cells in the cropland along the valley margins; therefore, the pattern has a physical location and is not an artifact of catchment averaging.

The seven river-reach wetlands are reported separately (Table 1) because their catchments are whole upstream basins (96-3,122 km^2), and their A reflects basin-scale yield, not local wetland pressure. The three estuarine sites are listed but not interpreted, RUSLE being inappropriate for tidal flats.

Catchment typology

Ordination summarizes the multivariate structure un-

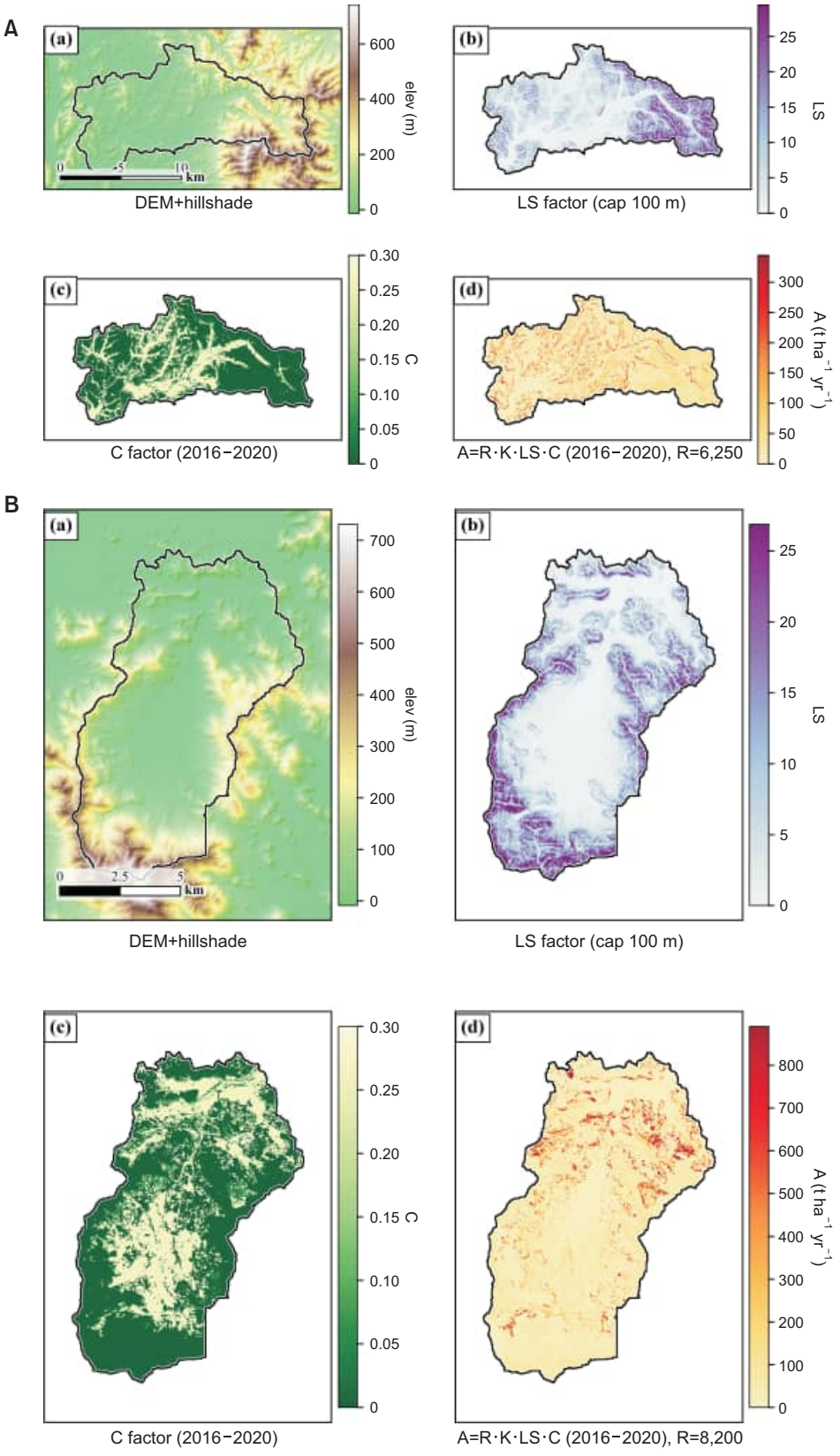

Fig. 5. RUSLE factor maps for Upo (A) and Hwapocheon, Gimhae (B), each panelled (a-d) as DEM with hillshade, LS, C (2016-2020), and soil loss A. Hotspots coincide with steep-LS, high-C cells at cultivated valley margins. Native resolution 30 m; continuous panels use bilinear display interpolation. RUSLE, Revised Universal Soil Loss Equation; DEM, digital elevation model; LS, slope length and steepness factor; C, cover management factor; A, soil loss; R, rainfall erosivity factor; K, soil erodibility factor.

derlying catchment differences (Supplementary Fig. 1). Principal component analysis (PCA) of the standardized RUSLE factors, land-cover composition, terrain, and trajectory metrics placed 39% of the variance in PC1 and 22% in PC2. PC1 is a cover–erosion gradient loading positively on the C factor, cropland, settlement, and mean A and negatively on forest, separating the intact forested montane and Jeju crater bogs from the cultivated and peri-urban catchments. PC2 is a terrain–size gradient (LS, slope, catchment area) that isolates the large river-reach basins. The dominant axis of variation among protected wetland catchments is therefore the forest-to-cultivation cover gradient, and the axis whose change over 1986-2020 was identified as the driver of the soil loss trend. Because A and the RUSLE factors that determine it (including C and the land-cover composition) are analyzed together in the same ordination, this PCA is a descriptive summary of how those inputs and outputs co-vary, not an independent validation of the soil-loss estimates. It is therefore expected to recover the cover-erosion structure by construction, and we interpret it accordingly, separate from the independently derived vegetation-index check below.

Thirty-five-year trajectories

Across the seven 5-year epochs (1986-1990→2016-2020), soil loss increased at 14 of the 18 local catchments and decreased at 4 (Table 1, Fig. 3B, Supplementary Fig. 2). The increases were large at a few sites (Hwaeomneup +166%, Madongho +75%, Mujechineup +59%, Waryong +44%, and Ungok +40%), while the decreases (Duung −46%, Jaeyaksan −36%, Doline −27%) occurred at catchments where cropland had reverted toward grass or forest. The trajectories swing between epochs, and the swings follow erosivity rather than cover; the epoch of lowest erosivity, 2013-2015, is also the epoch with the lowest R in 11 of the 18 local catchments. However, swings cannot be pinned to individual storm years. Erosivity peaked in 1996-2000 or 2016-2020, depending on the catchment, and in no local catchment peaked in 2001-2005. Therefore, although 2002 (Rusa) and 2003 (Maemi) were years of extreme rainfall erosivity in the annual station record (Section "RUSLE factors"), the 5-year majority compositing averages them (Section "Data and catchment delineation"); soil loss peaked in 2016-2020 at half the local catchments (9 of 18) and in 2001-2005 at only 3 (Supplementary Figs. 2, 3). Consistent with Shin *et al*. (2019), the monotonic epoch trend was statistically weak (Kendall's τ significant at only a few sites; 7 data points). Therefore, we described the trajectory by its direction and its attributed drivers rather than by a formal trend test.

Attribution: the two drivers act on different components

Decomposing each catchment's 35-year change into

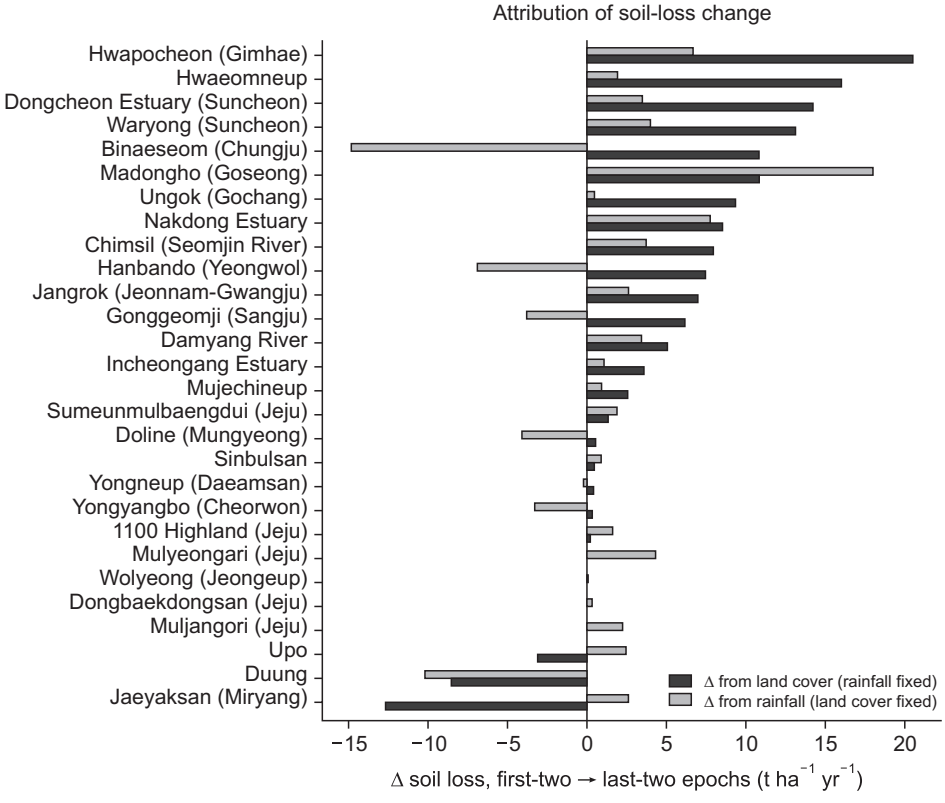

Fig. 6. Endpoint attribution. Change in soil loss (first-two to last-two epoch means) partitioned into land-cover (rainfall fixed) and rainfall (land cover fixed) components, per catchment.

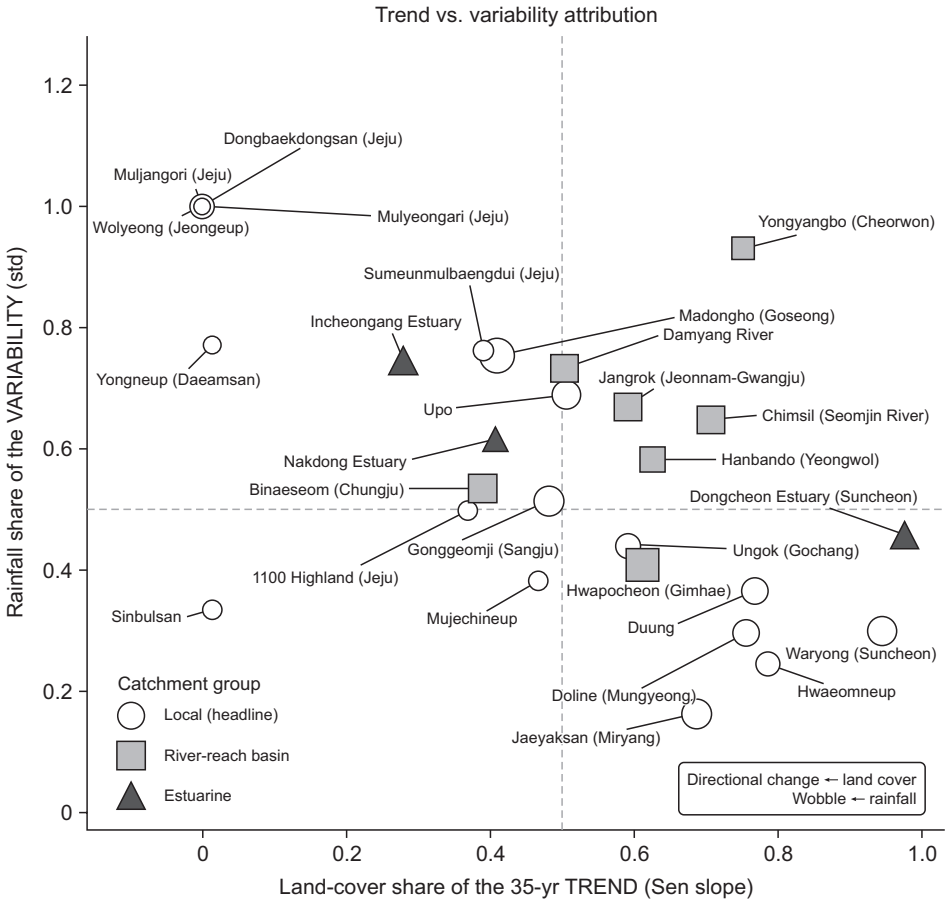

Fig. 7. Trend-versus-variability attribution. Land-cover share of the 35-year trend (x) against rainfall share of the inter-epoch variability (y), per catchment. Markers keyed to group by shape and fill, sized by mean A. A, soil loss.

a land-cover series ($R_0 \cdot S(t)$) and a rainfall series ($R(t) \cdot S_0$) separates two distinct signals (Figs. 6, 7, Table 1).

- Directional trend (land cover): Across the local group, the median land cover share of the (Sen-slope) trend was 0.44, with a 95% bootstrap interval of 0.20-0.67 that straddled an equal split (Section "Catchment sediment-source screening and robustness"). The share was high only where the cover actually moved in either direction: it reached 0.69-0.94 at five catchments (Waryong 0.94, Hwaeomneup 0.79, Duung 0.77, Doline 0.76, and Jaeyaksan 0.69) and was around 0.6 at Ungok and several river-reach basins. These five were not all expanding: Waryong and Hwaeomneup sit below advancing cropland and settlement, while at Duung, Doline, and Jaeyaksan, the cropland reverted; therefore, the share marked how much and not the direction in which the cover moved. These five were also among the smallest catchments in the group (all <2.2 km², 132-2,411 cells of 30 m), where a handful of reclassified cells moved the trend (Section "Limitations and conclusion" iv), and the bootstrap bounds are widest: the 0.69-0.94 range is a property of small, strongly changed catchments, not the group's central tendency. In contrast, the four wetlands whose land-cover map remained unchanged across all seven epochs (the Jeju crater bogs Mulyeongari, Muljangori, Dongbaekdongsan, and mainland Wolyeong) had a land-cover trend share of zero, a clean internal control showing that the decomposition did not produce a signal where none existed.
- Inter-epoch variability (rainfall): The standard-deviation decomposition attributes most of the epoch-to-epoch swing to rainfall (climate variability share>0.5 at half the local catchments, 9 of 18, and→1.0 at the crater wetlands whose only moving factor is R). Erosivity excursions explain this volatility.

The two signals differ in their roles. Land-cover change bent the long-term trajectory wherever it bent at all, upward where cultivation and settlement advanced, and downward where cropland reverted, while rainfall variability governed the swings around that trajectory. Only the role of rainfall was firmly resolved by seven epochs; the per-catchment land-cover shares were directional, but imprecise (Section "Catchment sediment-source screening and robustness"). The interaction residual ($\Delta A - \Delta A_{land} - \Delta A_{clim}$) is small at most sites ($|residual| < 5$ t ha^{-1} yr^{-1}) and is reported per catchment in Table 1.

Over the local catchments the 1986-1990→2016-

Table 4. Land-cover transition matrix over the local wetland catchments, 1986-1990 to 2016-2020 (ha)

From\to	Settlement	Cropland	Forest	Grass	Wetland	Barren	Water
Settlement	202	56	5	8	0	6	1
Cropland	409	7,342	934	551	4	64	56
Forest	104	698	15,663	426	2	42	139
Grass	201	794	427	746	0	18	0
Wetland	0	5	1	0	3	1	0
Barren	10	7	1	4	0	6	2
Water	4	5	5	0	2	4	428

Rows, initial class; columns, final class.

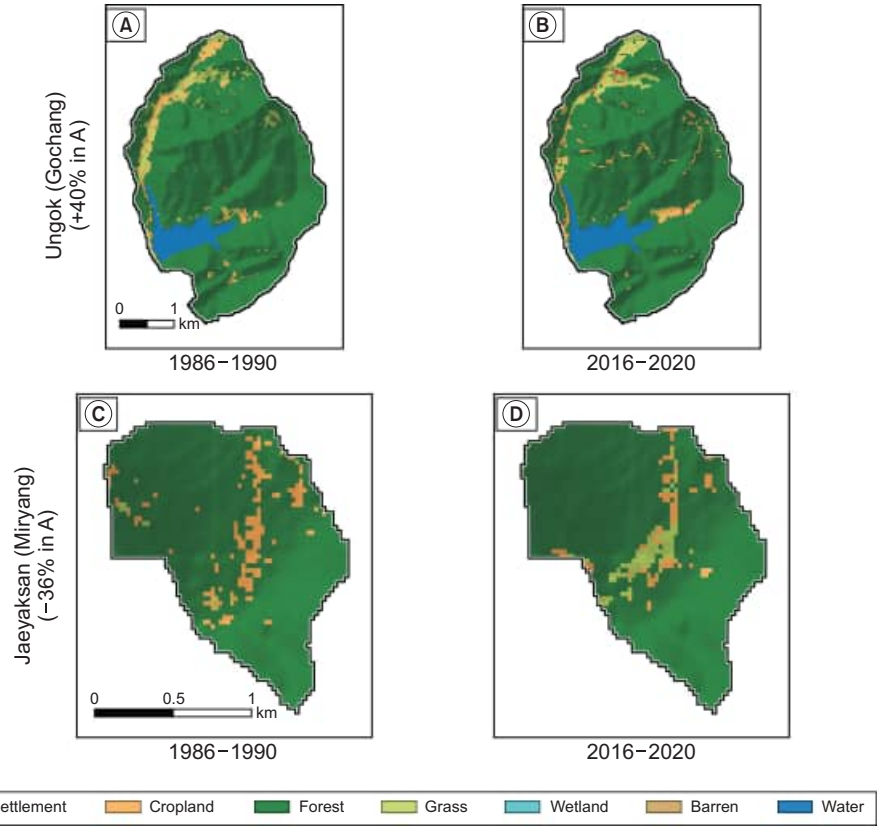

Fig. 8. Catchment land cover in 1986-1990 and 2016-2020. (A, B) Ungok (Gochang), where soil loss rose 40%; (C, D) Jaeyaksan (Miryang), where it fell 36% as cropland reverted to grass. Seven-class scheme as in the cover factor. A, soil loss.

2020 land-cover transition matrix (Table 4) showed the mechanism behind these trends: a large forest⇄cropland exchange (698 ha forest→cropland against 934 ha cropland→forest), plus 409 ha of cropland and 201 ha of grassland converted to settlement. The forest⇄cropland exchange was the erosive one: some hillslopes were cultivated (C rising from 0.007 toward 0.27) while others reverted from cropland to forest (C falling from 0.27 toward 0.007), aligning with the pattern of mixed increases and decreases described in Section "Thirty-five-year trajectories". The cropland/grassland→settlement conversion runs the other way in the model: settlement carries the lowest C of any class (0.001, Section "RUSLE factors"), below both cropland (0.27) and grassland (0.05). Therefore, paving over a hillslope lowers its modeled soil loss even though the land-cover change is visually as conspicuous as cultivation. We did not interpret settlement expansion as an erosive move, and any wetland whose rising trend is attributed to land cover is rising because of cultivation, not urbanization, on its catchment. Fig. 8 shows the erosive movements on the ground in a rising catchment (Ungok, cropland extending along the valley) and a falling catchment (Jaeyaksan, cropland giving way to grass).

Catchment sediment-source screening and robustness

Combining current soil loss, its 35-year direction, and the land-cover share of that direction (a manageable driver) yields a catchment sediment source management priority screening list (per-catchment scores in Supplementary Table 1), a ranking of potential hillslope pressure and its manageability, and not of sediment delivered to or retained within the wetland or of total catchment-scale erosion (Robustness, below). Specifically, each local catchment's screening score was the sum of three z-scored terms, each standardized (mean 0, unit variance) across the 18 local catchments: recent soil loss (A_end), the positive part of its 35-year change (chg_pct, clipped at zero; thus, only rising catchments were rewarded with this term), and the land cover trend share (land_trend_frac, taken as zero where undefined). Each term contributes equally (unweighted sum); a catchment ranks the highest by combining high current loss, rising trend, and land-cover-attributable trend and not by any one term alone. The five highest-screening-priority local wetlands were Hwaeomneup, Madongho (Goseong), Waryong (Suncheon), Ungok (Gochang), and Mujechineup, each carrying a rising, at least partly cover-driven trend; that is, a loss that catchment management could plausibly reduce. Four of the five also carry above-median recent loss (Madongho 79, Waryong 46, Hwaeomneup 34 and Ungok 32 t ha^{-1} yr^{-1} against a local median of 22). Mujechineup is the exception and enters on trajectory alone: its recent loss was 13 t ha^{-1} yr^{-1}, well below the median, but rose 59% over the record. In contrast, the Jeju crater wetlands and high-montane bogs ranked low for intervention; their losses were either small or driven by rainfall, which management cannot alter.

Three caveats cut across the list, all of which are quantified under Robustness below. First, it is built from the catchment-mean RUSLE rate (A, t ha^{-1} yr^{-1}), not from total (gross) soil loss (A×catchment area) or from delivered sediment: ranking the local catchments by gross soil loss instead of by rate reorders the list substantially (Spearman ρ=0.73 against the rate ranking, top-5 overlap 3/5; Supplementary Table 1)—Waryong and Hwaeomneup, both small, steep local catchments, rank 2nd and 5th by rate but fall to 6th and 13th by total tonnage, while larger catchments such as Ungok and Jaeyaksan rank higher by gross output than by rate. We used the rate, consistent with the relative framing of Section "Soil loss, trajectory, and attribution" and because it represents the sediment shed by the wetland's own hillslopes per unit area. However, the two metrics yield genuinely different rankings; managers weighing the total sediment source magnitude should consult Supplementary Table 1 rather than the rate ranking alone. Second, the soil-loss ranking that underlies the list is sensitive to the support-practice assumption, a factor that this land-cover product cannot resolve. At a paddy-like P, the cultivated sites fall relative to the forested bogs (per-catchment soil-loss rank for the 2016-2020 epoch under P=1, 0.5, 0.3, and 0.15 in Supplementary Table 1), although Madongho holds first place under every P tested and, together with Mulyeongari, is the only local catchment to remain in the top five under every P scenario; the screening score itself was not recomputed under each P. Third, the list ranks hillslope pressure, not delivered load: two of the five screening-priority sites (Madongho and Ungok) drain large catchments in which the most eroded ground lies far from the wetland; therefore, managers should read the ranking together with the delivery ratios below, rather than from the ranking alone. Establishing how the list would be reordered under the delivered load requires a coupled routing model that we do not attempt here (Section "Limitations and conclusion" vi).

Robustness

The ranking is stable against the cover and terrain choices but not against the support-practice assumption, and the distinction matters (Table 3, sensitivity_ranking.csv). Varying cropland and forest C by ±20%, and the LS slope-length cap over 50-200 m, changed individual catchment A by up to 28% but left the ranking essentially unchanged (Spearman ρ=0.990-0.997, Kendall's τ=0.952-0.974 against the baseline; top-8 overlap 8/8 in all cases except the 50 m LS cap, 7/8). The fixed-interval EI_{30} correction factor (1.40-1.90) is a per-catchment scalar and leaves both the ranking and the attribution fractions unchanged. Upgrading the rainfall network from 27 to 66 ≥30-year stations (bringing Jeju from long-range extrapolation to within-island interpolation) left the priority ranking, trajectories and attribution essentially identical (rank correlation ρ≥0.99 with the provisional run), which established that the conclusions do not depend on the erosivity-network density.

The support-practice factor is an exception. Setting P to a paddy-like value on the cropland class (Section "Robustness and corroboration") degrades the rank correlation progressively: Spearman ρ=0.95, 0.89 and 0.79 at P=0.5, 0.3 and 0.15, against ρ≥0.99 for every C and LS variant. At P=0.3, A fell 58% at Gonggeomji, 53% at Hwaeomneup, and 46 % at Upo, dropping them from local ranks 3, 2, and 4 to 9, 7, and 6, respectively, while Muljangori, Waryong, and Ungok move up. As P acts only on cropland, the cultivated catchments lost the most, while the four Jeju crater bogs contain no cropland, are unaffected by P, and therefore rise in rank only because the cultivated catchments fall. The sweep over-corrects, since the seven-class scheme lumps upland field and orchard (true P near 1) in with paddy. Thus, the effective ranking most plausibly lies between the P=1 ranking and the P=0.5 one (ρ=0.95, one change in the local top five)—

though not necessarily, since the true effective P depends on the unresolved proportions of paddy, upland field and orchard within each catchment's cropland, which this land-cover product cannot recover, and a catchment that happens to be paddy-dominated could in principle fall outside that range. The direction of the bias is unambiguous, however: P=1 favors the cultivated valley catchments relative to the forested bogs, and these are the catchments from which the priority list was built. Separating paddy fields from upland fields would sharpen the ranking more than any further work on C or LS.

Sediment connectivity checks require care. Re-weighting each cell by a flow-distance delivery ratio SDR=exp(–d/L) and normalizing by Σ(SDR) leaves the local order unchanged (Spearman ρ=0.94, 0.97 and 0.98 for L=500, 1,000 and 2,000 m). However, this statistic is a delivery-weighted mean erosion rate: the normalization divides the magnitude of delivery; therefore, the agreement shows only that near-wetland ground erodes much like the catchment as a whole and says nothing about whether the ranking would survive a sediment-delivery model. Nor are the local catchments uniformly compact: mean cell-level delivery is 0.97-1.00 at the small montane and crater bogs but 0.07-0.47 at the four largest and highest-ranked (Madongho 0.07, Gonggeomji 0.11, Upo 0.17, Ungok 0.47). Therefore, connectivity bears on the headline group, not only on the river reaches and estuarine basins, as reported separately.

Vegetation-index corroboration

A continuously valued vegetation index supports the cover management signal that underlies the soil loss estimates (Supplementary Fig. 4). Growing-season NDVI rose across most catchments over 1986-2020 (median catchment NDVI increasing from ≈0.66 to ≈0.75), consistent with the well-documented greening of South Korea's reforested hillslopes; the estuarine catchments sit near zero because open water dominates their area. More importantly, NDVI was negatively related to soil loss in the direction predicted by the RUSLE attribution. Within the headline local group, recent catchment NDVI was inversely related to mean soil loss (Spearman ρ=–0.57, 95 % bootstrap interval –0.86 to –0.11, n=18), and more strongly over all 28 catchments (ρ=–0.68, –0.87 to –0.38). We lead with the local figure because including open-water-dominated estuarine sites, where RUSLE is not meaningful (Section "Study area and target wetlands"), would inflate the coefficient by adding points that the model is not designed to represent. The 35-year change in NDVI is likewise inversely related to the change in soil loss: catchments whose soil-loss pressure rose greened the least (local: ρ=–0.55, –0.85 to –0.05; all: ρ=–0.48, –0.77 to –0.09). Every coefficient points in the same direction and every interval excludes zero, but the local intervals approach zero: 18 catchments fix the sign, not the strength (Section "Robustness and corroboration"). The direct correlation between the NDVI change and the C-factor change is weak and its interval spans zero (local: ρ=–0.17, 95% bootstrap interval –0.64 to +0.39), as expected: the reclassified seven-class C factor changes only slightly over these largely forested catchments, whereas NDVI integrates canopy density and condition that the discrete classes cannot resolve. This is not an independent validation: NDVI and the land-cover series come from the same Landsat archive and share cloud and shadow masking; therefore, the check is independent of the classifier and the C look-up table, a continuous measure of the canopy state against a discrete one, but not of the underlying imagery. Corroboration from a different sensor or against the measured sediment would be a stronger test, and neither was attempted here.

Attribution uncertainty

The epoch bootstrap shows what seven 5-year epochs can and cannot resolve (Supplementary Fig. 5). These epoch-bootstrap bounds are heuristic and not formal confidence intervals (Section "Robustness and corroboration"). Therefore, we reported them as bootstrap intervals throughout. The soil loss ranking and the direction of change were robust (the ranking to factor and network choices shown above, and to the vegetation index corroboration above; the ordination of Section "Soil loss and catchment typology" is descriptive, not an independent, cross-check), but the per-catchment attribution fractions were estimated with wide intervals. No local catchment had a land-cover trend share whose 95% bootstrap interval lay entirely above 0.5 (0 of 18): even the most strongly land-driven sites have broad bounds (Waryong 0.94, 95% bootstrap interval [0.26, 0.99]; Jaeyaksan 0.69 [0.16, 0.95]). At the group level, the median land-cover trend share across the local catchments was 0.44 (95 % bootstrap interval [0.20, 0.67]), which straddles 0.5, being pulled down by the stable, forested catchments in which there is little trend to attribute. The rainfall control on the inter-epoch variability was the more robustly resolved signal: seven of 18 local catchments have a rainfall variability share whose 95 % bootstrap interval lay entirely above 0.5, and the group median was 0.51 (95% bootstrap interval [0.39, 0.68]). Therefore, we interpreted the conditional statement of Section "Attribution: the two drivers act on different components" as directionally supported but not precisely resolved per catchment, whereas rainfall control on the swings was the more firmly resolved of the two attributions. A longer or annual series is needed to tighten the per-catchment trend attribution; the sediment source screening ranking, which rests on current and rising soil loss rather than on the exact attribution split, is unaffected. The widest intervals belonged to catchments with the

weakest trends in both drivers, where the share was a ratio of two small numbers and is correspondingly unstable (e.g. Sinbulsan, trend strength 0.071 t ha^{-1} yr^{-2}, among the weakest in the local group, share 0.01 [0.01, 0.92]); these sites contributed little to the screening ranking in any case. The per-catchment estimates, intervals, and trend strengths are presented in Supplementary Table 2.

Discussion

Drivers, mechanisms, and management implications

Two drivers resolved unequally

Neither driver beats the other; they act on different components of the signal, and the seven-epoch record resolves these two roles unequally. Rainfall control of inter-epoch swings was the more firmly resolved attribution (Section "Attribution: the two drivers act on different components"). The land cover set the direction of the trajectory where the cover shifted, but no catchment interval lay wholly above an equal split (Section "Catchment sediment-source screening and robustness"); therefore, its role is directional and not quantified. One part that requires no qualification is the internal control: the four wetlands whose cover never shifted return a land-cover trend share of zero; therefore, the decomposition does not manufacture a signal where none exists.

The distinction among these roles has direct management relevance. The rainfall-driven swings are climatic and cannot be managed, whereas directional drift associated with land-cover change, where present, is a signal that catchment-scale interventions can address. This also refines the prairie precedent of Skagen *et al*. (2016): in the monsoonal setting, the climate role arrives as high-variance storm-driven pulses, not as a slow precipitation trend. Therefore, a useful decomposition separates the trend from variability instead of partitioning a single change.

What drove the trends

The transition matrix (Table 4) locates the erosive driver: a two-way forest⇄cropland exchange, not the visually larger cropland/grassland-to-settlement conversion, which lowers modeled C and therefore runs against, not with, the rising trend (Section "Attribution: the two drivers act on different components"). Cultivation advanced on some hillslopes, while it retreated from others, which is why increases and decreases appeared side-by-side (Section "Thirty-five-year trajectories"). The factor maps localized the hotspots to cropland along the valley margins, where steep terrain meets high cover, which links the statistical attribution to specific areas that catchment management can target.

Absolute magnitude and the unit question

Our SI-consistent soil loss estimates were roughly one order of magnitude larger than those of several earlier Korean RUSLE results. This unit difference is not a physical disagreement: erosivity computed as SI EI_{30} (~5,000 MJ mm ha^{-1} h^{-1} yr^{-1}) is approximately 15-fold a customary-unit Toxopeus-type R (~490); therefore, any equation that pairs the latter with SI K, LS, and C understates absolute loss by that factor. Therefore, we treat the value of A as a relative measure and base every inference on rank, trajectory, and attribution, all of which are invariant to the erosivity scale (Section "Catchment sediment-source screening and robustness"). The direct-EI_{30} approach is the methodological contribution. It recovers the storm intensity signal that annual precipitation regressions lose (Lee & Heo, 2011; Panagos *et al*., 2017), and the station-level erosivity reproduces the known Korean pattern of summer monsoon dominance, with no significant long-term trend and extreme years coinciding with landfalling typhoons, as reported by Shin *et al*. (2019).

Management implications

Combining current potential hillslope soil loss pressure, trend direction, and manageable (land-cover) share of that trend yields an actionable sediment source screening list (Section "Catchment sediment-source screening and robustness"). It identifies pressure that catchment management could realistically reduce through cover retention or restoration on the contributing hillslopes, and it serves as a screening tool for prioritizing target areas rather than as a ranking of delivered sediment or ecological impact. Mujechineup, which enters the list on its trajectory alone with its loss still below the group median, is a case to be monitored rather than one requiring urgent attention. In contrast, the Jeju crater wetlands and high-montane bogs rank low for intervention; their loss is either small or rainfall-governed, and management cannot alter rain. Legal protection of the wetland polygon does not protect it from its catchment; several protected sites carry rising, cover-driven potential soil loss pressure originating outside the designated boundary, which argues for extending management attention from the wetland to its sediment shed.

Within a priority catchment, interventions can be targeted rather than applied uniformly. The soil loss maps (Fig. 5) show that loss is concentrated where the steep slope length (high LS) coincides with cultivated or bare cover (high C), typically on cultivated valley margins and steepened lower slopes. Retaining or restoring vegetation on these hotspot slopes, rather than treating the entire catchment uniformly, is where cover management would most efficiently reduce the potential hillslope soil loss pressure; a site-level, hillslope-resolved prioritization (from the same factor maps or field survey) is the natural op-

erational follow-up. The trend/variability split also frames the climate dimension; because the inter-epoch swings are governed by erosivity, which management cannot alter, the land cover trend is the controllable lever. Reducing the cover-driven baseline lowers the level from which rainfall-driven extremes depart, which is an adaptation argument as well as a conservation one. We do not attribute the swings to named typhoons; although individual storms dominate the annual erosivity record, their effects are averaged over 5-year epochs (Section "Thirty-five-year trajectories"). Thus, storm-scale and epoch-scale signals should not be conflated. Resolving the contribution of individual events requires an annual land-cover series.

Limitations and conclusion

Two limitations bear on the priority ranking, and both demote large cultivated catchments relative to compact bogs.

The first is the support-practice factor. P was set to 1.0 throughout because the seven-class cover cannot separate paddies from upland fields, and the sweep in Section "Catchment sediment-source screening and robustness" shows that the ranking is robust to the C and LS choices, but not to this one. The bias runs one-way and inflates the cultivated valley catchments that fill the priority list; therefore, a land-cover product separating paddies from upland fields would sharpen the ranking more than further work on C or LS would.

The second limitation is sediment delivery. RUSLE estimates hillslope soil loss, not what reaches the wetland, and this study does not close that gap. The connectivity weighting of Section "Catchment sediment-source screening and robustness" compares delivery-weighted erosion rates, not delivered loads. A coupled delivery and retention model, as used by Skagen *et al*. (2016), is the next step. More fundamentally, RUSLE represents only sheet-and-rill erosion on hillslopes and does not represent gully erosion, channel- and stream-bank erosion, landslides, or the retention and resuspension of sediment once it is within a wetland, any of which could add to, subtract from, or reroute the sediment source pressure estimated in this study at a given site.

Six further caveats bound the interpretation without touching on the ranking. (i) The seven-class, 5-year-composite cover cannot separate paddy/field/orchard or conifer/broadleaf; we used C values from existing literature and showed the ranking is robust to ±20% perturbation in these lumped classes. (ii) With only seven epochs, formal trend tests have low power, consistent with the weak Kendall's τ. Therefore, we lean on the direction of change and on the firmly resolved role of rainfall in explaining the variability. (iii) LS from raw upslope area overstates the factor in valley cells; we cap slope length at 100 m (RUSLE guidance), and show that the ranking is robust over 50-200 m. (iv) Small mountain-bog catchments turn on a few reclassified cells, which is why the five highest land-cover trend shares (0.69-0.94) belong to small catchments (132-2,411 cells) and carry the widest bounds: the high shares and the instability share a cause. The same small catchments carry a second, geometric source of uncertainty that the land-cover sensitivity does not capture: their D8 boundary from the 30 m DEM is drawn from only ≈130 cells (Section "Study area and target wetlands"); therefore, pit-filling and flat-resolution choices move their outer edge, not just their internal cover mix, by more than for the larger basins. (v) River-reach wetlands draining whole basins are reported separately, with one island bog falling outside the soil-map and land-cover coverage. (vi) Catchments are treated as independent for the correlation and ranking statistics. Although neighbors share climate, parent material, and land-use history, we did not test spatial autocorrelation, and a spatially explicit model would be the appropriate refinement.

These claims are unevenly bound. The order of magnitude separating the cultivated valley catchments from the intact montane and crater bogs survives every C and LS variant, the upgrade from 27 to 66 erosivity stations, and the vegetation index comparison (the ordination, Section "Soil loss and catchment typology," is descriptive rather than an independent check but is consistent with the same separation), and the factor maps locate it physically. What is open is the order within the cultivated group, where the P assumption and delivery gap both bite. The ranking is firm at the scale of the type of catchment and provisional at the scale of the site.

None of these displaced the headline patterns. Across South Korea's inland protected wetlands, potential hillslope soil-loss pressure spans more than one order of magnitude, has risen at most sites from 1986 to 2020, and is divided cleanly by driver: land-cover change has bent the long-term trajectory where it has bent at all, while monsoon erosivity governs the swings around it. Because the trend component is manageable, the results point to a short list of protected wetlands whose catchments warrant priority sediment source screening and management attention, and to the broader principle that protecting a wetland requires managing its catchment, not only its boundary, a principle that holds whatever fraction of the hillslope pressure is ultimately delivered to and retained within the wetland itself.

Author Contributions

Conceptualization: SML. Data curation: JCK. Funding acquisition: JCK. Resources: JCK. Software: SML. Supervision: JCK. Writing – original draft: SML. Writing – review & editing: JCK.

Conflict of Interest

The authors declare that they have no competing interests.

Acknowledgments

We thank the National Institute of Ecology for the EcoBank land-cover time series and national wetland spatial information, the Korea Meteorological Administration for ASOS hourly precipitation records, and the Rural Development Administration for providing a detailed soil map.

Funding

This study was supported by a research program of the National Institute of Ecology (NIE) funded by the Ministry of Climate, Energy, and Environment (MCEE), Republic of Korea (Grant no. NIE-B-2026-01).

References

Borselli, L., Cassi, P., and Torri, D. (2008). Prolegomena to sediment and flow connectivity in the landscape: a GIS and field numerical assessment. *CATENA*, 75, 268-277. https://doi.org/10.1016/j.catena.2008.07.006

Desmet, P.J.J., and Govers, G. (1996). A GIS procedure for automatically calculating the USLE LS factor on topographically complex landscape units. *Journal of Soil and Water Conservation*, 51, 427-433. https://doi.org/10.1080/00224561.1996.12457102

Gorelick, N., Hancher, M., Dixon, M., Ilyushchenko, S., Thau, D., and Moore, R. (2017). Google Earth Engine: planetary-scale geospatial analysis for everyone. *Remote Sensing of Environment*, 202, 18-27. https://doi.org/10.1016/j.rse.2017.06.031

Jung, K.H., Kim, W.T., Hur, S.O., Ha, S.K., Jung, P.K., and Jung, Y.S. (2004). USLE/RUSLE factors for national scale soil loss estimation based on the digital detailed soil map. *Korean Journal of Soil Science and Fertilizer*, 37, 199-206.

Kim, J.C., Choi, J.Y., Lee, S., and Jung, H.S. (2019). A comparative analysis of annual surface soil erosion before and after the river improvement project in the Geumgang basin using the RUSLE. *Korean Journal of Remote Sensing*, 35, 1351-1361. https://doi.org/10.7780/kjrs.2019.35.6.4.5

Kim, J.C., Lee, H.J., Choi, J.Y., Kim, S.K., and Jung, H.S. (2020). Topographical change in coastal areas arising from soil erosion in the Riparian zone. *Journal of Coastal Research*, 102, 101-106. https://doi.org/10.2112/si102-013.1

Kim, J.C., Yoon, J.D., Park, J.S., Choi, J.Y., and Yoon, J.H. (2018). Utilizing the Revised Universal Soil Loss Equation (RUSLE) technique comparative analysis of soil erosion risk in the Geumhogang Riparian area. *Korean Journal of Remote Sensing*, 34, 179-190. https://doi.org/10.7780/kjrs.2018.34.2.1.2

Lee, J.H., and Heo, J.H. (2011). Evaluation of estimation methods for rainfall erosivity based on annual precipitation in Korea. *Journal of Hydrology*, 409, 30-48. https://doi.org/10.1016/j.jhydrol.2011.07.031

Mitsch, W.J., and Gosselink, J.G. (2015). *Wetlands*. 5th ed. Wiley.

Moore, I.D., and Burch, G.J. (1986). Physical basis of the length-slope factor in the Universal Soil Loss Equation. *Soil Science Society of America Journal*, 50, 1294-1298. https://doi.org/10.2136/sssaj1986.03615995005000050042x

National Institute of Ecology. (2023). *Continuous time-series land cover maps for South Korea using Google Earth Engine* [*data set*]. Retrieved Jul 20, 2026 from https://doi.org/10.22756/GEO.20230000000838.

Ozsahin, E., Duru, U., and Eroglu, I. (2018). Land use and land cover changes (LULCC), a key to understand soil erosion intensities in the Maritsa Basin. *Water*, 10, 335. https://doi.org/10.3390/w10030335

Panagos, P., Borrelli, P., Meusburger, K., Yu, B., Klik, A., Lim, K.J., *et al*. (2017). Global rainfall erosivity assessment based on high-temporal resolution rainfall records. *Scientific Reports*, 7, 4175. https://doi.org/10.1038/s41598-017-04282-8

Renard, K.G., Foster, G.R., Weesies, G.A., McCool, D.K., and Yoder, D.C. (1997). *Predicting soil erosion by water: a guide to conservation planning with the Revised Universal Soil Loss Equation* (*RUSLE*). *USDA agriculture handbook 703*. United States Department of Agriculture.

Renard, K.G., and Freimund, J.R. (1994). Using monthly precipitation data to estimate the R-factor in the revised USLE. *Journal of Hydrology*, 157, 287-306. https://doi.org/10.1016/0022-1694(94)90110-4

Roy, D.P., Kovalskyy, V., Zhang, H.K., Vermote, E.F., Yan, L., Kumar, S.S., *et al*. (2016). Characterization of Landsat-7 to Landsat-8 reflective wavelength and normalized difference vegetation index continuity. *Remote Sensing of Environment*, 185, 57-70. https://doi.org/10.1016/j.rse.2015.12.024

Shin, J.Y., Kim, T., Heo, J.H., and Lee, J.H. (2019). Spatial and temporal variations in rainfall erosivity and erosivity density in South Korea. *CATENA*, 176, 125-144. https://doi.org/10.1016/j.catena.2019.01.005

Skagen, S.K., Burris, L.E., and Granfors, D.A. (2016). Sediment accumulation in prairie wetlands under a changing climate: the relative roles of landscape and precipitation. *Wetlands*, 36 (Suppl 2), 383-395. https://doi.org/10.1007/s13157-016-0748-5

Tucker, C.J. (1979). Red and photographic infrared linear combinations for monitoring vegetation. *Remote Sensing of Environment*, 8, 127-150. https://doi.org/10.1016/0034-4257(79)90013-0

Wischmeier, W.H. (1976). Use and misuse of the Universal Soil Loss Equation. *Journal of Soil and Water Conservation*, 31, 5-9.

Wischmeier, W.H., and Smith, D.D. (1978). *Predicting rainfall erosion losses-a guide to conservation planning. USDA agriculture handbook 537*. United States Department of Agriculture.

Yin, S., Xie, Y., Nearing, M.A., and Wang, C. (2007). Estimation of rainfall erosivity using 5- to 60-minute fixed-interval rainfall data from China. *CATENA*, 70, 306-312. https://doi.org/10.1016/j.catena.2006.10.011

Zarrinabadi, E., Lobb, D.A., Enanga, E., Badiou, P., and Creed, I.F. (2023). Agricultural activities lead to sediment infilling of wetlandscapes in the Canadian Prairies: assessment of soil erosion and sedimentation fluxes. *Geoderma*, 436, 116525. https://doi.org/10.1016/j.geoderma.2023.116525

PNIE PROCEEDINGS OF THE NATIONAL INSTITUTE OF ECOLOGY OF THE REPUBLIC OF KOREA

Original Article

PNIE 2026;7(4):173-180
https://doi.org/10.22920/PNIE.2026.7.4.173
pISSN 2765-2203, eISSN 2765-2211

Habitat Use of Sympatric *Onychodactylus sillanus* and *Hynobius* spp. Larvae in a Mountain Stream on the Southeastern Korean Peninsula

June Kim[1†], Min-Woo Park[2†], Jia Lee[3], Daesik Park[1,4*]

[1]Interdisciplinary Program in Earth Environmental System Science & Engineering, Kangwon National University, Chuncheon, Korea
[2]Research Center, Busan Metropolitan City Institute for Gifted Education & Promotion, Busan, Korea
[3]Interdisciplinary Program in Landscape Architecture, Seoul National University, Seoul, Korea
[4]Division of Science Education, Kangwon National University, Chuncheon, Korea

ABSTRACT

Amphibian larvae are suitable models for studying fine-scale niche differentiation. In the Republic of Korea, *Onychodactylus sillanus* and *Hynobius* spp. larvae often coexist in mountain streams of the southeastern Korean Peninsula. However, whether they show seasonal changes in spatial occupancy or use similar microhabitats during larval co-occurrence remains unclear. This study aimed to examine the microhabitat use of these species in mountain streams to determine whether they show spatial or temporal variations in habitat use. Monthly field surveys were performed at 17 sites between March and November 2024. *O. sillanus* and *Hynobius* spp. larvae used 55.7% (64 of 115) and 22.6% (26 of 115) of the available surveyed sites, respectively. Only *O. sillanus* larvae were found at the uppermost sites, whereas *Hynobius* larvae were more abundant at the downstream sites. Co-occurrence was noted at 17.4% (15 of 86) of the surveyed sites between March and September. Among the five measured microhabitat variables (altitude, water temperature, dissolved oxygen, pH, and stream width), only altitude varied between the sites occupied by the two groups. Thus, *O. sillanus* and *Hynobius* spp. larvae demonstrate differential habitat use and spatially and temporally limited co-occurrence in mountain valley streams. Comparative studies of sites with and without co-occurrence are required to further understand whether co-occurrence results in interspecific interactions.

Keywords: Co-occurrence, Hynobiidae, Microhabitat, Occupancy, Spatial partitioning

Introduction

Ecological niche theory explains how species or animal groups utilize resources, space, and time (Chesson, 2000). If ecologically similar species coexist, their niches may overlap, thereby increasing interspecific competition (HilleRisLambers *et al*., 2012). Sympatric species often show differences in microhabitat requirements, temporal activity, spatial occupancy, and resource utilization (Cimmaruta *et al*., 1999; Lunghi *et al*., 2022; Rosa *et al*., 2023; Waldron *et al*., 2024). Examining how the distribution of

Received July 20, 2026; **Revised** October 1, 2026;
Accepted October 6, 2026

***Corresponding author:** Daesik Park
e-mail parkda@kangwon.ac.kr
https://orcid.org/0000-0001-9209-0493

†These authors contributed equally to this work.

This is an Open Access article distributed under the terms of the Creative Commons Attribution Non-Commercial License (http://creativecommons.org/licenses/by-nc/4.0), which permits unrestricted non-commercial use, distribution, and reproduction in any medium, provided the original work is properly cited.

Copyright © National Institute of Ecology.

sympatric species in an area is partitioned at various environmental and spatial scales is necessary to understand the mechanisms of coexistence in an ecological system. Amphibian larvae are suitable models for studying fine-scale niche differentiation as aquatic environmental factors affect their distribution (Barr & Babbitt, 2002; Yeiser & Richter, 2015). In mountain streams, larval occurrence differs across short distances, depending on water temperature, stream width, dissolved oxygen (DO), pH, flow rate, altitude, and seasonal hydrology (Camp & Fortner, 2025). Fine-scale spatial and environmental differences may be particularly significant in narrow mountain streams where suitable aquatic habitats are limited, and seasonal alterations in water flow can rapidly change habitat availability (Zylstra *et al*., 2015).

The family Hynobiidae includes two *Onychodactylus* and seven *Hynobius* species that occur in the Republic of Korea (Borzée & Min, 2021; Borzée *et al*., 2022; Borzée, 2024). Three species, *Onychodactylus sillanus*, *Hynobius leechii*, and *Hynobius yangi*, have been previously reported (Baek *et al*., 2011; Kim *et al*., 2026). *O. sillanus* has degenerated lungs and, therefore, prefers mountain stream habitats with high DO concentrations (Borzée *et al*., 2022; Borzée, 2024). In contrast, *H. leechii* and *H. yangi* widely occur in the lowlands and mountain valleys (Borzée & Min, 2021; Um *et al*., 2025). *O. sillanus* has a larval stage of 2-3 years (Iwasawa & Kera, 1980; Lee *et al*., 2008), whereas *H. leechii* and *H. yangi* have relatively short larval stages, lasting approximately 3 months (Yoon *et al*., 1996). Although these species often coexist in mountain streams, whether they exhibit seasonal alterations in their spatial occupancy or use similar microhabitats during larval co-occurrence remains elusive.

Herein, we examined whether sympatric *O. sillanus* and *Hynobius* spp. larvae exhibited differential mountain stream habitat use by combining microhabitat and spatial occupancy analyses. Our findings contribute to the establishment and implementation of conservation plans for these threatened species.

Materials and Methods

Population survey

Surveys were performed along a mountain stream near Geumjeongsan, Yangsan-si, Gyeongsangnam-do, Republic of Korea (35.3119° N, 129.0608° E; Fig. 1) from March to November 2024. Seventeen survey sites were established at approximately 50 m intervals and designated S1-S17, starting at the site furthest upstream (Fig. 1). The straight-line distance between the study sites was 620 m, and altitude ranged from 99 to 231 m above sea level (Fig. 1B).

Onychodactylus sillanus larvae are easily distinguishable from the larvae of the other two species based on their morphology. However, *H. leechii* and *H. yangi* larvae are morphologically similar, warranting genetic identification (Koo *et al*., 2023; Lee & Park, 2016). Genetic analysis of all observed *Hynobius* larvae was not feasible, particularly considering that *H. yangi* is an endangered species in the Republic of Korea. Therefore, in this study, we categorized *H. leechii* and *H. yangi* larvae as *Hynobius* spp. larvae.

The number of larvae in each site was recorded for each survey. Two investigators conducted a 20-minute visual encounter survey at each site, carefully turning over rocks within a 50 m stream section. During the autumn surveys, the accumulated leaf litter was also slowly moved aside to enhance larval detection.

All data, including the number of larvae observed and the number of sites occupied by each group, were summarized by site and month. We constructed heat maps across the two species groups, nine survey months, and 17 survey sites to visualize the temporal and spatial distribution patterns of *O. sillanus* and *Hynobius* spp. larvae. Furthermore, we combined the numbers of larvae from the 17 sites to explore monthly changes in the overall

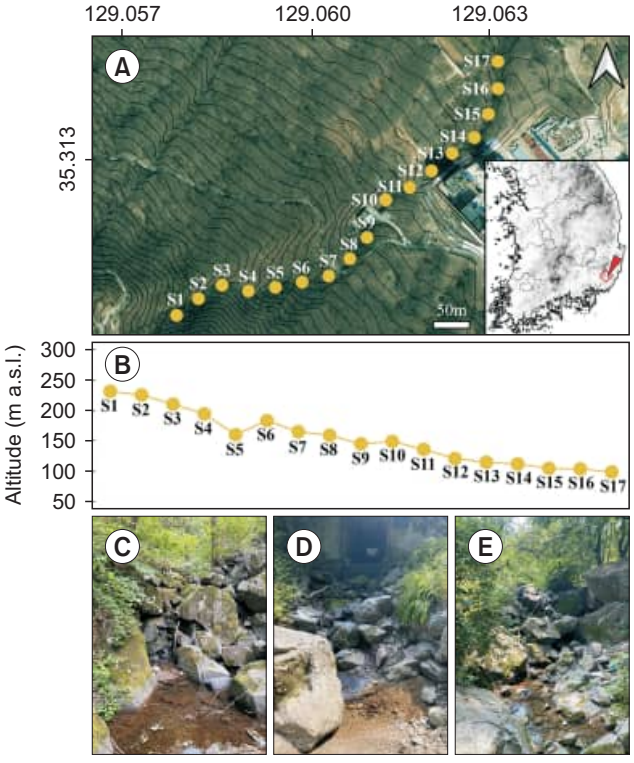

Fig. 1. The study stream near Mt. Geumjeong, Yangsan-si, Gyeongsangnam-do, Republic of Korea and the 17 survey sites (A) at approximately 50 m intervals along the stream, numbered from the uppermost to the lowermost site (B). (C-E) Several representative sites: (C) upstream (S1, 231 m a.s.l.), (D) midstream (S10, 149 m a.s.l.), and (E) downstream (S14, 112 m a.s.l.). a.s.l., above sea level.

number of observed larvae.

In this study, *Hynobius* larvae were detected between March and September, which was therefore defined as the period of larval co-occurrence. We calculated the monthly co-occurrence rate as the number of sites with co-occurrence divided by the total number of available sites per month to determine the spatial overlap between the sites occupied by the two larval groups during this period. Available sites were defined as those where water quality measurements were recorded or where at least one larval group was detected. Additionally, we calculated the Jaccard index (*J*) to evaluate the occupancy similarity:

$$J = \frac{a}{a + b + c}$$

where a is the number of sites occupied by *O. sillanus* and *Hynobius* spp., b is the number of sites occupied only by *O. sillanus*, and c is the number of sites occupied only by *Hynobius* spp. (Koleff *et al*., 2003). The analysis excluded sites where neither group was detected.

Special permits were not required because we did not capture any animals during the study. All procedures were performed in accordance with the guidelines of the Society for the Study of Amphibians and Reptiles (SSAR) and the American Society of Ichthyologists and Herpetologists (ASIH) for the use of live amphibians in the field (ASIH, 2004).

Microhabitat use

During the field surveys, we measured five microhabitat variables at each site: water temperature, stream width, DO, pH, and altitude. The water quality was measured using a YSI ProQuatro meter (YSI Inc., Yellow Springs, OH, USA). Water quality measurements were not performed if the water level was extremely low (i.e., if the site was nearly or completely dry). Nevertheless, we counted all larvae observed at these sites, if present.

We compared five microhabitat variables (water temperature, stream width, DO, pH, and altitude) for the sites occupied by *O. sillanus* and *Hynobius* spp. larvae using the Mann–Whitney U-test after the Shapiro–Wilk normality test to determine whether microhabitat use differed between the two species groups. Subsequently, we performed a principal component analysis (PCA) after Z-score standardization (Jolliffe & Cadima, 2016) to explore which microhabitat variables best explained the overall microhabitat variation between the sites occupied by each species during the co-occurrence period.

All analyses were conducted using R version 4.4.2 (R Foundation for Statistical Computing, Vienna, Austria). All data are presented as mean±1 standard deviation unless otherwise mentioned.

Results

Population survey

Onychodactylus sillanus larvae were observed in the upper (S1-S5) and middle-lower reaches (S7-S15; Fig. 2C). We found *O. sillanus* larvae at 14 of the 17 sites, with a monthly average of 7.1±2.7 sites (range: 1-10 sites; Fig. 2C). July was the month with the most sites occupied by *O. sillanus* larvae (ten sites). *Hynobius* spp. larvae were observed between S5 and S17 (Fig. 2B, C) at 11 of the 17 sites, with a monthly average of 2.9±3.3 sites (range: 0-8 sites; Fig. 2A). May and June were the months with the most sites occupied by *Hynobius* spp. larvae (eight sites each). No larvae were observed at S6 or S16, and *Hynobius* spp. larvae were not found at S1-S4 (Fig. 2B, C).

A total of 484 *O. sillanus* larvae were recorded between March and November, with the highest monthly abundance observed in May (n=100; Fig. 2A). The monthly abundance of *O. sillanus* revealed a roughly unimodal pattern, increasing from May to July and gradually declining from August onward (Fig. 2A). A total of 95 *Hynobius* spp. larvae were observed from March to September. Furthermore, they revealed a unimodal monthly abundance pattern, with relatively high abundances in May (n=37) and June (n=35), followed by a steep decline from July onward (Fig. 2B). *Hynobius* spp. larvae were not detected in October (Fig. 2A, B).

Between March and September, *O. sillanus* and *Hynobius* spp. larvae co-occurred from S5-S13 at a monthly average of 2.14±1.57 sites (range: 0-4 sites; Fig. 2). The four site surveys with the highest co-occurrence values were performed in May and June (Fig. 2B). The average co-occurrence rate among the available sites was 17.9±13.7% (range: 0-36.4%). The highest monthly co-occurrence rate was observed in June.

The average monthly Jaccard index for the sites occupied by the two groups was 0.21±0.14 (range: 0.00-0.38). The largest overlap was observed in April (J=0.375). No overlap was observed for March (J=0.000). The Jaccard index decreased from July to August to September (0.200, 0.125, and 0.111, respectively), with the reduction in the abundance of *Hynobius* spp. larvae.

Microhabitat use

Considering the five microhabitat variables at the sites occupied by the two groups, *O. sillanus* larvae (mean: 162.5 m±39.7 m) used significantly higher altitude sites than *Hynobius* spp. larvae (mean: 130.9 m±18.4 m; W=625.5, n=62, P<0.01). The remaining four variables (water temperature, stream width, pH, and DO) did not differ between the two groups (all P>0.05), although their values varied across sites and seasons (Fig. 3).

In the PCA, the first three PCs had eigenvalues >1, which together explained 76.6% of the total microhabi-

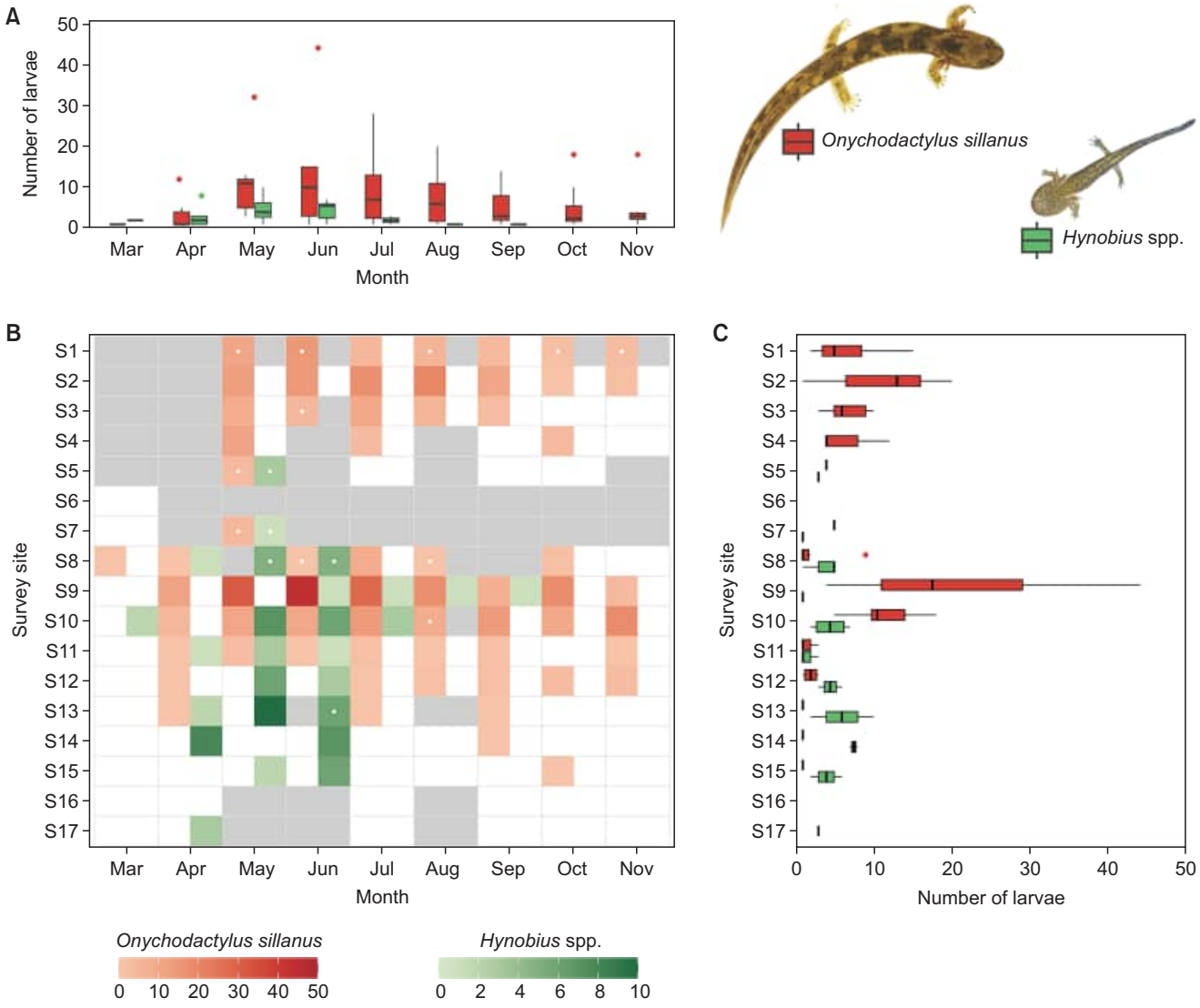

Fig. 2. The number of *Onychodactylus sillanus* (red brown) and *Hynobius* spp. (green) larvae recorded across the different months (March-November, A) and the 17 survey sites (S1-S17, C). In the box plots, the horizontal line indicates the median, the box represents the interquartile range, the whiskers represent the range of the data, and the dots show outliers. The heatmap (B) illustrates the spatial (survey site) and temporal (month) patterns of the number of larvae found. Color gradients indicate different larvae numbers. Inserted photographs in the (A) panel indicate *Onychodactylus sillanus* and *Hynobius* spp. larvae.

tat variation (Table 1). PC1 explained 33.9% of the total variation and was mainly linked to water temperature, pH, and DO; PC2 explained 22.1% and was related to the stream width (Fig. 4A); and PC3 explained 20.6% and was linked to the altitude (Fig. 4B). No clear separation in the microhabitat use of *O. sillanus* and *Hynobius* spp. larvae was observed (Fig. 4).

Discussion

This study investigated patch-level occupancy, seasonal occurrence, and microhabitat use of sympatric *O. sillanus* and *Hynobius* spp. larvae in a mountain stream in the Republic of Korea. During the co-occurrence period (March to September), 17.4% of the sites were shared. Only *O. sillanus* larvae were found in the uppermost sites, whereas more *Hynobius* larvae were observed in the lower reaches of the stream. Our findings revealed a certain degree of spatial habitat partitioning between the two species.

Onychodactylus sillanus larvae are more common than *Hynobius* spp. larvae in mountain valley streams of the southeastern Korean Peninsula. *O. sillanus* and *Hynobius*

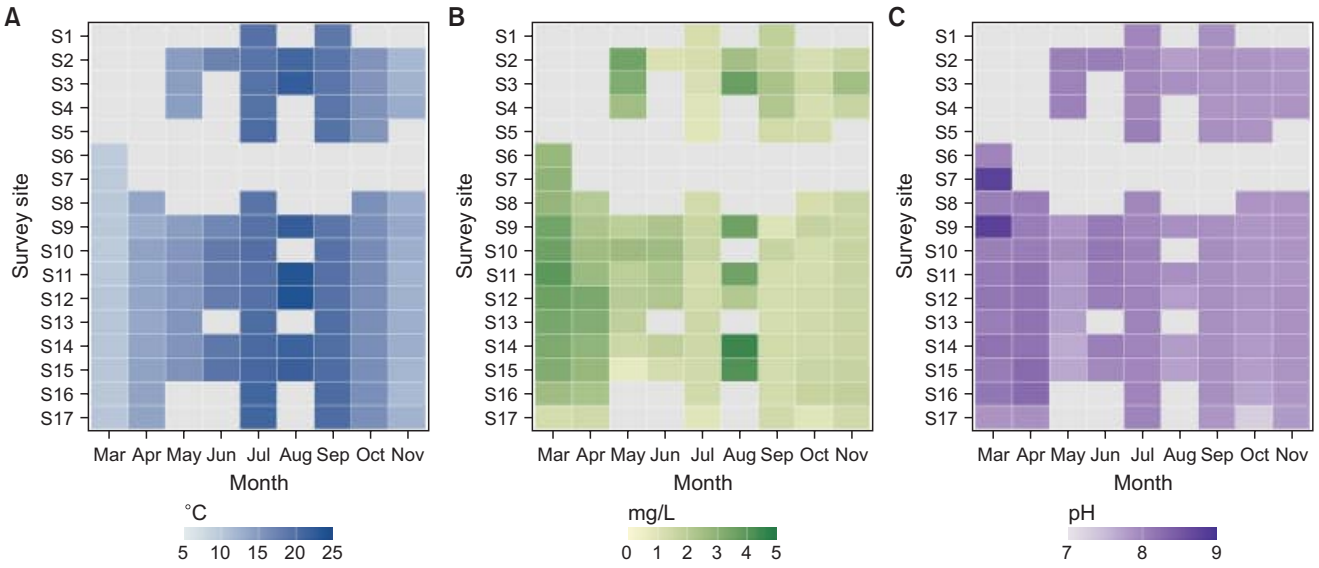

Fig. 3. Changes in microhabitat variables across the temporal (monthly survey; March-November) and spatial (survey sites; S1-S17) scales. (A) Water temperature, (B) dissolved oxygen, and (C) pH. Grey cells indicate sites where variables were not measured owing to drying out. S1 was upstream and S17 downstream.

Table 1. Results of PCA of microhabitat variables

Variable	PC1	PC2	PC3
Loadings			
Water temperature (°C)	−0.615	−0.244	0.154
Stream width (cm)	0.186	0.867	−0.016
Dissolved oxygen (mg/L)	0.490	−0.312	0.348
pH	0.578	−0.237	0.056
Altitude (m)	−0.114	0.188	0.923
Variance explained			
Eigenvalue	1.695	1.104	1.032
Proportion of variance (%)	33.9	22.1	20.6
Cumulative variance (%)	33.9	56.0	76.6

Loadings of five microhabitat variables on the first three principal components, with eigenvalues, proportion of variance (%), and cumulative variance (%). Data were collected during the co-occurrence period (March-September).
PCA, principal component analysis.

spp. larvae use 55.7% and 22.6% of the available sites, respectively. Notably, *O. sillanus* occurred exclusively at the high-altitude sites S1-S4, and no *Hynobius* spp. larvae were observed. The limited distribution of *Hynobius* spp. larvae in this area may be the result of local avoidance. The headwaters in the upper reaches of the steep mountain valley streams of the southern Korean Peninsula are recharged year-round (Son *et al*., 2002). However, the recharge of groundwater substantially reduces during the dry period (Kim *et al*., 2008), causing the middle reaches to dry out. In contrast, the lower reaches do not generally dry out owing to baseflow contributions (Choi *et al*., 2023). Headwaters are often situated underground with very little visible water and relatively low temperatures. Unlike *O. sillanus*, *Hynobius* spp. have a short larval period of two to three months (Yoon *et al*., 1996). They may avoid cooler upper reaches and prefer the mid-lower reaches where water is continuously available and the water temperature is higher (Andersen *et al*., 2022) to accelerate their development at high water temperatures (Kukita *et al*., 2015; Moriya, 1983). In contrast, *O. sillanus* larvae may use the uppermost reaches and parts of the middle reaches, where water is available, the temperature is low, and upflow of the cool spring water occurs (Borzée, 2024). Additionally, *O. sillanus* larvae prefer low-temperature areas with high DO values because of the small size of their external gills relative to their body length (Ghosh *et al*., 2025; Yoshikawa & Matsui, 2022). Furthermore, unlike *Hynobius* spp. larvae, *Onychodactylus* species larvae have claws that allow secure attachment to substrates such as bedrock in fast-flowing environments (Borzée, 2024; Poyarkov *et al*., 2012). This may have enabled a stable habitation in the upstream reaches, potentially contributing to the broader spatial distribution observed in this study.

Temporal and spatial variation in the number of larvae noted in the valley stream could provide information on the potential breeding sites of *O. sillanus* and *Hynobius* spp. Considering their emergence patterns, *O. sillanus* may breed underground near the uppermost reaches of the stream and site S9. Given this distribution, the larvae at

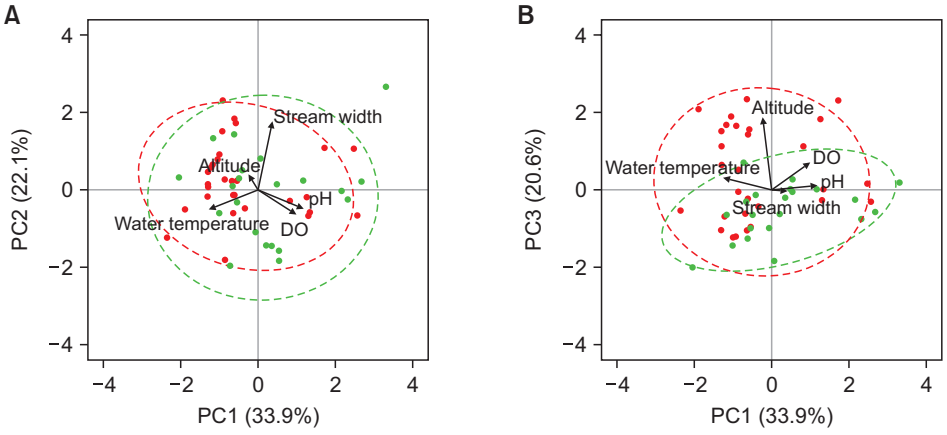

Fig. 4. Principal component analysis of the five microhabitat variables (water temperature, stream width, dissolved oxygen [DO], pH, and altitude) measured at sites occupied by *Onychodactylus sillanus* (red) and *Hynobius* spp. (green) larvae during the co-occurrence period (March-September). The dashed circles indicate the 95% confidence ellipse for each species group. Arrows represent the loadings of each variable on the PCs. (A) PC1 vs. PC2, (B) PC1 vs. PC3.

sites S1-S5 likely originated from higher-altitude breeding sites, whereas the larvae at sites S9-S15 likely originated near site S9. These separate breeding sites may reflect the steep valley stream structure and supply patterns of groundwater and stream water along the upper, middle, and lower reaches of the stream (Kim *et al*., 2008; Son *et al*., 2002). Unlike *O. sillanus*, *Hynobius* spp. might have mainly bred between sites S8 and S15, where water was continuously supplied during the larval period. Within the stream, the longitudinal movements of *Hynobius* spp. larvae are likely limited, especially toward the upper reaches (Borzée, 2024). Some larvae were found in the lower reaches; however, areas such as S16 and S17, which are frequently dry, may not have been utilized as breeding sites. Despite the temporally unimodal emergence of *O. sillanus* larvae, they could not be used to determine the breeding period in this stream. Larval emergence into streams from underground spawning sites can vary substantially depending on the yolk absorption period, microhabitat characteristics, and the effects of passive stream flow on hatchlings (Akita & Miyazaki, 1991; Lee *et al*., 2008; Park *et al*., 2026; Solkin, 1993). Breeding sites, larval movement, and groundwater flow were not directly evaluated in this study. Therefore, these proposed explanations need further investigation.

The two groups exhibited limited spatial and temporal co-occurrence, suggesting differential habitat partitioning within the mountain valley streams. Major habitat sharing occurred for only three months from April to June, despite co-occurrence in the stream between March and September. Along the stream, co-occurrence was limited to seven sites, S5, S7-S11, and S13, where stream water was continuously supplied throughout the year. Additionally, the co-occurrence rate was as low as 17.4% and the Jaccard occupancy similarity value was 0.21. Despite the low co-occurrence rate, the two groups tended to use similar microhabitat resources in terms of water temperature, DO, and pH. This suggests the potential for interspecific interactions. For example, competition can delay larval development and growth and occasionally induce adaptive traits via developmental plasticity in amphibians (Hloušková *et al*., 2018; Relyea, 2002). To better understand whether such co-occurrence leads to interspecific competition and its potential effects, comparative studies on growth rates, body conditions, and affected physical or morphological traits at sites with and without co-occurrence are warranted. Our findings suggest differential habitat use and a spatially and temporally limited co-occurrence of *O. sillanus* and *Hynobius* spp. larvae in mountain valley streams.

Our study revealed the temporal and spatial habitat use of *O. sillanus* and *Hynobius* spp. larvae in a mountain valley stream on the southeastern Korean Peninsula. *Hynobius yangi* has been designated an endangered species by the Korean Ministry of Climate, Energy, and Environment (Ministry of Environment, 2017). The distribution range of *O. sillanus* is limited to a small pocket surrounded by the Nakdong and Hyeongsan Rivers (Kim *et al*., 2026). Recent climate change modeling has revealed that climate change can significantly reduce the distribution of both species (Borzée *et al*., 2022; Lee *et al*., 2026). Our results contribute to the establishment and implementation of conservation plans for these threatened species.

Author Contributions

Conceptualization: JK, MWP. Data curation: JK. Formal analysis: JK, MWP. Funding acquisition: DP. Investigation:

JK, JL. Methodology: JK, JL. Project administration: JK, JL. Resources: JK, JL. Software: JK, MWP. Supervision: DP. Validation: JK, MWP. Visualization: JK, MWP. Writing – original draft: JK, MWP, DP. Writing – review & editing: JK, MWP, DP.

Conflict of Interest

The authors declare that they have no competing interests.

Acknowledgments

We thank the Laboratory of Herpetology, Kangwon National University, for their assistance with this study.

Funding

This research was supported by the Basic Science Research Program of the National Research Foundation of Korea (NRF), funded by the Ministry of Education (RS-2024-00346579; RS-2025-25415913).

References

Akita, Y., and Miyazaki, K. (1991). Migration and breeding cycle of *Onychodactylus japonicus* on Mt. Hodatsu. *Japanese Journal of Herpetology,* 14, 29-38. https://doi.org/10.5358/hsj1972.14.2_29

American Society of Ichthyologists and Herpetologists (ASIH). (2004). *Herpetological Animal Care and Use Committee (HACC). Guidelines for Use of Live Amphibians and Reptiles in Field and Laboratory Research*. 2nd ed. ASIH.

Andersen, D., Chuang, M.F., Choe, M., Kim, A., Kwon, S., Jang, Y., *et al*. (2022). Elevational distribution of amphibians: resolving distributions, patterns, and species communities in the Republic of Korea. *Zoological Studies,* 61, e25. https://doi.org/10.6620/ZS.2022.61-25

Baek, H.J., Lee, M.Y., Lee, H., and Min, M.S. (2011). Mitochondrial DNA data unveil highly divergent populations within the genus *Hynobius* (Caudata: Hynobiidae) in South Korea. *Molecules and Cells,* 31, 105-112. https://doi.org/10.1007/s10059-011-0014-x

Barr, G.E., and Babbitt, K.J. (2002). Effects of biotic and abiotic factors on the distribution and abundance of larval two-lined salamanders (*Eurycea bislineata*) across spatial scales. *Oecologia,* 133, 176-185. https://doi.org/10.1007/s00442-002-1029-y

Borzée, A. (2024). *Continental Northeast Asian Amphibians: Origins, Behavioural Ecology, and Conservation*. Elsevier Science & Technology.

Borzée, A., and Min, M.S. (2021). Disentangling the impacts of speciation, sympatry and the island effect on the morphology of seven *Hynobius* sp. salamanders. *Animals,* 11, 187. https://doi.org/10.3390/ani11010187

Borzée, A., Shin, Y., Poyarkov, N.A., Jeon, J.Y., Baek, H.J., Lee, C.H., *et al*. (2022). Dwindling in the mountains: description of a critically endangered and microendemic *Onychodactylus* species (Amphibia, Hynobiidae) from the Korean Peninsula. *Zoological Research,* 43, 750-755. https://doi.org/10.24272/j.issn.2095-8137.2022.048

Camp, C.D., and Fortner, E.M. (2025). Differences in larval microhabitat between two cryptic, sympatric salamander species (*Desmognathus folkertsi* and *D. amphileucus*) in northeastern Georgia, USA. *Animals,* 15, 1479. https://doi.org/10.3390/ani15101479

Chesson, P. (2000). Mechanisms of maintenance of species diversity. *Annual Review of Ecology and Systematics,* 31, 343-366. https://doi.org/10.1146/annurev.ecolsys.31.1.343

Choi, H., Lee, C., Jo, H.J., and Shim, B.O. (2023). Assessment of groundwater recharge and connectivity with surface water in a mountainous watershed using natural tracers in Daejeon, Korea. *Environmental Earth Sciences,* 82, 530. https://doi.org/10.1007/s12665-023-11209-2

Cimmaruta, R., Forti, G., Nascetti, G., and Bullini, L. (1999). Spatial distribution and competition in two parapatric sibling species of European plethodontid salamanders. *Ethology Ecology & Evolution,* 11, 383-398. https://doi.org/10.1080/08927014.1999.9522821

Ghosh, D., Fan, L., and Borzée, A. (2025). First report on water quality parameters for larvae of two species of clawed salamanders (*Onychodactylus zhaoermii and Onychodactylus zhangyapingi*). *Russian Journal of Herpetology,* 32, 33-39. https://doi.org/10.30906/1026-2296-2025-32-1-33-39

HilleRisLambers, J., Adler, P.B., Harpole, W.S., Levine, J.M., and Mayfield, M.M. (2012). Rethinking community assembly through the lens of coexistence theory. *Annual Review of Ecology, Evolution, and Systematics,* 43, 227-248. https://doi.org/10.1146/annurev-ecolsys-110411-160411

Hloušková, M., Balogová, M., Kršáková, V., and Gvoždík, L. (2018). No trade-offs in interspecific interference ability and predation susceptibility in newt larvae. *Ecology and Evolution,* 8, 9095-9104. https://doi.org/10.1002/ece3.4465

Iwasawa, H., and Kera, Y. (1980). Normal stages of development of the Japanese lungless salamander, *Onychodactylus japonicus* (Houttuyn). *Japanese Journal of Herpetology,* 8, 73-89. https://doi.org/10.5358/hsj1972.8.3_73

Jolliffe, I.T., and Cadima, J. (2016). Principal component analysis: a review and recent developments. *Philosophical Transactions of the Royal Society A, Mathematical, Physical and Engineering Sciences,* 374, 20150202. https://doi.org/10.1098/rsta.2015.0202

Kim, T.W., Jung, J.Y., Ham, S.E., Lee, J.H., Son, G.T., Ryu, S.M., *et al*. (2008). Time series and groundwater recharge analyses using water fluctuation data in Mountain Geumjeong area. *Journal of the Korean Environmental Sciences Society,* 17, 257-267. https://doi.org/10.5322/JES.2008.17.2.257

Kim, Y., Nam, H., Park, J., Park, J., and Park, D. (2026). Distribution and potential dispersal corridors of two *Onychodactylus* species in the Republic of Korea. *Diversity,* 18, 57. https://doi.org/10.3390/d18010057

Koleff, P., Gaston, K.J., and Lennon, J.J. (2003). Measuring beta diversity for presence–absence data. *Journal of Animal Ecology,* 72, 367-382. https://doi.org/10.1046/j.1365-2656.2003.00710.x

Koo, K., Kim, E., Kim, H., Im, J., and Kim, Y. (2023). Problem in morphological identifications of the five newly described

Korean *Hynobius* salamander species in South Korea. *Korean Journal of Herpetology,* 13, 9-17.

Kukita, S., Gouda, M., Ikeda, S., Ishibashi, S., Furuya, T., and Nakamura, K. (2015). Effects of photoperiod and temperature on growth and development in clouded salamander (*Hynobius nebulosus*) larvae. *Zoological Science,* 32, 266-271. https://doi.org/10.2108/zs140220

Lee, J., Ra, N., Eom, J., and Park, D. (2008). Population dynamics of the long-tailed clawed salamander larva, *Onychodactylus fischeri*, and its age structure in Korea. *Journal of Ecology and Field Biology,* 31, 31-36. https://doi.org/10.5141/jefb.2008.31.1.031

Lee, J.H., Chang, M.H., Shin, M.S., Lee, E.S., Lee, J.S., and Seo, C.W. (2026). Ensemble species distribution modeling of climate change impacts on endangered amphibians and reptiles in South Korea. *Animals,* 16, 95. https://doi.org/10.3390/ani16010095

Lee, J.H., and Park, D. (2016). *The Encyclopedia of Korean Amphibians*. Nature and Ecology.

Lunghi, E., Corti, C., Biaggini, M., Zhao, Y., and Cianferoni, F. (2022). The trophic niche of two sympatric species of salamanders (Plethodontidae and Salamandridae) from Italy. *Animals,* 12, 2221. https://doi.org/10.3390/ani12172221

Ministry of Environment. (2017). *Enforcement rule of the wildlife protection and management act, appendix 1* (*Ministry of Environment Ordinance No. 737*). Retrieved Oct 18, 2026 from https://www.law.go.kr.

Moriya, T. (1983). The effect of temperature on the action of thyroid hormone and prolactin in larvae of the salamander *Hynobius* retardatus. *General and Comparative Endocrinology,* 49, 1-7. https://doi.org/10.1016/0016-6480(83)90001-1

Park, M.W., Park, J., Kim, J., Park, J., Joo, N., Nam, H., *et al*. (2026). Integrated environmental DNA analysis and population assessment revealed a biannual breeding season of the Korean clawed salamander (*Onychodactylus koreanus*). *PLoS One,* 21, e0342469. https://doi.org/10.1371/journal.pone.0342469

Poyarkov, N.A., Jr., Che, J., Min, M., Kuro-o, M., Yan, F., Li, C., *et al*. (2012). Review of the systematics, morphology and distribution of Asian Clawed Salamanders, genus *Onychodactylus* (Amphibia, Caudata: Hynobiidae), with the description of four new species. *Zootaxa,* 3465, 1-106. https://doi.org/10.11646/zootaxa.3465.1.1

Relyea, R.A. (2002). Competitor-induced plasticity in tadpoles: consequences, cues, and connections to predator-induced plasticity. *Ecological Monographs,* 72, 523-540. https://doi.org/10.1890/0012-9615(2002)072[0523:cipitc]2.0.co;2

Rosa, G., Salvidio, S., and Costa, A. (2023). Disentangling exploitative and interference competition on forest dwelling salamanders. *Animals,* 13, 2003. https://doi.org/10.3390/ani13122003

Solkin, V. (1993). On the ecology of the salamander *Onychodactylus fischeri* (Caudata: Hynobiidae). *Herpetozoa,* 6, 29-36.

Son, M., Hamm, S., Kim, I., Song, W., Lee, Y., Jung, H., *et al*. (2002). Fracture analysis for evaluation of groundwater flow around the Geumjeong Mountain, Busan. *Journal of the Korean Society of Engineering Geology,* 12, 305-317.

Um, T.E., Bliss, D.A., Borzée, A., and Jang, Y. (2025). Biogeographic barriers and environmental gradients reveal distribution limits in *Hynobius* salamanders. *Scientific Reports,* 15, 38345. https://doi.org/10.1038/s41598-025-22226-5

Waldron, B.P., Campbell, C.A., and Kuchta, S.R. (2024). Specialist or refugee: microhabitat use and competition between two sympatric woodland salamanders. *Journal of Zoology,* 323, 45-56. https://doi.org/10.1111/jzo.13151

Yeiser, J.M., and Richter, S.C. (2015). Microhabitat conditions influence mesohabitat associations and distribution of larval salamanders in headwater streams. *Hydrobiologia,* 751, 175-187. https://doi.org/10.1007/s10750-015-2185-5

Yoon, I., Lee, S., and Yang, S. (1996). The study on prey resource and life history of *Hynobius leechii* Boulenger and *Onychodactylus fischeri* Boulenger (Amphibia; Salientia). *Korean Journal of Environmental Biology,* 14, 195-203.

Yoshikawa, N., and Matsui, M. (2022). A new salamander of the genus *Onychodactylus* from central Honshu, Japan (Amphibia, Caudata, Hynobiidae). *Current Herpetology,* 41, 82-100. https://doi.org/10.5358/hsj.41.82

Zylstra, E.R., Steidl, R.J., Swann, D.E., and Ratzlaff, K. (2015). Hydrologic variability governs population dynamics of a vulnerable amphibian in an arid environment. *PLoS One,* 10, e0125670. https://doi.org/10.1371/journal.pone.0125670

PNIE PROCEEDINGS OF THE NATIONAL INSTITUTE OF ECOLOGY OF THE REPUBLIC OF KOREA

Original Article

PNIE 2026;7(4):181-189
https://doi.org/10.22920/PNIE.2026.7.4.181
pISSN 2765-2203, eISSN 2765-2211

Functional Traits and Competitor-Stress-Tolerator-Ruderal Strategies of *Phragmites australis* in Southwestern Korean Estuaries

Dong-Ho Son[1], Seok Yeoul Ko[2], Kyoung Hoon Yang[3], Min Jae Kim[3], Jong-Wook Kim[3]*, Hyeon-Ho Myeong[4]

[1]Ecological and Natural Map Team, National Institute of Ecology, Seocheon, Korea
[2]Invasive Alien Species Team, National Institute of Ecology, Seocheon, Korea
[3]Department of Biological Science, Mokpo National University, Muan, Korea
[4]Ecology Research Department, Korea National Park Research Institute, Korea National Park Service, Wonju, Korea

ABSTRACT

Reed beds dominated by *Phragmites australis* have long supplied coastal societies with thatching materials, livestock fodder, and cultural symbolism, making them ideal sentinels for linking plant strategy theory to ecocultural value. We quantified functional trait differentiation among 14 plant communities spanning saline estuarine margins and adjacent freshwater marshes and interpreted the results through canonical correspondence analysis (CCA) and Grime's competitor-stress-tolerator-ruderal (CSR) framework. The CCA revealed that total organic carbon (TOC) strongly aligns with the positive side of CCA1, indicating it is a key driver distinguishing sites along this axis, whereas nitrite nitrogen (Nitri-N) shows a strong positive influence on CCA2. In the CSR space, most communities were clustered along the competitor–stress-tolerator (C–S) continuum, indicating the prevalence of competitive and stress-tolerant tactics in brackish settings. *P. australis*-rich stands epitomize the stress-tolerator–competitor (SC) strategy blend, thriving where fluctuating salinity imposes physiological stress, yet their dense culms facilitate space pre-emption. By embedding these patterns in an ecocultural context, our findings highlighted how the traditional reed uses coincide with habitats maximizing both cultural ecosystem services and ecological resilience. Recognizing the strategic underpinnings of reed communities can guide sustainable harvesting, habitat restoration, and cultural heritage conservation along dynamic coastlines.

Keywords: CCA, CSR strategies, Cultural ecosystem services, Estuaries, *Phragmites australis*, Plant dispersal

Introduction

Coastal wetlands in southwestern South Korea represent dynamic ecotones shaped by the convergence of marine influences, terrestrial inputs, and a historical human reliance on common reeds (*Phragmites australis*) (Lee *et al*., 2020). Traditionally harvested from diverse coastal habitats, including salt marshes, dune systems, and estuarine

Received September 7, 2026; **Revised** October 13, 2026; **Accepted** October 14, 2026

***Corresponding author:** Jong-Wook Kim
e-mail keco@mokpo.ac.kr
https://orcid.org/0000-0002-6275-2940

This is an Open Access article distributed under the terms of the Creative Commons Attribution Non-Commercial License (http://creativecommons.org/licenses/by-nc/4.0), which permits unrestricted non-commercial use, distribution, and reproduction in any medium, provided the original work is properly cited.

Copyright © National Institute of Ecology.

margins, *P. australis* supports cultural practices such as thatching, bedding for livestock, and artisanal weaving. In modern contexts, these reeds contribute to ecosystem services, including eco-parks, shoreline protection, and water purification.

Understanding the persistence and distribution of *P. australis* within these ecocultural systems requires synthesizing abiotic gradients, biotic processes, and historical land-use patterns. Evidence from fieldwork and lab analyses suggests that factors such as salinity, inundation regimes, soil particle size, exchangeable cations (Ca^{2+}, Mg^{2+}, K^{+}), total organic carbon (TOC), and total phosphorus (TP) exert a strong influence over vegetation composition across coastal landscapes like dunes, salt marshes, polders, and estuarine flats (Son *et al*., 2020). These abiotic variables interact with biological drivers, including competitive hierarchies, herbivory, invasive pressure, and stress tolerance, to collectively shape plant community dynamics (Lee & Kim, 2018).

Existing along a transitional marine–terrestrial interface, these habitats experience rapid changes in hydrology and soil salinity, resulting in a patchwork of environments ranging from hypersaline flats to nearly freshwater marshes (Elmas, 2017; Ihm *et al*., 2007). Extensive land reclamation throughout East Asia has transformed many tidal flats into agricultural or industrial landscapes, initially retaining coastal characteristics but gradually desalinizing them depending on precipitation, topography, and sediment properties (Hong *et al*., 2010; Min & Kim, 1999; 2000; Yang *et al*., 2021). Vegetation succession typically begins with salt-tolerant pioneers such as *Suaeda*, followed by peak species richness within a decade post-reclamation, with clear zonation patterns aligned with elevation and creek structure (Cho *et al*., 2017).

Soil chemistry, particularly pH, organic matter, and nitrate levels, plays a pivotal role in facilitating the spread of ruderal competitors, such as *P. australis* and other halophytic species (Bornette & Puijalon, 2011; Rooney & Kalff, 2000). These species leverage extensive rhizome systems and clonal reproduction to capitalize on nutrient inputs and withstand fluctuating salinity, rendering them key ecological engineers and culturally important resources.

This study investigated plant functional traits and water chemistry across 14 estuarine wetland sites to (1) apply Grime's competitor-stress-tolerator-ruderal (CSR) strategy framework for species classification and (2) examine the spatial variation in plant strategies across estuarine zones. By emphasizing the cultural and ecological significance of *P. australis*, we sought to bridge trait-based plant ecology with practical approaches to wetland conservation, sustainable reed use, and adaptive strategies for coastal ecosystem management under environmental change.

Materials and Methods

Study area and ecocultural context

Fourteen reed-dominated wetlands were surveyed between July and August 2021 along the coastline of southwestern Korea (Fig. 1, Table 1). Because these estuarine flats supply the thatching, fodder, and weaving materials that underpin local reed festivals and craft cooperatives, the sites were stratified to include both actively harvested stands and conservation zones. The latitude, longitude, and coverage (%) of each site are listed in Table 1.

Vegetation sampling

Within each wetland, three 1×1 m quadrats were established within the prevailing *P. australis* zone, yielding a total of 42 quadrats (three quadrats×14 wetlands). The quadrats within the wetlands were spaced at least 10 m apart. Four additional quadrats were placed in adjacent herb–shrub mosaics only to describe community transitions qualitatively; these were excluded from the canonical correspondence analysis (CCA), CSR analysis, and summary statistics. All vascular plants were identified in situ, and the percentage cover was visually estimated for each species.

Sampling and statistical units

The three quadrats within a wetland were not independent of one another; therefore, they were treated as subsamples rather than replicates. Species cover, trait values, and water variables were initially averaged across the three quadrats for each wetland; the wetland (site) was the sole statistical unit in all analyses. Therefore, the final dataset contained 14 sites, each representing a distinct *P. australis* community (14 relevés in the CCA; Table 2). Each wetland was treated as an independent sampling

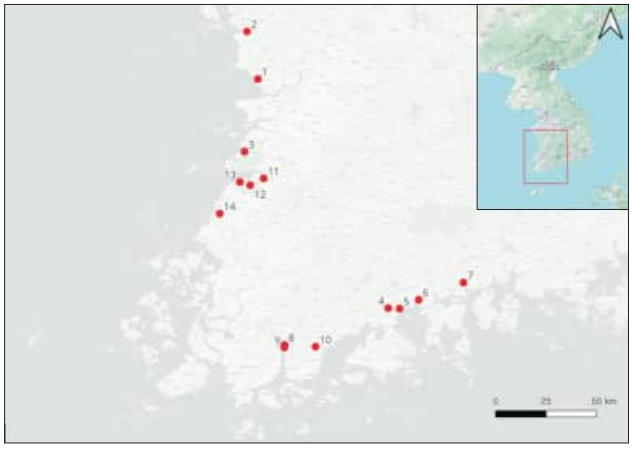

Fig. 1. Map of study areas along the southwestern coast of South Korea.

Table 1. *Phragmites* communities study sites in estuary along the southwestern coast of South Korea

Site number	Local name	Latitude	Longitude	Coverage (%)
1	Seocheon-gun Hanseong-ri	N 36.08698	E 126.6419	100
2	Boryeong-si Naehang-dong	N 36.34679	E 126.5825	100
3	Buan-gun Baekryeon-ri	N 35.69272	E 126.5693	100
4	Boseong -gun Jangjwa-ri	N 34.84049	E 127.3520	100
5	Suncheon-si Guryong-ri	N 34.83745	E 127.4134	100
6	Suncheon-si Seonhak-ri	N 34.88593	E 127.5179	100
7	Gwangyang-si Seonso-ri	N 34.97942	E 127.7616	95
8	Gangjin-gun Hogye-ri	N 34.64008	E 126.7870	100
9	Gangjin-gun Samsin-ri	N 34.62626	E 126.7855	100
10	Jangheung-gun Punggil-ri	N 34.63043	E 126.9559	100
11	Gochang-gun Suang-ri	N 35.54691	E 126.6735	100
12	Gochang-gun Yongsan-ri	N 35.50992	E 126.6001	100
13	Gochang-gun Dueo-ri	N 35.52703	E 126.5438	100
14	Yeonggwang-gun Gusu-ri	N 35.35487	E 126.4341	95

Table 2. Eigenvalues, explained variation, pseudo-canonical correlation and explained fitted variation in CCA of 14 relevés and 8 explanatory estuary water factors

Statistic	Axis 1	Axis 2	Axis 3	Axis 4
Eigenvalues	1.0000	0.9999	0.9991	0.9932
Explained variation (cumulative)	7.96	15.92	23.87	31.77
Pseudo-canonical correlation	1.0000	1.0000	1.0000	0.9999
Explained fitted variation (cumulative)	12.96	25.92	38.86	51.73

CCA, canonical correspondence analysis.

Table 3. Functional traits used for CSR strategy assessment

Symbol	Trait (unit)	Ecological relevance
CH	Canopy height (mm)	Competitive potential
LS	Lateral spread (mm)	Space occupancy & rhizome reach
LA	Leaf area (mm^2)	Light interception
LDW	Leaf dry weight (mg)	Structural investment
LDMC	Leaf dry matter content (%)	Stress tolerance
SLA	Specific leaf area ($mm^2\ mg^{-1}$)	Growth rate
Cov	Canopy cover (%)	Dominance
FP	Flowering period (mo)	Reproductive window
FS	Flowering start (mo)	Phenology

CSR, competitor-stress-tolerator-ruderal.

unit because the sites were situated in separate estuaries or tidal-channel systems; the closest pair (Sites 8 and 9 in Gangjin-gun) was approximately 1.5 km apart, with all other pairs separated by more than 5 km. As no test was performed at the quadrat level, quadrats from the same wetland were never counted as independent observations, precluding pseudoreplication.

Plant functional traits

Within each of the 42 quadrats, five canopy shoots of *P. australis*, the dominant species across all quadrats, were randomly selected, yielding 15 shoots per wetland (210 shoots in total). This standardized protocol was applied across all wetlands. Nine traits were recorded (Table 3): canopy height (CH), lateral spread (LS), leaf area (LA), leaf dry weight (LDW), leaf dry matter content (LDMC), specific leaf area (SLA), canopy cover (Cov), flowering period (FP) and flowering start (FS), following Hodgson *et al*. (1999) and Pierce *et al*. (2013) (Tables 3, 4). Seven of these traits (CH, LS, LDW, LDMC, SLA, FP, and FS) were inputs for the CSR allocation method proposed by Hodgson *et al*. (1999), whereas LA, LDMC, and SLA were inputs for the method by Pierce *et al*. (2013); Cov was recorded to quantify dominance. The traits were selected to fulfill the requirements of the two CSR classification methods, while collectively describing plant size and competitive ability (CH, LS, and LA), leaf economics (LDMC and SLA), and phenology (FP and FS).

Table 4. Summary statistics of the plant functional traits of *Phragmites australis* across the 14 study sites (N=number of sites)

	Canopy height (mm)	Leaf dry matter content (%)	FP (No. of mo)	LS (six-point model)	Leaf dry weight (mg)	Specific leaf area (mm^2 mg^{-1})	FS (mo)
Means	2,929	44	2	6	0.523	10	6
SD	182	10	0	0	0	4	0
N	14	14	14	14	14	14	14
MAX	3,000	65.2	2	6	0.746	20.983	6
MIN	2,500	32.4	2	6	0.267	5.928	6
Range	500	32.8	0	0	0.480	15.055	0

Statistics were calculated from site means, each the mean of 15 shoots (five shoots in each of three quadrats). LS, FP and FS are categorical scores of Hodgson *et al*. (1999).
FP, flowering period; LS, lateral spread; FS, flowering start; SD, standard deviation.

Table 5. Summary statistics of water factors across the 14 study sites (N=number of sites)

	Ammonium-N (mg/L)	Nitrite-N (mg/L)	Nitrate-N (mg/L)	Phosphate (mg/L)	TN (mg/L)	TOC (mg/L)	Salinity (PSU)	Electrical conductivity (mS/cm)	Density (%)
Means	0.819	0.038	0.791	0.260	3.792	8.258	6.976	7.254	99
SD	1.171	0.046	0.397	0.417	3.939	4.766	7.618	7.393	2
N	14	14	14	14	14	14	14	14	14
MAX	4.401	0.135	1.172	1.569	16.836	17.410	18.290	18.527	100
MIN	0.009	0.006	0.010	0.008	1.003	2.337	0.060	0.076	95
Range	4.392	0.129	1.162	1.561	15.833	15.073	18.230	18.451	5

Statistics were calculated from site means, each the mean of the pore-water samples from the three quadrats.
TN, total nitrogen; TOC, total organic carbon; PSU, practical salinity unit; SD, standard deviation.

Trait definitions and measurement

CH was measured in the field as the vertical distance from the soil surface to the highest photosynthetic tissue on each shoot. Cov represents the visually estimated percentage cover of *P. australis* in each quadrat. For the leaf traits, one fully expanded, undamaged, and sun-exposed leaf was collected from each shoot, sealed in a moist plastic bag, and stored in a cool box. In the laboratory, leaves were rehydrated in water at 4°C in the dark for at least 6 hours, blotted dry, and weighed to determine the water-saturated fresh mass. LA was measured from scanned images using ImageJ software (National Institutes of Health, Bethesda, MD, USA). Leaves were then oven-dried at 60°C for 72 hours and weighed to determine LDW. LDMC was calculated as leaf dry mass divided by water-saturated fresh mass (%), and SLA as LA divided by leaf dry mass (mm^2 mg^{-1}), following Pérez-Harguindeguy *et al*. (2013). LS, FP, and FS are categorical scores in the Hodgson *et al*. (1999) method; these were assigned based on field observations of rhizome spread and from flowering records from the plant field guide, remaining constant across sites (Table 4). All other trait values were derived from field and laboratory measurements, and no trait database was used.

Physico-chemical properties of stem-adjacent water

Triplicate pore water samples (0-10 cm depth) were extracted from each quadrat using a sterile bottle and analyzed within 24 hours (Table 5) for salinity, electrical conductivity (EC), nitrate-N, nitrite-N, ammonium-N, total nitrogen (TN), phosphate-P, and TOC, following Lee *et al*. (2020).

Data analysis

Canonical correspondence analysis

The site-level mean species cover (for 14 sites, excluding the four transition quadrats) was correlated to the eight water variables (Table 5) using CANOCO 5.10 (Ter Braak & Šmilauer, 2018). The site scores were centered and standardized, and the significance of the first two axes was tested using 999 permutations.

Competitor-stress-tolerator-ruderal strategy assignment

Because *P. australis* accounted for 95-100% of the cover in every quadrat, the trait value of each community was calculated as the mean of the 15 shoots measured at that site. This value represents the community-weighted mean (CWM=$\Sigma p_i x_i$, where p_i is the relative cover of species i and x_i its mean trait value), given that $p_i \approx 1$ for *P. australis*. These site-level values were integrated into the CSR allocation routine of Hodgson *et al*. (1999) to plot each community within Grime's CSR triangle (Grime, 1974). A triangular plot (Fig. 2) was drawn with the site number for each community alongside the reference communities listed in Table 6.

Results

Dominance and functional strategy of *Phragmites australis*

P. australis overwhelmingly dominated all 14 estuarine communities, accounting for 95-100% of the Cov (Fig. 1, Table 1). Trait-based ordination located the species along the competitor (C)/stress-tolerator–competitor (SC) and SC sectors, confirming its dual ability to monopolize light while enduring fluctuating salinity (Fig. 2).

Key structural traits of harvested culms

- CH: 2,500-3,000 mm, representing an ideal stem length for roofing bundles.
- LDMC: 32.4-65.2%, this high dry-matter content imparts rot resistance in mats.
- SLA: 5.93-20.98 $mm^2\ mg^{-1}$, these relatively low values indicate tough, slow-decomposing leaves, suited for livestock bedding and reedboard manufacture.

Fig. 3 show the ralationship between LDMC and SLA. Fig. 4 shows the relationship between the environmental variables and the study sites.

TOC strongly aligned with the positive side of CCA1, indicating it as a key driver distinguishing sites along this axis. Nitri-N (nitrite nitrogen) shows a strong positive influence on CCA2. Salinity and EC were positively correlated with CCA2, indicating a salinity gradient driving species distribution in the upper part of the plot. Ammonium Nitrogen (Amm-N) and TN pointed leftwards, demonstrating a negative correlation with CCA1. Sites 3 and 6 were associated with high TOC, whereas sites 5 and 10 were associated with higher salinity and EC. Sites with high salinity and EC support plants with shorter CH. Sites with higher TOC were associated with plants with higher LDW, indicating faster resource acquisition. The first two CCA axes (eigenvalues of 1.0000 and 0.9999; 61.53% of the total constrained variance) segregated the communities into three hydronutrient groups.

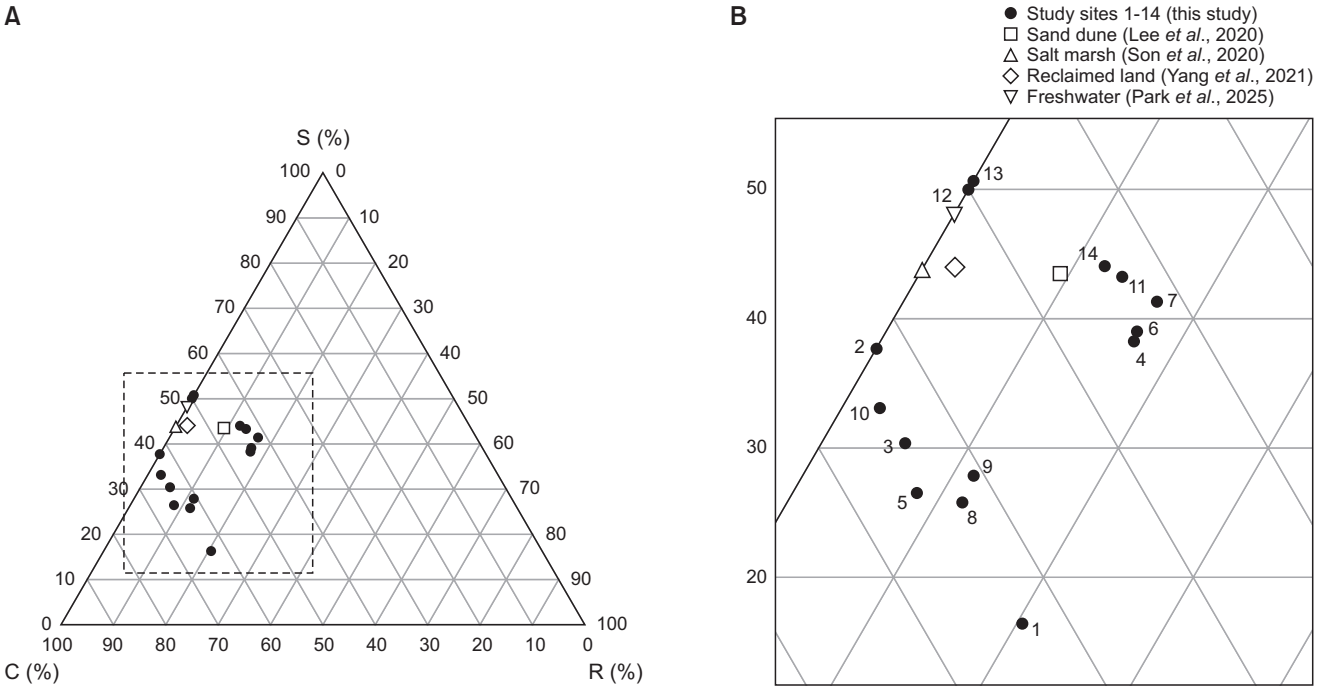

Fig. 2. CSR classification by plant factors from Hodgson *et al*. (1999) and Pierce *et al*. (2013) in 14 *Phragmites australis* communities. (A) All communities in the C–S–R triangle, (B) enlarged view of the dashed area in (A). Filled circles are the 14 *P. australis* communities of this study, labelled with their site numbers (Table 1). Open symbols are reference communities from sand dunes (Lee *et al*., 2020), salt marshes (Son *et al*., 2020), reclaimed land (Yang *et al*., 2021) and freshwater wetlands (Park *et al*., 2025) (Table 6). CSR, competitor-stress-tolerator-ruderal.

Table 6. C, S, and R values, and CSR strategies based on Hodgson *et al*. (1999), collected from *Phragmites australis* communities along the southwestern coastal estuaries of South Korea

Site number	C (%)	S (%)	R (%)	Strategy type
1	63.3	16.3	20.4	C/CR
2	62.4	37.6	0.0	C/SC
3	64.2	30.3	5.6	C/SC
4	44.9	38.2	17.0	SC/CSR
5	65.3	26.4	8.3	C/SC
6	44.3	38.9	16.8	SC/CSR
7	41.8	41.2	17.0	SC
8	62.6	25.7	11.7	C/SC
9	60.8	27.8	11.4	C/SC
10	64.5	33.0	2.5	C/SC
11	43.1	43.1	13.7	SC
12	50.1	49.9	0.0	SC
13	49.4	50.6	0.0	SC
14	43.9	43.9	12.1	SC
Sand dune (Lee *et al*., 2020)	47.2	43.4	9.4	SC
Salt marsh (Son *et al*., 2020)	56.3	43.7	0.0	SC
Reclaimed land (Yang *et al*., 2021)	54.0	43.9	2.1	SC
Freshwater (Park *et al*., 2025)	52.0	48.0	0.0	SC

C, competitor; S, stress-tolerator; R, ruderal.

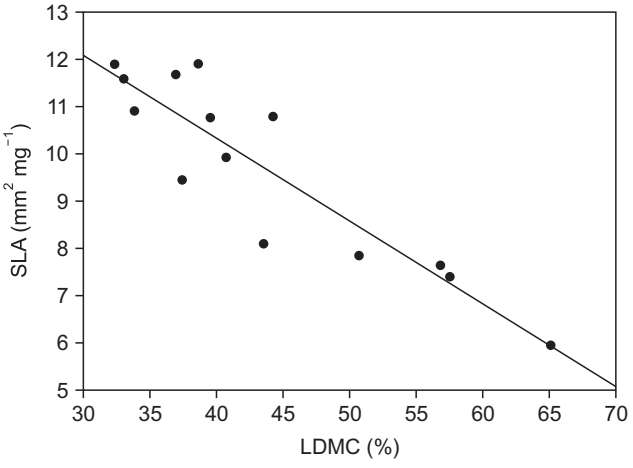

Fig. 3. Relationship between LDMC and SLA. LDMC, leaf dry matter content; SLA, specific leaf area.

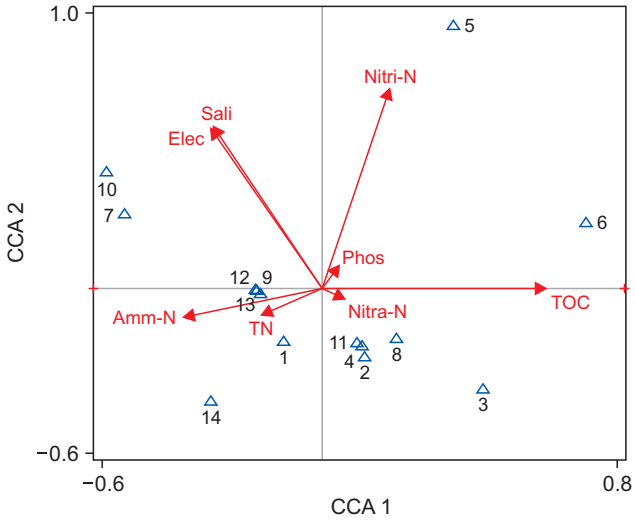

Fig. 4. CCA bi-plot diagram in estuary *Phragmites australis* communities. Axes 1 and 2 are the vegetation plots and the water factors. Water factors are visualized as arrows. See Table 1 for site names. CCA, canonical correspondence analysis; Nitri-N, nitrite nitrogen; Sali, salinity; Elec, electrical conductivity; Phos, phosphate; Nitra-N, nitrate-n; Amm-N, ammonium-n; TN, total nitrogen; TOC, total organic carbon.

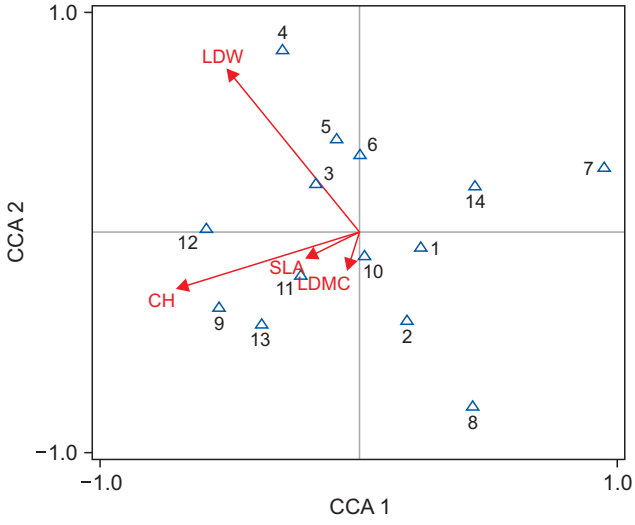

Fig. 5. CCA bi-plot diagram. The 14 community scores are plotted along 1 and 2 axes and clustered into several traits in estuary *Phragmites australis* communities. See Table 1 for site names. CCA, canonical correspondence analysis; LDW, leaf dry weight; CH, canopy height; SLA, specific leaf area; LDMC, leaf dry matter content.

Fig. 5 shows the relationship between the plant functional traits and the study sites. LDW and CH show a strong influence on the CCA2 axis. Sites 9, 12, and 13

were positioned near the CH vectors, suggesting a dominance of species with taller structures and denser leaves, which were likely more competitive. Sites 3, 4, 5, and 6 were associated with a high LDW, suggesting a combination of trait strategies. These trait-environment relationships were reflected in spatial patterns, substantiating that environmental gradients shape functional trait distributions in estuarine vegetation. The first two CCA axes (eigenvalues of 0.9943 and 0.9783; 30.37% of the total constrained variance) segregated the communities into four plant groups.

Community-level competitor-stress-tolerator-ruderal allocation

CSR triangle plots (Fig. 2, Table 6) placed all 14 communities along a CSR continuum; each point in Fig. 2 is labeled with its site number (Table 1), and the reference communities from other coastal habitats are denoted with separate symbols:

- C/SC stands (n=6): Sites 2, 3, 5, 8, 9, and 10.
- SC stands (n=5): Sites 7, 11, 12, 13, and 14.
- SC/CSR stands (n=2): Sites 4 and 6.
- C/CR stand (n=1): Site 1, where ruderal forbs invaded the cutover ground.

Synthesis

Across the southwestern estuarine mosaic, *P. australis* translates its C/SC–SC strategy into tangible cultural and economic benefits, such as lignified shoots for roofing, silica-rich leaves for bedding, and a rhizomatous matrix that stabilizes tidal margins. Variations in water chemistry fine-tune community CSR positions, suggesting that adaptive harvest regimes timed to local nutrient signatures can maintain both reed quality and wetland health.

Discussion

Multivariate ordination revealed that estuarine wetlands in southwestern Korea are primarily structured by stress-tolerant and competitive plant strategies, aligning with global trends observed in similar brackish ecosystems (Bornette & Puijalon, 2011; Lee *et al*., 2020). When interpreted through an ecological framework, these patterns offer actionable insights for site-based management.

- C/SC assemblages (43% of surveyed sites: 2, 3, 5, 8, 9, 10) were typically located on elevated levees, historically valued for their straight, woody reed stems used in thatching and fencing.
- SC-dominated communities (36% of surveyed sites: 7, 11, 12, 13, 14) prevail in low-lying back-marsh zones prone to salinity fluctuations and inundation, where traditional harvesting would be constrained.

These observations resonate with findings from adjacent coastal habitat types (Table 6):

- Dune ecosystems: Salinity and moisture gradients in sandy terrains favor rhizomatous SC-type species that anchor to dunes, although their limited height restricts their suitability for thatching (Lee *et al*., 2020).
- Salt marshes: Son *et al*. (2020) reported that SC strategists can cope with both competition and episodic disturbances. When mechanical harvesting intensifies, our findings indicate that similar edge communities may emerge, highlighting the need for spatially staggered harvesting regimes.
- Reclaimed polder land: The initial post-diking stages often support SC species (Min & Kim, 2000; Yang *et al*., 2021). Our analysis suggests that progressive desalination promotes a shift along the competitor–stress-tolerator (C–S) continuum, potentially enabling sustainable reed use within a decade if leaching and grazing are appropriately managed.

By positioning both species and community means within Grime's CSR triangle, we developed a process-based understanding of how wetland plants negotiate productivity, stress, and disturbance. When combined with ecological knowledge, this framework serves as an applied tool for:

1. Optimizing harvest schedules: C and C/SC stands can be harvested earlier for high-quality thatch, whereas SC stands should be left until late season to maintain coastal resilience.
2. Locating nutrient-removal zones: CCA results showed strong associations between specific plant guilds and nitrogen compounds. Targeted harvesting in these areas may help remove excess nutrients while sustaining traditional economies.
3. Informing restoration strategies: To rapidly stabilize reclaimed or disturbed shores, the use of native SC or C/SC reed genotypes can support both ecological succession and craft heritage.

Although *P. australis* is often considered an invasive species, it has sustained centuries of cultural practice, from regional reed festivals to modern composite materials. Understanding its expression along the C/SC–SC axis explains its resilience in saline and harvested environments, and provides a framework for reconciling ecological, hydrological, and cultural priorities. This study demonstrates that embedding trait-based ecological models within lived and practical contexts enhances both scientific understanding and stewardship. The CSR triangle not only classifies species strategy, but also reveals the cultural logic behind traditional reed harvesting—when, where, and how to cut.

Conclusion

P. australis is the dominant species across the estuarine wetlands of the southwestern Korean coastline, exhibit-

ing distinct expression along the C–S axis of Grime's plant strategy model. In saline-influenced and frequently inundated habitats, *P. australis* persists through stress-tolerance strategies associated with salinity resistance and disturbance adaptation, whereas in less saline and more resource-rich environments, competitive traits promote enhanced vertical growth and biomass accumulation. These spatially differentiated strategies demonstrate that the ecological success of *P. australis* is not attributable to a single functional strategy but rather to its capacity to adjust along environmental gradients.

By integrating the CSR theory with community-level analysis and traditional ecological knowledge, this study provides a process-based framework for understanding the persistence, distribution, and utilization of *P. australis* in coastal wetlands. The C–S continuum identified here offers practical guidance for sustainable reed management, including optimizing harvest timing, identifying potential nutrient-removal zones, and selecting appropriate plant communities to restore disturbed coastal habitats.

These findings further highlight that *P. australis* is not merely a dominant wetland plant but also is an ecological component intertwined with long-standing cultural practices. The relationship between plant strategy, environmental stress, and traditional harvesting demonstrates that ecological resilience and human use can be jointly considered in coastal wetland stewardship. By linking functional plant ecology to cultural landscapes, this study provides insights into balancing biodiversity conservation, ecosystem management, and the sustainable use of reed-dominated wetlands.

Author Contributions

Conceptualization: DHS, JWK. Data curation: DHS, SYK. Formal analysis: DHS, KHY, MJK. Funding acquisition: JWK. Investigation: DHS, SYK, KHY, MJK, HHM. Methodology: DHS, JWK. Project administration: JWK. Resources: KHY, MJK. Software: SYK. Supervision: JWK, HHM. Validation: DHS, KHY, MJK. Visualization: DHS, SYK. Writing – original draft: DHS. Writing – review & editing: DHS, SYK, KHY, MJK, JWK, HHM.

Conflict of Interest

The authors declare that they have no competing interests.

Funding

This research was supported by a grant (RS-2018-NR033226) from the Basic Science Research Program through the National Research Foundation of Korea (NRF), funded by the Ministry of Education, Republic of Korea.

References

Bornette, G., and Puijalon, S. (2011). Response of aquatic plants to abiotic factors: a review. *Aquatic Sciences*, 73, 1-14. https://doi.org/10.1007/s00027-010-0162-7

Cho, J.S., Lee, J.S., and Kim, J.W. (2017). Distribution of *Phragmites australis* communities with different habitat salinity. *Journal of Coastal Research*, 33, 1210-1216. https://doi.org/10.2112/jcoastres-d-16-00065.1

Elmas, E. (2017). Ecophysiological characteristics and CSR strategies of four dune species. *Annales Botanici Fennici*, 54, 353-360. https://doi.org/10.5735/085.054.0617

Grime, J.P. (1974). Vegetation classification by reference to strategies. *Nature*, 250, 26-31. https://doi.org/10.1038/250026a0

Hodgson, J.G., Wilson, P.J., Hunt, R., Grime, J.P., and Thompson, K. (1999). Allocating C-S-R plant functional types: a soft approach to a hard problem. *Oikos*, 85, 282-294. https://doi.org/10.2307/3546494

Hong, S.K., Koh, C.H., Harris, R.R., Kim, J.E., Lee, J.S., and Ihm, B.S. (2010). Land use in Korean tidal wetlands: impacts and management strategies. *Environmental Management*, 45, 1014-1026. https://doi.org/10.1007/s00267-006-0164-3

Ihm, B.S., Lee, J.S., Kim, J.W., and Kim, J.H. (2007). Coastal plant and soil relationships along the southwestern coast of South Korea. *Journal of Plant Biology*, 50, 331-335. https://doi.org/10.1007/bf03030663

Lee, J.S., and Kim, J.W. (2018). Dynamics of zonal halophyte communities in salt marshes in the world. *Journal of Marine and Island Cultures*, 7, 84-106. https://doi.org/10.21463/jmic.2018.07.1.06

Lee, J.S., Son, D.H., Lee, S.H., Myeong, H.H., Cho, J.S., Lee, J.C., *et al*. (2020). Canonical correspondence analysis ordinations and competitor, stress tolerator, and ruderal strategies of coastal dune plants in South Korea. *Journal of Coastal Research*, 36, 528-535. https://doi.org/10.2112/jcoastres-d-19-00106.1

Min, B.M., and Kim, J.H. (1999). Plant distribution in relation to soil properties of reclaimed lands on the West Coast of Korea. *Journal of Plant Biology*, 42, 279-286. https://doi.org/10.1007/bf03030341

Min, B.M., and Kim, J.H. (2000). Plant succession and interaction between soil and plants after land reclamation on the West Coast of Korea. *Journal of Plant Biology*, 43, 41-47. https://doi.org/10.1007/bf03031035

Park, S.B., Yang, K.H., Ko, S.Y., Cho, J.S., You, C., Son, D.H., *et al*. (2025). Distribution of freshwater plant communities and halophytes in coastal region, Muan-gun, South Korea. *Journal of Marine and Island Cultures*, 14, 74-87. https://doi.org/10.21463/jmic.2025.14.1.05

Pérez-Harguindeguy, N., Díaz, S., Garnier, E., Lavorel, S., Poorter, H., Jaureguiberry, P., *et al*. (2013). New handbook for standardised measurement of plant functional traits worldwide. *Australian Journal of Botany*, 61, 167-234. https://doi.org/10.1071/bt12225

Pierce, S., Brusa, G., Vagge, I., and Cerabolini, B.E.L. (2013). Allocating CSR plant functional types: the use of leaf economics and size traits to classify woody and herbaceous vascular plants. *Functional Ecology*, 27, 1002-1010. https://doi.org/10.1111/1365-2435.12095

Rooney, N., and Kalff, J. (2000). Inter-annual variation in submerged macrophyte community biomass and distribution: the influence of temperature and lake morphometry. *Aquatic Botany*, 68, 321-335. https://doi.org/10.1016/s0304-3770(00)00126-1

Son, D.H., Lee, J.S., Kim, D.E., Lee, S.H., Hong, S.K., Myeong, H.H., *et al*. (2020). Importance of biotic and soil factors in determining the distribution strategies of coastal salt marsh plants. *Journal of Marine and Island Cultures*, 9. https://doi.org/10.21463/jmic.2020.09.2.01

Ter Braak, C.J.F., and Šmilauer, P. (2018). *Canoco reference manual and user's guide: software for ordination (version 5.10)*. Wageningen University & Research.

Yang, K.H., Park, S.B., Kim, S.Y., Cho, J.S., Lee, J.S., You, C., *et al*. (2021). Distribution strategies of vascular plants at the reclaimed lands at the Saemangum Sea Dike. *Journal of Marine and Island Cultures*, 10, 45-57. https://doi.org/10.21463/jmic.2021.10.2.03

PNIE PROCEEDINGS OF THE NATIONAL INSTITUTE OF ECOLOGY OF THE REPUBLIC OF KOREA

Original Article

PNIE 2026;7(4):190-199
https://doi.org/10.22920/PNIE.2026.7.4.190
pISSN 2765-2203, eISSN 2765-2211

Time-Series Analysis of Spatial Cluster Changes in Grade 1 Zones of the Ecological and Nature Map: 2007-2025

Ha-Eun Lee, Hye-Yeon Yoon*

Ecological and Natural Map Team, National Institute of Ecology, Seocheon, Korea

ABSTRACT

This study analyzed the temporal changes in the spatial distribution and clustering patterns of grade 1 zones in the Ecological and Nature Map of South Korea from 2007 to 2025. Grade 1 zone data for 2007, 2017, 2021, and 2025 were analyzed at the sigungu level using the 2025 administrative boundaries as a common spatial framework. Five indicators were calculated for each sigungu: ratio, total area, patch count, mean patch area, and maximum patch area of the grade 1 zones. K-means clustering was applied to a pooled dataset of 1,008 observations after z-score standardization to classify spatial characteristics under a consistent temporal criterion. The total area of grade 1 zones increased from 7,300.5 km^2 in 2007 to 9,134.6 km^2 in 2017 and 9,206.5 km^2 in 2021, but decreased to 8,573.2 km^2 in 2025. From 2007 to 2025, 183 and 61 sigungu exhibited an increase and decrease in the ratio of grade 1 zones, respectively, while 8 remained stable. Pooled clustering identified four types: low-ratio small-scale, mid-ratio few large-patch, mid-to-high ratio multi-patch, and high-ratio large-area concentrated types. These results show that grade 1 zones have been spatially reorganized over time, while remaining concentrated in mountainous and highly natural regions.

Keywords: Area change, Ecological and Nature Map, Grade, K-means, Spatial cluster

Introduction

The Ecological and Nature Map (ENM) is prepared by grading the natural environment according to ecological value and naturalness, pursuant to Article 34 of the Natural Environment Conservation Act and the Guidelines for Preparing the ENM (Korea Law Information Center, 2025a; 2025b). The map divides the entire country into approximately 800 map sheets and evaluates the natural environment of each area based on four criteria: vegetation, endangered wildlife, topography, and wetlands. The results are then integrated and classified into grade 1, 2, and 3 zones and separately managed zones (National Institute of Ecology, 2025a; 2025b). As representative environmental spatial information that comprehensively reflects the ecological value and natural environmental characteristics of the national territory, the ENM is used as an important baseline dataset for nature conservation and national land-use planning. In particular, grade 1 zones are recognized as areas with high ecological conservation value and should be prioritized in spatial decision-making processes related to development and conservation.

Since it was first officially announced in 2007, the

Received July 2, 2026; **Revised** July 27, 2026;
Accepted July 28, 2026

***Corresponding author:** Hye-Yeon Yoon
e-mail gis82@nie.re.kr
https://orcid.org/0009-0002-2920-7729

This is an Open Access article distributed under the terms of the Creative Commons Attribution Non-Commercial License (http://creativecommons.org/licenses/by-nc/4.0), which permits unrestricted non-commercial use, distribution, and reproduction in any medium, provided the original work is properly cited.

Copyright © National Institute of Ecology.

ENM has been continuously revised based on the results of the National Ecosystem Survey and 15 other ecosystem surveys. In 2017, the first nationwide revision of approximately 800 maps was completed using the results of the Third National Ecosystem Survey. Subsequently, a second revision was conducted in 2021 based on data from the Fourth National Ecosystem Survey, and a third revision was conducted in 2025 based on data from the Fifth National Ecosystem Survey. Given that the ENM is not a static product but a dataset that is continuously updated according to natural environment survey results and policy considerations, the spatial characteristics of grade 1 zones cannot be sufficiently understood from a single time point. Therefore, it is necessary to compare and analyze data from different periods to identify how the distribution and structure of grade 1 zones have changed over time.

Previous studies have mainly focused on the preparation of the ENM, the current status of spatial distribution, and changes in the characteristics of specific areas (Ko *et al*., 2024; Lee *et al*., 2023; Yoon & Oh, 2025). However, relatively few studies have analyzed both time-series changes and typological characteristics at the national scale using a common analytical unit. In particular, the range of map sheets and update targets reflected in the ENM differ by period, which limits direct comparisons of changes within the same spatial extent. Consequently, it has been difficult to consistently interpret changes in the area ratio, spatial distribution, patch structure, and clustering characteristics of grade 1 zones. In this context, comparing the 2007, 2017, 2021, and 2025 versions of the ENM, each providing nationwide coverage, helps minimize limitations on interpretation arising from differences in the map sheets included. This comparison also enables the systematic identification of the spatial distribution and change patterns of grade 1 zones associated with the accumulation of ecosystem survey data and revisions to the mapping guidelines.

Given that the ENM polygon data may vary across periods in both number of grade 1 zone patches and the mapping criteria used, direct comparisons among temporal datasets may be limited. To improve comparability, sigungu was used as a common analytical unit, and indicators such as the proportion of land classified as grade 1 zones, patch count, mean patch area, and maximum patch area were calculated for each sigungu. In addition, we applied cluster analysis to these indicators to group sigungu with similar characteristics and systematically interpret the differences in spatial distribution across periods.

Therefore, this study aimed to build a spatial database to facilitate comparisons over time using grade 1 zone data from the 2007, 2017, 2021, and 2025 versions of the ENM. Spatial indicators were calculated at the sigungu level to analyze distributional changes by period and long-term change patterns. Furthermore, spatial cluster analysis was conducted to identify sigungu types and explore their spatial distribution and temporal reorganization.

Materials and Methods

The target of this study was the grade 1 zones of the ENM, and the spatial scope comprised 252 sigungu units across South Korea, which served as the analytical units (Fig. 1). The data used in the analysis were the ENM data for 2007, 2017, 2021, and 2025. The 2007 map was prepared based on the Second National Ecosystem Survey (1997-2003), the 2017 map was prepared based on the Second and Third National Ecosystem Surveys (2006-2013), and the 2021 map was prepared based on the Fourth National Ecosystem Survey (2014-2018) and related data. The 2025 map was prepared based on the Fourth and Fifth National Ecosystem Surveys (2014-2023) and related data.

The ENM data were constructed as vector data using a geographic information system (GIS). Standardization and spatial alignment of spatial data are essential for enabling time-series comparisons among datasets. Therefore, the ENM data for each period were integrated into a single GIS database. Nationwide sigungu was defined as the common analytical unit, and the area, ratio, and patch characteristics of grade 1 zones were calculated. The sigungu boundary data were obtained from the census administrative boundary data provided by the Statistical

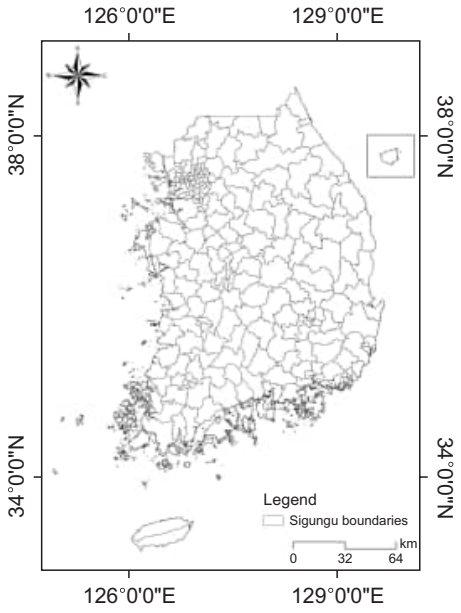

Fig. 1. Study area and analytical units.

Geographic Information Service (SGIS) of the Ministry of Data and Statistics (2025) (https://sgis.kostat.go.kr/).

The 2025 sigungu administrative boundary, consisting of 252 units, was used as a common spatial framework to ensure temporal comparability. Grade 1 zone polygons for 2007, 2017, 2021, and 2025 were overlaid with this common boundary, and all area-based and patch-related indicators were recalculated for each sigungu unit in 2025. This standardization minimized inconsistencies caused by administrative boundary changes among periods.

Data preprocessing, spatial overlay analysis, sigungu-level indicator calculation, and cluster analysis were performed in an Anaconda virtual environment running Python 3.12.7 (Python Software Foundation, Wilmington, DE, USA). GeoPandas and Pyogrio were used for spatial data processing, pandas and NumPy were used for data processing, and the K-means algorithm, implemented in scikit-learn, was used for cluster analysis. Map visualization was conducted using ArcGIS 10.8 (ESRI, Redlands, CA, USA), and all analytical data were unified to the World Geodetic System 1984 (WGS 1984) ellipsoid and the geographic coordinate system.

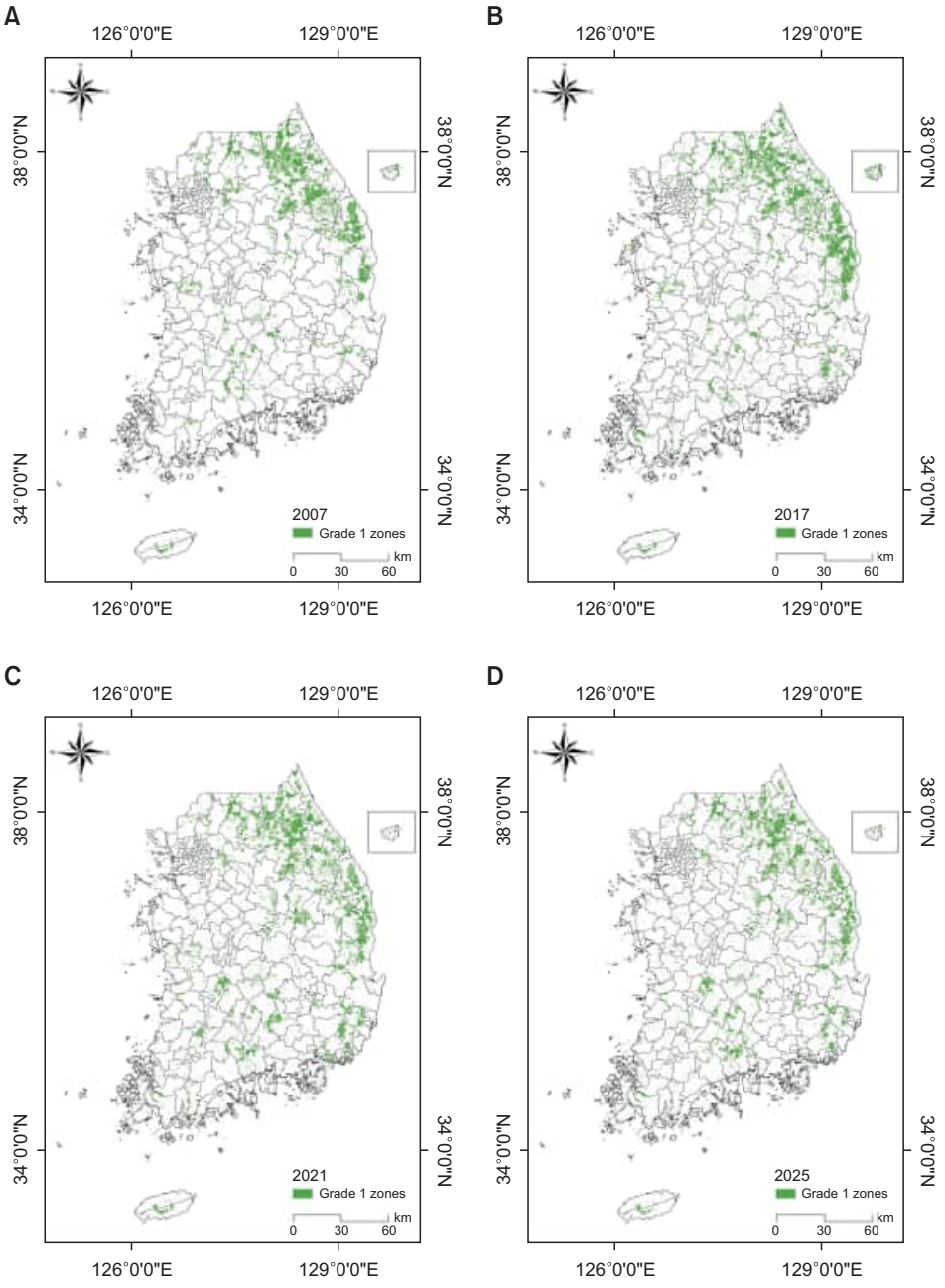

Fig. 2. Spatial distribution of grade 1 zones in the Ecological and Nature Map by period. (A) 2007, (B) 2017, (C) 2021, and (D) 2025.

Results

Spatial distribution of grade 1 zones by period

A comparison of the ratio of grade 1 zones in the ENM by period showed a common pattern in which high values were generally found in forested areas, whereas low values were found in urban and plain areas (Fig. 2). In 2007, the total area of grade 1 zones was 7,300.5 km^2. The ratio of grade 1 zone area was relatively high in northern and eastern Gangwon and northeastern Gyeongbuk, whereas it was generally low in the Seoul metropolitan area, west coast, and southern regions (Fig. 2A). This indicates that grade 1 zones of the ENM are generally concentrated in areas with high naturalness.

In 2017, the total area of grade 1 zones was 9,134.6 km^2, an increase of 1,834.1 km^2 compared with 2007. The spatial concentration of grade 1 zones became more distinct (Fig. 2B). High ratios were observed in northern Gangwon, the east coast, and northeastern Gyeongbuk, and some areas showed higher ratios compared with those in 2007. Meanwhile, the Seoul metropolitan area, major urban areas, southern Gyeonggi, urban areas in inland Chungcheong, and southwestern plain areas remained at low levels. This suggests that, with the incorporation of survey data by period, grade 1 zones were relatively more widely distributed in mountainous and coastal areas with high conservation value.

In 2021, the total area of grade 1 zones was 9,206.5 km^2, showing a slight increase compared to that in 2017. Although some areas with large grade 1 zone areas showed reductions or spatial reorganization, the overall spatial structure did not change substantially (Fig. 2C). As in the previous periods, high area ratios of grade 1 zones were found in the mountainous inland areas of Gangwon, regions adjacent to the east coast, and northeastern Gyeongbuk, whereas low ratios were maintained in the Seoul metropolitan area, major metropolitan cities, and areas with intensive industrial and agricultural land use. In particular, a contrast was observed between mountainous areas with high naturalness and urban areas with intensive human land use.

In 2025, the total area of grade 1 zones decreased to 8,573.2 km^2, a reduction of 633.3 km^2 compared to 2021. However, the basic structure of the spatial distribution of grade 1 zones remained similar (Fig. 2D). The areas with high ratios of grade 1 zones appeared to be less concentrated than in 2017, and only relative increases and decreases in some areas were reflected in a spatial distribution pattern similar to that of 2021. Across the four periods, grade 1 zones in 2025 were not uniformly distributed nationwide but showed spatial heterogeneity, with concentrations in mountainous and highly natural areas and low values in urban and plain areas.

Changes in grade 1 zones from 2007 to 2025

An analysis of changes in the ratio of grade 1 zones at the sigungu level from 2007 to 2025 showed that the mean ratio increased from approximately 4.0% in 2007 to approximately 5.6% by 2025. However, this pattern was not uniform across all regions but differed among sigungu. Among the 252 sigungu, 183 showed an increase in the ratio, 61 showed a decrease, and 8 areas remained stable, indicating that the number of increasing areas was larger (Fig. 3).

Spatially, increasing trends were relatively distinct in parts of Busan and Gyeongnam, the east coast of Gangwon, and parts of the Seoul metropolitan area, whereas decreasing trends were observed in northern and inland Gangwon and northern Gyeonggi. Thus, the long-term changes from 2007 to 2025 showed spatial heterogeneity, with both increases and decreases depending on the region rather than a uniform national trend.

The top 10 areas with the largest increases in the ratio of grade 1 zones were Buk-gu, Busan (39.2 percentage points), Geumjeong-gu, Busan (31.6 percentage points), Yangsan-si (18.1 percentage points), Mapo-gu, Seoul (16.8 percentage points), Donghae-si (16.0 percentage points), Hadong-gun (15.0 percentage points), Wanju-gun (13.5 percentage points), Yecheon-gun (13.3 percentage points), Yeongdeungpo-gu, Seoul (13.0 percentage points), and Jinhae-gu, Changwon-si (12.6 percentage points) (Fig. 4A). Conversely, the top 10 areas with the largest decreases were Nowon-gu, Seoul (–18.5 percentage points), Jeongseon-gun (–13.7 percentage points), Uijeongbu-si (–12.3 percentage points), Inje-gun (–12.1

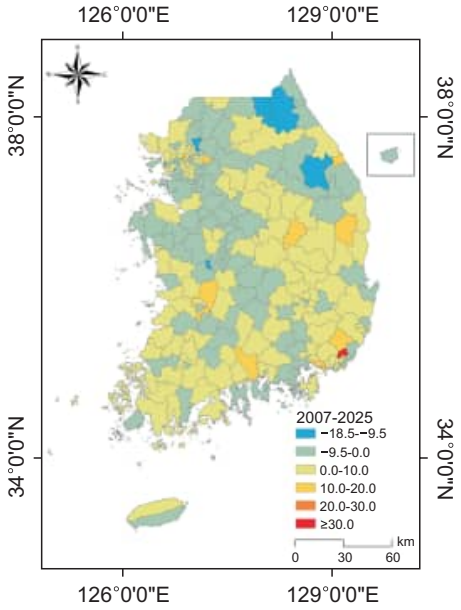

Fig. 3. Changes in the ratio of grade 1 zones in the Ecological and Nature Map, 2007-2025.

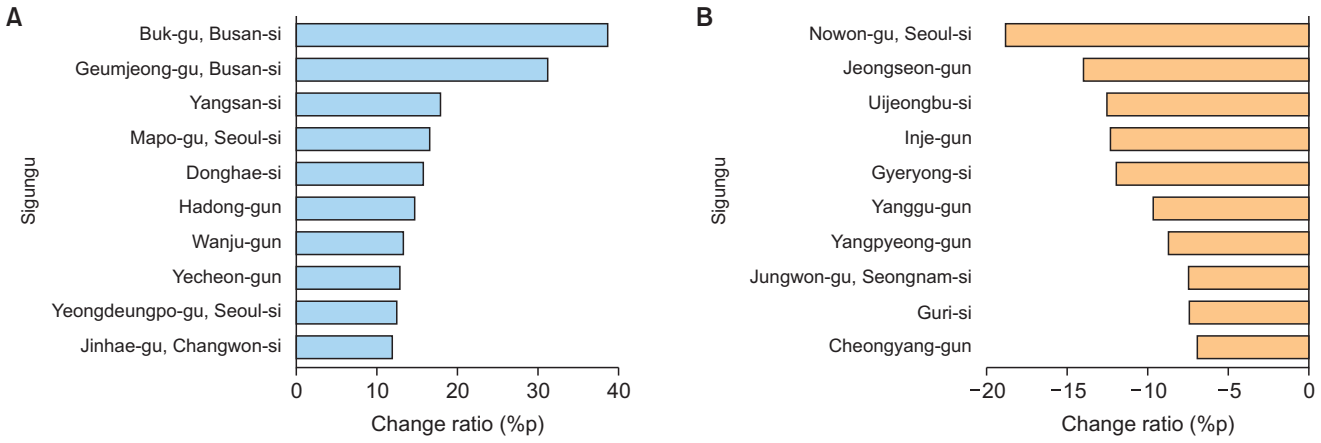

Fig. 4. Top 10 sigungu showing the largest increase (A) and decrease (B) in the ratio of grade 1 zones in the Ecological and Nature Map, 2007-2025.

Table 1. Cluster validity indices for different numbers of clusters

k	Silhouette	Calinski-Harabasz index	Davies-Bouldin index
2	0.700	668.572	0.883
3	0.560	625.777	1.077
4	0.580	587.596	0.981
5	0.538	575.320	0.965
6	0.451	582.637	1.016
7	0.467	561.693	1.017
8	0.470	556.040	1.014
9	0.465	547.595	1.019
10	0.474	540.195	0.981

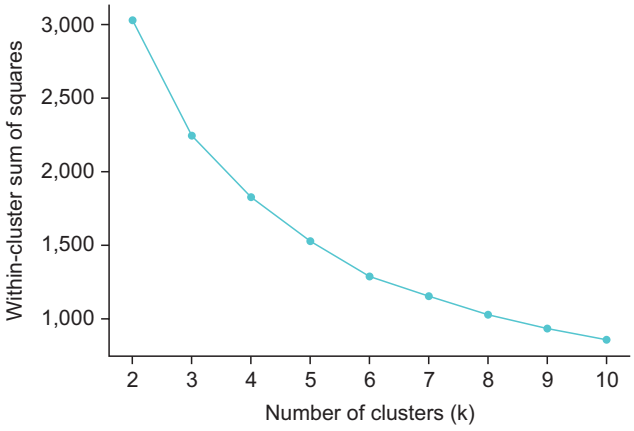

Fig. 5. Elbow plot of the within-cluster sum of squares for pooled K-means clustering.

percentage points), Gyeryong-si (−11.8 percentage points), Yanggu-gun (−9.5 percentage points), Yangpyeong-gun (−8.6 percentage points), Jungwon-gu, Seongnam-si (−7.3 percentage points), Guri-si (−7.3 percentage points), and Cheongyang-gun (−6.8 percentage points) (Fig. 4B). These results show that grade 1 zones increased in mountainous and coastal areas and in some urban fringe areas, whereas they decreased in the northern Seoul metropolitan areas and parts of inland Gangwon.

The mean ratio of the grade 1 zone area by period increased to 5.3% in 2017 and 6.3% in 2021, reaching its highest level in 2021, and then decreased slightly to 5.6% in 2025. In other words, the ratio of grade 1 zones generally increased after 2007. However, as the ratio decreased in some areas after 2021, the overall mean slightly declined. Nevertheless, the mean in 2025 remained higher than that in 2007, indicating that more sigungu experienced the long-term expansion of grade 1 zones.

Cluster characteristics based on pooled K-means clustering

To compare cluster transitions under a consistent temporal criterion, the sigungu-level indicators for 2007, 2017, 2021, and 2025 were combined into a single pooled dataset. The pooled dataset consisted of 1,008 observations, representing 252 sigungu units across four time points. Five indicators were used for clustering: the ratio of grade 1 zones, patch count, mean patch area, maximum patch area, and total area of grade 1 zones. As these variables had different units and scales, they were standardized using z-scores prior to clustering. K-means clustering was then applied to the standardized pooled dataset. Among the tested k values, k=2 showed the highest silhouette coefficient and Calinski–Harabasz index and the lowest Davies–Bouldin index. However, k=2 provided only a broad distinction between low- and high-value areas and was insufficient for interpreting the differences in patch configuration and area concentration. Therefore,

k=4 was selected as the final number of clusters because it maintained an acceptable silhouette coefficient of 0.580 and allowed for ecologically meaningful differentiation among the low-ratio small-scale, mid-ratio few large-patch, mid-to-high ratio multi-patch, and high-ratio large-area concentrated types (Table 1). The elbow plot also showed that the decrease in within-cluster sum of squares became more gradual after k=4, further supporting the selection of k=4 when both clustering performance and ecological interpretability were considered (Fig. 5).

A comparison of the original-scale mean values for each pooled cluster revealed that the four clusters differed in terms of the ratio of grade 1 zones, patch count, mean patch area, maximum patch area, and total area (Table 2). Cluster C1 was characterized by a low proportion and small total area of grade 1 zones and was classified as a low-ratio small-scale type. Cluster C2 had a moderate ratio of grade 1 zones, a small number of patches, and the largest mean patch area, and was interpreted as a mid-ratio few large-patch type. Cluster C3 showed a relatively high ratio of grade 1 zones and a large number of patches, corresponding to a mid-to-high ratio multi-patch type. Cluster C4 had the highest ratio, patch count, maximum patch area, and total area of grade 1 zones, and was interpreted as a high-ratio large-area concentrated type. These results indicate that grade 1 zones in the ENM exhibit distinct spatial characteristics in terms of areal extent, patch count and patch size.

The annual distribution of cluster membership showed that C1 was the dominant type during all periods (Fig. 6). The number of C1 sigungu was 199 in 2007, 205 in 2017, 182 in 2021, and 199 in 2025, accounting for 79.0%, 81.3%, 72.2%, and 79.0% of all sigungu, respectively. This indicates that, in most administrative districts, grade 1 zones consistently accounted for a low proportion of land and a small total area of grade 1 zones.

C2, the mid-ratio type with few large-patches, included 21 sigungu in 2007, but this number decreased to 3 in 2017. It temporarily increased to 10 in 2021 before declining to 3 in 2025. This pattern suggests that areas characterized by a moderate ratio of grade 1 zones and a small number of relatively large patches were limited and temporally unstable.

C3, the mid-to-high ratio multi-patch type, increased from 27 sigungu in 2007 to 33 in 2017 and 54 in 2021, before decreasing to 38 in 2025. The increase in C3 until 2021 suggests that the mid-to-high ratio and multi-patch characteristics became more pronounced during this period. However, the subsequent decrease in 2025 indicates that some of these areas were reorganized into other cluster types.

C4, the high-ratio large-area concentrated type, was limited to a small number of sigungu throughout the study period, but increased from 5 in 2007 to 11 in 2017, decreased to 6 in 2021, and increased again to 12 in 2025. This indicates that high-ratio and large-area grade 1 zones were spatially concentrated in a limited number of administrative districts, but such areas persisted over time.

Overall, the results indicate that the sigungu types of grade 1 zones in the ENM were characterized by the dominance and persistence of the low-ratio small-scale type in all periods. In contrast, the mid-to-high ratio multi-patch and high-ratio large-area concentrated types appeared in a smaller number of sigungu, mainly in mountainous and highly natural regions. This indicates that, although grade 1 zones expanded or were reorganized in some regions, most sigungu nationwide maintained low-ratio small-scale characteristics.

Temporal transitions of cluster types

As the cluster types were derived from pooled K-means clustering, the cluster transitions across periods can be interpreted as changes in cluster membership under a consistent classification criterion. The transition matrices showed that C1 was the most stable cluster throughout the study period (Fig. 7). Of the 199 sigungu classified as C1 in 2007, 184 remained as C1 in 2017 (Fig. 7A). Similarly, 172 of the 205 sigungu classified as C1 in 2017 remained as C1 in 2021 (Fig. 7B), and 180 of the 182 sigungu classified as C1 in 2021 remained as C1 in 2025 (Fig. 7C).

From 2007 to 2017, the most frequent transition was

Table 2. Cluster profile results based on the original-scale mean values

Cluster	Eco ratio (%)	Patch count	Mean patch area (km^2)	Max patch area (km^2)	Total eco area (km^2)	Profile (type)
C1	2.2	264.1	0.034	1.07	8.66	Low-ratio small-scale
C2	9.1	52.8	0.335	2.73	13.73	Mid-ratio few large-patch
C3	14.8	1,707.6	0.078	7.61	91.67	Mid-to-high ratio multi-patch
C4	30.0	8,005.2	0.062	11.31	381.51	High-ratio large-area concentrated

The values represent the cluster-wise means on the original scale. K-means clustering was performed using z-score-standardized variables.

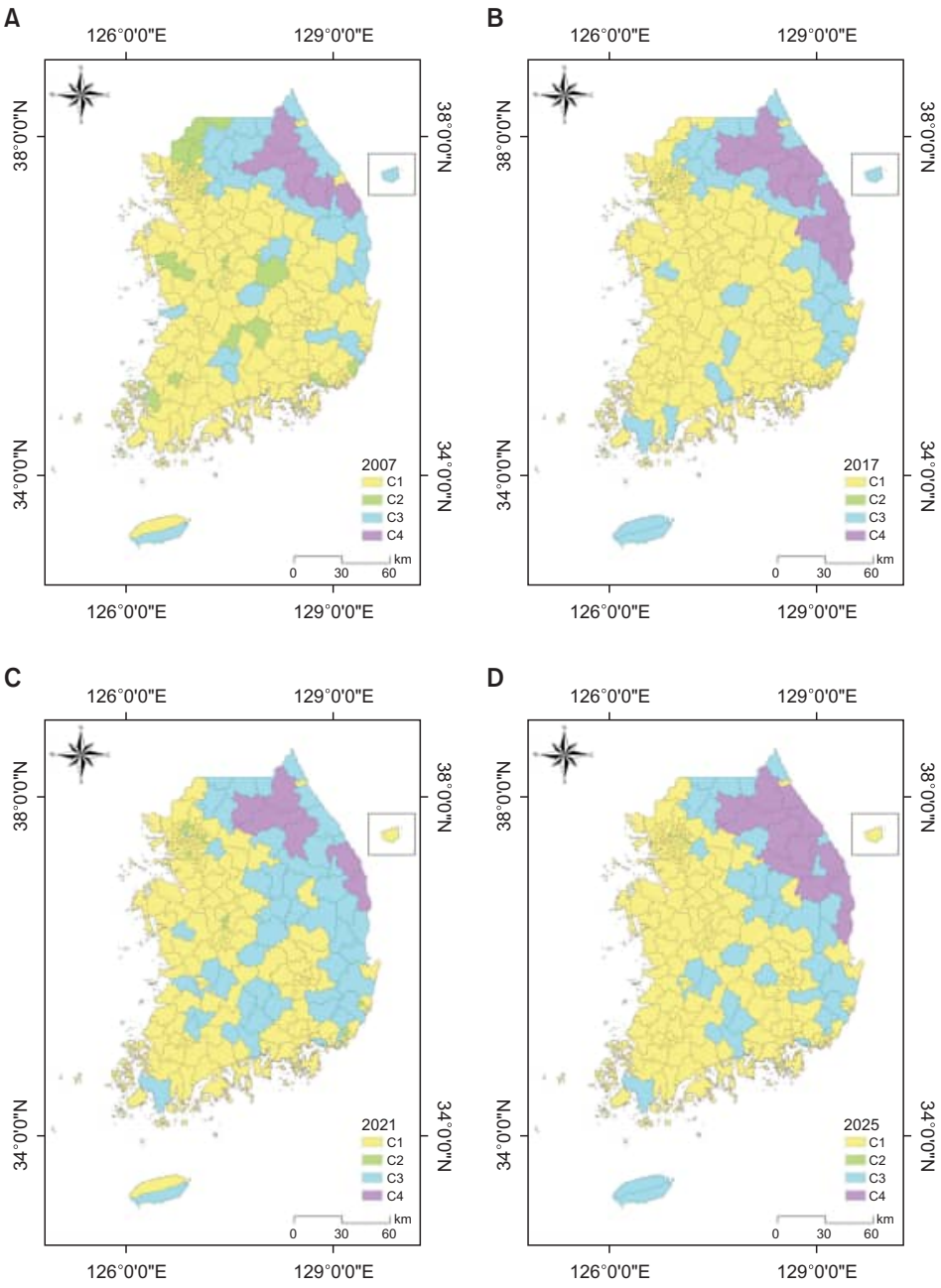

Fig. 6. Spatial distribution of cluster types derived from pooled K-means clustering by year. (A) 2007, (B) 2017, (C) 2021, and (D) 2025.

C1→C1, followed by C2→C1 and C3→C3 (Fig. 7A). This indicates that most low-ratio small-scale areas remained stable, whereas many areas classified as mid-ratio few large-patch type in 2007 were reclassified as low-ratio small-scale areas in 2017. From 2017 to 2021, 23 sigungu changed from C1 to C3, contributing to an increase in the mid-to-high ratio multi-patch type in 2021 (Fig. 7B). Between 2021 and 2025, 12 sigungu that were classified as C3 in 2021 changed to C1 in 2025, whereas 6 changed from C3 to C4 (Fig. 7C). This suggests that part of the mid-to-high ratio multi-patch type was reorganized into either a low-ratio small-scale type or a high-ratio large-area concentrated type during this period.

Analysis of the representative cluster transition paths further confirmed the persistence of the low-ratio small-scale type (Fig. 8). The most frequent path was C1→C1→C1→C1, which was observed in 158 sigungu. This indicates that the low-ratio small-scale type was not only the most common cluster but also the most stable temporal pattern. The second most frequent path was C3→C3→C3→C3, observed in 13 sigungu, followed by C2→C1→C1→C1, observed in 11 sigungu. These results

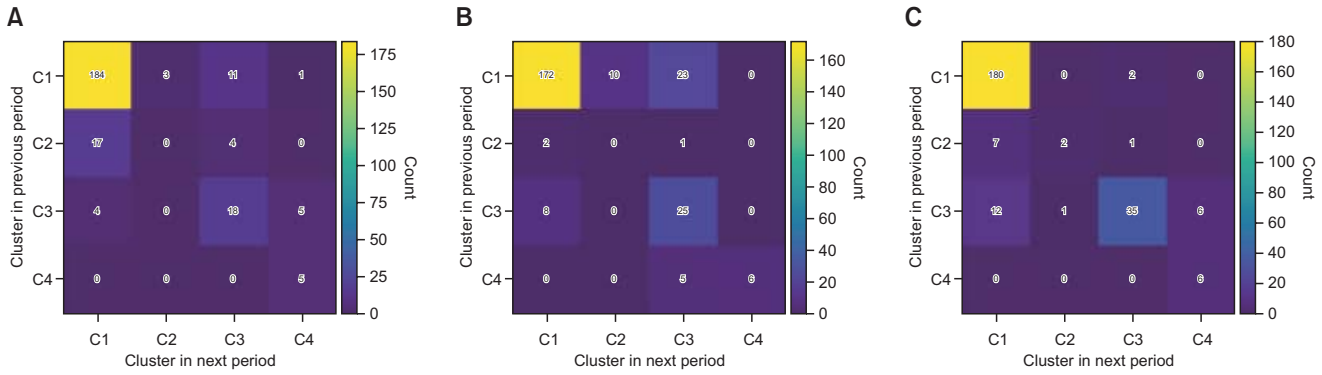

Fig. 7. Cluster transition matrices based on pooled K-means clustering. (A) 2007-2017, (B) 2017-2021, and (C) 2021-2025.

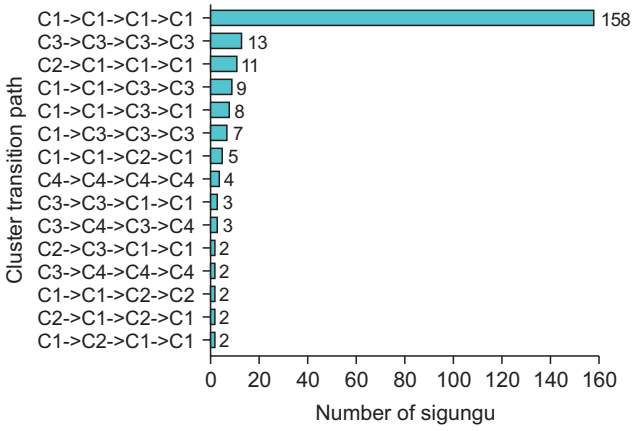

Fig. 8. Frequency of dominant cluster transition paths based on pooled K-means clustering.

suggest that the overall cluster structure of grade 1 zones was dominated by persistent low-ratio small-scale areas, although a limited number of sigungu maintained mid-to-high ratio multi-patch characteristics or shifted from the mid-ratio few large-patch type to the low-ratio small-scale type (Fig. 8).

Several other transition paths involved changes among multiple cluster types, indicating that some sigungu experienced temporal reorganization in terms of the ratio, patch count, mean patch area, maximum patch area, and total area of grade 1 zones. Therefore, although the overall cluster structure was dominated by stable low-ratio small-scale areas, localized changes in cluster membership occurred in specific regions over time. However, because this analysis was conducted at the sigungu level, it may not have fully captured fine-scale changes in patch configuration or ecological quality within administrative units.

Discussion

This study built a time-series spatial database at the nationwide sigungu level using grade 1 zone data from the ENM for 2007, 2017, 2021, and 2025. It analyzed the changes in the spatial distribution and reorganization of the cluster structure of grade 1 zones based on the area ratio, patch count, mean patch area, maximum patch area, and total area.

The results showed that grade 1 zones consistently had high area ratios in highly natural areas across all periods, such as the northern and eastern mountainous regions of Gangwon and mountainous and coastal regions of northeastern Gyeongbuk. In contrast, low ratios were observed in the Seoul metropolitan area, other metropolitan areas, plains, and urban regions. This spatial distribution was maintained relatively consistently despite temporal increases and decreases in area, indicating that the distribution of grade 1 zones was closely related to naturalness and land-use characteristics.

The long-term change from 2007 to 2025 showed that more sigungu experienced increases rather than decreases in the ratio of grade 1 zones, indicating an overall expansion trend. However, increases and decreases differed by region. Grade 1 zones increased in mountainous and coastal areas and in some urban fringe areas, whereas decreases were observed in the northern Seoul metropolitan area and parts of inland Gangwon. Therefore, changes in grade 1 zones should not be understood as a simple nationwide increase or decrease but as spatial reorganization that differs according to regional characteristics and survey data.

The decrease in the total area of grade 1 zones after 2021 can be interpreted in several ways. First, this reduction may reflect changes in the classification or evaluation processes associated with the revision of the ENM. As updated survey data are incorporated, some areas previously classified as grade 1 may be reclassified based on more recent ecological information. Second, land-use

changes, such as urban expansion, infrastructure development, or development pressure in peri-urban areas, may have contributed to localized reductions in grade 1 zones. Third, the decrease does not necessarily indicate a nationwide decline in ecological value, because the overall spatial pattern of grade 1 zones remained concentrated in mountainous and highly natural areas. Therefore, the reduction observed in 2025 should be interpreted as a spatial reorganization of grade 1 zones rather than a simple loss of ecologically valuable areas.

Pooled K-means clustering classified sigungu into four types: low-ratio small-scale, mid-ratio few large-patch, mid-to-high ratio multi-patch, and high-ratio large-area concentrated types. The low-ratio small-scale type accounted for the largest share in all periods, indicating that most sigungu had relatively low proportions and small total areas of grade 1 zones. In contrast, the mid-to-high ratio multi-patch and high-ratio large-area concentrated types appeared in a smaller number of sigungu, mainly in mountainous and highly natural areas. Cluster transition and representative path analyses showed that the low-ratio small-scale type was the most persistent temporal pattern, whereas some sigungu shifted toward mid-to-high ratio multi-patch or high-ratio large-area concentrated characteristics over time.

These findings suggest that the ENM is a dynamic ecological spatial information system that reflects updated survey data, revised criteria, and changes in spatial interpretation rather than a fixed spatial dataset. In addition, conservation planning should consider not only the total area of grade 1 zones but also their spatial configuration, regional concentration, and temporal persistence. The mid-to-high ratio multi-patch and high-ratio large-area concentrated types are important for examining conservation priorities and ecological network continuity, whereas areas showing decreased or persistent low-ratio characteristics require additional review in relation to land use, developmental pressure, and ecological connectivity. Although the pooled clustering approach allows cluster transitions to be interpreted under consistent classification criteria, this study was conducted at the sigungu level. Therefore, the transition matrices and path analysis indicated changes in cluster membership at the administrative-unit level rather than detailed patch-level transitions within each sigungu. Although the sigungu-level analysis is useful for nationwide comparisons, it has limitations in explaining fine-scale patches or qualitative ecological changes within administrative districts.

Conclusion

This study analyzed the long-term spatial changes and clustering characteristics of grade 1 zones in the ENM of South Korea from 2007 to 2025. The total area of grade 1 zones increased from 2007 to 2021 and then decreased by 2025; however, the overall distribution pattern remained concentrated in mountainous and highly natural areas. At the sigungu level, more areas showed an increase rather than a decrease in the ratio of grade 1 zones; however, spatial changes varied substantially by region. Cluster analysis showed that the low-ratio small-scale type dominated most sigungu, whereas the mid-to-high ratio multi-patch and high-ratio large-area concentrated types were differentiated in specific mountainous and highly natural regions. These results provide baseline information for interpreting long-term ENM updates and supporting conservation planning and ecological spatial management.

Author Contributions

Conceptualization: HEL, HYY. Data curation: HYY. Funding acquisition: HYY. Methodology: HEL. Resources: HYY. Software: HYY. Validation: HEL. Visualization: HYY. Writing – original draft: HEL. Writing – review & editing: HYY.

Conflict of Interest

The authors declare that they have no competing interests.

Funding

This research was funded by the Ministry of Climate, Energy and Environment (MCEE) and supported by the National Institute of Ecology (NIE) “Development of Total GIS-DB on Nature and Environment” project (NIE-A-2026-03).

References

Ko, E.J., Kang, T.H., and Yoon, H.Y. (2024). Preparation an ecological map using data from the third survey on national environment. *GEO DATA*, 6, 290-297. https://doi.org/10.22761/GD.2024.0130

Korea Law Information Center. (2025a). *Natural Environment Conservation Act*. Retrieved Jun 16, 2026 from https://www.law.go.kr/lsInfoP.do?lsiSeq=279793&efYd=&ancYnChk=undefined#0000.

Korea Law Information Center. (2025b). *Methods of Drawing Ecology and Nature Maps*. Retrieved Jun 16, 2026 from https://www.law.go.kr/admRulLsInfoP.do?admRulSeq=2100000199219.

Lee, S.J., Choo, C.O., Jeong, J.T., and Kim, J.T. (2023). Analysis and comparison of physicochemical characteristics of first-grade soils from ecological and nature map-focused on igneous rocks area. *The Journal of Engineering Geology*, 33, 61-68. https://doi.org/10.9720/kseg.2023.1.061

Ministry of Data and Statistics. (2025). Administrative boundaries for census purposes. *Statistical Geographic Information*

Service. Retrieved Jun 16, 2026 from https://sgis.mods.go.kr/view/pss/openDataIntrcn.

National Institute of Ecology. (2025a). *Ecology and Natural Map Guide Book*. National Institute of Ecology.

National Institute of Ecology. (2025b). *Development of Total GIS-DB on Nature and Environment*. National Institute of Ecology.

Yoon, H.Y., and Oh, W.S. (2025). Area analysis by grade and province of the ecology and nature map (2022-2025). *GEO DATA*, 7, 123-136.

PNIE PROCEEDINGS OF THE NATIONAL INSTITUTE OF ECOLOGY OF THE REPUBLIC OF KOREA

Original Article

PNIE 2026;7(4):200-212
https://doi.org/10.22920/PNIE.2026.7.4.200
pISSN 2765-2203, eISSN 2765-2211

Long-Term Tidal Flat Area Variation at the Nakdong River Estuary Measured from Multi-Temporal Sentinel-1 with Tidal and Seasonal Correction

Won-Kyung Baek[1], Moung-Jin Lee[2], Jun-Ho Lee[3], Keunyong Kim[1], Sung-Hwan Park[4], Joo-Hyung Ryu[1,5]*

[1]Korea Ocean Satellite Center, Korea Institute of Ocean Science and Technology, Busan, Korea
[2]Division for Environmental Planning, Korea Environment Institute, Sejong, Korea
[3]Peru-Korea Joint Ocean Research Center, Korea Institute of Ocean Science and Technology, Busan, Korea
[4]Marine Natural Disaster Research Department, Korea Institute of Ocean Science and Technology, Busan, Korea
[5]External Relations Division, Korea Institute of Ocean Science and Technology, Busan, Korea

ABSTRACT

Tidal flats in estuaries change continuously in response to tides, seasonal effects, and human activities. Monitoring their long-term area variation is important for understanding coastal changes and managing ecological resources. However, tidal flat areas detected from satellite imagery depends strongly on the tidal level and season at the time of acquisition, which can introduce large errors in long-term trend analysis. In this study, we analyzed the long-term tidal flat area variation at the Nakdong River Estuary (NRE), Korea, using 162 multi-temporal Sentinel-1 synthetic aperture radar (SAR) images acquired from November 2014 to March 2023. Tidal flat areas were extracted from each SAR image by thresholding the calibrated backscatter intensity. A polynomial fitting approach was used to correct for tidal and seasonal dependencies in the measured area time series. Pixel-frequency maps were constructed before and after the permanent floodgate opened in February 2022 to detect topographical anomalies. The corrected area anomalies tended to decrease from 2015 to 2017, followed by a slight increase or stabilization. The pixel frequency comparison identified five distinct change zones (A-E): erosion along the eastern main channel downstream of the opened floodgates (zones D and E), and deposition on the western landward flat (zone A). This spatial pattern is consistent with the east-west asymmetry expected under the gate-operation regime. Tidal and seasonal corrections are therefore necessary for reliable long-term monitoring and provide baseline information for assessing the impact of the NRE floodgate opening on estuarine geomorphology.

Keywords: Floodgate opening, Nakdong River Estuary, Pixel-frequency, Sentinel-1, Tidal correction, Tidal flat

Received July 23, 2026; **Revised** August 31, 2026; **Accepted** September 1, 2026

***Corresponding author:** Joo-Hyung Ryu
e-mail jhryu@kiost.ac.kr
https://orcid.org/0000-0003-4514-5214

Introduction

Tidal flats are coastal wetlands formed by tidal and fluvial sedimentation. They provide ecological and economic functions, whose values depend on the extent and elevation of the exposed flats (Barbier *et al.*, 2011). As habitats

This is an Open Access article distributed under the terms of the Creative Commons Attribution Non-Commercial License (http://creativecommons.org/licenses/by-nc/4.0), which permits unrestricted non-commercial use, distribution, and reproduction in any medium, provided the original work is properly cited.

Copyright © National Institute of Ecology.

and nursery grounds, tidal flats support fisheries and biodiversity; in particular, the tidal flats of the Republic of Korea are a globally important stopover and wintering site for migratory shorebirds along the East Asian-Australasian flyway, so that a contraction or spatial redistribution of exposed flat reduces the low-tide foraging area available to these birds and is a key consideration in habitat conservation planning (Lee *et al.*, 2023a). Tidal flats also store substantial organic carbon in their sediments and act as blue carbon sinks; changes in their extent and elevation alter carbon burial and are relevant to blue carbon accounting (Chen & Lee, 2022).

Tidal flats and their associated barrier islands dissipate wave energy and attenuate storm surges, buffering the mainland against typhoons and coastal flooding and provide natural coastal protection (Möller *et al.*, 2014; Narayan *et al.*, 2017). These landforms change continuously in response to tides, ocean waves, river discharge, human activities, and seasonal effects, and their global extent is rapidly changing (Murray *et al.*, 2019). As such changes propagate into the habitats, fisheries, carbon, and coastal protection functions noted above, the long-term monitoring of tidal flat areas and topography is essential for informed coastal management.

Satellite remote sensing is widely used for large-scale tidal flat monitoring because it provides spatially consistent observations over long periods. Of the available sensors, the synthetic aperture radar (SAR) is well suited for wetland analysis because it operates independently of weather conditions and provides a strong intensity contrast between water and non-water surfaces (Baek & Jung, 2019; Ryu *et al.*, 2002). Existing satellite methods for intertidal topography fall into two broad categories. In the waterline method, a digital elevation model (DEM) is reconstructed by tracing the boundary between water and exposed land across images acquired at different tidal levels (Liu *et al.*, 2013; Mason *et al.*, 2001; Ryu *et al.*, 2002). Multi-sensor implementations have recently been optimized for rapid and extensive mapping (Lee *et al.*, 2025a); however, this approach requires many clear acquisitions that are well distributed at the tidal level and are sensitive to waterline-extraction error.

In the pixel-frequency (inundation/exposure-frequency) method, intertidal topography is derived from how frequently each pixel is exposed across a long time series (Bishop-Taylor *et al.*, 2019; Kim *et al.*, 2021; Sagar *et al.*, 2017), with recent optical variants for complex estuaries (Chen *et al.*, 2023). This approach is more robust to individual-image errors because it aggregates many acquisitions but it has generally been applied to a single period and without explicit correction of the tidal and seasonal dependence of the measured area. Baek *et al.* (2023) applied the pixel-frequency approach to multi-temporal Sentinel-1 data in Gochang, Korea, and demonstrated the detection of geomorphological change but again, for a single period and without a long-term, tidally, and seasonally-corrected area time series.

For Nakdong River Estuary (NRE), long-term morphological changes have been documented from nautical charts (Yoo *et al.*, 2006), bathymetric surveys (Park *et al.*, 2014), geological and sedimentological analyses (Jeong *et al.*, 2022; 2024), and multi-temporal optical imagery (Kim *et al.*, 2024; Lee *et al.*, 2025b). These studies are however limited by sparse temporal sampling or, for optical sensors, by cloud cover, and none of them provide an all-weather, long-term SAR area time series corrected for acquisition conditions. This is because the tidal flat area detected in any single SAR image depends strongly on the tidal level and seasonal conditions at acquisition: higher tidal levels submerge more of the flat and reduce the detected area, whereas seasonal variation in river discharge, wave climate, and biological activity add fluctuations unrelated to genuine long-term change such that an apparent multi-year pattern may simply reflect the acquisition conditions. Strategies for decoupling such environmental influences from satellite time series have been demonstrated in related settings (e.g., caldera-lake water levels; Lee *et al.*, 2026); however, to our knowledge, an explicit tidal and seasonal correction of a long SAR-derived tidal flat area time series, combined with a pre-/post-event pixel-frequency spatial analysis, has not been reported for estuaries such as NRE. The present study addresses this gap in the literature.

The NRE in the southeastern part of the Korean Peninsula near Busan is a suitable site for studying long-term tidal flat change. It is a designated migratory bird sanctuary and one of the most important waterbird habitats in Korea. Barrier islands, tidal flats, and reed marshes support large wintering and passage populations of waterbirds, whose distribution closely follows the physical configuration of the tidal flats (Lee *et al.*, 2010). Over the past 90 years, the area has undergone considerable geomorphological change driven by human activities, including the construction of the Noksan dam (1934) and the NRE dam (1987), land reclamation, and periodic dredging for shipping channel maintenance (Lee *et al.*, 2023b). Barrier islands, such as Jinudo, Daemadeung, Baekhapdeung, Sinjado, and Doyodeung, have formed and evolved in response to these interventions. After an experimental floodgate opening period from 2018 to 2021, the NRE floodgates were opened permanently in February 2022 for the first time in 35 years, which changed the hydrodynamic conditions and sedimentation patterns of the estuary.

A preliminary version of the tidally- and seasonally-corrected area time series for the NRE was presented at a conference (Baek *et al.*, 2024). The present study substantially extends previous work by constructing pixel-frequency maps before and after the permanent floodgate

opening to resolve the spatial pattern of topographic change by checking this pattern for consistency against independent geological and optical studies of the same estuary and by examining its ecological implications.

In the current study, the long-term tidal flat area variation in NRE was analyzed using multi-temporal Sentinel-1 SAR data that span approximately 9 years (November 2014 to March 2023). The objectives were to: (1) extract tidal flat areas from 162 Sentinel-1 images and build a time series of tidal flat areas; (2) develop and apply a polynomial fitting approach that corrected for tidal level and seasonal dependencies, thereby isolating genuine long-term area anomalies; and (3) compare pixel-frequency maps between the pre- and post-floodgate opening periods to detect spatial patterns of topographical change.

Materials and Methods

Study area and data

Nakdong River Estuary

The study area covered the tidal flat wetlands of the NRE at the southeastern tip of the Korean Peninsula in Busan, Republic of Korea (Fig. 1). The NRE includes several barrier islands and tidal flats, including Eulsukdo, Daemadeung, Maenggeummurideung, Jinudo, Baekhapdeung, Sinjado, and Doyodeung, which developed through the interaction between fluvial sediment supply and tidal dynamics. Historical marine chart analyses have documented a century-scale, seaward expansion of these sand barriers (Yoo *et al.*, 2006). Over the past century, human activity has strongly affected this area. Jinudo and Daemadeung formed naturally in the 1910s; the Noksan Dam was constructed in 1934; Baekhapdeung emerged as a sandbar island in 1955; the NRE dam was completed in 1987, blocking natural tidal flow; and Sinjado and Doyodeung formed in 1975 and 1988, respectively (Lee *et al.*, 2023b). After the experimental floodgate openings from 2018 to 2021, the NRE dam floodgates were permanently opened in February 2022, restoring tidal exchange for the first time in 35 years. In the same year, dredging was conducted in Daemadeung to maintain the shipping channel.

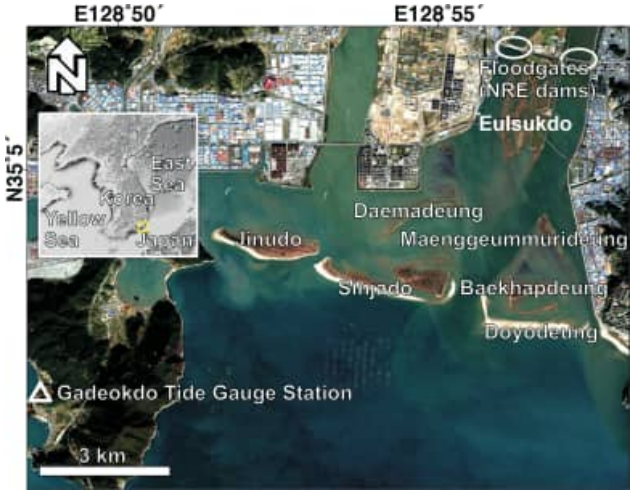

Fig. 1. Study area of the Nakdong River Estuary shown in a Sentinel-2 optical image acquired on November 1, 2016. The white box indicates the study area. Major barrier islands and tidal flats are labeled: Eulsukdo, Daemadeung, Maenggeummurideung, Jinudo, Baekhapdeung, Sinjado, and Doyodeung. The locations of the NRE floodgates (NRE dams), the tidal level gauging station (Gadeokdo).

Sentinel-1 data

A total of 162 Sentinel-1 single-look complex (SLC) images acquired in the interferometric wide swath mode with VV polarization from an ascending orbit were obtained. The data period spanned November 2014 to March 2023, with a nominal revisit interval of 12 days. The images were divided into two subsets based on the NRE floodgate opening: pre-opening period (November 2014 to February 2022; 135 images) and post-opening period (February 2022 to March 2023; 27 images). All images were acquired at 18:23 local time (KST, UTC+9) in the same relative orbit with an identical imaging geometry. After a 4:1 (range:azimuth) multi-look, the slant-range and azimuth pixel spacings were 9.32 m and 13.97 m, respectively, and the incidence angle over the study area was approximately 36.9°. Images with substantial mis-segmentation or missing tidal-level data were excluded to ensure data quality.

Auxiliary data

Two auxiliary datasets were used. First, the Copernicus DEM at 30-m resolution, derived from the TanDEM-X mission (2011-2015), was used to mask land areas from the SAR images (https://spacedata.copernicus.eu). Second, time-series tide-level data from the Gadeokdo gauging station were obtained from the Korea Hydrographic and Oceanographic Agency (http://www.khoa.go.kr/) at 1-min intervals. The tidal level at each SAR acquisition time was estimated by averaging the measurements within ±3 min of the acquisition time (18:23 KST); scenes with missing tidal records were excluded. The acquisition dates and corresponding tidal levels for all 162 scenes are shown in Fig. 2.

Methodology

Overall processing pipeline

The data processing pipeline consisted of four main stages (Fig. 3):

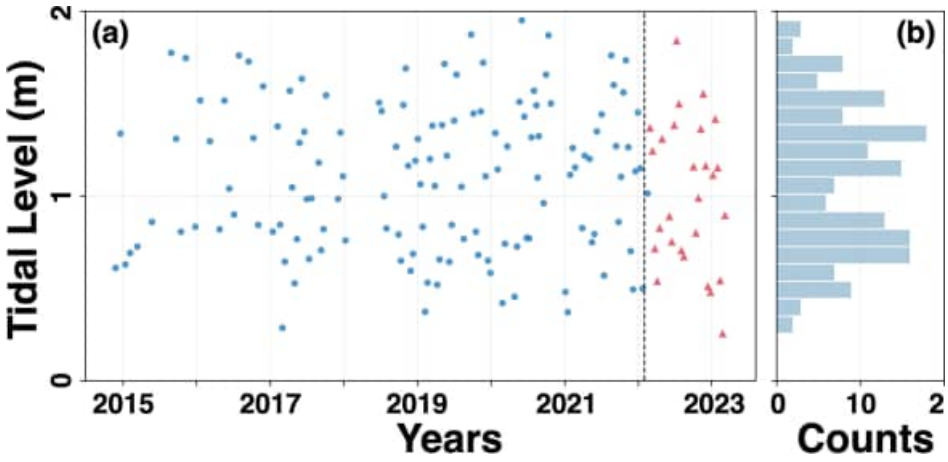

Fig. 2. Tidal levels at the Sentinel-1 acquisition times. (a) Tidal level at each of the 162 acquisitions plotted against the acquisition date; blue circles and red triangles denote the pre-opening (n=135) and post-opening (n=27) periods, respectively, and the vertical dashed line marks the permanent floodgate opening (February 2022). (b) Distribution of the tidal levels at the acquisition times. The acquisitions span a tidal-level range of 0.26-1.95 m.

(I) SAR data pre-processing, including radiometric calibration, speckle filtering, co-registration, and land masking; (II) tidal flat detection by backscatter thresholding; (III) pixel-frequency analysis for topographical change anomaly detection; and (IV) time-series area computation with tidal and seasonal correction. The stages are described in the following subsections.

All processing was conducted in the radar (slant range-azimuth) coordinate system without full geocoding or terrain correction. After the 4:1 range multi-look, the slant-range and azimuth pixel spacings were 9.32 m and 13.97 m, respectively. To obtain physically reasonable areas, the slant-range pixel area was converted to ground range by dividing by the sine of the incidence angle ($\theta \approx 36.9°$). This flat-earth conversion is appropriate for the near-flat relief of tidal flats; thus, the areas reported in this study are ground-range areas. As all 162 images were acquired in the same relative orbit with an identical imaging geometry and were co-registered to a common reference, this conversion applied a common, time-invariant factor and did not affect the relative temporal variations of the area (i.e., anomalies) or pixel-wise frequency comparisons at fixed image coordinates on which the conclusions rest. Full geocoding and terrain correction were not applied because an accurate intertidal topography of the study area was not available, and the near-flat relief of tidal flats rendered terrain-induced geometric distortions negligible.

As all maps are shown in radar (range-azimuth) coordinates, their orientation differs from a conventional north-up map projection. For the ascending, right-looking acquisition geometry used here, the radar coordinate display was inverted relative to the geographic north-up orientation. Geographic directions referred to in the text (e.g., east and west, or landward and seaward) and the assignment of the change zones to specific locations are therefore made after accounting for this radar-geometry orientation rather than read directly from the figures.

SAR data preprocessing

The raw Sentinel-1 SLC products were first converted to calibrated backscatter intensity (σ^0) on a decibel (dB) scale, and a 4:1 (range:azimuth) multi-look was applied to reduce speckle noise and improve the signal-to-noise ratio, giving slant-range and azimuth pixel spacings of 9.32 m and 13.97 m, respectively. The non-local means (NL-means) filter was then applied to suppress the remaining speckle while preserving the edges, which is important for accurate boundary delineation between the water and tidal flat surfaces (Buades *et al.*, 2011; Kim *et al.*, 2016; Penna & Mascarenhas, 2018). The NL-means filter estimates the noise-free value of each pixel as a weighted average of the pixels with similar local neighborhoods across the image, where the weights decrease as the patches become more dissimilar. All images were then co-registered to a common reference image (the visually-cleanest scene acquired on March 17, 2019) to remove the relative geometric offsets between the acquisitions. Finally, the Copernicus 30-m DEM was used to generate a land mask that excluded permanent land areas from the subsequent analysis.

Tidal flat detection

Tidal flat areas were extracted by thresholding the calibrated backscatter intensity. As open-water surfaces produce low, approximately Gaussian-distributed back-

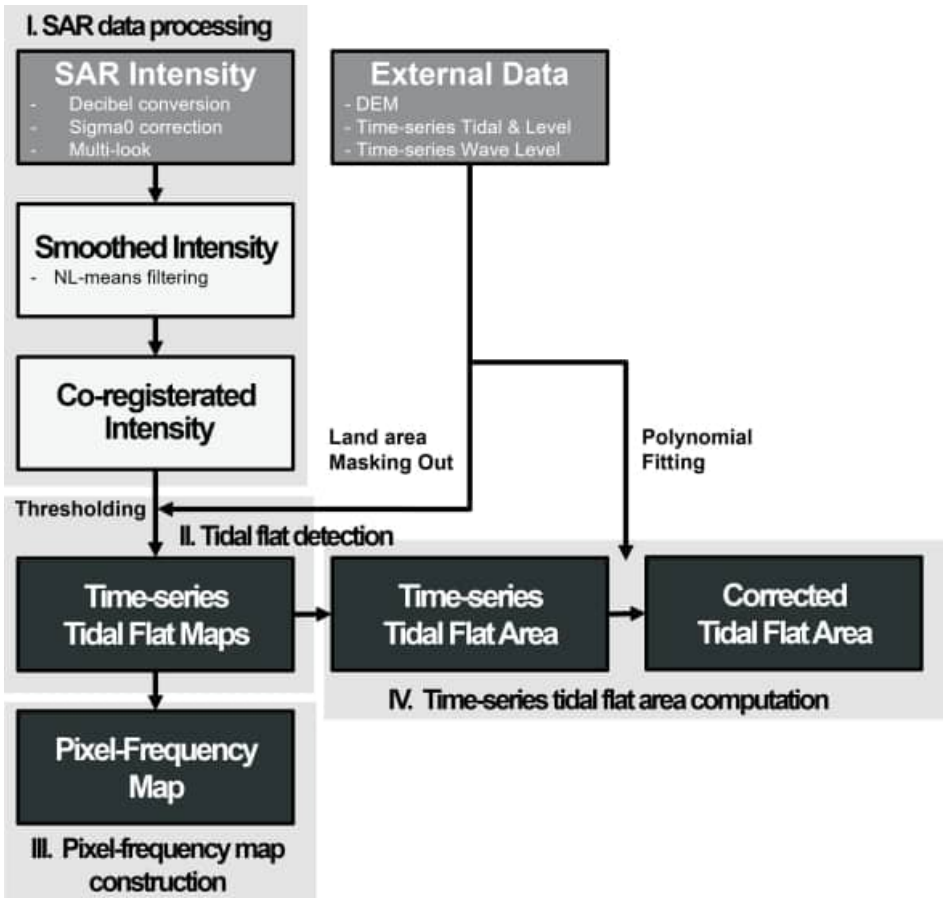

Fig. 3. Overall data processing pipeline. Stage I: synthetic aperture radar (SAR) data preprocessing including decibel conversion, sigma0 correction, multi-look, non-local-means (NL-means) filtering, co-registration, and land masking using a digital elevation model (DEM). Stage II: tidal flat detection using backscatter thresholding to produce time-series tidal flat maps. Stage III: pixel-frequency map construction for topographic change anomaly analysis. Stage IV: time-series tidal flat area computation with polynomial fitting correction for tidal level and seasonal effects, yielding corrected-area anomaly.

scatter, a single backscatter threshold was determined from the water backscatter distribution of the visually-cleanest scene of the time series (the March 17, 2019, acquisition, which was also used as the co-registration reference) and fixed at σ^0=−14.3 dB. This global threshold was applied over the cropped area of interest in a single pass, without per-image or iterative adjustment: pixels with σ^0 above −14.3 dB were classified as tidal flat (non-water) and those below as water. Regions that did not contain exposed sandbars (permanently open water) were removed using a fixed mask. The input scenes were preferentially selected for calm sea-surface (low-roughness) conditions to minimize false detection over water; from 192 candidate acquisitions, images that showed visually-evident mis-segmentation (predominantly from rough sea state) were excluded by visual inspection, leaving the 162 scenes used here (Park, 2016).

Pixel-frequency analysis

To analyze the spatial patterns of topographical changes before and after the NRE floodgate opening, the pixel-frequency method was applied (Baek *et al.*, 2023; Kim *et al.*, 2021; Liu *et al.*, 2013). For a set of multi-temporal binary tidal flat maps, the pixel frequency at each location is the ratio of the number of times that pixel is classified as a tidal flat to the total number of observations:

$$f(x, y)=Ntf(x, y)/Ntotal \quad (1)$$

where f(x, y) is the pixel frequency at location (x, y), Ntf is the number of tidal flat classifications, and Ntotal is the total number of images. Higher frequency values indicate locations that are more frequently exposed (i.e., at higher elevations), and lower values indicate areas that are predominantly submerged. Thus, the frequency map represents the relative topographical surface of the tidal flat.

Separate pixel-frequency maps were constructed for the pre-opening period (135 images from November 2014 to February 2022) and post-opening period (27 images from February 2022 to March 2023). Comparing the two maps identified spatial anomalies in the topographic changes associated with the floodgate opening. To verify that this comparison reflected genuine topographical changes rather than differing acquisition conditions, the tidal-level statistics (mean and standard deviation) of the two periods at the SAR acquisition times were compared (Fig. 2); the values and their interpretation are reported in Results section.

Tidal and seasonal correction of area time series

The total tidal flat area in each SAR image was computed by summing all the tidal flat pixels and multiplying by the pixel area. The raw area measurements depended strongly on the tidal level at the time of acquisition. To isolate the long-term area variation from these short-term fluctuations, a two-step polynomial correction was applied. More sophisticated multivariate approaches to environmental signal decoupling have recently been proposed (e.g., a deep-learning-based correction of hydro-meteorological influences on lake water levels; Lee *et al.*, 2026) but a simple polynomial formulation was adopted here as a first-order approximation appropriate for a feasibility-level analysis.

In the first step, the relationship between the measured tidal flat area and the tidal level was modeled using a second-order polynomial:

$$\hat{A}=a_1h^2+b_1h+c_1 \quad (2)$$

where $\hat{A}$ is the predicted tidal flat area (km²), h is the tidal level (m), and a_1, b_1, c_1 are the fitted polynomial coefficients.

The tidal area anomaly was computed as the residual: $\Delta A_{tidal}=A_{observed}-\hat{A}$. This eliminated the dominant tidal dependency from the area time series.

In the second step, the remaining seasonal component in the tidal-corrected anomaly was modeled as a function of the decimal day of the year using another second-order polynomial:

$$\Delta A_{seasonal}=a_2d^2+b_2d+c_2 \quad (3)$$

where d is the decimal day of year (0-1), and a_2, b_2, c_2 are the fitted polynomial coefficients.

The final, corrected area anomaly, representing the long-term variation, was obtained by subtracting this seasonal component: $\Delta A_{final}=\Delta A_{tidal}-\Delta A_{seasonal}$. This two-step correction removed the dominant short-term fluctuations caused by tidal level and seasonal effects and enabled the identification of genuine long-term patterns in tidal flat area.

Results

SAR intensity and tidal flat maps

Fig. 4 shows the annual, preprocessed SAR intensity images from 2015 to 2022 in the radar coordinate system, and Fig. 5 shows the corresponding thresholded water/non-water binary segmentation maps. The effect of tidal level on the detected tidal flat extent is clear: images acquired at lower tidal levels (e.g., 0.80-0.84 m) showed much larger, exposed, tidal flat areas than did those acquired at higher tidal levels (e.g., 1.49-1.56 m). This comparison shows why tidal correction is necessary for reasonable analysis of long-term area patterns. The NL-means filtered intensity images showed a clear contrast between the water (dark) and exposed tidal flat surfaces (bright), which supports the accurate delineation of the tidal flat boundary.

Pixel-frequency maps and topographical change anomaly

Fig. 6 shows the pixel frequency maps generated before and after the opening of the permanent floodgate in February 2022 (pre-opening: 135 images; post-opening: 27 images). A comparison of the two maps indicated five distinct zones of topographical change, labeled A-E. The geographical position of each zone accounted for the radar-geometry orientation of the maps. In zone A, on the tidal flat between Jinudo and the Noksan industrial complex on the western side of the estuary, the pixel frequency increased in the post-opening period compared with that in the pre-opening period, indicating an increase in elevation. In contrast, zones B-E had a reduced pixel frequency, suggesting erosion or subsidence. The reductions in zone E, on the wetland immediately south of Eulsukdo

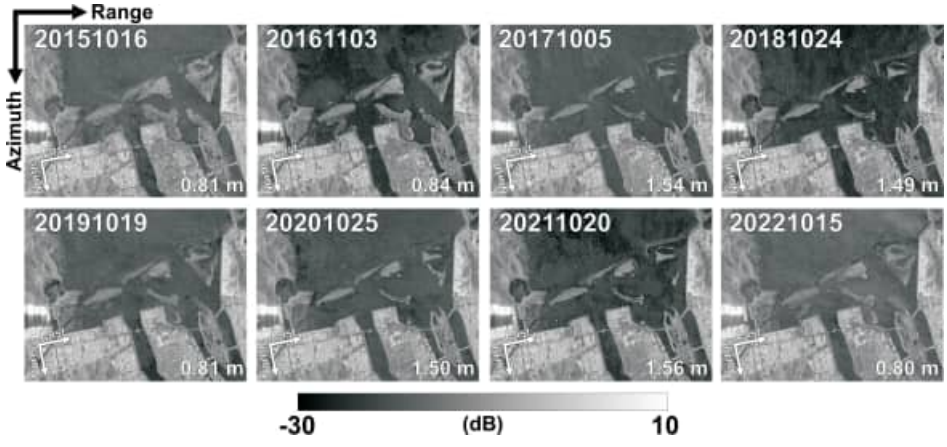

Fig. 4. Examples of the preprocessed Sentinel-1 synthetic aperture radar intensity images in the radar coordinate system (annual representatives, 2015-2022). The tidal level at the time of acquisition is annotated for each image: 0.81 m (2015.10.16), 0.84 m (2016.11.03), 1.54 m (2017.10.05), 1.49 m (2018.10.24), 0.81 m (2019.10.19), 1.50 m (2020.10.25), 1.56 m (2021.10.20), and 0.80 m (2022.10.15).

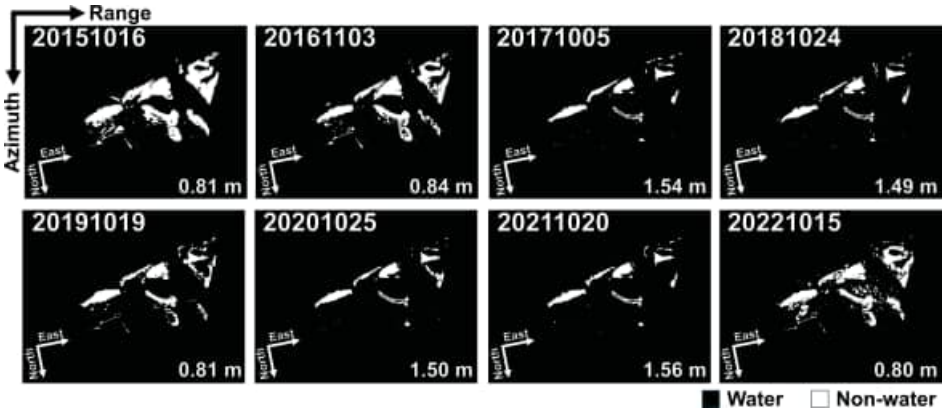

Fig. 5. Examples of the thresholded synthetic aperture radar data (water/non-water binary segmentation maps) in the radar coordinate system, corresponding to the images in Fig. 4. Note the clear inverse relationship between tidal level and exposed tidal flat extent.

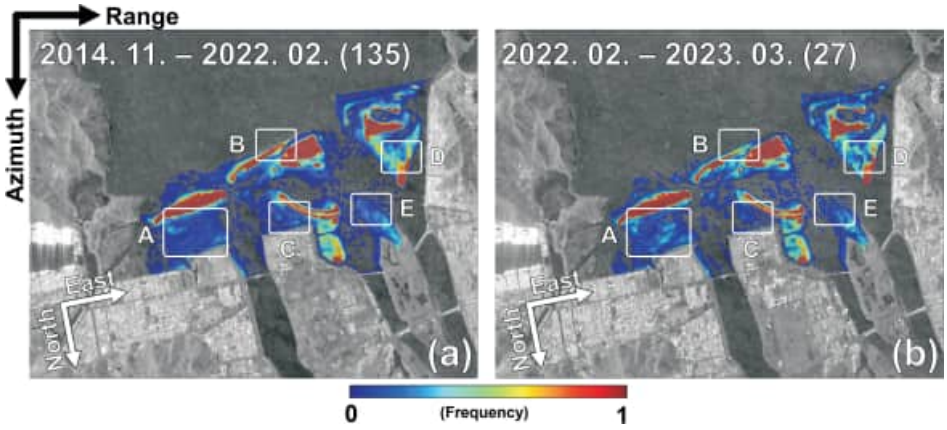

Fig. 6. Pixel-frequency maps generated before (a; 135 images) and after (b; 27 images) the permanent NRE floodgate opening in February 2022, shown in the radar coordinate system. Five change zones (A-E) are identified: zone A (between Jinudo and the Noksan industrial complex, western side) shows increased frequency (deposition); zones B-E show decreased frequency (erosion/subsidence). Zone E (wetland immediately south of Eulsukdo, directly downstream of the floodgates) and zone D (between Maenggeummurideung and Baekhapdeung) lie along the eastern main channel; zone C (between Daemadeung and the landward side) coincides spatially with dredging for shipping channels; and zone B, located on the seaward (southern) front of Sinjado, is interpreted to show a relative decrease in elevation due to erosion, possibly associated with a temporary increase in ocean wave energy. The frequency scale ranges from 0 (always submerged) to 1 (always exposed).

and thus directly downstream of the opened floodgates, and in zone D, between Maenggeummurideung and Baekhapdeung along the eastern main channel, were consistent with enhanced erosion under increased tidal flow after the permanent floodgate opening. Zone C, between Daemadeung and the landward side of the estuary, coincided spatially with the dredging carried out for shipping channel maintenance. Zone B, located on the seaward (southern) front of Sinjado, was interpreted as showing a relative decrease in elevation due to erosion, possibly associated with a temporary increase in ocean wave energy.

To assess the validity of the pixel-frequency comparison, tidal-level statistics for the two periods were compared (Figs. 2, 7). The mean tidal levels during SAR acquisition were 1.10 m for the pre-opening and 1.01 m for the post-opening period, with standard deviations of 0.40 m and 0.39 m, respectively. The two distributions were broadly similar, with a mean difference of approximately 0.09 m. This supports the interpretation that the observed changes in the pixel frequency patterns mainly reflect topographic changes rather than systematic differences in tidal conditions between the two periods.

Time-series tidal flat area and tidal correction

The tidal level and total tidal flat area time series derived from the 162 Sentinel-1 images are shown in Fig. 8a, b. The measured area (converted to ground range) varied substantially from 2-12 km^2.

Across most of the observed tidal ranges, the tidal flat area decreased as the tidal level increased (an approximately inverse relationship). The second-order polynomial fit yielded $A=4.0h^2-13.7h+14.5$, where A is the area (km^2)

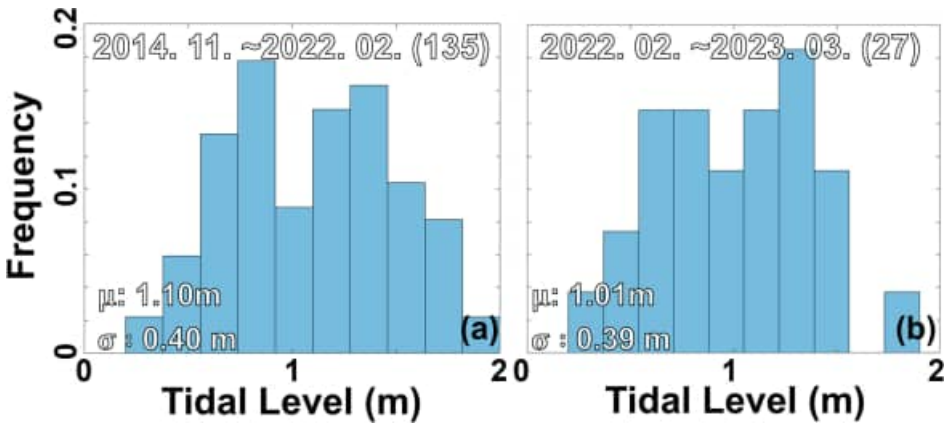

Fig. 7. Histograms of tidal level at the synthetic aperture radar acquisition times for the (a) pre- and (b) post-opening periods (before and after February 2022). The mean tidal levels are 1.10 m (pre-opening; 135 images) and 1.01 m (post-opening; 27 images), with standard deviations of 0.40 m and 0.39 m, respectively.

and h is the tidal level (m) (Fig. 8c). This empirical fit was used only as a hypsometric approximation within the observed tidal range and was not extrapolated beyond it. After the tidal correction, the area anomaly (ΔA_{tidal}) showed reduced variability while preserving the underlying long-term signal (Fig. 8d).

Seasonal correction and final area anomaly

The tidal-corrected area anomaly exhibits a seasonal pattern when plotted against the decimal day of the year (Fig. 8e). A second-order polynomial fit ($\Delta A_{seasonal}=-3.5d^2+3.8d-0.7$) was applied to model and remove this seasonal component. The resulting corrected area anomaly is shown in Fig. 8f. The two-step correction reduced the standard deviation of the area time series from 2.26 km² before correction to 1.00 km² after the tidal correction and 0.96 km² after the additional seasonal correction, confirming that most of the acquisition-condition-driven variability had been removed. The tidal flat area tended to decrease from 2015 to 2017, followed by a slight increase or stabilization; a linear fit indicated a decrease of approximately –0.32 km²/year from 2015-2017, after which, the rate stabilized (approximately –0.03 km²/year).

The periods of the experimental floodgate opening (2018-2021) and the permanent opening (from February 2022) are annotated in the Fig. 8. Although the post-opening period was relatively short (~1 year), no apparent drastic shift in the corrected area anomaly was observed at the whole-estuary scale, suggesting that localized changes (as identified in the pixel-frequency analysis) may not have appeared in the aggregate area metric. Quantifying such an internal redistribution would require a zone-wise decomposition of the corrected area time series together with an assessment of its sampling uncertainty, which was outside the scope of this study.

Discussion

The multi-temporal Sentinel-1 SAR data, combined with correction for tidal and seasonal effects, indicated a long-term tidal flat area variation that short-term acquisition-condition dependencies would otherwise obscure. The raw area time series varied by more than 4 km² around the mean, mainly because of tidal level differences among the acquisitions. Without correction, this variability could be mistaken for genuine geomorphological changes. A two-step polynomial correction reduced this noise and isolated a more coherent long-term signal. The reduction from 2015 to 2017, followed by stabilization, may reflect a mix of natural sediment dynamics and the cumulative effects of earlier human interventions, although attributing specific causes requires additional evidence from field observations and hydrodynamic modeling.

These results can be compared with earlier work on the geomorphology of the NRE, although differences in the method, area definition, and observation period limit the comparison to the direction and timing of the change rather than absolute area values. Early marine chart analyses spanning nearly a century (1927-1995) documented the long-term changes in the intertidal and sand barrier areas of the estuary, including a net increase in the sand barrier area after the 1980s (Yoo *et al.*, 2006). Bathymetric surveys of the Jinudo-Sinjado shoreface between 2007 and 2012 reported an overall depositional pattern that was strongly correlated with suspended sediment discharge from the Nakdong River, albeit with pronounced local variability (Park *et al.*, 2014). Satellite studies have extended these observations over the past decade. A multi-temporal optical analysis estimated the NRE tidal flat area at 9.4-9.9 km² for 2019-2023 and reported a relative stabilization, with inter-annual fluctuations of up to approximately 5.4% that were attributed to natural sediment dynamics rather than human forcing (Kim *et al.*, 2024). Sandbar morphology has also been tracked with SPOT imagery over similar periods (Lee *et al.*, 2025b). The

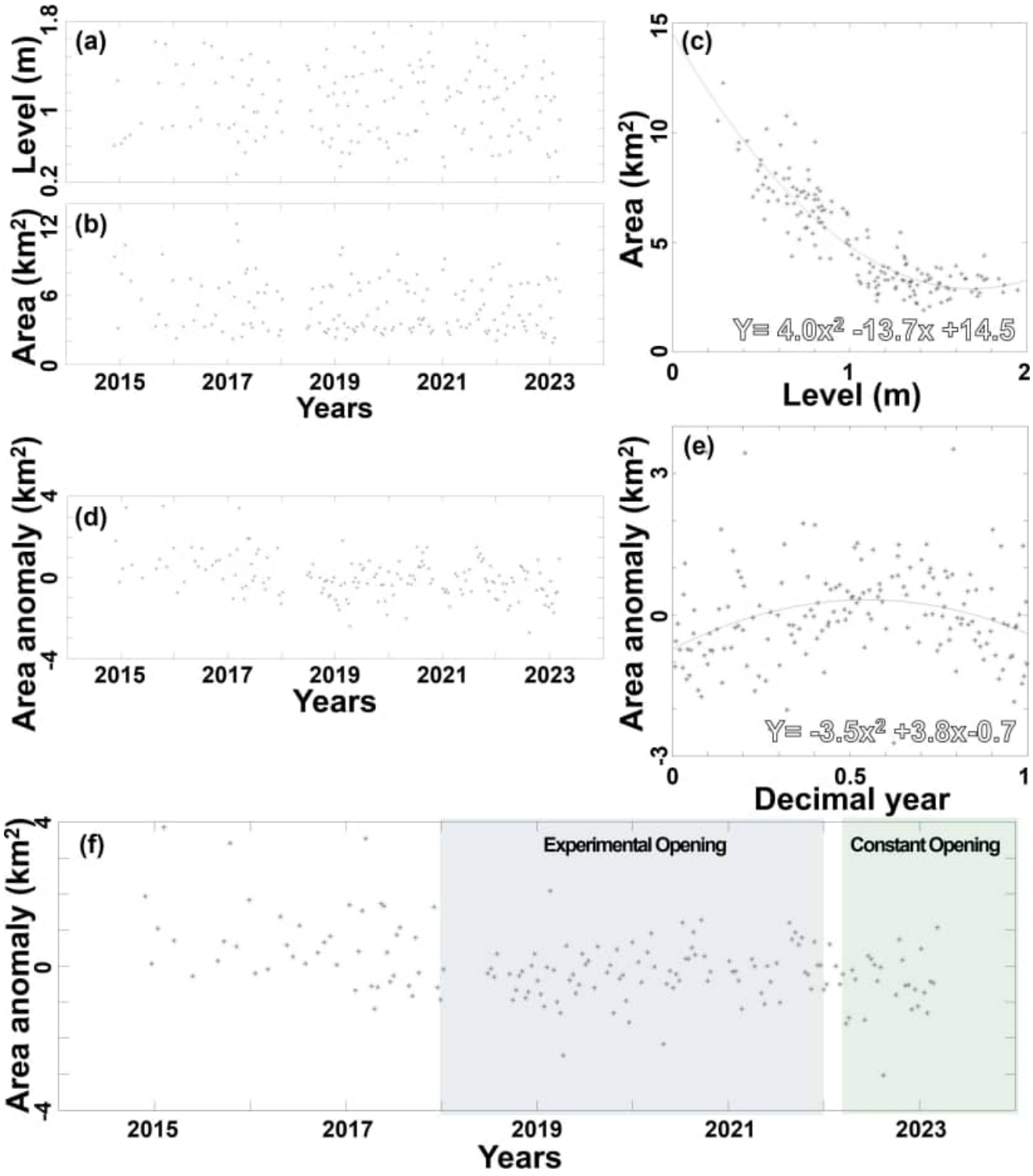

Fig. 8. Time-series area anomaly variation: (a) tidal level at the synthetic aperture radar acquisition times; (b) tidal flat area; (c) the relationship between tidal level and tidal flat area with the fitted second-order polynomial ($A=4.0h^2-13.7h+14.5$); (d) tidal flat area anomaly after correcting the tidal level effect; (e) seasonal effects of the tidal flat area anomaly with the fitted seasonal polynomial ($\Delta A_{seasonal}=-3.5d^2+3.8d-0.7$); (f) final tidal flat area anomaly after correcting both tidal level and seasonal effects. The periods of experimental floodgate opening (2018-2021) and permanent opening (from February 2022) are annotated in (f).

stabilization in that optical record is consistent with the leveling-off of the current corrected-area anomaly after 2017, and the description of several percent inter-annual variability as a natural, acquisition-independent signal supports the need for the tidal and seasonal correction applied here. However, the mid-2010s decrease resolved in the current time series could not be directly cross-validated against the optical record, which lacks annual coverage from 2013 to 2019; a more detailed comparison must await denser and longer optical and radar time series. Consistent with the interpretation that the estuary has been approaching a quasi-equilibrium configuration after a century of human modification (Jeong *et al.*, 2022), the current SAR-based, tidal- and seasonally-corrected time series provides a complementary, all-weather record that isolates the long-term component of the area signal that the acquisition conditions would otherwise obscure.

The pixel frequency comparison between the pre- and post-floodgate opening periods provides spatially explicit indications of topographic changes that coincide with the restoration of tidal exchange. The erosion patterns near the floodgates (zones D and E) were consistent with the geological response recently documented for the same estuary. Using bathymetric and sedimentological surveys, Jeong *et al.* (2024) found that the regular opening of the eastern NRE dam gates enhanced the ebb tidal prism and produced erosional topography and landward-migrating (transgressive) barrier islands on the eastern side, in contrast to the depositional, seaward-prograding regime maintained by the predominantly-closed, western (Noksan) gates. After accounting for the radar-geometry orientation of the current maps, the spatial arrangement of the change zones was consistent with this asymmetry: the frequency reductions in zone E, immediately south of Eulsukdo and thus directly downstream of the opened gates, and in zone D, further along the eastern main channel between Maenggeummurideung and Baekhapdeung, lie on the eastern discharge path; whereas the frequency increase in zone A was on the western flat between Jinudo and the Noksan industrial complex, where the Noksan gates were predominantly closed.

A quantitative, zone-wise assessment of these changes, including their significance against pixel-frequency sampling uncertainty, is beyond the scope of the present feasibility level analysis, thus warranting further studies. This spatial correspondence is also supported by long-term sedimentological monitoring, which shows that the total barrier-island area of the NRE, which declined after the 1987 dike-gate construction, has undergone marked morphological changes as the system shifted to wave-, tide-, and discharge-dominated conditions (Lee *et al.*, 2023b). The permanent floodgate opening and dredging at Daemadeung occurred in the same year; therefore, the individual contributions of these concurrent drivers could not be separated from the present data. The spatial coincidence of zone C with the reported dredging shows both the sensitivity of the pixel-frequency method to localized change and the difficulty of attributing any single cause. Overall, these spatial patterns are consistent with the current understanding of NRE dynamics; however, the agreement should be regarded as a qualitative consistency check rather than a quantitative validation, given the absence of direct field data for the study period.

This study has some limitations. The post-opening period contained only 27 images spanning approximately 1 year, which limited the robustness of the conclusions regarding the long-term impact of the floodgate opening. As the accuracy of pixel-frequency-derived tidal flat topography improves as the number of acquisitions increases (Lee *et al.*, 2025a; Liu *et al.*, 2013), the frequency map derived from the 27 post-opening images carried a larger error than that derived from the 135 pre-opening images. The two maps therefore differ in their expected error magnitude, and the pre- versus post-opening comparison is interpreted qualitatively rather than as an exact measure of the magnitude of topographic change. As Sentinel-1 data continue to be archived, re-analysis using an extended post-opening dataset is essential.

The tidal and seasonal corrections are based on second-order polynomial fitting, which assumes smooth, stationary relationships between the area and these factors; the seasonal term is a polynomial in the decimal day of the year and does not enforce continuity across the year boundary. This simple form was retained because the seasonal term served only to remove a nuisance signal; the correction reduced the variance of the area series linearly and the long-term tendency was dominated by the inter-annual signal and was thus more robust than the seasonal model (the implied year-boundary discontinuity was small, ~0.3 km², versus the >4 km² raw variability). Additional corrections for wave height, river discharge, precipitation, exposure duration, and a cyclic formulation, such as harmonic regression, could refine the correction in future work.

The analysis was conducted for the entire study area as a single unit. Given the complex channel geometry of the NRE, with distinct sediment transport regimes in different subareas, a segment-by-segment analysis is planned for future work. No concurrent in situ survey was available for the study period such that the detected changes were at a qualitative to semi-quantitative level, and a formal per-pixel classification validation (e.g., confusion matrix, F1-score, Intersection over Union) was not conducted, consistent with common practice for pixel-frequency and waterline topographic studies whose conclusions rest on aggregated relative quantities rather than single-scene classification accuracy. In particular, the magnitude of topographic change between the two pixel-frequency

maps should ultimately be evaluated through propagation of the expected pixel-wise elevation errors; such uncertainty estimates for pixel-frequency-derived topography are not yet available for the study area, and their rigorous derivation is beyond the scope of this feasibility-level analysis. The integration with field survey data, SAR-derived DEMs, and other satellite observations would strengthen the validation of these findings.

The tidal levels used to characterize each acquisition were obtained from the Gadeokdo gauging station, which lies at some distance from the study area. As tidal amplitude and phase vary spatially within and around the estuary, these values may not exactly represent the tidal level over the barrier islands and flats at each acquisition time, introducing an additional source of uncertainty into the tidal correction.

Some isolated bright pixels remained over the water surface in the binary and pixel-frequency maps. Additional spatial filtering was not applied in areas of expected topographic change because each pixel-frequency map was averaged over many acquisitions such that spatially random, transient misclassifications would have been suppressed in proportion to the number of images; whereas a persistent change would accumulate across dates into a coherent pattern. The SAR data alone could not distinguish a transient misclassification from a genuine short-lived change; therefore, aggressive filtering would risk removing real signals. Permanent open water was masked beforehand, and the scenes were preselected for a calm sea state, which further limited false detection. This residual, largely tide-independent noise mainly affected individual scene area estimates rather than the relative long-term anomalies.

In addition to their geomorphological significance, the long-term area and topographic changes documented in this study have ecological implications for NRE. The NRE is a globally important habitat for migratory waterbirds whose distribution is closely tied to the physical configuration of the tidal flats (Lee *et al.*, 2010); therefore, a sustained contraction or spatial redistribution of exposed tidal flats, such as the 2015-2017 decrease and the localized erosion near the floodgates found here, may reduce or shift the intertidal foraging area available to shorebirds during low tide. This link underlies the conservation value of Korean tidal flats as flyway stopover sites (Lee *et al.*, 2023a). Changes in tidal flat extent and elevation may also affect their function as blue-carbon sinks because unvegetated tidal flats store substantial sedimentary carbon (Chen & Lee, 2022), and the global pattern of tidal flat loss shows the value of the long-term, satellite-based monitoring demonstrated here (Murray *et al.*, 2019). The present analysis did not quantify these ecological responses; establishing them would require integration with in situ biological and sedimentological observations, which were identified as an important direction for future research.

Despite these limitations, this study provides a long-term, SAR-based baseline record of tidal flat area variation at NRE spanning the 2022 permanent floodgate opening, together with a practical procedure for correcting acquisition-condition dependencies that is applicable to other estuarine and coastal environments monitored by multi-temporal SAR. The combination of area correction and pixel-frequency analysis provides complementary information: the former captures aggregated patterns and the latter indicates spatial patterns of change. Future work should also examine the response of individual barrier islands and tidal flats to specific events such as typhoons, nearby construction, and seasonal flood pulses, which can directly affect sedimentation and erosion patterns at NRE.

Conclusion

This study analyzed the long-term tidal flat area variation in the NRE using 162 multi-temporal Sentinel-1 SAR images from November 2014 to March 2023. A two-step polynomial correction was applied to remove the tidal levels and seasonal dependencies from the raw area time series, such that genuine long-term area anomalies could be extracted. The corrected area anomalies tended to decrease from 2015 to 2017, followed by a slight increase or stabilization. Pixel-frequency maps constructed for the pre- and post-floodgate opening periods identified five zones of topographic change (A-E), with erosion along the eastern main channel downstream of the opened floodgates and deposition on the western landward flat. This spatial pattern was consistent with the east-west asymmetric hydrodynamic response expected under the gate operation regime.

The main contributions of this study are three-fold: (1) a long-term record of tidal flat area variation at NRE from multi-temporal SAR data with explicit correction for tidal and seasonal dependencies, (2) evidence that this correction is essential for reliable long-term monitoring because uncorrected area measurements show variability that can mask genuine patterns, and (3) spatial identification of topographic change zones associated with the 2022 permanent floodgate opening using the pixel-frequency method, checked for consistency against independent geological and optical studies of the same estuary.

Future work will focus on (1) extending the analysis with newly-archived Sentinel-1 data to strengthen the post-opening tendency assessment; (2) analyzing the corrected area change separately for each channel-bounded sub-area of the estuary to resolve the internal spatial redistribution that the whole-estuary metric could not capture; (3) incorporating additional correction factors,

including wave height, river discharge, and exposure duration; and (4) validating the detected changes through integration with field survey data and complementary satellite observations.

Author Contributions

Conceptualization: WKB. Data curation: MJL, KK. Formal analysis: WKB. Funding acquisition: JHR. Investigation: JHL. Methodology: WKB. Software: WKB. Supervision: JHR. Validation: JHL. Visualization: KK. Writing – original draft: WKB. Writing – review & editing: MJL, SHP, JHR.

Conflict of Interest

The authors declare that they have no competing interests.

Acknowledgments

The authors thank the European Space Agency for providing Sentinel-1 and Sentinel-2 imagery and the Korea Hydrographic and Oceanographic Agency for the tidal data used in this study.

Funding

This research was supported by the Korea Institute of Marine Science and Technology (KIMST) funded by the Ministry of Oceans and Fisheries, Korea (RS-2023-00254717).

References

Baek, W., and Jung, H. (2019). A review of change detection techniques using multi-temporal synthetic aperture radar images. *Korean Journal of Remote Sensing,* 35, 737-750. https://doi.org/10.7780/kjrs.2019.35.5.1.10

Baek, W., Lee, M., Lee, J., Kim, K., Lee, J., Kwak, G., *et al*. (2024). *Measurement of long-term tidal flat area variation using multi-temporal Sentinel-1 at Nakdong River Estuary via tidal and seasonal effect mitigation*. Paper presented at *IGARSS 2024 - 2024 IEEE International Geoscience and Remote Sensing Symposium,* Athens, Greece.

Baek, W., Lee, M., Yu, H., Ryu, J., and Kim, J. (2023). Topographical change mapping of estuarine wetland, Gochang, Korea via multi-temporal pixel-frequency approach using Sentinel-1. *Korean Journal of Remote Sensing,* 39, 1747-1761. https://doi.org/10.7780/kjrs.2023.39.6.3.7

Barbier, E.B., Hacker, S.D., Kennedy, C., Koch, E.W., Stier, A.C., and Silliman, B.R. (2011). The value of estuarine and coastal ecosystem services. *Ecological Monographs,* 81, 169-193. https://doi.org/10.1890/10-1510.1

Bishop-Taylor, R., Sagar, S., Lymburner, L., and Beaman, R.J. (2019). Between the tides: modelling the elevation of Australia's exposed intertidal zone at continental scale. *Estuarine, Coastal and Shelf Science,* 223, 115-128. https://doi.org/10.1016/j.ecss.2019.03.006

Buades, A., Coll, B., and Morel, J. (2011). Non-local means denoising. *Image Processing On Line,* 1, 208-212. https://doi.org/10.5201/ipol.2011.bcm_nlm

Chen, C., Zhang, C., Tian, B., Wu, W., and Zhou, Y. (2023). Tide2Topo: a new method for mapping intertidal topography accurately in complex estuaries and bays with time-series Sentinel-2 images. *ISPRS Journal of Photogrammetry and Remote Sensing,* 200, 55-72. https://doi.org/10.1016/j.isprsjprs.2023.05.004

Chen, Z.L., and Lee, S.Y. (2022). Tidal flats as a significant carbon reservoir in global coastal ecosystems. *Frontiers in Marine Science,* 9, 900896. https://doi.org/10.3389/fmars.2022.900896

Jeong, J.B., Jung, H., Lee, J., Park, K.K., Kim, S.Y., and Woo, H.J. (2022). Evolution and sedimentation mechanisms of estuarine beach in the Nakdong River estuary, Korea: natural and human impact. *Ocean Science Journal,* 57, 451-466. https://doi.org/10.1007/s12601-022-00070-2

Jeong, J.B., Woo, H.J., Jung, H., Ryu, J., Kim, K., and Kang, J. (2024). Morphological and geological responses of barrier estuaries to dam-opening systems. *Geo-Marine Letters,* 44, 19. https://doi.org/10.1007/s00367-024-00781-6

Kim, D., Jung, H., and Baek, W. (2016). Comparative analysis among radar image filters for flood mapping. *Journal of the Korean Society of Surveying, Geodesy, Photogrammetry and Cartography,* 34, 43-52. https://doi.org/10.7848/ksgpc.2016.34.1.43

Kim, K., Jung, H.C., Choi, J., and Ryu, J. (2021). Statistical analysis for tidal flat classification and topography using multi-temporal SAR backscattering coefficients. *Remote Sensing,* 13, 5169. https://doi.org/10.3390/rs13245169

Kim, M., Park, J., and Hyun, C. (2024). Evaluating changes in blue carbon storage by analyzing tidal flat areas using multi-temporal satellite data in the Nakdong River estuary, South Korea. *Korean Journal of Remote Sensing,* 40, 191-202. https://doi.org/10.7780/kjrs.2024.40.2.6

Lee, C., Jang, J., Jeong, K., Kim, D., and Joo, G. (2010). Patterning habitat preference of avifaunal assemblage on the Nakdong River estuary (South Korea) using self-organizing map. *Ecological Informatics,* 5, 89-96. https://doi.org/10.1016/j.ecoinf.2009.09.014

Lee, E., Park, S., Baek, W., Jung, H., Lee, H., and Park, S. (2026). Deep learning-based decoupling of hydro-meteorological signals from Cheonji caldera lake water levels for volcanic precursor detection. *ISPRS Journal of Photogrammetry and Remote Sensing,* 240, 89-113. https://doi.org/10.1016/j.isprsjprs.2026.07.006

Lee, J., Kim, I., Lee, S., Son, J., Jang, J., and Sung, H. (2023a). International importance of tidal flats in the Republic of Korea as shorebird stopover sites in the East Asian–Australasian flyway. *Avian Conservation and Ecology,* 18, 23. https://doi.org/10.5751/ace-02449-180123

Lee, J., Kim, K., Kwak, G., Baek, W., Jang, Y., and Ryu, J. (2025a). Optimization of a multi-sensor satellite-based waterline method for rapid and extensive tidal flat topography mapping. *Estuarine, Coastal and Shelf Science,* 318, 109235. https://doi.org/10.1016/j.ecss.2025.109235

Lee, J., Woo, H.J., Jung, H., Jeong, J.B., and Park, K. (2023b). Characteristics of sedimentation based on data from the Nakdong estuary information service system (NEISS), South Korea. *Estuarine, Coastal and Shelf Science,* 293, 108479. https://doi.org/10.1016/j.ecss.2023.108479

Lee, S., Hyun, C., and Kim, S. (2025b). Assessing sandbar morphology in the Nakdong River Estuary using SPOT series satellite imagery. *Marine Georesources & Geotechnology,* 43, 1013-1023. https://doi.org/10.1080/1064119x.2024.2378074

Liu, Y., Li, M., Zhou, M., Yang, K., and Mao, L. (2013). Quantitative analysis of the waterline method for topographical mapping of tidal flats: a case study in the Dongsha Sandbank, China. *Remote Sensing,* 5, 6138-6158. https://doi.org/10.3390/rs5116138

Mason, D.C., Davenport, I.J., Flather, R.A., Gurney, C., Robinson, G.J., and Smith, J.A. (2001). A sensitivity analysis of the waterline method of constructing a digital elevation model for intertidal areas in ERS SAR scene of eastern England. *Estuarine, Coastal and Shelf Science,* 53, 759-778. https://doi.org/10.1006/ecss.2000.0789

Möller, I., Kudella, M., Rupprecht, F., Spencer, T., Paul, M., van Wesenbeeck, B.K., *et al*. (2014). Wave attenuation over coastal salt marshes under storm surge conditions. *Nature Geoscience,* 7, 727-731. https://doi.org/10.1038/ngeo2251

Murray, N.J., Phinn, S.R., DeWitt, M., Ferrari, R., Johnston, R., Lyons, M.B., *et al*. (2019). The global distribution and trajectory of tidal flats. *Nature,* 565, 222-225. https://doi.org/10.1038/s41586-018-0805-8

Narayan, S., Beck, M.W., Wilson, P., Thomas, C.J., Guerrero, A., Shepard, C.C., *et al*. (2017). The value of coastal wetlands for flood damage reduction in the northeastern USA. *Scientific Reports,* 7, 9463. https://doi.org/10.1038/s41598-017-09269-z

Park, J., Khim, B., Lee, H.J., and Lee, S.R. (2014). Recent morphological changes off the shoreface of Jinwoodo and Sinjado in the Nakdong River Estuary: 2007-2012. *Ocean and Polar Research,* 36, 87-101. https://doi.org/10.4217/opr.2014.36.2.087

Park, S. (2016). Detection of water bodies from Kompsat-5 SAR data. *Korean Journal of Remote Sensing,* 32, 539-550. https://doi.org/10.7780/kjrs.2016.32.5.11

Penna, P.A.A., and Mascarenhas, N.D.A. (2018). (Non-)homomorphic approaches to denoise intensity SAR images with non-local means and stochastic distances. *Computers & Geosciences,* 111, 127-138. https://doi.org/10.1016/j.cageo.2017.11.006

Ryu, J., Won, J., and Min, K. (2002). Waterline extraction from Landsat TM data in a tidal flat: a case study in Gomso Bay, Korea. *Remote Sensing of Environment,* 83, 442-456. https://doi.org/10.1016/s0034-4257(02)00059-7

Sagar, S., Roberts, D., Bala, B., and Lymburner, L. (2017). Extracting the intertidal extent and topography of the Australian coastline from a 28 year time series of Landsat observations. *Remote Sensing of Environment,* 195, 153-169. https://doi.org/10.1016/j.rse.2017.04.009

Yoo, C., Yoon, H., Ryu, C., and Lee, I. (2006). Spatiotemporal changes of the sand barrier using marine charts analysis in the Nakdong River estuarine. *Journal of Ocean Engineering and Technology,* 20, 54-60.

PNIE PROCEEDINGS OF THE NATIONAL INSTITUTE OF ECOLOGY OF THE REPUBLIC OF KOREA

Original Article

PNIE 2026;7(4):213-224
https://doi.org/10.22920/PNIE.2026.7.4.213
pISSN 2765-2203, eISSN 2765-2211

U-Net Semantic Segmentation of Quadrat Underwater Imagery for Automated Benthic Cover Classification

Sung-Hwan Park[1], Nam-Hoon Kim[1], Won-Kyung Baek[2], Soonyoung Choi[3,4], Jong-Seok Lee[1], Euiyoung Jeong[5]*

[1]Marine Natural Disaster Research Department, Korea Institute of Ocean Science and Technology, Busan, Korea
[2]Korea Ocean Satellite Center, Korea Institute of Ocean Science and Technology, Busan, Korea
[3]Dokdo Research Center, East Sea Research Institute, Korea Institute of Ocean Science and Technology, Uljin, Korea
[4]Division of Science Education, Kangwon National University, Chuncheon, Korea
[5]Marine Infra Support Team, Korea Institute of Ocean Science and Technology, Busan, Korea

ABSTRACT

Quadrat-based underwater photography is a widely used tool that assesses the status of coastal benthic ecosystems. However, the interpretation of benthic cover is still performed manually by experts, making it labor-intensive and subjective. This study investigated how accurately U-Net segmentation can classify benthic cover in quadrat underwater imagery and evaluated three hierarchical tasks: quadrat frame detection (two classes), detection of the region of interest inside the quadrat (ROI-in; three classes), and benthic cover classification (six classes). A ResNet34-based U-Net pretrained on ImageNet was trained on 69 quadrat images (768×1,280 pixels) acquired along the east coast of Korea using labels produced through visual interpretation as the ground truth. Model performance was assessed using five-fold cross-validation, in which images containing benthic fauna were evenly distributed among the folds. Frame and ROI-in detection achieved overall accuracies (OA) of 0.986 and 0.974, respectively. The baseline six-class model reached an OA of 0.912, but rarely detected benthic fauna, which accounted for less than 0.4% of all pixels (F1=0.26). In contrast, the rare-class-enhanced model, which assigned larger weights to this rare class, raised the F1 score to 0.45 and recall to 0.63, with a slight decrease in OA to 0.891. These results indicate that redesigning the loss function effectively mitigates the learning failure of extremely rare benthic classes, highlighting the feasibility of automating quadrat benthic cover surveys.

Keywords: Benthic cover classification, Class imbalance, Focal loss, Quadrat underwater imagery, Semantic segmentation, U-Net

Received August 11, 2026; **Revised** September 3, 2026; **Accepted** September 7, 2026

***Corresponding author:** Euiyoung Jeong
e-mail eyjeong@kiost.ac.kr
https://orcid.org/0009-0008-3083-4213

Introduction

Quadrat surveys are widely used to quantify the status of coastal benthic ecosystems. In a typical survey, the seabed inside a quadrat is photographed, and benthic cover is estimated by point counting, in which the substrate

This is an Open Access article distributed under the terms of the Creative Commons Attribution Non-Commercial License (http://creativecommons.org/licenses/by-nc/4.0), which permits unrestricted non-commercial use, distribution, and reproduction in any medium, provided the original work is properly cited.

Copyright © National Institute of Ecology.

type beneath randomly placed points is counted on each image. However, this procedure requires an expert to classify the points image-by-image; thus, it is labor-intensive, and the results vary with the experience and subjectivity of the interpreter (Kohler & Gill, 2006; Williams *et al*., 2019). These limitations have motivated the use of deep-learning-based segmentation to automate the interpretation of quadrat imagery.

Several semi-automated software packages have been developed to reduce the burden of interpretation. Coral Point Count with Excel extensions implements random point counting in a spreadsheet environment (Kohler & Gill, 2006), and photoQuad supports point counting of quadrat images and compares the errors of four photo-quadrat methods (Trygonis & Sini, 2012). More recently, CoralNet, an automated annotation platform, has substantially reduced the interpretation burden of large benthic image collections (Williams *et al*., 2019). However, these tools still rely on point sampling or semi-automated annotation and do not provide full pixel-wise segmentation of the entire image.

However, segmentation studies based on convolutional neural networks (CNNs) have moved beyond point counting and achieved pixel-wise automation for benthic and underwater imagery. Representative examples include coral segmentation from sparse annotations (Alonso *et al*., 2019), benthic community segmentation from orthographic imagery (Pavoni *et al*., 2020), neural network recognition of marine benthos and corals (Raphael *et al*., 2020), and seagrass habitat segmentation using drone imagery (Jeon *et al*., 2021). The need for automated annotation was also emphasized in an early study that directly addressed the large variability among human experts (Beijbom *et al*., 2015). However, few studies have addressed the interpretation of extremely rare classes together with hierarchical cover classifications at the quadrat scale.

From a methodological perspective, the U-Net with encoder transfer learning is the standard approach for segmenting small image datasets (Kattenborn *et al*., 2021; Wagner *et al*., 2019). Several loss functions have been proposed to address class imbalance. For example, previous studies have reported that the learning failure of minority classes substantially degrades CNN performance (Buda *et al*., 2018), and focal loss (Lin *et al*., 2020) and its variants improve the imbalanced segmentation of medical images (Yeung *et al*., 2022). However, few studies have

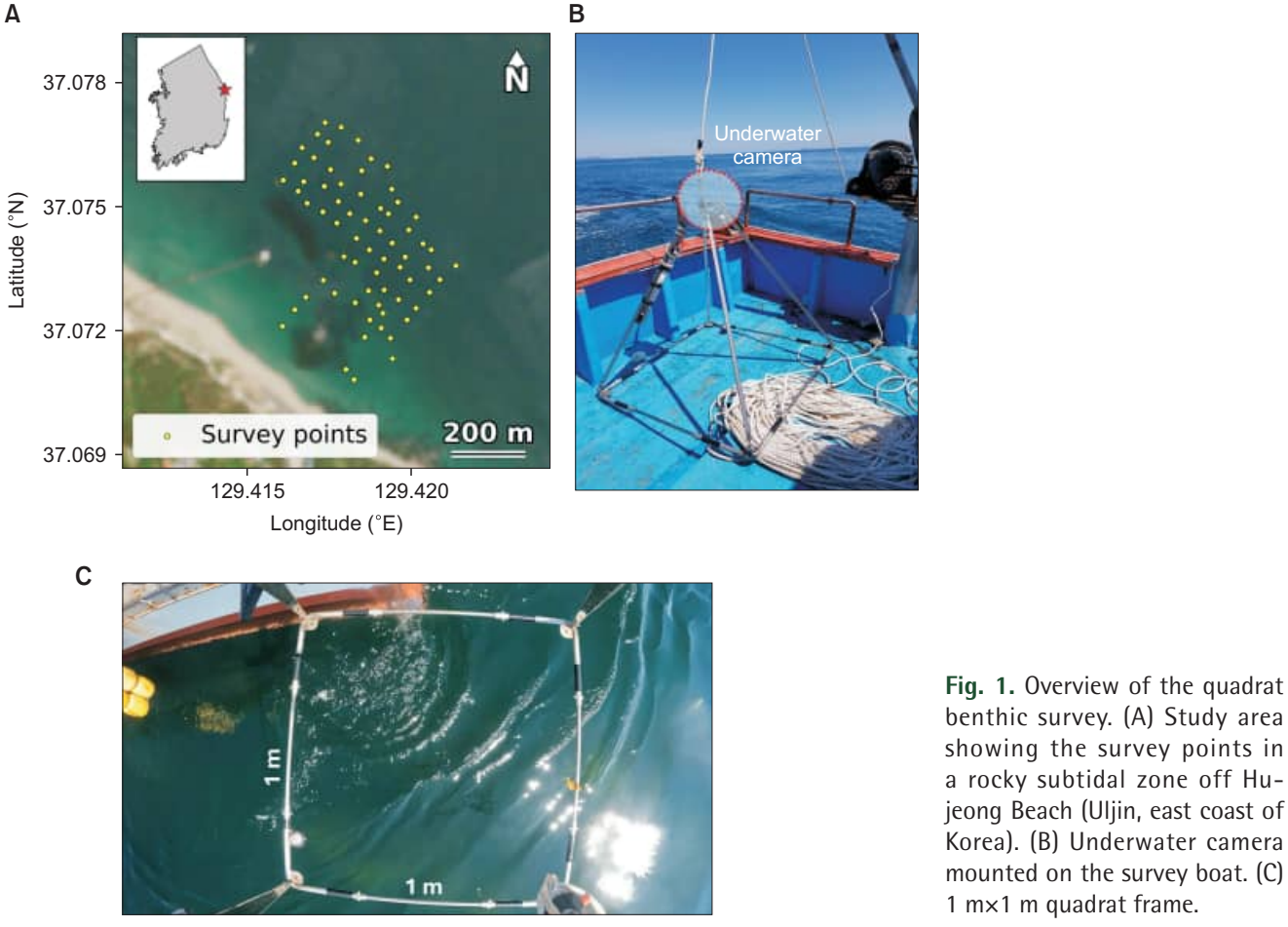

Fig. 1. Overview of the quadrat benthic survey. (A) Study area showing the survey points in a rocky subtidal zone off Hujeong Beach (Uljin, east coast of Korea). (B) Underwater camera mounted on the survey boat. (C) 1 m×1 m quadrat frame.

compared the performance before and after modifying the loss function for small quadrat-scale datasets.

Therefore, this study had the following three objectives. First, six-class semantic segmentation of the benthic cover and detection of the region of interest (ROI; two and three classes) were performed using independent U-Nets. Second, class-weighted cross-entropy combined with focal loss was applied to mitigate the learning failure of the extremely rare benthic fauna classes. Third, the model performance was verified statistically by five-fold cross-validation, in which images containing benthic fauna were evenly distributed across the folds. The underlying hypothesis was that redesigning the loss function can recover the minority benthic fauna class without substantially degrading the overall accuracy (OA).

Materials and Methods

A quadrat survey was conducted using an underwater imaging frame in a rocky subtidal zone off Hujeong Beach, Uljin-gun, Gyeongsangbuk-do, on the east coast of South Korea (Fig. 1A). In conventional quadrat surveys, divers place a square quadrat at randomly selected locations; therefore, the results are not easily generalized to the entire seabed. To overcome this limitation, the imaging frame was lowered from the survey vessel to the seabed at stations with 50-m intervals. The frame has a square-pyramidal shape and is equipped with an underwater camera (HERO10 Black, GoPro Inc., San Mateo, CA, USA); its base forms a 1 m×1 m square quadrat (Fig. 1B, C). During the survey on May 26, 2022, underwater

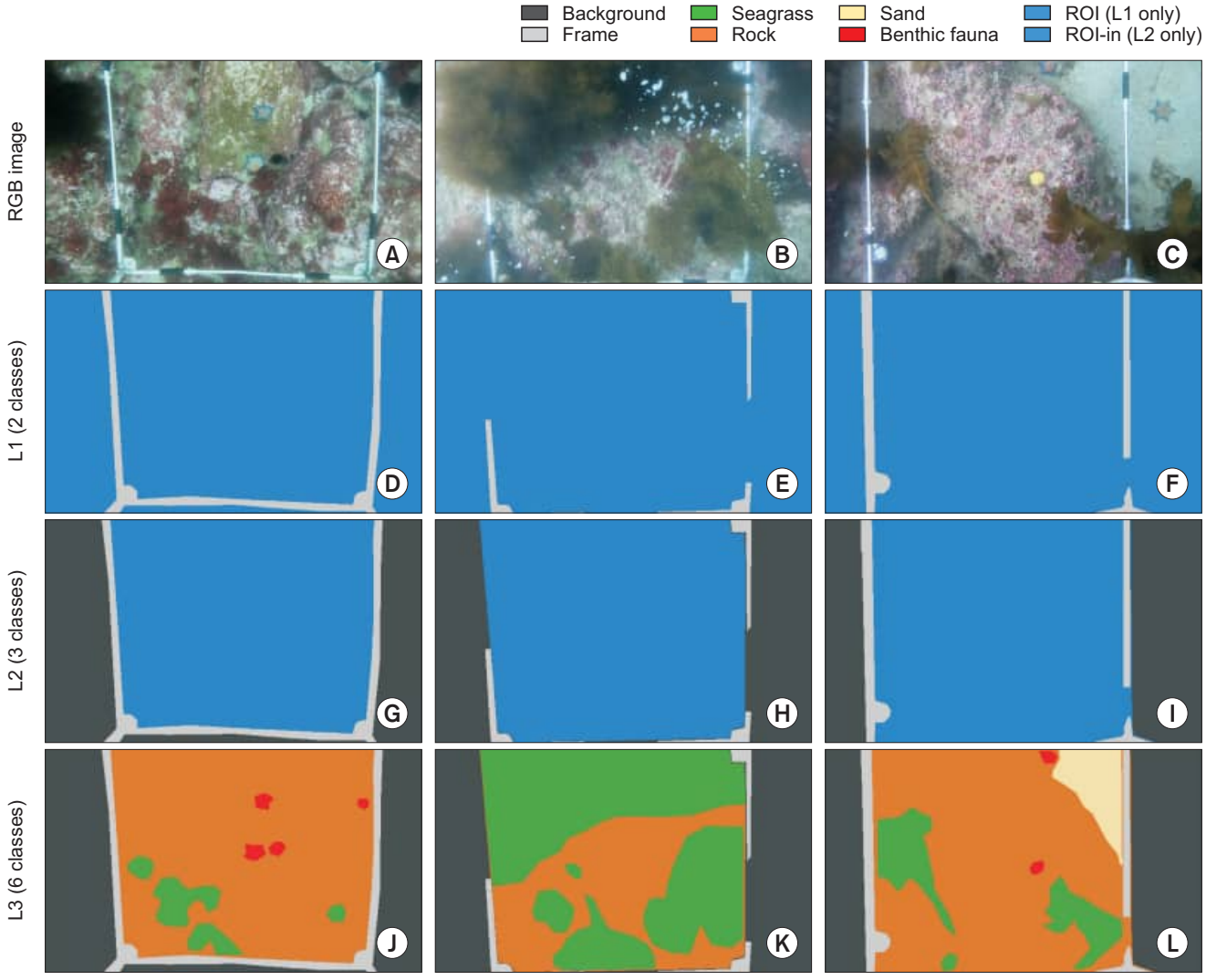

Fig. 2. Hierarchical labeling scheme (L1: 2-class, L2: 3-class, L3: 6-class) of the quadrat underwater images. (A-C) RGB images of three example stations. (D-F) L1 labels showing the frame and the ROI. (G-I) L2 labels that add the background outside the quadrat. (J-L) L3 labels that divide the ROI-in into four cover classes. Each column shows the same image.

images with a resolution of 3,840×2,160 pixels were acquired at 69 stations, excluding shallow stations that the vessel could not approach.

The ground-truth labels were constructed using visual interpretation. Based on this interpretation, three hierarchical label sets were produced: L1 (two classes), L2 (three classes), and L3 (six classes) (Fig. 2). The six classes consisted of background, frame, seagrass, rock, sand, and benthic fauna. The pixel distribution of the six classes was highly imbalanced: sand (30.9%) and background (29.7%) accounted for approximately 60% of all pixels, followed by rock (22.3%) and seagrass (11.3%), whereas frames accounted for only 5.5% (Table 1). In particular, benthic fauna accounts for only 0.4% of all pixels, approximately 80 times less than that of sand, which is the most abundant class, and is therefore the most difficult class to learn.

Table 1. Six-class pixel distribution of the dataset (768×1,280 labels, 69 images)

Code	Class	Pixels	Proportion (%)
1	Background	20,123,666	29.7
2	Frame	3,713,507	5.5
3	Seagrass	7,682,488	11.3
4	Rock	15,132,790	22.3
5	Sand	20,926,519	30.9
6	Benthic fauna	250,790	0.4
Total		67,829,760	100.0

The three hierarchical tasks were designed to verify different objectives. The two-class task detects the quadrat frame and treats the remaining region as the ROI. The three-class task divides the image into the background outside the quadrat, frame, and ROI inside the quadrat (ROI-in). The six-class task classifies the benthic cover inside the quadrat, excluding the area outside it. Therefore, the three tasks represent a stepwise increase in difficulty from frame detection to area separation, and finally to cover classification. The overall workflow, from input imagery and hierarchical annotation to independent model training and a common evaluation protocol, is summarized in Fig. 3.

A U-Net with a ResNet34 encoder pretrained on ImageNet was adopted as the network (Fig. 4, Table 2). Exploiting pretrained weights through transfer learning is a standard procedure that improves training stability and accuracy in the segmentation of small image datasets (LeCun *et al.*, 2015; Wagner *et al.*, 2019). The three tasks were each trained as an independent U-Net; that is, the three task models were not combined sequentially. Instead, each model was evaluated for the entire image.

Training was performed on images resized to

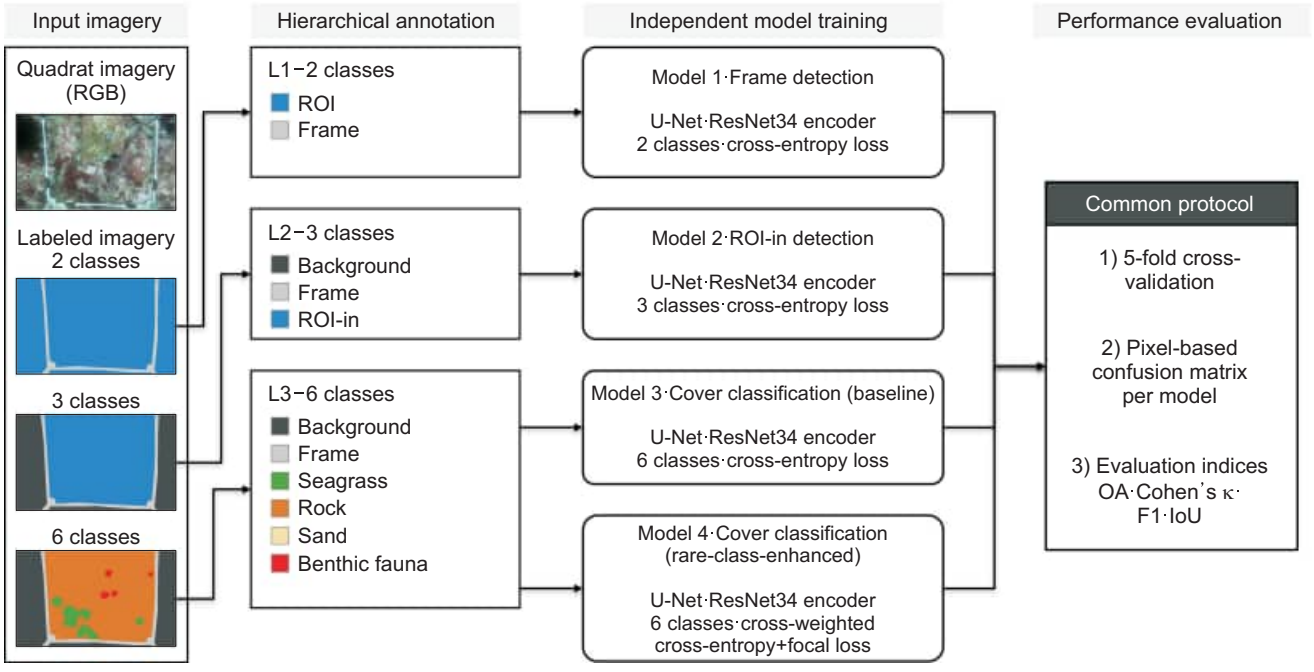

Fig. 3. Overall workflow of this study, from input quadrat imagery and hierarchical annotation (L1-L3) to independent training of the four U-Net models and the common evaluation protocol (five-fold cross-validation; pixel-based confusion matrices; OA, Kappa, F1, and IoU). ROI, region of interest; ROI-in, ROI inside the quadrat; OA, overall accuracy; IoU, intersection over union.

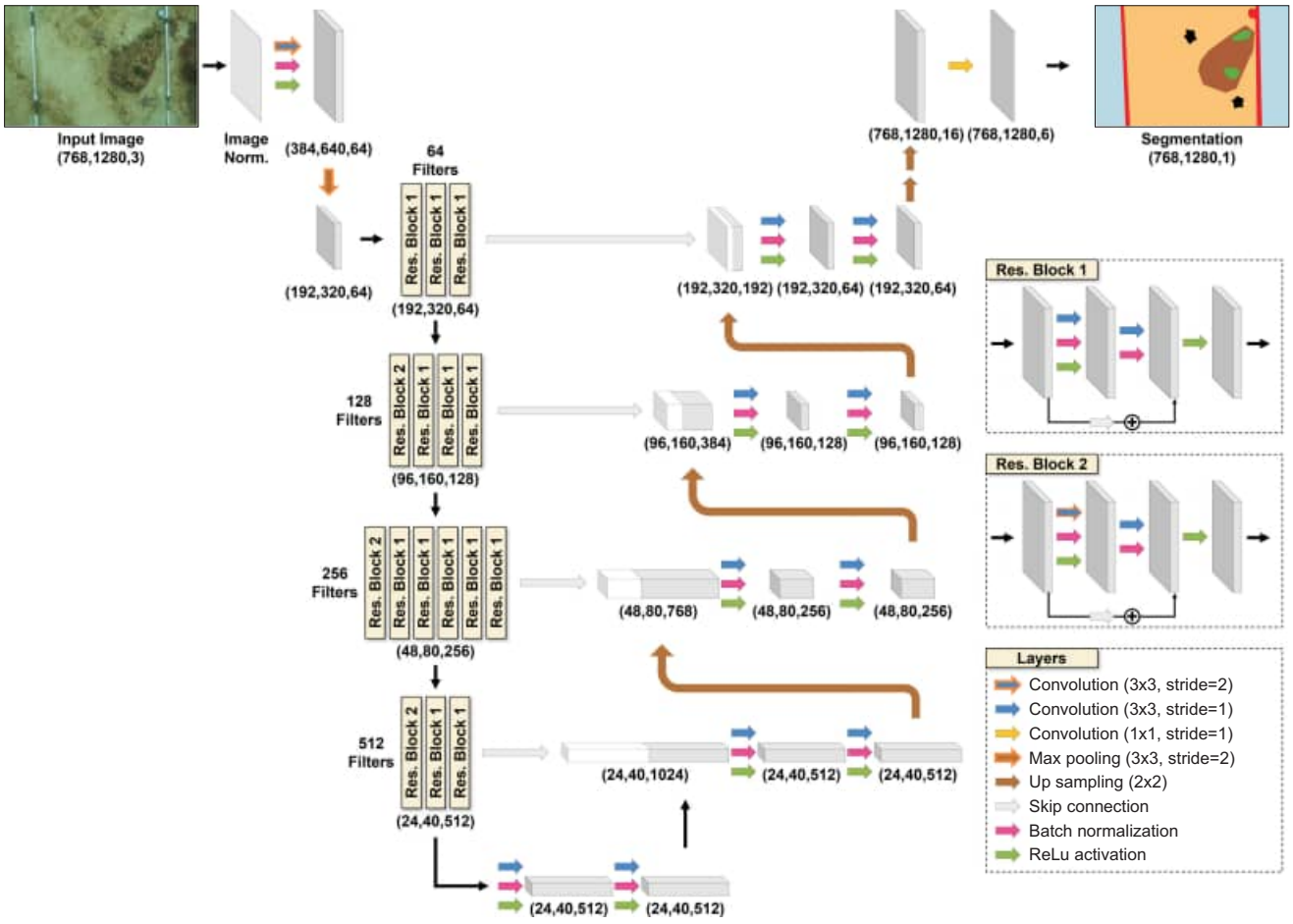

Fig. 4. Architecture of the U-Net used for benthic cover segmentation.

Table 2. Training configuration of the U-Net models

Item	Value
Input size (RGB)	768×1,280 whole image (normalized to [0, 1])
Optimizer	Adam
Learning rate	2×10^{-5}
Batch size	8
Epochs	300
Augmentation	Random horizontal+vertical flip
Cross-validation	5-fold, stratified by benthic fauna presence
Loss – 2/3-class & 6-class base	Cross-entropy
Loss – 6-class rare-class-enhanced	Class-weighted Cross-entropy+Focal loss (γ=2)
Random seed	42 (data split, initialization, shuffling, augmentation)

768×1,280 pixels using horizontal and vertical flip augmentation (Nanni *et al.*, 2021; Shorten & Khoshgoftaar, 2019). A five-fold cross-validation was used, with the folds partitioned such that the benthic fauna class was distributed evenly. The folds were split at the image level. Each of the 69 images was acquired at a different station; therefore, no station appeared more than once. Within each fold, 49 or 50 images were used for training, six for validation, and 13 or 14 for testing. Four models were trained: a two-class model for quadrat frame detection, a three-class model for ROI-in detection, a six-class baseline model using cross-entropy for benthic cover classification, and a six-class rare-class-enhanced model using class-weighted cross-entropy combined with focal loss. Among these, the six-class baseline and rare-class-enhanced models were compared with the loss function as the only controlled variable, thereby isolating the effect of the loss-function redesign.

The six-class baseline model was trained using standard cross-entropy loss L_{CE} (Eq. 1):

$$L_{CE} = -\frac{1}{N_p}\sum_{i} log(p_{t,i}) \quad \text{(Eq. 1)}$$

where L_{CE} denotes the cross-entropy loss of the baseline model, N_p is the total number of pixels, and i is the pixel index. Additionally, $p_{t,i}$ denotes the probability that pixel i is predicted as its ground truth class.

For the rare-class-enhanced model, a composite loss L_{CWF}, formed by summing class-weighted cross-entropy and weighted focal loss terms, was used (Eq. 2). The focal term reduces the contribution of easily predicted pixels by a factor of $(1-p_{t,i})^{\gamma}$, thereby concentrating training on the rare classes (Buda *et al*., 2018; Lin *et al*., 2020; Yeung *et al*., 2022). Class weights are defined as the reciprocal of the pixel frequency of each class normalized by the mean of these reciprocals across all classes (Eq. 3). These weights are computed separately for each fold using only the training images of the fold. Validation and test images were excluded from the computations.

$$L_{CWF} = -\frac{1}{N_p}\sum_{i} w_{y_i}\left[1+\left(1-p_{t,i}\right)^{\gamma}\right] log(p_{t,i}) \quad \text{(Eq. 2)}$$

$$w_c = \frac{\frac{1}{n_c}}{\frac{1}{C}\sum_k\left(\frac{1}{n_k}\right)} \quad \text{(Eq. 3)}$$

where L_{CWF} denotes the loss of the rare-class-enhanced model, y_i is the ground-truth class of pixel i, and w_{yi} (=w_c) is the weight assigned to the ground-truth class. Parameter γ is the focusing strength that reduces the contribution of easily classified pixels (γ=2). Terms n_c and n_k denote the numbers of pixels belonging to classes c and k, respectively, and C denotes the total number of classes. Optimization was performed with the Adam optimizer, using a learning rate of 2×10^{-5} and batch size of eight (Table 2).

The evaluation is based on pixel-wise confusion matrices. OA, the Kappa coefficient (McHugh, 2012), class-wise precision, recall, F1 score, and the intersection over union (IoU) were computed as the mean±standard deviation over the five folds (Taha & Hanbury, 2015). Additionally, an out-of-fold confusion matrix, obtained by aggregating the validation predictions of all five folds, is presented.

Results

High performance was obtained for both quadrat frame detection with two classes and ROI-in detection with three classes. An OA of 0.986 and Kappa coefficient of 0.862 were recorded for the two-class model, indicating stable detection of the quadrat frame (Table 3). Additionally, the areas inside and outside the quadrat were separated reasonably well by the three-class model, with an OA of 0.974 and Kappa coefficient of 0.947 (Table 3). The small errors observed in both tasks can be attributed to the distinct geometric structure of the frame, which is readily learned by the network.

Representative predictions of the six-class benthic cover classification were qualitatively compared for the four scenes (Figs. 5-8). Each figure shows the input image, ground-truth label, baseline model prediction, and rare class-enhanced model prediction. In addition, class-wise coverage proportions (%) were annotated for the ground truth label and rare-class-enhanced model prediction.

In the sand-dominated scene, the ground-truth sand coverage of 64.9% was closely reproduced by both the baseline (65.1%) and rare-class-enhanced models (65.3%) (Fig. 5). In contrast, benthic fauna was extremely rare in the ground-truth label at 0.4%, and only 0.1% was detected by the baseline model; therefore, most were missed. In contrast, 0.4% was detected in the rare-class-enhanced model, and the starfish was thus located. However, the shape of the starfish was not fully reproduced by the rare-class-enhanced model, and part of the region outside the quadrat was misclassified as sand.

In the seagrass-dominated scene (Fig. 6), the quadrat frame was occluded by seagrass and was barely discernible, even in the original image, and the frame accounted for 1.7% of the ground-truth label. Owing to this occlusion, the left boundary was not segmented correctly in either the three- or six-class models, and the shape of the benthic cover classification area within the quadrat consequently collapsed. Nevertheless, the seagrass and rock coverage obtained from the rare-class-enhanced model were 57.1% and 15.2%, respectively, which were similar

Table 3. Overall segmentation performance per model (five-fold cross-validation, mean±SD)

Model	OA	Kappa	Macro-F1	Mean-IoU
2-class (L1 region)	0.986±0.002	0.862±0.019	0.931±0.009	0.877±0.015
3-class (L2 region)	0.974±0.006	0.947±0.013	0.938±0.009	0.889±0.016
6-class base (L3 cover)	0.912±0.022	0.881±0.028	0.796±0.068	0.684±0.047
6-class rare-class-enhanced (L3 cover)	0.891±0.012	0.854±0.016	0.788±0.033	0.682±0.032

SD, standard deviation; OA, overall accuracy; IoU, intersection over union.

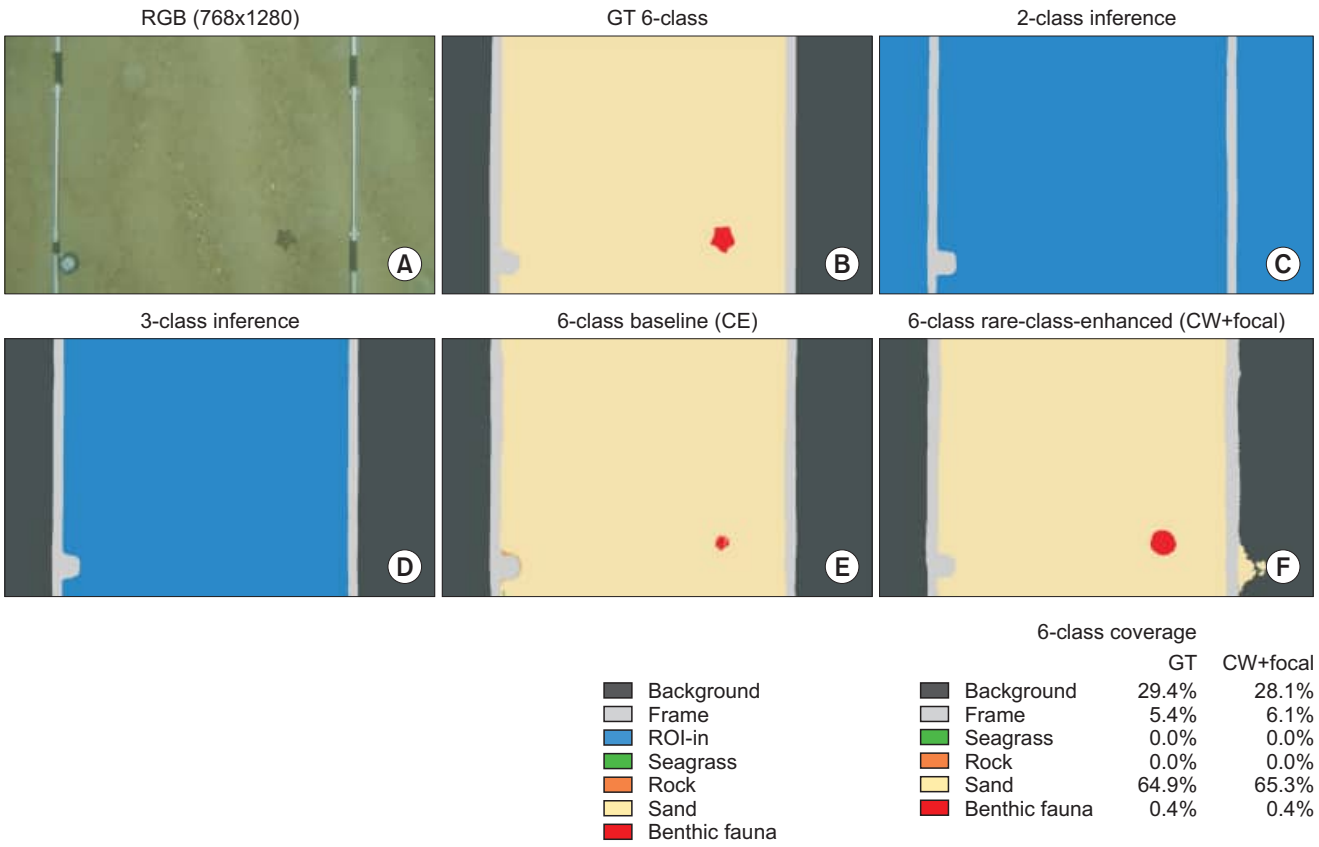

Fig. 5. Qualitative comparison for a sand-dominated scene: (A) RGB input, (B) ground-truth six-class label, (C) two-class prediction, (D) three-class prediction, (E) six-class baseline (CE) prediction, and (F) six-class rare-class-enhanced (CW+Focal; class-weighted CE+Focal loss) prediction. Per-class coverage (%) is annotated in each panel. GT, ground truth; CE, cross-entropy; CW, class-weighted; ROI-in, region of interest inside the quadrat.

to the corresponding ground-truth values of 55.8% and 13.0%.

In the scene composed of rock and benthic fauna (Fig. 7; rock ground truth, 63.4%), misclassification was observed in which the rare-class-enhanced model generated seagrass (1.2%) and sand (0.2%) that were absent from the ground truth. Owing to the limitation in reproducing its shape, the benthic fauna increased from 1.2% in the baseline model to 3.7% in the rare-class-enhanced model and was overdetected relative to the ground truth (2.6%). However, the rare-class-enhanced model successfully identified ten of the 11 benthic fauna positions.

For the complex scene in which several benthic covers were intermixed, the constituent covers were classified successfully by both the baseline and rare-class-enhanced models. Sand was classified as 31.2% using the rare-class-enhanced model, a value close to the ground truth of 34.0% (Fig. 8). However, the rock was overestimated at 25.1% relative to a ground truth of 15.5%, whereas the seagrass was underestimated at 8.4% relative to a ground truth of 16.2%, indicating that the rock and seagrass were mutually confused. Additionally, part of the area outside the quadrat was classified as benthic cover.

In terms of the quantitative performance of the six-class benthic cover classification, the OA of the baseline and rare-class-enhanced models differed only marginally. An OA of 0.912 was obtained for the baseline model, and one of 0.891 was obtained for the rare-class-enhanced model, corresponding to a decrease of 0.021 (Table 3, Fig. 9). This indicates that redesigning the loss function slightly lowers OA. This decrease was consistent across all five folds. The rare-class-enhanced model showed a lower OA for every fold (Table 4). The per-fold decrease ranged from 0.003-0.039.

In contrast, at the cost of this modest reduction in OA, the performance of the extremely rare benthic fauna class was substantially recovered in the rare-class-enhanced model. The F1 score for benthic fauna increased from 0.26 in the baseline model to 0.45 in the rare-class-enhanced model, and the IoU increased from 0.14 to 0.30 (Figs. 9, 10, Table 5). The recall of benthic fauna was reported under two aggregation schemes. Out-of-fold recall rose

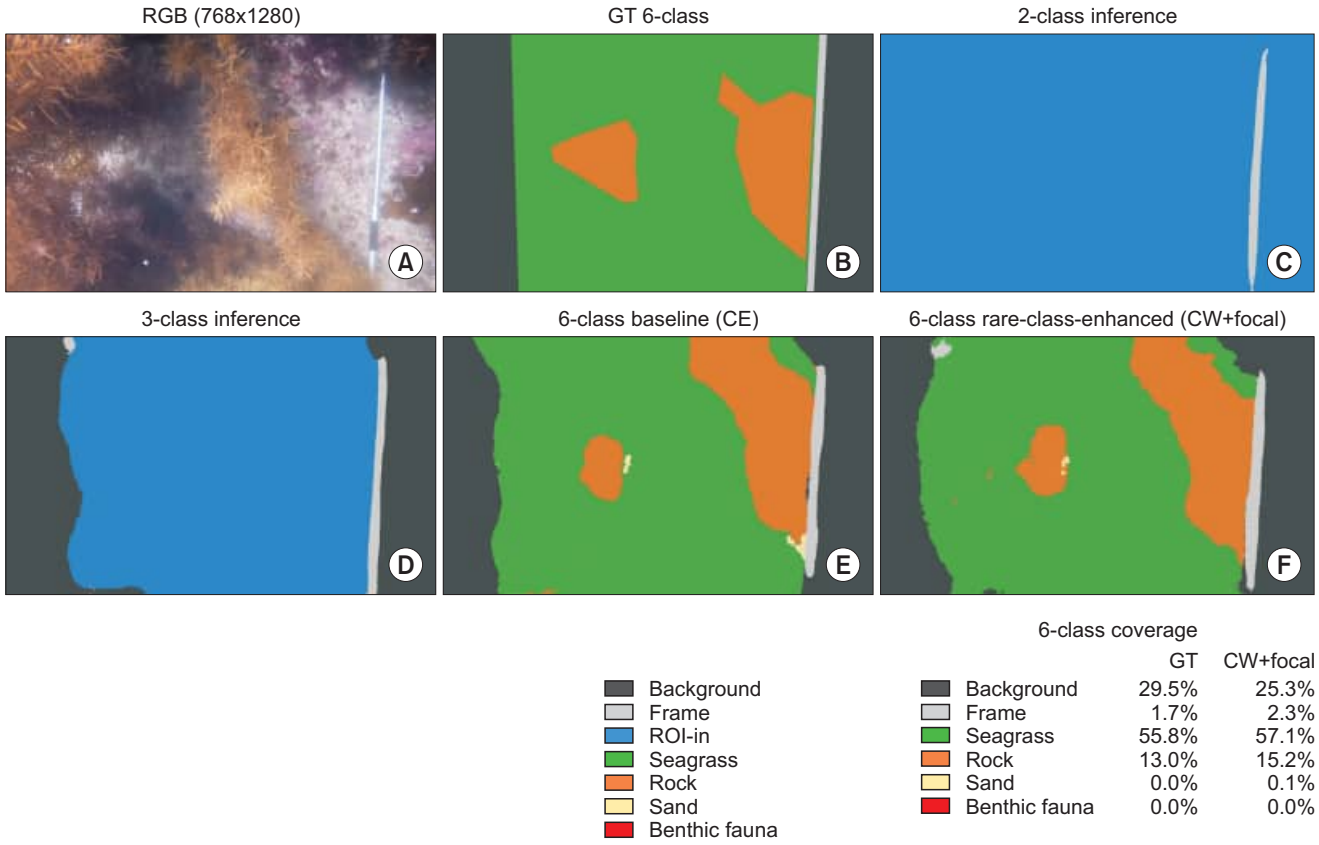

Fig. 6. Qualitative comparison for a seagrass-dominated scene; panels as in Fig. 5. (A) RGB input, (B) ground-truth six-class label, (C) two-class prediction, (D) three-class prediction, (E) six-class baseline (CE) prediction, and (F) six-class rare-class-enhanced (CW+Focal) prediction. Per-class coverage (%) is annotated in each panel. GT, ground truth; CE, cross-entropy; CW, class-weighted; ROI-in, region of interest inside the quadrat.

from 0.13-0.63. A five-fold increase in the average recall rose from 0.15-0.69. Detection performance for the benthic fauna class in the rare-class-enhanced model was thus approximately 1.7 times higher in F1 (from 0.26-0.45) and approximately 2.1 times higher in IoU (from 0.14-0.30) than that in the baseline model. The five non-fauna classes showed small declines in F1 between 0.013 and 0.036 (Table 5).

Discussion

The three segmentation tasks empirically demonstrated the feasibility of automating quadrat-based benthic cover surveys. The detection of the quadrat frame (two classes) and ROI-in detection (three classes) stably separated the quadrat structure with OA of 0.986 and 0.974, respectively. Therefore, these two steps can replace preprocessing, in which the effective ROI is designated prior to visual interpretation. The six-class cover classification also distinguished the major cover types, including background, sand, rock, and seagrass, with high accuracy using a dataset of only 69 images. In particular, the extremely rare benthic fauna class was partially recovered by redesigning the loss function, confirming its potential for detecting scarce but ecologically important targets.

The combination of class-weighted cross-entropy and focal loss mitigated the training failure of the extremely rare benthic fauna class at the cost of a slight loss in the OA. These results are consistent with earlier reports indicating that minority classes are prone to training failure under imbalanced data (Buda *et al.*, 2018), and focal-type losses alleviate this failure (Yeung *et al.*, 2022). The present results also fall within the context of studies that address training improvements in benthic community segmentation models (Pavoni *et al.*, 2020). The five non-fauna classes lost between 0.013 and 0.036 in the F1 score. Therefore, the cover estimates remained reliable. In contrast, the baseline model missed almost all the benthic fauna. A class that is never detected does not provide monitoring information. Because benthic cover surveys aim to detect rare but ecologically important organisms, accepting a slight decrease in OA to secure the recall of benthic fauna is a meaningful trade-off consistent with the survey objective.

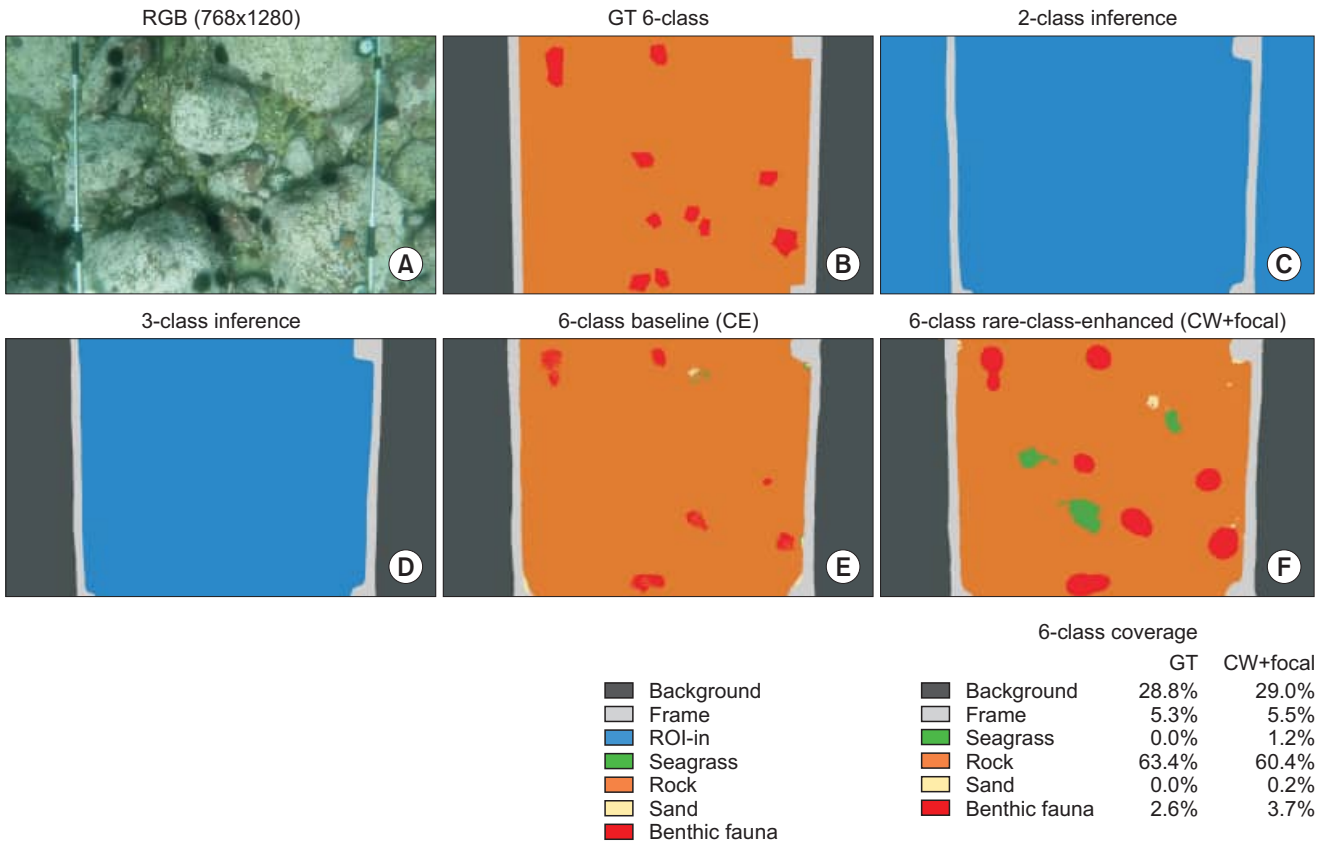

Fig. 7. Qualitative comparison for a rock-and-benthic-fauna scene; panels as in Fig. 5. (A) RGB input, (B) ground-truth six-class label, (C) two-class prediction, (D) three-class prediction, (E) six-class baseline (CE) prediction, and (F) six-class rare-class-enhanced (CW+Focal) prediction. Per-class coverage (%) is annotated in each panel. GT, ground truth; CE, cross-entropy; CW, class-weighted; ROI-in, region of interest inside the quadrat.

However, although the benthic fauna class was recovered by focal loss, its F1 score remained at approximately 0.45, indicating that is difficult to overcome through a loss function design alone. The rare-class-enhanced model achieved a recall of 0.69 but had a precision of 0.38. Therefore, it detected, but overpredicted, most benthic fauna pixels. Benthic fauna occupied small areas with irregular outlines. Individuals were often partially occluded by seagrass or rocks. Under these conditions, the class boundary becomes ambiguous, and false positives increase. This limitation is primarily attributed to the absolute scarcity of samples of the extremely rare class, which accounted for less than 0.4% of all pixels in the dataset. Small sample sizes inflate the variance in validation performance, and such variability makes stable estimation difficult (Varoquaux, 2018). Therefore, redesigning the loss function serves only as a means of fully exploiting the available data and cannot substitute for the insufficiency of the samples themselves.

The data used in this study are limited in generalizability as they comprise only 69 images acquired on a single survey date (May 26, 2022) and within a single region. Therefore, the images represent a single season and set of water conditions. The model performance in other seasons, depths, or water clarities is not known. Additional surveys across seasons and regions are required before operational use. To reinforce statistical stability, a five-fold cross-validation was performed with the folds partitioned such that the benthic fauna class was evenly distributed. Nevertheless, the spatiotemporal representativeness remains limited when both the large validation error associated with small samples (Varoquaux, 2018) and the variability inherent in expert visual interpretation (Beijbom *et al.*, 2015) are considered. All benthic animals were labeled as a single class. They were not separated into taxa, such as sea stars, urchins, or gastropods. Benthic fauna accounted for less than 0.4% of all the pixels. Splitting this class into taxa resulted in too few pixels for the training. Therefore, taxa-level labels have been left for future studies using a larger image set.

Consequently, portions of the region outside the quadrat were misclassified as benthic cover by the rare-class-enhanced model (Figs. 5, 8). However, the inside and outside of the quadrats were separated with high accuracy

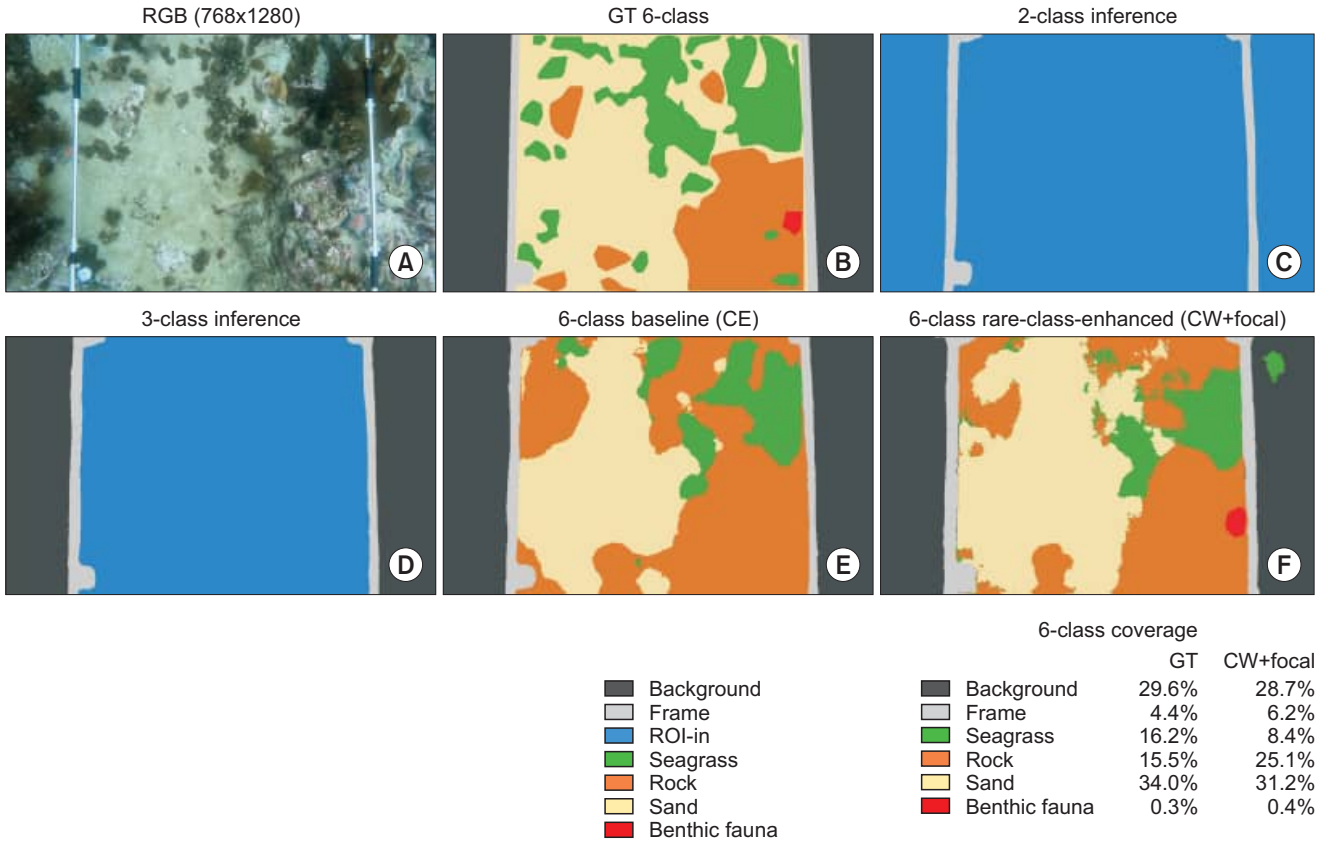

Fig. 8. Qualitative comparison for a mixed-cover scene; panels as in Fig. 5. (A) RGB input, (B) ground-truth six-class label, (C) two-class prediction, (D) three-class prediction, (E) six-class baseline (CE) prediction, and (F) six-class rare-class-enhanced (CW+Focal) prediction. Per-class coverage (%) is annotated in each panel. GT, ground truth; CE, cross-entropy; CW, class-weighted; ROI-in, region of interest inside the quadrat.

Table 4. Per-fold OA of the two six-class models (five-fold cross-validation)

Fold	6-class base	6-class rare-class-enhanced	Difference
1	0.896	0.881	−0.015
2	0.901	0.898	−0.003
3	0.933	0.894	−0.039
4	0.887	0.875	−0.012
5	0.942	0.907	−0.035
Mean±SD	0.912±0.022	0.891±0.012	−0.021±0.015

SD, standard deviation; OA, overall accuracy.

using the three-class model (OA=0.974). Using three-class prediction as a mask to remove regions outside the quadrat from the six-class output can effectively suppress such misclassification. This indicates a direction for subsequent refinement, in which ROI-in detection and benthic cover classifications are combined.

Future research should proceed in one of three directions. First, the dataset could be expanded to cover a wider range of imaging periods, regions, and water depths to increase both the representativeness and absolute volume of the samples. Second, the benthic cover classes can be further subdivided to construct a classification scheme suited to the objectives of a survey. Third, ROI-in detection and benthic cover classification can be developed into a single automated workflow that can be applied to operational benthic surveys (Jeon *et al.*, 2021; Raphael *et al.*, 2020). Through such extensions, quadrat benthic cover surveys can be automated and implemented in a practical monitoring framework.

Conclusion

Unlike conventional visual interpretation, U-Net semantic segmentation combined with a redesigned loss function enables the automated benthic cover classification of quadrat underwater images. Quadrat frame detection (two classes) and ROI-in detection (three classes) separated the quadrat structure stably with OA of 0.986 and 0.974, re-

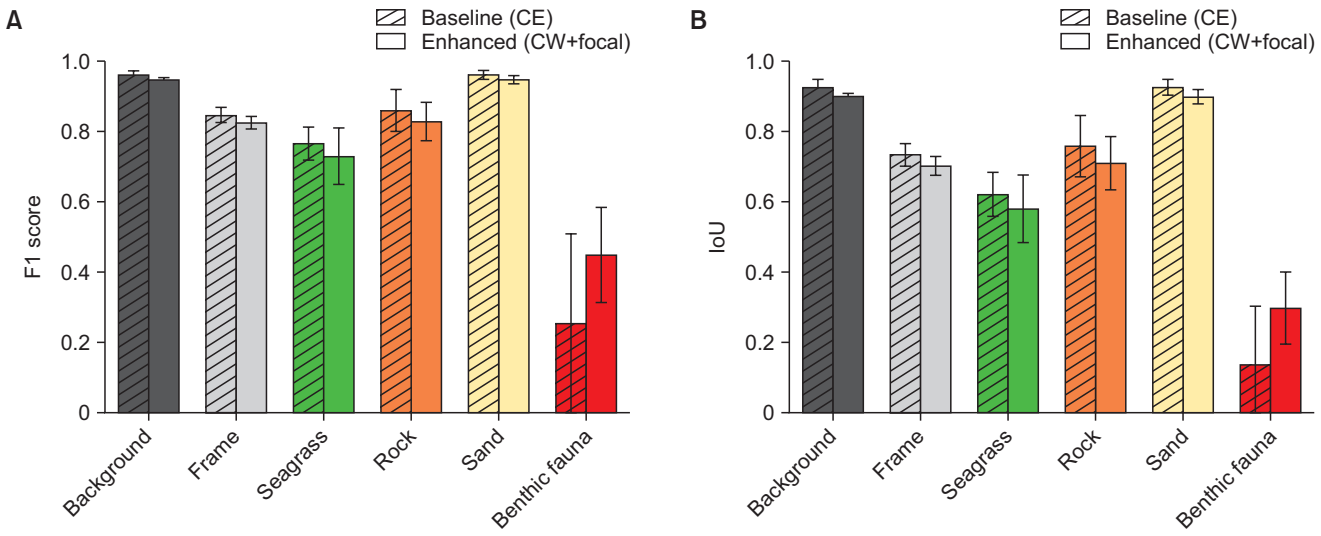

Fig. 9. Per-class (A) F1 scores and (B) IoU of the six-class baseline vs. rare-class-enhanced models. CE, cross-entropy; CW, class-weighted; IoU, intersection over union.

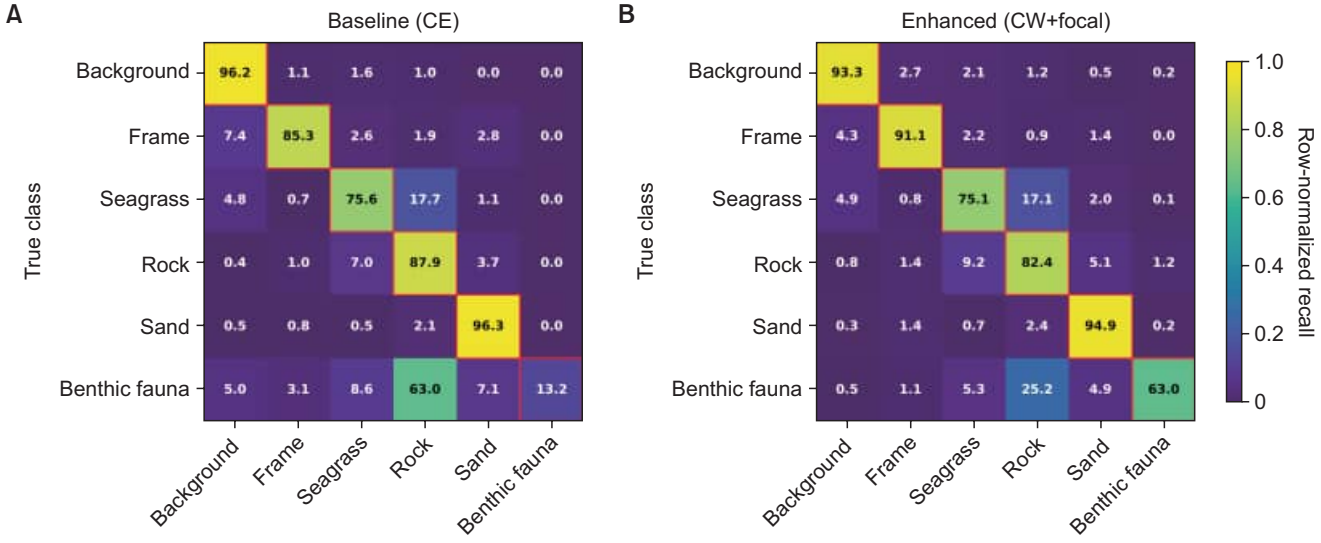

Fig. 10. Out-of-fold confusion matrices of the six-class baseline model (A) and rare-class-enhanced model (B). CE, cross-entropy; CW, class-weighted.

Table 5. Six-class per-class F1 and IoU, baseline vs. rare-class-enhanced loss (five-fold cross-validation, mean±SD)

Class	F1 (base)	F1 (rare-class-enhanced)	IoU (base)	IoU (rare-class-enhanced)
Background	0.961±0.012	0.948±0.005	0.925±0.023	0.901±0.009
Frame	0.846±0.022	0.825±0.018	0.734±0.032	0.702±0.026
Seagrass	0.765±0.047	0.729±0.080	0.622±0.063	0.580±0.096
Rock	0.860±0.060	0.828±0.055	0.759±0.088	0.710±0.076
Sand	0.962±0.012	0.947±0.011	0.926±0.023	0.899±0.020
Benthic fauna	0.255±0.254	0.449±0.135	0.137±0.167	0.298±0.102

SD, standard deviation; IoU, intersection over union.

spectively. The rare-class-enhanced model, in which class-weighted cross-entropy and focal loss were applied, recovered the F1 score of the extremely rare benthic fauna class from 0.26-0.45. This indicates that redesigning the loss function mitigates the learning failure of the minority benthic fauna class without substantially compromising the OA. These findings contribute to the automation of quadrat benthic cover surveys and provide a basis for the development of operational coastal benthic monitoring through data expansion and finer class subdivisions.

Author Contributions

Conceptualization: EJ. Methodology: SHP. Software: SHP. Validation: NHK. Investigation: WKB. Formal analysis: SC. Funding acquisition: SC, EJ. Data curation: JSL. Writing – original draft: SHP. Writing – review & editing: NHK, WKB, SC, JSL, EJ.

Conflict of Interest

The authors declare that they have no competing interests.

Funding

This work was supported by an in-house grant from the Korea Institute of Ocean Science and Technology (KIOST; PKB0011) under the project "Development of original technology to verify factors influencing barren ground on the East Sea coast according to climate change."

References

Alonso, I., Yuval, M., Eyal, G., Treibitz, T., and Murillo, A.C. (2019). CoralSeg: learning coral segmentation from sparse annotations. *Journal of Field Robotics*, 36, 1456-1477. https://doi.org/10.1002/rob.21915

Beijbom, O., Edmunds, P.J., Roelfsema, C., Smith, J., Kline, D.I., Neal, B.P., *et al*. (2015). Towards automated annotation of benthic survey images: variability of human experts and operational modes of automation. *PLoS One*, 10, e0130312. https://doi.org/10.1371/journal.pone.0130312

Buda, M., Maki, A., and Mazurowski, M.A. (2018). A systematic study of the class imbalance problem in convolutional neural networks. *Neural Networks*, 106, 249-259. https://doi.org/10.1016/j.neunet.2018.07.011

Jeon, E., Kim, S., Park, S., Kwak, J., and Choi, I. (2021). Semantic segmentation of seagrass habitat from drone imagery based on deep learning: a comparative study. *Ecological Informatics*, 66, 101430. https://doi.org/10.1016/j.ecoinf.2021.101430

Kattenborn, T., Leitloff, J., Schiefer, F., and Hinz, S. (2021). Review on Convolutional Neural Networks (CNN) in vegetation remote sensing. *ISPRS Journal of Photogrammetry and Remote Sensing*, 173, 24-49. https://doi.org/10.1016/j.isprsjprs.2020.12.010

Kohler, K.E., and Gill, S.M. (2006). Coral Point Count with Excel extensions (CPCe): a Visual Basic program for the determination of coral and substrate coverage using random point count methodology. *Computers & Geosciences*, 32, 1259-1269. https://doi.org/10.1016/j.cageo.2005.11.009

LeCun, Y., Bengio, Y., and Hinton, G. (2015). Deep learning. *Nature*, 521, 436-444. https://doi.org/10.1038/nature14539

Lin, T.Y., Goyal, P., Girshick, R., He, K., and Dollár, P. (2020). Focal loss for dense object detection. *IEEE Transactions on Pattern Analysis and Machine Intelligence*, 42, 318-327. https://doi.org/10.1109/TPAMI.2018.2858826

McHugh, M.L. (2012). Interrater reliability: the kappa statistic. *Biochemia Medica*, 22, 276-282. https://doi.org/10.11613/bm.2012.031

Nanni, L., Paci, M., Brahnam, S., and Lumini, A. (2021). Comparison of different image data augmentation approaches. *Journal of Imaging*, 7, 254. https://doi.org/10.3390/jimaging7120254

Pavoni, G., Corsini, M., Callieri, M., Fiameni, G., Edwards, C., and Cignoni, P. (2020). On improving the training of models for the semantic segmentation of benthic communities from orthographic imagery. *Remote Sensing*, 12, 3106. https://doi.org/10.3390/rs12183106

Raphael, A., Dubinsky, Z., Iluz, D., and Netanyahu, N.S. (2020). Neural network recognition of marine benthos and corals. *Diversity*, 12, 29. https://doi.org/10.3390/d12010029

Shorten, C., and Khoshgoftaar, T.M. (2019). A survey on image data augmentation for deep learning. *Journal of Big Data*, 6, 60. https://doi.org/10.1186/s40537-019-0197-0

Taha, A.A., and Hanbury, A. (2015). Metrics for evaluating 3D medical image segmentation: analysis, selection, and tool. *BMC Medical Imaging*, 15, 29. https://doi.org/10.1186/s12880-015-0068-x

Trygonis, V., and Sini, M. (2012). photoQuad: a dedicated seabed image processing software, and a comparative error analysis of four photoquadrat methods. *Journal of Experimental Marine Biology and Ecology*, 424-425, 99-108. https://doi.org/10.1016/j.jembe.2012.04.018

Varoquaux, G. (2018). Cross-validation failure: small sample sizes lead to large error bars. *NeuroImage*, 180, 68-77. https://doi.org/10.1016/j.neuroimage.2017.06.061

Wagner, F.H., Sanchez, A., Tarabalka, Y., Lotte, R.G., Ferreira, M.P., Aidar, M.P.M., *et al*. (2019). Using the U-net convolutional network to map forest types and disturbance in the Atlantic rainforest with very high resolution images. *Remote Sensing in Ecology and Conservation*, 5, 360-375. https://doi.org/10.1002/rse2.111

Williams, I.D., Couch, C.S., Beijbom, O., Oliver, T.A., Vargas-Angel, B., Schumacher, B.D., *et al*. (2019). Leveraging automated image analysis tools to transform our capacity to assess status and trends of coral reefs. *Frontiers in Marine Science*, 6, 222. https://doi.org/10.3389/fmars.2019.00222

Yeung, M., Sala, E., Schönlieb, C.B., and Rundo, L. (2022). Unified Focal loss: generalising Dice and cross entropy-based losses to handle class imbalanced medical image segmentation. *Computerized Medical Imaging and Graphics*, 95, 102026. https://doi.org/10.1016/j.compmedimag.2021.102026

PNIE PROCEEDINGS OF THE NATIONAL INSTITUTE OF ECOLOGY OF THE REPUBLIC OF KOREA

Case Report

PNIE 2026;7(4):225-232
https://doi.org/10.22920/PNIE.2026.7.4.225
pISSN 2765-2203, eISSN 2765-2211

A Checklist of the Subfamily Epipaschiinae (Lepidoptera, Pyralidae) from Korea, with Two Newly Recorded Species

Hanul Kim[1], Jae-Ho Ko[2], Ulziijargal Bayarsaikhan[1]*

[1]Convergence Research Center for Insect Vectors, Incheon, Korea
[2]DASARI Research Institute of BioResources, Daejeon, Korea

ABSTRACT

The subfamily Epipaschiinae Meyrick, 1884 (Lepidoptera: Pyralidae) comprises approximately 737 described species worldwide, with most species distributed in tropical and temperate regions. Although most species are associated with forest ecosystems, several are known to feed on economically important agricultural and horticultural crops. In Korea, 22 species belonging to nine genera have previously been recorded. This study reports *Lamida obscura* (Moore, 1888) and *Lista haraldusalis* (Walker, 1859) as new records for the Korean fauna and documents *Lamida* Walker, 1859 as a genus newly recorded from the country. Illustrations of the adults and genitalia of the examined species are provided, along with an updated checklist of Korean Epipaschiinae. Information on the host plants of the newly recorded species is also provided.

Keywords: Korea, Lepidoptera, Moths, Pyraloidea, Taxonomy

Introduction

The subfamily Epipaschiinae Meyrick, 1884, belongs to the family Pyralidae within the superfamily Pyraloidea. Approximately 737 species have been described worldwide, with most distributed in tropical and temperate regions (Nuss *et al.*, 2003-2024).

Epipaschiinae moths are mostly medium-sized and can be recognized by their upturned labial palpi and somber wing coloration. Epipaschiinae can be distinguished by the following combination of characteristics: simple antennae, a scape sometimes bearing long tuft in males, an ocellus and chaetosema, and labial palpi always upturned and slender, with the second segment sometimes swollen in males. In the male genitalia, the uncus is variously shaped and is mostly as long as the vinculum; the valva is usually simple, ovate, or elongated; the juxta is variously shaped, mostly distinct, and the phallus is simple, usually elongated. In female genitalia, papillae are triangular, the setose apices, the ostium bursae is cup-shaped, the ductus bursae is membranous, sometimes with a sclerotized part, and the corpus bursae has a pair of signa (Solis, 1993).

The Korean fauna of Epipaschiinae was first documented by Park (1983), who recorded 13 species from Korea. Subsequent studies have gradually expanded knowledge of the Korean Epipaschiinae fauna (Bae, 2004; Bae *et al.*, 2008; Ju, 1999). Paek (2010) reported 19 species belonging to 11 genera of Epipaschiinae in Korea. Recently, Kim and Paek (2020) and Kim *et al.* (2021; 2023) reported ad-

Received June 15, 2026; **Revised** August 21, 2026; **Accepted** August 24, 2026

***Corresponding author:** Ulziijargal Bayarsaikhan
e-mail uug228@naver.com
https://orcid.org/0000-0002-9274-4060

This is an Open Access article distributed under the terms of the Creative Commons Attribution Non-Commercial License (http://creativecommons.org/licenses/by-nc/4.0), which permits unrestricted non-commercial use, distribution, and reproduction in any medium, provided the original work is properly cited.

Copyright © National Institute of Ecology.

ditional species records for the country.

A total of 22 species belonging to nine genera of the subfamily Epipaschiinae have been recorded in Korea (Bae *et al.*, 2008; Kim & Paek, 2020; Kim *et al.*, 2021; 2023). In adjacent countries, 85 species have been reported in China (Wang *et al.*, 2021) and 26 species have been reported in Japan (Yamanaka, 2013).

In the present study, two species, *Lamida obscura* (Moore, 1888) and *Lista haraldusalis* (Walker, 1859) are recorded for the first time in Korea. The adults and genitalia of the newly recorded species are illustrated, and an updated checklist of Korean Epipaschiinae is provided. With these additions, Korean Epipaschiinae now comprises 24 species belonging to 10 genera.

Case Report

Materials and methods

The present study was based on specimens collected in Korea. Specimens were collected using a 220 V/200 W mercury vapor lamp (Dongseong Co., Busan, Korea) and four ultraviolet lamp (20 W, FL20SbL/18; Kumho Co., Gwangju, Korea) and four ultraviolet lamps (20 W, FL20SbL/18; Kumho Co., city, Korea). The genitalia were dissected and examined using a Leica EZ4 stereomicroscope (CMS GmbH, Wetzlar, Germany). Images of adults and their genitalia were captured using a Canon EOS 50D digital camera attached to a Canon EF 100 mm F2.8 Macro USM lens (Canon Inc., Tokyo, Japan) and a Leica DM 2500 microscope attached to a Leica ICC50 E (Leica Microsystems, CMS GmbH, Wetzlar, Germany). Voucher specimens were deposited in the Bio-Resource and Environmental Center, Incheon National University (INU), Korea.

Taxonomic accounts

Family Pyralidae Latreille, 1809

Subfamily Epipaschiinae Meyrick, 1884

Genus *Lamida* Walker, 1859

Lamida Walker, 1859a:252. TS: *Lamida moncusalis* Walker, 1859. Type locality (TL): Hindustan.

Allata Walker, 1863:110. TS: *Allata penicillata* Walker, 1862. TL: Hindustan.

Lamida obscura (Moore, 1888) (Fig. 1)

Orthaga obscura Moore, 1888:201. TL: India (Darjeeling).

Macalla obscura: Shibuya, 1927:346; Marumo, 1942:11; Inoue, 1955:143.

Macalla sordidalis Hampson, 1916:136. TL: India (Sikhim).

Macalla proximalis Caradja, 1925:390. TL: China (Canton).

Lamida obscura: Inoue and Yamanaka, 1975:109, pl. 1, Fig. 17; pl. 3, Fig. 22; pl. 8, Fig. 45; Solis, 1992:283; Yamanaka, 1998:112, pl. 143:12; Yamanaka, 2013:331, pl. 47, Figs. 10, 11.

Adult (Fig. 1A, B): Wingspan 25-28 mm in both sexes. Head covered with brown, mixed with grayish-yellow scales; ocellus present; chaetosema present; labial palpus slender, upturned, brown, mixed with grayish-yellow scales. Patagium grayish yellow, mixed with light brown scales; tegula with grayish yellow scales. Ground color of forewing grayish dark brown; basal area with irregular dark brown spots; postmedial band dark brown, irregularly dentate; adterminal line dark brown; fringe broad, light brown, mixed with dark brown scales. Ground color of hindwing grayish brown. Abdomen brown, mixed with grayish-brown.

Male genitalia (Fig. 1C): Uncus elongated and bifurcated at the apex, with hair present. Gnathos absent. Valva broad, rounded, and covered with hair. Vinculum orbicular. Saccus rounded and U-shaped. Juxta weakly sclerotized, slender, elongated, spine-shaped, acuminate at apex. Phallus cylindrical, slightly curved, and nearly the same length as the valva; aedeagus without cornutus.

Female genitalia (Fig. 1D): Papillae anales broadly triangular, with hairs at the apex. Posterior and anterior apophyses of nearly the same length. Apophyses anteriores 1.5 times broader than apophyses posteriores. Ostium bursae weakly sclerotized and cup-shaped. Ductus bursae short, half the length of the corpus bursae, membranous. Corpus bursae broad, ovate, and membranous, with a pair of semicircular signa.

Material examined: 3♂, 2♀, Mt. Cheonggye, Gwacheon-si (Gyeonggi Province [GG]), Korea, 20. VIII.1976 (Park), genitalia slides no. INU-10562, 10580; 1♂, Yeongjong-do, Incheon (GG), Korea, 03. VI.1995 (Paek & Ryu); 1♀, Mt. Gyemyeong, Chungju-si (Chungcheongbuk Province [CB]), Korea, 11-12. VII.2002 (Choi & Yeom), genitalia slide no. INU-10564; 1♂, Mt. Mudeung, Gwangju (Jeollanam Province [JN]), Korea, 11. VII.2000, (Lee, Yu, Kim & Park).

Distribution: Korea (new record), China, Taiwan, Japan, Nepal, India, and Malaysia.

Host plants: Fagaceae-*Castanopsis sieboldii* (Yamanaka, 2013).

Remarks: The genus *Lamida* Moore, 1885 was recorded in Korea for the first time and is represented by *Lamida obscura* (Moore, 1888) in the present study.

Genus *Lista* Walker, 1859

Lista Walker, 1859b:877. Type species (TS): *Lista genisusalis* Walker, 1859. TL: Borneo (Sarawak).

Paracme Lederer, 1863:338. TS: *Paracme insulsalis* Lederer, 1863.

Craneophora Christoph, 1881:1. TS: *Craneophora ficki* Christoph, 1881.

Belonepholis Butler, 1889:17, 89. TS: *Belonepholis striata* Butler, 1889. TL: India (Dharamshala).

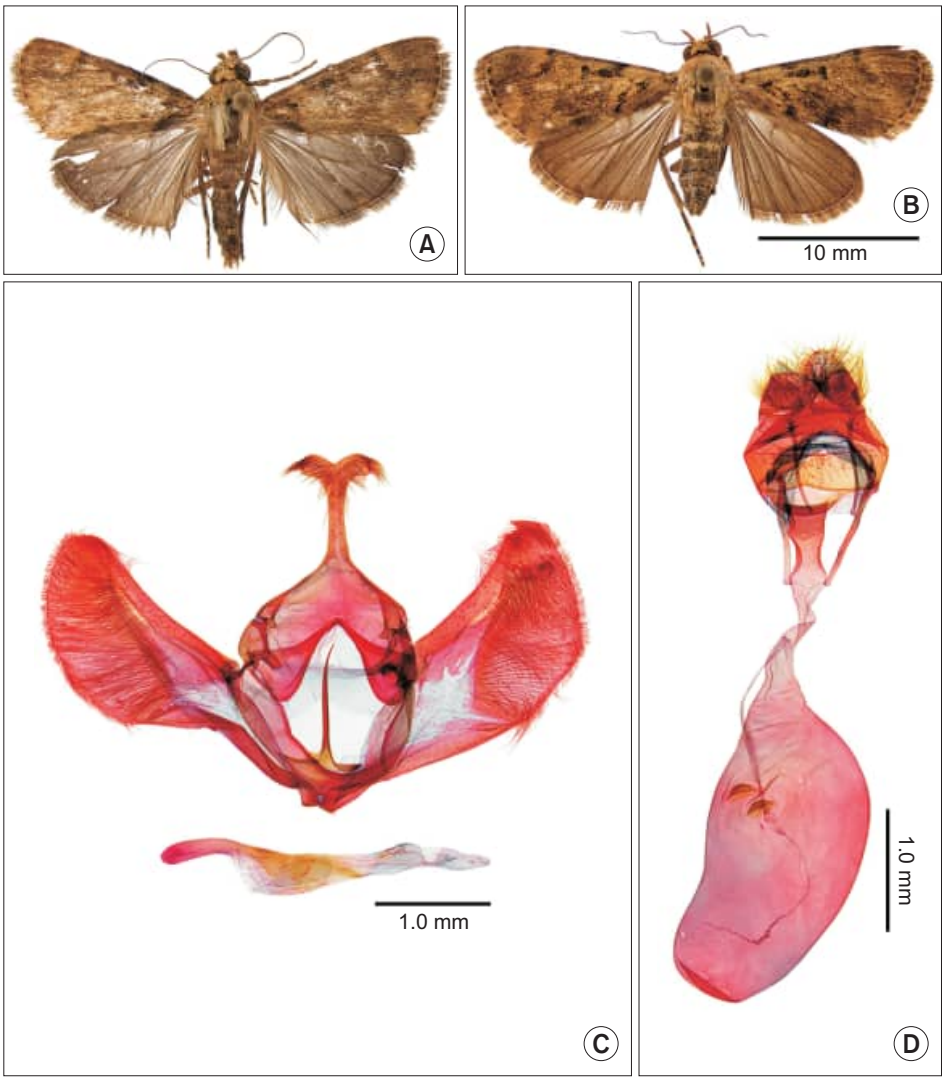

Fig. 1. *Lamida obscura* (Moore, 1888). (A) Male, (B) female, (C) male genitalia (INU-10599), and (D) female genitalia (INU-10564).

***Lista haraldusalis* (Walker, 1859) (Fig. 2)**

Locastra haraldusalis Walker, 1859a:160. TL: Borneo (Sarawak).

Lista genisusalis Walker, 1859b:877. TL: Borneo.

Stericta haraldusalis (Walker): Hampson, 1896:121, Fig. 70; Leech, 1901:416; Marumo, 1920:270; Shibuya, 1928:105.

Lista haraldusalis (Walker): Swinhoe, 1900:424; Solis, 1992:283.

Craneophora haraldusalis (Walker): Janse, 1931:474; Mutuura, 1957:105.

Lista ficki (Walker): Yamanaka, 2000:67; Figs. 1385, 1939 (misidentified).

Adult (Fig. 2A, B): Forewing length 10-11 mm in both sexes. Head covered with light-yellow scales; ocellus present; chaetosema present; labial palpus slender, upturned, light yellow, mixed with brown scales. Thorax grayish yellow mixed with brown scales. Ground color of forewing: brownish orange; basal area: dark brown; medial band: dark yellow; postmedial band: light yellow; distal area: brown; fringe: light yellow. Ground color of hindwing brownish-orange and the same pattern as forewing without an antemedial band. Abdomen light brown, mixed with dark brown scales.

Male genitalia (Fig. 2C): Uncus broad, acuminate on both sides, and apex rounded. Gnathos with approximately five small apical spines. Valva trapeziform, curved outward, costal margin sclerotized, and haired. Fibula thickly spine-shaped. Sacculus thickly sclerotized. Vinculum and saccus broadly U-shaped. Juxta orbicular, with two spines at the apex. Phallus rod-shaped, slightly curved, nearly the same length as the valva; aedeagus with a spine-shaped cornutus.

Female genitalia (Fig. 2D): Papillae: Anales ovoid, with setose apices. Posterior and anterior apophyses of nearly the same length. Ostium bursae sclerotized and deeply

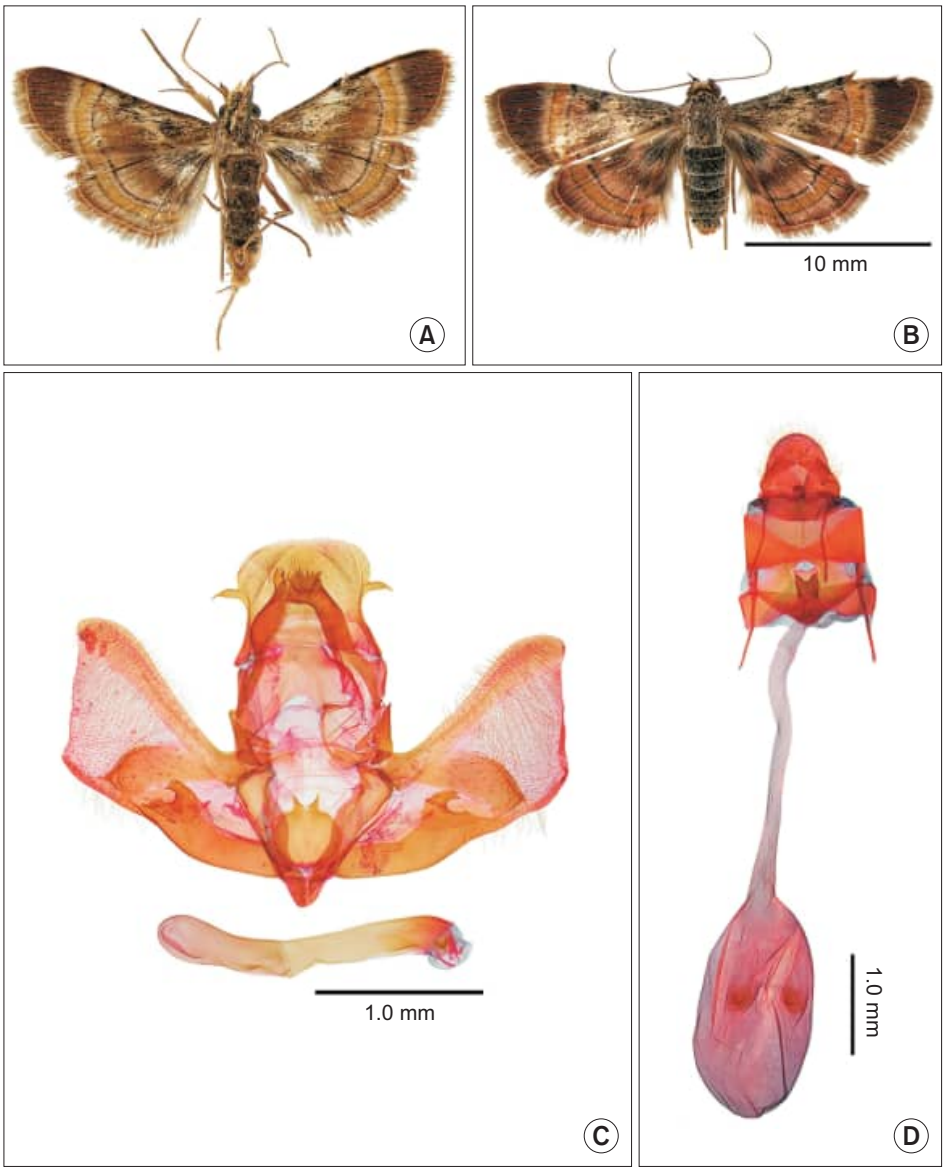

Fig. 2. *Lista haraldusalis* (Walker, 1859). (A) Male, (B) female, (C) male genitalia (INU-10594), and (D) female genitalia (INU-10595).

clefted distally. Ductus bursae membranous, approximately 1.5 times longer than corpus bursae. Corpus bursae ovate, membranous, with pair of ovoid sign, placed in first half of bursae.

Material examined: 1♀, Byeongbangchi, Jeongseon-gun (Gangwon Province [GW]), Korea, 06. VIII.2015, (Kim, Kim & Jung); 1♀, Mt. Chiak, Wonju-si (GW), Korea, 05. VIII.1998, (Ahn & Kim); 1♂, Imwon-ri, Samcheok-si (GW), Korea, 20. VI.2008, (Kim, Ju & Chae), genitalia slide no. INU-10592; 1♂, 2♀, Malgeunmul-pension, Hoengseong-gun (GW), Korea, 01. VII.2016, (Bae Y.S., Park B.S., Na S.M., Bayarsaikhan U. & Ko J.H.), genitalia slide no. INU-10553; 1♀, Mt. Sambang, Yeongwol-gun (GW), Korea, 09. VII.2001, (Bae Y.S., Kim Y.K. & Lee C.M.), genitalia slide no. INU-10510; 1♀, Daeseong Reservoir, Paltan-myeon, Hwaseong-si (GG), Korea, 03. VIII.1998, (Paek & Lee); 1♂, Mt. Gwanmo, Incheon (GG), Korea, 05. VIII.2003, (Bae *et al.*); 1♀, Mt. Kwangdeok, Hwacheon-gun (GW), Korea, 20. VII.1996 (Bae, Paek, Lee, Ahn & Jeon), genitalia slide no. INU-10524; 1♀, Mt. Myeongseong, Cheorwon-gun (GW), Korea, 20. VII.1999, (Paek, Lee & Oh); 1♀, Mt. Taehwa, Gwangju-si (GG), Korea, 21. VI.2018, (Na S.M., Lee D.J., Ko J.H., Lee T.G., Kim H.K. & Cha Y.B.); 1♀, Mt. Waebong, Gapyeong-gun (GG), Korea, 05. VI.2018, (36°48′17″N, 127°28′32″E), (Lee D.J., Kim H.K. & Jang C.M.); 1♂, Mt. Yongmun, Yangpyeong-gun (GG), Korea, 11. VIII.1998 (Lee, Ahn & Kim), genitalia slide no. INU-10511; 1♂, Mt. Baegam, Yeongyang-gun (Gyeongsangbuk Province [GB]), Korea, 15. VII.1999 (Lee, Kim & Kim), genitalia slide no. INU-10523; 1♀, Nari Basin,

Ulleung-gun (GB), Korea, 17. VII.2014, (Bae *et al.*); 1♂, Mungyeongsaejae Resort, Mungyeong-si (GB), Korea, 01. IX.2020, (36°44′21.4″N, 128°09′40.4″E), (Ko J.H., Cha Y.B. & Kim H.U.), genitalia slide no. INU-10598; 1♂, Mt. Jiri, Sancheong-gun (Gyeongsangnam Province [GN]), Korea, 25-28. VI.2001, (U.I.B.), genitalia slide no. INU-10594; 1♀, Mt. Chilgap, Cheongyang-gun (Chungcheongnam Province [CN]), Korea, 12. VII.2000, (Kim, Lee & Oh); 1♀, Hanseo University, Seosan-si (CN), Korea, 19. VII.2016, (Lee D.J. & Ko J.H.), genitalia slide no. INU-10595.

Distribution: Korea (new record), China, Japan, Nepal, India, and Malaysia.

Host plants: Juglandaceae-*Platycarya strobilacea* (Liu *et al.*, 2015).

Remarks: The genus *Lista* Walker was previously represented in Korea as a single species: *Lista ficki* Christoph. In this study, *L. haraldusalis* (Walker) is reported as a new record of Korean fauna.

A checklist of the subfamily Epipaschiinae from Korea

Genus *Epilepia* Janse, 1931

TS: *Macalla melanosparsalis* Janse, 1922.

Epilepia dentatum (Matsumura & Shibuya, 1927)

Macalla dentatum Shibuya, 1927:349. TL: Japan.

Distribution: Korea (GW, GG, GB, GN, Jeollabuk Province [JB], JN, and Jeju Island [JJ]), Taiwan, and Japan.

Genus *Lamida* Walker, 1859

TS: *Lamida moncusalis* Walker, 1859.

Lamida obscura (Moore, 1888) (Fig. 1)

Orthaga obscura Moore, 1888:201. TL: India (Darjeeling).

Distribution: Korea (new record), China, Taiwan, Japan, Nepal, India, and Malaysia.

Genus *Lista* Walker, 1859

TS: *Lista genisusalis* Walker, 1859.

Lista ficki (Christoph, 1881)

Craneophora ficki Christoph, 1881:2. TL: Russia (Amur).

Distribution: Korea (GW, GG, and CB), Russia, China, Japan, and Nepal.

Lista haraldusalis (Walker, 1859) (Fig. 2)

Locastra haraldusalis Walker, 1859a:160. TL: Borneo (Sarawak).

Distribution: Korea (GW, GG, GB, GN, and CN), China, Nepal, India, and Malaysia.

Genus *Locastra* Walker, 1859

TS: *Locastra maimonalis* Walker, 1859.

Locastra muscosalis (Walker, 1866)

Taurica muscosalis Walker, 1866:1268. TL: China.

Distribution: Korea (GG, GB, JN, and JJ), China, Taiwan, Japan, Nepal, India, Sri Lanka, and Malaysia.

Genus *Noctuides* Staudinger, 1892

TS: *Noctuides melanophia* Staudinger, 1892.

Noctuides melanophia Staudinger, 1892

Noctuides melanophia Staudinger, 1892:466, pl. 3, Fig. 22. TL: China and Russia (Amur).

Distribution: Korea (GW and GG), China, Japan, Russia, and Vietnam.

Genus *Orthaga* Walker, 1859

TS: *Orthaga euadrusalis* Walker, 1859.

Orthaga achatina (Butler, 1878)

Glossina achatina Butler, 1878:56. 38, Fig. 10. TL: Japan (Yokohama).

Distribution: Korea (GW, GG, CB, GB, and GN), China, Japan, and Russia.

Orthaga euadrusalis Walker, 1859

Orthaga euadrusalis Walker, 1859a:191. TL: Borneo (Sarawak).

Distribution: Korea (GW, GG, and JJ), China, Taiwan, Japan, Nepal, India, Malaysia, and Sri Lanka.

Orthaga olivacea (Warren, 1891)

Hyperbalanotis olivacea Warren, 1891:433. TL: Japan.

Distribution: Korea (GW, GG, CN, GB, JN, and JJ), China, Taiwan, Japan, and Russia.

Orthaga onerata (Butler, 1879)

Bleptina onerata Butler, 1879:447. TL: Japan.

Distribution: Korea (GW, GG, GB, GN, and JN), Japan, and Russia.

Genus *Stericta* Lederer, 1863

TS: *Glossina divitalis* Guenée, 1854.

Stericta kiiensis (Marumo, 1920)

Lepidogma kiiensis Marumo, 1920:266, pl. 16, Figs. 14-16. TL: Japan.

Distribution: Korea (GW, GG, GB, CN, and JN), China, Japan, Nepal, and India.

Stericta melanobasis (Hampson, 1906)

Lepidogma melanobasis Hampson, 1906:129. TL: Japan.

Distribution: Korea (GW, GG, GB, CB, CN, and JN), China, Taiwan, Japan, India, and Malaysia.

Stericta kogii Inoue and Sasaki, 1995

Stericta kogii Inoue and Sasaki, 1995:245, Figs. 1-3.

Distribution: Korea (GW, GG, CN, GB, and JN), China, Japan, and Russia.

Stericta flavopuncta Inoue and Sasaki, 1995

Stericta flavopuncta Inoue and Sasaki, 1995:247; Figs. 5-6. TL: Japan.

Distribution: Korea (GW, GG, CB, and CN), China, and Japan.

Stericta angusta (Inoue, 1988)
Jocara angusta Inoue, 1988:85, Figs. 1-3. TL: Japan.
Distribution: Korea (GG, CN, and JN) and Japan.
Genus *Teliphasa* Moore, 1888
TS: *Teliphasa orbiculifer* Moore, 1888.

Teliphasa amica (Butler, 1879)
Locastra amica Butler, 1879:447. TL: Japan.
Distribution. Korea (GW, GG, GB, GN, JB, and JN), China, Japan, and Russia.

Teliphasa albifusa (Hampson, 1896)
Macalla albifusa Hampson, 1896:113. TL: India (Sikhim).
Distribution: Korea (GW, GG, GB, GN, JB, and JN), China, Japan, and Russia.

Teliphasa elegans (Butler, 1881)
Locastra elegans Butler, 1881:581. TL: Japan (Yokohama).
Distribution: Korea (GW, GG, CB, GB, and GN), China, Japan, and Russia.
Genus *Termioptycha* Meyrick, 1889
TS: *Termioptycha cyanopa* Meyrick, 1889.

Termioptycha bilineata (Wileman, 1911)
Macalla bilineata Wileman, 1911:364. TL: Japan (Shibuya).
Distribution: Korea (GG and JN), China, and Japan.

Termioptycha inimica (Butler, 1879)
Locastra inimica Butler, 1879:448. TL: Japan.
Distribution: Korea (GW, GG, CB, and GB), China, Japan, and Russia.

Termioptycha margarita (Butler, 1879)
Locastra margarita Butler, 1879:66. pl. 57, Fig. 4. TL: Japan (Yokohama).
Distribution: Korea (GW, GG, GB, JB, JN, and JJ), China, Taiwan, Japan, India, Malaysia, Sri Lanka, and Borneo.

Termioptycha eucarta (Felder *et al.*, 1875)
Ethnistis eucarta Felder *et al.*, 1875:28. TL: Indonesia (Moluccas).
Distribution: Korea (GW and GG), China, Japan, Indonesia, Papua New Guinea, and Australia.

Termioptycha nigrescens (Warren, 1891)
Parasarama nigrescens Warren, 1891:428. TL: Japan (Yesso).
Distribution: Korea (GW and GG), Japan, and Russia.
Genus *Trichotophysa* Warren, 1896
TS: *Trichotophysa olivalis* Warren, 1896.

Trichotophysa jucundalis (Walker, 1866)
Bleptina jucundalis Walker, 1866: 1164. TL: Sri Lanka.
Distribution: Korea (GG and JN), China, and Japan.

Discussion

In this study, *Lamida obscura* (Moore, 1888) and *Lista haraldusalis* (Walker, 1859) were recorded for the first time in Korea, and the genus *Lamida* Walker, 1859 was newly recorded in the Korean fauna. With these additions, the Korean Epipaschiinae now comprises 24 species belonging to 10 genera.

Both species are distributed in East and Southeast Asia and adjacent regions. Considering their broad distribution in East and Southeast Asia, the occurrence of these species in Korea was not unexpected. Their previous lack of records in Korea is likely due to limited collection efforts and insufficient taxonomic studies on Epipaschiinae in Korea.

The available host plant records indicate that host plants suitable for both newly recorded species are widely available in South Korea. Additional surveys are required to clarify their distribution, host–plant associations, and ecology.

The discovery of two previously unrecorded species and one previously unrecorded genus highlights the fact that the diversity of Epipaschiinae in Korea remains incompletely understood. Additional faunistic and taxonomic studies, particularly in forest habitats and under-surveyed regions, are likely to reveal further unrecorded taxa and contribute to a better understanding of the Korean pyralid fauna.

Author Contributions

Conceptualization: HK, JHK, UB. Data curation: HK. Formal analysis: HK. Funding acquisition: JHK. Investigation: HK. Methodology: HK, JHK. Visualization: HK. Writing – original draft: HK. Writing – review & editing: HK, JHK, UB.

Conflict of Interest

The authors declare that they have no competing interests.

Acknowledgments

We express our gratitude to Professor Yang-Seop Bae (Incheon National University, Incheon, Republic of Korea), Dr. Tak-Gi Lee (Yangpyeong Insect Museum, Yangpyeong-gun, Republic of Korea), and Dr. Yeong-Bin Cha (Division of Forest Biodiversity, Korea National Arboretum, Pocheon, Republic of Korea) for their assistance with specimen collection.

Funding

This work was supported by a grant from the National Institute of Biological Resources (NIBR), funded by the Ministry of Climate, Energy, and Environment (MCEE) of the Republic of Korea (NIBR201801201).

References

Bae, Y.S. (2004). *Superfamily Pyraloidea II (Phycitinae & Crambinae etc.), Economic Insects of Korea 22. Insecta Koreana Supplement 29*. National Institute of Agricultural Science and Technology.

Bae, Y.S., Byun, B.K., and Paek, M.K. (2008). *Pyralid Moths of Korea (Lepidoptera, Pyraloidea)*. Korea National Arboretum.

Butler, A.G. (1878). *Illustrations of typical specimens of Lepidoptera Heterocera in the collection of the British Museum. Pt. II.* British Museum.

Butler, A.G. (1879). LI. Descriptions of new species of Lepidoptera from Japan. *Annals and Magazine of Natural History*, 4, 349-374, 437-457. https://doi.org/10.1080/00222937908679865

Butler, A.G. (1881). Descriptions of new genera and species of heterocerous Lepidoptera from Japan. *Transactions of the Royal Entomological Society of London*, 29, 579-600. https://doi.org/10.1111/j.1365-2311.1881.tb00882.x

Butler, A.G. (1889). *Illustrations of typical specimens of Lepidoptera Heterocera in the collection of the British Museum. Part VII*. British Museum.

Caradja, A.V. (1925). Ueber Chinas Pyraliden, Tortriciden, Tineiden nebst kurze Betrachtungen, zu denen das Studium dieser Fauna Veranlassung gibt: (Eine biogeographische Skizze). *Memoriile Sectiunii Stiintifice. Academia Romana*, 3, 257-383. *German*.

Christoph, H.T. (1881). Neue Lepidopteren des Amurgebietes. *Bulletin de la Société impériale des naturalistes de Moscou*, 56, 1-80.

Felder, C., Felder, R., and Rogenhofer, A.F. (1875). Heterocera. In C. Felder, R. Felder, and A.F. Rogenhofer (Eds.), *Voyage of the Austrian Frigate Novara Around the World in the Years 1857, 1858, and 1859 under the Command of Commodore B. von Wüllerstorf-Urbair. Zoological Part*. (pp. 1-20). Kaiserlich-Königliche Hof- und Staatsdruckerei. *German*.

Hampson, G.F. (1896). *The Fauna of British India, including Ceylon and Burma. Moths. Vol. 4*. Taylor & Francis.

Hampson, G.F. (1906). XVII. On new Thyrididae and Pyralidae. *Annals and Magazine of Natural History*, 17, 112-147.

Hampson, G.F. (1916). Descriptions of new Pyralidae of the subfamilies Epipaschiinae, Chrysauginae, Endotrichinae, and Pyralinae. *Annals and Magazine of Natural History*, 18, 126-160.

Inoue, H. (1955). *Check List of the Lepidoptera of Japan. Part 2: Alucitidae–Epicopeidae*. Rikusuisha.

Inoue, H. (1988). A new species of the Epipaschiinae from Japan, with some synonymic notes on the Pyralidae from East Asia (Lepidoptera). *Tinea*, 12, 85-95.

Inoue, H., and Sasaki, H. (1995). On the eastern Palaearctic Stericta atribasalis Hampson, with description of a new species (Pyralidae, Epipaschiinae). *Lepidoptera Science*, 45, 245-250. https://doi.org/10.18984/lepid.45.4_245

Inoue, H., and Yamanaka, H. (1975). A revision of the Japanese species formerly assigned to the genus *Macalla* Walker (Lepidoptera: Pyralidae). *Bulletin of Faculty of Domestic Sciences of Otsuma Woman's University*, 11, 95-112.

Janse, A.J.T. (1931). A contribution towards the study of the genera of the Epipaschiinae (family Pyralidae). *Transactions of the Royal Entomological Society of London*, 79, 439-492. https://doi.org/10.1111/j.1365-2311.1931.tb00712.x

Ju, J.S. (1999). Additional records on the fauna of lepidopterous insects from Is. Chin-do, Chollanam-do, Korea. *Journal of the Lepidopterological Society of Korea*, 11, 29-32.

Kim, H., Lee, T.G., Cha, Y.B., Jang, C.M., Kim, J.N., Bayarsaikhan, U., *et al*. (2021). Review of the genus Stericta Lederer (Lepidoptera: Pyralidae: Epipaschiinae) from Korea. *Journal of Asia-Pacific Biodiversity*, 14, 371-377. https://doi.org/10.1016/j.japb.2021.04.003

Kim, H., Lee, T.G., Cha, Y.B., Jang, C.M., Kim, J.N., Bayarsaikhan, U., *et al*. (2023). A review of the genus Termioptycha Meyrick (Lepidoptera: Pyralidae: Epipaschiinae) from Korea. *Journal of Asia-Pacific Biodiversity*, 16, 590-596. https://doi.org/10.1016/j.japb.2023.03.010

Kim, S.S., and Paek, M.K. (2020). *A photographic guide to Korean moths*. Nature and Ecology.

Lederer, J. (1863). [Contribution to the knowledge of pyralid moths]. *Wiener Entomologische Monatschrift*, 7, 243-280. *German*.

Leech, J.H. (1901). XV. Lepidoptera Heterocera from China, Japan, and Corea. *Transactions of the Royal Entomological Society of London*, 49, 385-514. https://doi.org/10.1111/j.1365-2311.1901.tb01371.x

Liu, J., Yang, M., Hu, J., Shang, X., Song, Q., Li, B., *et al*. (2015). Investigation on the resource and utilization situation of insect tea in Guizhou. *Guizhou Agricultural Sciences*, 43, 62-65.

Marumo, N. (1920). A revision of the Japanese Pyralidae. Part I (Subfamily Epipaschiinae). *Journal of the College of Agriculture, Imperial University of Tokyo*, 6, 265-274.

Marumo, N. (1942). Studies on rice borers VI: classification of the subfamily Pococerinae in Japan. *Department of Agriculture, Ministry of Agriculture and Forestry*, 161, 1-29.

Moore, F. (1888). Pyralidae, Crambidae, Geometridae, Tortricidae, Tineidae. In W.C. Hewitson, F. Moore (Eds.), *Descriptions of new Indian lepidopterous insects from the collection of the late Mr. W.S. Atkinson*. (pp. 199-299). Asiatic Society of Bengal.

Mutuura, A. (1957). Pyralidae. In T. Esaki, S. Issiki, A. Mutuura, H. Inoue, H. Ogata, H. Okagaki, *et al*. (Eds.), *Icones Heterocerorum Japonicorum in Coloribus Naturalibus. vol. 1.* (pp. 93-147). Hoikusya.

Nuss, M., Landry, B., Mally, R., Vegliante, F., Tränkner, A., Bauer, F., *et al*. (2003-2024). Global information system on pyraloidea. *GlobIZ*. Retrieved May 1, 2026 from https://www.pyraloidea.org/.

Paek, M.K., Hwang, J.M., Jung, K.S., Kim, T.W., Kim, M.C., Lee, Y.J., *et al*. (2010). *Checklist of Korean insects*. Nature and Ecology.

Park, K.T. (1983). Pyralidae. In Y.H. Shin, and S.H., Nam (Eds.), *Illustrated Flora & Fauna of Korea Vol. 27, 9* (pp. 298-444). Ministry of Education.

Shibuya, J. (1927). A study on the Japanese Epipaschiinae. *Transactions of the Natural History Society of Formosa*, 17, 339-359.

Shibuya, J. (1928). The systematic study on the Pormosan Pyralidae. *Journal of the Faculty of Agriculture, Hokkaido Imperial University*, 22, 1-300.

Solis, M.A. (1992). Checklist of the old world Epipaschiinae and the related new world genera Macalla and Epipaschia (Pyralidae). *Journal of the Lepidopterists' Society,* 46, 280-297.

Solis, M.A. (1993). A phylogenetic analysis and reclassification of the genera of the Pococera complex (Lepidoptera: Pyralidae: Epipaschiinae). *Journal of the New York Entomological Society,* 101, 1-83.

Staudinger, O. (1892). [The following species illustrated on Plate III will be described in the next volume of this journal]. *Deutsche entomologische Zeitschrift Iris*, 5, 466. *German*.

Swinhoe, C. (1900). Epipaschiidae. In C. Swinhoe, L. Walsingham, J.H. Durrant (Eds.), *Catalogue of Eastern and Australian Lepidoptera Heterocera in the collection of the Oxford University Museum Part II*. (pp. 421-426). Clarendon Press.

Walker, F. (1859a). *List of the specimens of lepidopterous insects in the collection of the British Museum 16*. British Museum.

Walker, F. (1859b). *List of the specimens of lepidopterous insects in the collection of the British Museum 19*. British Museum.

Walker, F. (1863). *List of the specimens of lepidopterous insects in the collection of the British Museum 27*. British Museum.

Walker, F. (1866). *List of the specimens of lepidopterous insects in the collection of the British Museum 34*. British Museum.

Wang, M., Chen, F., Zhu, C., and Wu, C. (2021). Checklist of Epipaschiinae in China (Lepidoptera: Pyralidae). *Zoological Systematics*, 46, 328-341. https://doi.org/10.11865/zs.2021407

Warren, W. (1891). LVII. Descriptions of new genera and species of Pyralidae contained in the British-Museum collection. *Annals and Magazine of Natural History*, 7, 423-438, 494-501. https://doi.org/10.1080/00222939109460654

Wileman, A.E. (1911). XV. New and unrecorded species of Lepidoptera Heterocera from Japan. *Transactions of the Royal Entomological Society of London*, 59, 189-407. https://doi.org/10.1111/j.1365-2311.1911.tb03088.x

Yamanaka, H. (1998). Pyralidae of Nepal, II. In T. Haruta (Ed.), *Moths of Nepal, Part 5. Tinea Vol. 15 (Supplement 1) (pp. 99-114).* The Japan Heterocerists' Society.

Yamanaka, H. (2000). Pyralidae of Nepal (III). In T. Haruta (Ed.), *Moths of Nepal part 6. Tinea Vol. 16 (Supplement 1) (pp. 63-69).* The Japan Heterocerists' Society.

Yamanaka, H. (2013). Epipaschiinae, Pyralidae. In Y. Nasu, T. Hirowatari, Y. Kishida (Eds.), *The standard of moths in Japan IV* (pp. 62, 329-334). Gakken Education Publishing. *Japanese*.

Instruction for Authors

PNIE PROCEEDINGS OF THE NATIONAL INSTITUTE OF ECOLOGY OF THE REPUBLIC OF KOREA

Enacted August 5, 2020
Revised March 19, 2024
Revised June 23, 2025

AIMS AND SCOPE

Proceedings of the National Institute of Ecology of the Republic of Korea (PNIE; pISSN 2765-2203, eISSN 2765-2211) is an open access and online journal aimed at promoting outcomes of basic ecological research carried out in Korea and abroad. The journal focuses on basic ecological research on terrestrial and aquatic populations, communities, ecosystems, and landscapes, as well as applied issues such as data science and climate change in the context of ecological research.

GENERAL INFORMATION

PNIE is the official English language journal of the National Institute of Ecology (NIE) of the Republic of Korea. PNIE started its first issue on November 1, 2020. PNIE is published quarterly in a year (February 1, May 1, August 1, November 1). The journal publishes research papers, invited reviews and data papers. This multidisciplinary journal is a showcase of original research being conducted by ecologists in Korea and abroad. PNIE is also committed to representing ecological research from the Asia-Pacific region. Worldwide cooperative research initiatives are also welcome. PNIE is indexed in Google Scholar and KCI (Korea Citation Index).

CONTACTS

For subscription and all other information visit our website available from: https://acoms.accesson.kr/pnie/oprs/main/jrnlMain.do. To subscribe to this journal or renew your current subscription, please contact us through Tel (+82-41-950-5421), or E-mail: pnie@nie.re.kr.

OPEN ACCESS

This is an open access journal available free of charge. Articles published in PNIE are distributed under the terms of the Creative Commons Attribution Non-Commercial License (https://creativecommons.org/licenses/by-nc/4.0/), which permits unrestricted noncommercial use, distribution, and reproduction in any medium, provided the original work is properly cited. For any commercial use of material from the open access version of the journal, permission must be obtained from the Editorial Board.

EDITORIAL POLICIES AND ETHICAL CONSIDERATIONS

PNIE adheres to the research and publication ethics policies outlined in International Standards for Editors and Authors (https://publicationethics.org/resources/international-standards-for-editors-and-authors) and Recommendations for the Conduct, Reporting, Editing, and Publication of Scholarly Work in Medical Journals (https://www.icmje.org/recommendations); International Committee of Medical Journal Editors (ICMJE). Any studies involving human subjects must comply with the principles of the World Medical Association Declaration of Helsinki (2024; https://www.wma.net/policies-post/wma-declaration-of-helsinki/). Clinical research should be approved by the Institutional Review Board (IRB), as well as through patient consent. A patient's personal information cannot be published in any form. However, if it is absolutely necessary to use a patient's personal information, the consent of the patient or their guardian will be needed before publishing. Animal studies should be performed in compliance with all relevant guidelines, including the standards described in the National Institutes of Health (NIH) Guide for the Care and Use of Laboratory Animals and the guidelines provided by the Institutional Animal Care and Use Committee (IACUC).

Cases that require editorial expressions of concern or retraction shall follow the Committee on Publication Ethics (COPE) flowcharts available from: https://publicationethics.org/resources/flowcharts. If a correction is needed, it will follow the ICMJE Recommendation for Corrections, Retractions, Republications and Version Control available from: https://www.icmje.org/recommendations/browse/publishing-and-editorial-issues/corrections-and-version-control.html.

Honest errors are a part of science and publishing and require publication of a correction when they are detected. Corrections are needed for errors of fact. Minimum standards are as follows: First, it shall publish a correction notice as soon as possible, detailing changes from and citing the original publication on both an electronic and numbered print page that is included in an electronic or a print Table of Contents to ensure proper indexing; Second, it shall post a new article version with details of the changes from the original version and the date(s) on which the changes were made through K-Mark; Third, it shall archive all prior versions of the ar-

ticle. This archive shall be directly accessible to readers; and Fourth, previous electronic versions shall prominently note that there are more recent versions of the article via K-Mark.

1. Copyright

The copyright for all publications is owned by NIE. Permission must be obtained from the NIE for any commercial use of materials. All authors must sign a "Copyright Transfer Agreement" and submit it online through the PNIE electronic submission system (https://acoms.accesson.kr/pnie/oprs/main/jrnlMain.do).

2. Copyright Transfers

Any usage rights are regulated through the Creative Commons License. NIE Publishers uses a Creative Commons Attribution Non-Commercial License (CC-BY-NC), which permits reusers to distribute, remix, adapt, and build upon the material in any medium or format for non-commercial purposes only if attribution is provided.

Authors of approved manuscripts shall acknowledge that the copyright of the manuscript is held by the NIE and shall agree that NIE holds the rights to publish, transmit, sell, and distribute the manuscript through academic journals or other media.

3. Data Sharing and Data Accessibility

Authors should include a data accessibility statement, including a link to the repository they have used, in order that this statement can be published alongside their paper. This journal follows the data sharing policy described in "Data Sharing Statements for Clinical Trials: A Requirement of the International Committee of Medical Journal Editors". The ICMJE's policy regarding trial registration is explained at https://www.icmje.org/recommendations/browse/publishing-and-editorial-issues/clinical-trial-registration.html. If the data sharing plan changes after registration, this should be reflected in the statement submitted and published with the manuscript, and updated in the registry record.

4. Desk Rejection

During the pre-review evaluation the Editor-in-Chief or Subject Editors check the manuscript for compliance with the journal's guidelines, focus, and scope. At this point, they may reject a manuscript prior to sending it out for peer review, specifying the reasons. The most common ones are non-conformity with the journal's focus, scope, and policies and/or low scientific or linguistic quality. In such cases, authors are encouraged to substantially improve their manuscript and resubmit it for review. We encourage authors whose manuscripts have been desk rejected due to being out of the scope of this journal to consider another potentially suitable title from the PNIE Editorial Board.

If the manuscript is suitable for the journal but has to be corrected technically or linguistically, it will be returned to the authors for improvement. The authors will need to re-submit.

5. Peer Review

The acceptance criteria for all papers are the quality and originality of the research and its significance to our readership. Except where otherwise stated, manuscripts are peer reviewed by two anonymous reviewers and the Editor. We adopt single-blind peer review, in which reviewers are aware of the authors' identities, but authors do not know the identities of the reviewers. Final acceptance or rejection rests with the Editorial Board, which reserves the right to refuse any material for publication.

Authors should abide by the decision made, and if asked to submit a revised version of their manuscript, do so by the designated due date.

Manuscripts should be written in a clear, concise, direct style. Where contributions are judged as acceptable for publication on the basis of scientific content, the Editor and the Publisher reserve the right to modify manuscripts to eliminate ambiguity and repetition and to improve communication between authors and readers. If extensive alterations are required, the manuscript will be returned to the authors for revision.

6. Ethical Considerations

Any experiments involving animals must be ethically acceptable and, where relevant, conform to national guidelines for the use of animals in research.

In taxonomic papers, type specimens and type repositories must be clearly designated and indicated. Authors are required to deposit the name-bearing type material in internationally recognized institutions (not private collections).

When the research is carried out in areas for which research permits are required (e.g., nature reserves), or when it deals with organisms for which collection or import/export permits are required (e.g., protected species), the authors must clearly detail how they obtained these permits in the Acknowledgments section.

7. Authorship Policy

All listed authors must have contributed significantly to the paper, and all authors must be in agreement with the content of the submitted manuscript and must approve of the final version. Please see "Research and Publication Ethics" for detailed information on authorship and author's responsibilities.

8. Conflicts of Interest

The journal requires that all authors disclose any potential sources of conflict of interest. Any interest or relationship, financial or otherwise, that might be perceived as influenc-

ing an author's objectivity is considered a potential source of conflict of interest. These must be disclosed when directly relevant or directly related to the work that the authors describe in their manuscript. Potential sources of conflict of interest include, but are not limited to, patent or stock ownership, membership of a company board of directors, membership of an advisory board or committee for a company, and consultancy for or receipt of speaker's fees from a company. The existence of a conflict of interest does not preclude publication. It is the responsibility of the corresponding author to review this policy with all authors and collectively to disclose with the submission ALL pertinent commercial and other relationships. If there are no competing interests, the statement should read, "The authors declare that they have no competing interests." Additionally, potential conflicts of interest of editorial board members should also be disclosed in the manuscript.

9. Publication Ethics

This journal is a member of the COPE. Note this journal uses the iThenticate tool of the Similarity Check program to screen published and submitted content for originality. For more information on Similarity Check, see https://www.crossref.org/services/similarity-check/. All manuscripts submitted to PNIE are subject to screening using the iThenticate tool for textual similarity to other previously published works.

Reproduction of Copyright Material. If excerpts from copyrighted works owned by third parties are included, credit must be shown in the contribution. It is the author's responsibility to also obtain written permission for reproduction from the copyright owners.

MANUSCRIPT SUBMISSION

1. Select Article Type

• Original (Research) Articles

Original (Research) Article publishes research on basic ecology of terrestrial and aquatic populations, communities, ecosystems, and landscapes, as well as ecological research in general. Manuscripts include a title page (with a running title), abstract and keywords, text (introduction, materials and methods, results, and discussion), author contributions, conflicts of interest, acknowledgments, funding, references, tables, figures, and figure legends.

• Review Articles

Review Article is expected to be a focused discussion of defined topics relevant to the scope of PNIE. General remarks are the same as those for the original article. Manuscripts include a title page (with a running title), abstract and keywords, text, author contributions, conflicts of interest, acknowledgments, funding, references, tables, figures, and figure legends.

• Case Reports

Unique cases that make an important teaching point or scientific observation may be suitable for a case report. This should consist of a title page, abstract, text (including introduction, case report, and discussion), author contributions, conflicts of interest, acknowledgments, funding, references, tables, figures, and figure legends.

2. Submission

Thank you for your interest in PNIE. Note that submission implies that the content has not been published or submitted for publication elsewhere except as a brief abstract in the proceedings of a scientific meeting or symposium.

Once you have prepared your submission in accordance with the Guidelines, manuscripts should be submitted online at https://acoms.accesson.kr/pnie/oprs/main/jrnlMain.do.

- At least two files should be submitted.
  The covering letter and the manuscript. The covering letter should be uploaded as a file not for review. Figures and tables should also be uploaded as separate files.
- Submissions should be double-spaced.
  The top, bottom and side margins should be at least 30 mm. All pages should be numbered consecutively in the top right-hand corner, beginning with the title page.
- MS Word format is preferred.
  The submission system will prompt you to use an Open Researcher and Contributor ID (ORCiD) to help distinguish your work from that of other researchers.

For help with submissions, please contact:
- Homepage: https://www.nie.re.kr
- E-mail: pnie@nie.re.kr
- Tel: +82-41-950-5421

We look forward to your submission.

3. Publication Charges

There are no charges to publish an article in PNIE. There is also no submission fee. PNIE is an academic journal published with the support of the NIE.

4. Preparing Your Submission

Submissions should be double-spaced. The top, bottom and side margins should be at least 30 mm. All pages should be numbered consecutively in the top right-hand corner, beginning with the title page.

- The entire article should be supplied as a single file; only figures and tables should be supplied as separate files.
- Figures must be supplied as high resolution .tif or .eps

files. For more information, refer to 'Figures' later in this document.
- Specify the first author's surname, the journal title and the manuscript number.
- MS Word format is preferred.

1) Covering Letter
Papers are accepted for publication in the journal on the understanding that the content has not been published or submitted for publication elsewhere. This must be stated in the covering letter.

The covering letter must also contain an acknowledgment that all authors have contributed significantly, and that all authors are in agreement with the content of the manuscript. The role of each author should be written.
Authors must declare any financial support or relationships that may pose conflict of interest.

If tables or figures have been reproduced from another source, a letter from the copyright holder (usually the Publisher), stating authorization to reproduce the material, must be attached to the covering letter.

2) Pre-submission English-language Editing
Authors for whom English is a second language may be recommended to have their manuscript professionally edited before submission to improve the English.

3) Style of the Manuscript
Spelling. The journal uses US spelling and authors should therefore follow the latest edition of the Merriam–Webster's Collegiate Dictionary.

Units. All measurements must be given in SI or SI-derived units.

Abbreviations. Abbreviations should be used sparingly – only where they ease the reader's task by reducing repetition of long, technical terms. Initially use the word in full, followed by the abbreviation in parentheses. Thereafter use the abbreviation only.

Trade names. Chemical substances should be referred to by the generic name only. Trade names should not be used.

Zoological nomenclature. All papers must conform to the latest edition of the International Code of Zoological Nomenclature. Upon its first use in the title, abstract and text, the common name of a species should be followed by the scientific name (genus, species and authority) in parentheses. Genus names should not be abbreviated at the beginning of paragraphs.

Genetic nomenclature. Standard genetic nomenclature should be used.
Nucleotide sequence data can be submitted in electronic form to any of the three major collaborative databases: DDBJ, EMBL or GenBank. It is only necessary to submit to one database as data are exchanged between DDBJ, EMBL and GenBank on a daily basis. The suggested wording for referring to accession-number information is: "These sequence data have been submitted to the DDBJ/EMBL/GenBank databases under accession number U12345."

Addresses are as follows:
DNA Data Bank of Japan (DDBJ) https://www.ddbj.nig.ac.jp
EMBL Nucleotide Sequence Submissions https://www.ebi.ac.uk
GenBank https://www.ncbi.nlm.nih.gov

MANUSCRIPT ORGANIZATION AND FORMAT

1. Word Length
The length of an article (including references, tables and appendices) should not exceed 20 printed pages for research papers and invited reviews.

2. Parts of the Manuscript
Manuscripts should be presented in the following order: (i) title page, (ii) abstract and keywords, (iii) text, (iv) author contributions, (v) conflicts of interest, (vi) acknowledgments, (vii) funding, (viii) supplementary information, (ix) references, (x) tables (each table complete with title and footnotes), (xi) figure legends and (xii) appendices. Figures and supporting information should be supplied in separate files, if relevant. Footnotes to the text are not allowed and any such material should be incorporated into the text as parenthetical matter.
Divide your article into clearly defined sections. Each subsection is given a brief heading. Each heading should appear on a separate line.

1) Title Page
The title page should contain:
(i) a short informative title that contains the major key words. The title should not contain abbreviations;
(ii) a short running title of less than 40 characters;
(iii) the full names and ORCIDs of the authors;
(iv) the author's institutional affiliations at which the work was carried out.
The present address of any author, if different from that where the work was carried out, should be supplied in a footnote.

2) Abstract and Keywords
All articles must have a brief abstract that states in 250 words or fewer the purpose, basic procedures, main findings and principal conclusions of the study. The abstract should not contain abbreviations or references.

Up to six key words (for the purposes of indexing) should be supplied below the abstract in alphabetical order. For the selection of keywords, refer to Medical Subject Heading in Index Medicus or in internet site, https://www.nlm.nih.gov/mesh/MBrowser.html.

3) Text

Authors should use the following subheadings to divide the sections of their manuscript: Introduction, Materials and Methods, Results, and Discussion.

(1) Introduction

Study rationale and relevant background information should be described clearly and concisely.

(2) Materials and Methods

Study materials and methods should be described in the following order: study design, materials and methods.

Ensure correct use of the terms sex (when reporting biological factors) and gender (identity, psychosocial or cultural factors), and, unless inappropriate, report the sex and/or gender of study participants, the sex of animals or cells, and describe the methods used to determine sex and gender. If the study was done involving an exclusive population, for example in only one sex, authors should justify why, except in obvious cases (e.g., prostate cancer). Authors should define how they determined race or ethnicity and justify their relevance.

Any study using human subjects or materials should be approved by the IRB, as well as through patient consent. Affiliation name of IRB and approval number must be clearly stated as follows: "This study was approved by the IRB of [Name of Affiliation] (Approval Number)". Any study using animals should state the IACUC approval and number. Any other ethics approvals should also be listed. If no ethical approvals were achieved or required, please state the reason (e.g., "In this study, the IRB of [Name of Affiliation] approved the exemption and allowed authors to review the patient's records with no need for informed consent.")

(3) Results

Study results should be reported in a clear and logical manner.

(4) Discussion

The results must be explained in relation to the hypotheses proposed in the Introduction. Keep in mind that the Discussion must not be a mere restatement of the results. Authors must emphasize new and important discoveries of the study and state the conclusions drawn from the results in relation to the purpose of the study. The shortcomings and limitations of the study must also be mentioned.

(5) Author Contributions

Enter all author contributions in the submission system during submission. The contributions of all authors must be described using the CRediT Taxonomy of author roles. Read the policy. To qualify for authorship, all contributors must meet at least one of the seven core contributions (conceptualization, methodology, software, validation, formal analysis, investigation, and data curation), as well as at least one of the writing contributions (original draft preparation, review, and editing). Authors may also satisfy the other remaining contributions; however, these alone will not qualify them for authorship. Contributions will be published with the final article, and they should accurately reflect contributions to the work. The submitting author is responsible for completing this information at submission, and it is expected that all authors will have reviewed, discussed, and agreed to their individual contributions prior to manuscript submission.

• Example of author contributions:

Conceptualization: ***, ***. Data curation: ***, ***. Formal analysis: ***, ***. Funding acquisition: ***, ***. Investigation: ***, ***. Methodology: ***, ***. Project administration: ***, ***. Resources: ***, ***. Software: ***, ***. Supervision: ***, ***. Validation: ***, ***. Visualization: ***, ***. Writing – original draft: ***, ***. Writing – review & editing: ***, ***.

(6) Conflicts of Interest

The authors must disclose any potential conflicts of interest possibly influencing the research or interpretation of data at the time of submission. In particular, all sources of funding for a study should be explicitly stated. Statements on conflict of interest have no influence on the editorial decision to publish. If there are no competing interests, the statement should read, "The authors declare that they have no competing interests." Additionally, potential conflicts of interest of editorial board members should also be disclosed in the manuscript.

(7) Acknowledgments

Any persons that contributed to the study or the manuscript, but who do not meet the requirements of authorship, could be placed here. For mentioning any persons or any organizations in this section, there should be a written permission from them.

(8) Funding

For each source of funds, both the research funder and the grant number should be listed here. If there is no funding source, the following is an example of a sentence that can be used: "None".

4) References

The Harvard (author, date) system of referencing is used (examples are given below). In the text, give the author's name followed by the year in parentheses: Smith (2000). If there are two authors use 'and': Smith and Jones (2001); but if cited within parentheses use '&': (Smith & Jones, 2001).

When reference is made to a work by three or more authors, the first name followed by et al. should be used: MacDonald *et al*. (2002). In the reference list, references should be listed in alphabetical order.
In the reference list, cite the names of all authors when there are six or fewer; when seven or more, list the first six followed by *et al*. Do not use *ibid*. or *op cit*. Reference to unpublished data and personal communications should not appear in the list but should be cited in the text only (e.g. A. Smith, unpubl. data, 2005). All citations mentioned in the text, tables or figures must be listed in the reference list.
Authors are responsible for the accuracy of the references.

(1) Journal Article
Sugumaran, M., Saul, S.J., and Ramesh, N. (1985). Endogenous protease inhibitors prevent undesired activation of prophenoloxidase in insect haemolymph. *Biochemical and Biophysical Research Communications*, 132, 1124–1129. https://doi.org/10.1016/0006-291x(85)91923-0

(2) Book
Chapman, R.F. (1971). *The Insects: Structure and Function*, 3rd ed. Elsevier.

(3) Web Sites
Chapman, K., and Brown, M. (2010). The future of digital library in Asia. *Digital Libraries*, 7, 111-119. Retrieved May 5, 2010 from https://www.diglib.org/publist.htm.
GBIF. (2024). *Global biodiversity information facility*. Retrieved Dec 9, 2024 from www.gbif.org.

(4) Chapter in a Book
Driever, M. (1993). Maternal control of anterior development in the Drosophila embryo. In M. Bate, and A.M. Aris (Eds.), *The Development of Drosophila melanogaster* (pp. 387–424). Cold Spring Harbor Laboratory Press.

(5) Conference Abstract
Hong, K.D., and Kim, L.P. (1997). *The sources and migratory pathway of locusts in Korea*. Paper presented at The 50th Annual Meeting of The Entomological Society of Korea, Seoul, Korea.

References in articles
We recommend the use of a tool such as EndNote or Reference Manager for reference management and formatting. EndNote reference styles can be searched for here: https://www.endnote.com/support/enstyles.asp. Reference Manager reference styles can be searched for here: https://www.refman.com/support/rmstyles.asp.

5) Tables
Tables should be self-contained and complement, but not duplicate, information contained in the text. Number tables consecutively in the text in Arabic numerals. Type tables on a separate page with the legend above. Legends should be concise but comprehensive – the table, legend and footnotes must be understandable without reference to the text. Vertical lines should not be used to separate columns. Column headings should be brief, with units of measurement in parentheses; all abbreviations must be defined in footnotes. Footnote symbols: †, ‡, §, ¶, should be used (in that order) and *, **, *** should be reserved for *P*-values. Statistical measures such as SD or SEM should be identified in the headings.

6) Figure Legends
Type figure legends on a separate page. Legends should be concise but comprehensive – the figure and its legend must be understandable without reference to the text. Include definitions of any symbols used and define/explain all abbreviations and units of measurement.

(1) Figures
All illustrations (line drawings and photographs) are classified as figures. Figures should be cited in consecutive order in the text. Figures should be sized to fit within the column (80 mm), intermediate (110 mm) or the full text width (167 mm).

Do not embed figures in the Word document – they must be supplied in separate files. Figures must be supplied as high resolution (at least 300 d.p.i.) files, saved as .eps or .tif. Line figures should be supplied in .eps format as at least 600 d.p.i. For very simple line figures, .xls and .ppt files will be accepted. Combination figures (with an image and text) should be in .eps format as at least 600 d.p.i. They can be supplied as .tif files but if so should be at least 600 d.p.i. and line work should not appear jagged. Line figures should be supplied as sharp, black and white graphs or diagrams, drawn professionally or with a computer graphics package. Lettering must be included and should be sized to be no larger than the journal text.

Magnifications should be indicated using a scale bar on the illustration.

7) Appendices
Appendices will be published after the references. For submission they should be supplied as separate files but referred to in the text.

8) Supplementary Information
Supplementary information is information that is not essential to the article but that provides greater depth and background. It is hosted online, and appears without editing or typesetting. It may include tables, figures, videos, datasets, etc.

9) Other Manuscript Formats
General guidelines are the same as for original articles.

(1) Case Reports
Unique cases that make an important teaching point or scientific observation may be suitable for a case report. Abstract should be written in English within 150 words in one paragraph. This should consist of title page, abstract, text (including Introduction, Case Report, and Discussion), author contributions, conflicts of interest, acknowledgments, funding, references, tables, figures, and figure legends.

(2) Review Articles
A Review Article is expected to be a focused examination of defined topics relevant to the scope of PNIE. General remarks are the same as for original article. Manuscripts include a title page (with a running title), abstract and keywords, text, author contributions, conflicts of interest, acknowledgments, funding, references, tables, and figures. Abstract should be written in English within 150 words in one paragraph. The text can be written in free style. The review articles should be submitted in the same way as regular papers and receive the same review process.

AUTHOR LICENSING

If your paper is accepted, the author identified as the formal corresponding author will receive an e-mail prompting them to complete a copyright license agreement on behalf of all authors of the paper.

PUBLICATION PROCESS AFTER ACCEPTANCE

1. Accepted Article Received in Production
When your accepted article is received by the production team, you (corresponding authors) will receive an e-mail asking you to log in to sign a publication license.

2. Proofs
Authors will receive an e-mail notification with a link and instructions for accessing HTML page proofs online. Page proofs should be carefully proofread for any copyediting or typesetting errors. Online guidelines are provided within the system. No special software is required, all common browsers are supported. Authors should also make sure that any renumbered tables, figures, or references match text citations and that figure legends correspond with text citations and actual figures. Proofs must be returned within 48 hours of receipt of the e-mail. Return of proofs via e-mail is possible in the event that the online system cannot be used or accessed.

PNIE PROCEEDINGS OF THE NATIONAL INSTITUTE OF ECOLOGY OF THE REPUBLIC OF KOREA

Enacted August 5, 2020
Revised July 26, 2022
Revised June 23, 2025

The *Proceedings of the National Institute of Ecology of the Republic of Korea* (PNIE) adheres to the ethical guidelines for research and publication described in Guidelines on Good Publication (http://publicationethics.org/resources/guidelines), the International Committee of Medical Journal Editors (ICMJE) Guidelines (http://www.icmje.org), and Principles of Transparency and Best Practice in Scholarly Publishing (http://doaj.org/bestpractice). PNIE follows the international standards for editors and authors press release (https://publicationethics.org/resources/international-standards-for-editors-and-authors) and the Committee on Publication Ethics (COPE) flowcharts, https://publicationethics.org/resources/flowcharts.

All authors of a manuscript must have agreed to its submission and are responsible for its content, including appropriate citations and acknowledgments; they must also have agreed that the corresponding author has the authority to act on their behalf on all matters pertaining to the publication of the paper. By publishing in this journal, the authors agree that the National Institute of Ecology has the right to protect the manuscript from misappropriation. Illustrations in published articles will not be returned to the authors.

1. Authorship

PNIE follows the recommendations for authorship by the ICMJE (https://www.icmje.org/recommendations/). Authorship credit should be based on 1) substantial contributions to the conception or design of the work; or the acquisition, analysis, or interpretation of data for the work; 2) drafting the work or reviewing it critically for important intellectual content; 3) final approval of the version to be published; and 4) agreement to be accountable for all aspects of the work in ensuring that questions related to the accuracy or integrity of any part of the work are appropriately investigated and resolved. Authors should meet the conditions of 1, 2, 3, and 4. After the initial submission of a manuscript, any changes whatsoever in authorship (adding author(s), deleting author(s), or re-arranging the order of authors) must be explained by a letter to the editor from the authors concerned. This letter must be signed by all authors of the paper. Copyright assignment must also be completed by every author.

- Corresponding author and first author: PNIE does not allow multiple corresponding authors for one article. Only one author should correspond with the editorial office and readers for one article. PNIE does accept notice of equal contribution for the first author when the study was clearly performed by co-first authors.
- Correction of authorship after publication: PNIE does not correct authorship after publication unless a mistake has been made by the Editorial Staff. Authorship may be changed before publication but after submission when an authorship correction is requested by all of the authors involved with the manuscript.

2. Review Process

PNIE is a peer-reviewed (single-blind peer review) journal, and the manuscripts are reviewed by two referees with extensive research experience in the relevant fields of the submitted manuscript, and the final editorial decision is made by the Editorial Committee, based on the referees' evaluations. After reviewing, the manuscript is returned to the corresponding author for revision; the revised manuscript must be re-submitted within one month. If it is not re-submitted within the designated period without a valid reason, such manuscript is deemed to be withdrawn from evaluation voluntarily.

3. Ethical Aspects

The author should not use ideas, research, or records of others without citing them. The corresponding author is responsible for all the contents of the manuscript. Authors must deposit data, strains or other materials in scientific collections (e.g., culture collections, herbaria, GenBank, etc.) to make it possible to repeat the experiments and perform future research. Research published in the PNIE must have been conducted in accordance with institutional, national and international guidelines concerning the use of animals in research and/or the sampling of endangered species. For the policies on research and publication ethics that are not stated in these instructions, the Guidelines on Good Publication (https://publicationethics.org/resources/guidelines), Publication of Scholarly Work in Medical Journals (https://www.icmje.org/icmje-recommendations.pdf) and the Principles of Transparency and Best Practice in Scholarly Publishing (https://doaj.org/bestpractice) will be applied.

4. Conflicts of Interest Statement

The corresponding author is responsible for disclosing any potential conflicts of interest that may influence the interpretation of the study's data or findings. Potential conflicts include, but are not limited to, financial support or affiliations with pharmaceutical companies, as well as academic or institutional relationships that could affect objectivity.

All sources of funding relevant to the research must be clearly stated. If no competing interests exist, the authors should include the following statement:
"The authors declare that they have no competing interests."
Additionally, any potential conflicts of interest involving members of the editorial board should be disclosed within the manuscript.

5. Secondary Publication

It is possible to republish manuscripts if the manuscripts satisfy the conditions of secondary publication of the ICMJE Recommendations (https://www.icmje.org/recommendations/).

6. Originality, Plagiarism and Duplicate Publication

All submitted manuscripts should be original and should not be under consideration by other scientific journals for publication at the same time. No part of the accepted manuscript should be duplicated in any other scientific journal without the prior permission of the Editorial Board. Submitted manuscripts are screened for possible plagiarism or duplicate publication by Similarity Check upon arrival. If plagiarism or duplicate publication is detected, the manuscripts may be rejected, the authors will be announced in the journal, and their institutions will be informed. There will also be penalties for the authors. Submission of a manuscript implies that: 1) the work has not been previously published; 2) it is not under consideration for publication elsewhere; and 3) its publication has been approved by all co-authors.

7. Process for Managing Research and Publication Misconduct

When the journal faces suspected cases of research and publication misconduct such as redundant (duplicate) publication, plagiarism, fraudulent or fabricated data, changes in authorship, undisclosed conflicts of interest, ethical problems with a submitted manuscript, a reviewer who has appropriated an author's idea or data, complaints against editors, and so on, the resolution process will follow the flowchart provided by the COPE (https://publicationethics.org/resources/flowcharts). The discussion and decision on the suspected cases are carried out by the PNIE Editorial Board and Research Ethics Committee of the National Institute of Ecology (https://www.nie.re.kr/nieEng/main/contents.do?menuNo=400093).

8. Process for Handling Article Correction, Retraction, and Editorial Expression of Concern

Cases that require editorial expressions of concern or retraction shall follow the COPE flowcharts available from: https://publicationethics.org/resources/flowcharts. If a correction is needed, it will follow the ICMJE Recommendation for Corrections, Retractions, Republications and Version Control available from: https://www.icmje.org/recommendations/browse/publishing-and-editorial-issues/corrections-and-version-control.html.
Honest errors are a part of science and publishing and require publication of a correction when they are detected. Corrections are needed for errors of fact. Minimum standards are as follows: First, it shall publish a correction notice as soon as possible detailing changes from the original publication and citing it on both an electronic and numbered print page that is included in an electronic or a print Table of Contents to ensure proper indexing; Second, it shall post a new article version with details of the changes from the original version and the date(s) on which the changes were made through K-Mark; Third, it shall archive all prior versions of the article. This archive should be directly accessible to readers. Fourth, previous electronic versions shall prominently note that there are more recent versions of the article via K-Mark.

9. Editorial Responsibilities

The Editorial Board will continuously work to monitor and safeguard publication ethics: guidelines for retracting articles; maintenance of the integrity of the academic record; preclusion of business needs from compromising intellectual and ethical standards; publishing corrections, clarifications, retractions, and apologies when needed; and excluding plagiarism and fraudulent data. The editors maintain the following responsibilities: responsibility and authority to reject and accept articles; avoiding any conflicts of interest with respect to articles they reject or accept; promoting publication of corrections or retractions when errors are found; and preserving the anonymity of reviewers.

10. Copyright Information

The copyright for all publications is owned by National Institute of Ecology. Permission must be obtained from the NIE for any commercial use of materials. All authors must sign a "Copyright Transfer Agreement" and submit it online through the PNIE electronic submission system (https://acoms.accesson.kr/pnie/oprs/main/jrnlMain.do).
PNIE is an open access journal available free of charge. Articles published in PNIE are distributed under the terms of the Creative Commons Attribution Non-Commercial License (https://creativecommons.org/licenses/by-nc/4.0/), which permits unrestricted noncommercial use, distribution, and reproduction in any medium, provided the original work is properly cited. For any commercial use of material from the open access version of the journal, permission must be obtained from the Editorial Board.
PNIE has an author self-archiving policy (Blue : Post-print) and allows self-archiving in compliance with the following.
Public Place: All or part of the article is posted on the author's personal website, the website of the institution or organization to which the author belongs, the website of the organization that supported the research fund, etc.

Disclosure Conditions: Self-archiving is permitted for personal and educational purposes, provided the author complies with CC-BY-NC regulations, inserts hyperlinks in publications, and posts prints after review.

11. Archiving

The journal is accessible without barrier from KoreaScience (https://koreascience.or.kr/) or National Lbrary of Korea (https://nl.go.kr) in the event a journal is no longer published.

Editor's & Reviewer's Guide

PNIE PROCEEDINGS OF THE NATIONAL INSTITUTE OF ECOLOGY OF THE REPUBLIC OF KOREA

Enacted August 5, 2020
Revised June 23, 2025

Editor's Guide

Editors have the following responsibilities:

- To acknowledge receipt of submitted manuscripts within a few days of receipt and to ensure the efficient, fair and timely review process of submitted manuscripts.
- To ensure that submitted manuscripts are handled in a confidential manner, with no details being disclosed to anyone, with the exception of the referees, without the permission of the author, until a decision has been taken as to whether the manuscript is to be published.
- To invite reviewers, particularly considering the use of an author's suggested referees for their submitted article, but to ensure that the suggestions do not lead to a positive bias (e.g. co-authors of previous publications, mentor). The editor maintains the right to use referees of their own choice.
- Not to use referees whom an author has requested not to be consulted, unless the editor reasonably considers there to be a significant overriding interest in so doing.
- To ensure the confidentiality of the names and other details of referees; adjudication and appeal referees may be informed of the names of prior referees, if appropriate.
- To make the final decision concerning acceptance or rejection of a manuscript with reasonable speed and to communicate the decision in a clear and constructive manner.
- To decide to accept or reject a manuscript for publication with reference only to the manuscript's importance, originality and clarity, and its relevance to the journal.
- To respect the intellectual independence of authors.
- To make known any conflicts of interest that might arise. Specifically, in cases where an editor is an author of a submitted manuscript, the manuscript must be passed to another editor for independent peer review.
- Not to use work reported in unpublished submitted articles for their own research.
- To respond to any suggestions of scientific misconduct, usually through consultation with the author. This may require the publication of a formal retraction or correction.
- To deal fairly with an author's appeal against the rejection of a submitted manuscript.
- To monitor and ensure the fairness, timeliness, and thoroughness of the peer review process.

Reviewer's Guide

Reviewers have the following responsibilities:

- To provide written, unbiased, and informative feedback in a timely manner on the scientific value of the work, rating the work's composition, scientific accuracy, originality, and interest to readers.

- To treat the manuscript as confidential; not sharing it with third parties, discussing it with others, or disclosing the information in the reviewed paper.

- Without undue delay, to return, destroy, or erase the manuscript and to inform the editor should they be unqualified to review the manuscript, or lack the time to review the manuscript.

- To judge the manuscript objectively and in a timely manner. Referees should not make personal criticism in their reviews.

- To return the manuscript without review to the editor if there is a conflict of interest.
  Specifically, referees should not review manuscripts authored or co-authored by a person with whom the referee has a close personal or professional relationship, if this relationship could be reasonably thought to bias the review.

- To explain and support their judgments so that editors and authors may understand the basis of their comments, and to provide reference to published work, where appropriate.

- To inform the editor of any similarity between the submitted manuscript and another either published or under consideration by another journal to the best of their knowledge.

- To ensure that all unpublished data, information, interpretation and discussion in a submitted article remain confidential and not to use reported work in unpublished, submitted articles for their own research.

- To alert the editor if a manuscript contains plagiarized material or falsified data to the best of their knowledge.

Principles of Transparency and Best Practice in Scholarly Publishing

PNIE PROCEEDINGS OF THE NATIONAL INSTITUTE OF ECOLOGY OF THE REPUBLIC OF KOREA

Enacted October 26, 2022
Revised June 23, 2025

1. Name of Journal

The official journal title is *Proceedings of the National Institute of Ecology of the Republic of Korea*. Abbreviated title is PNIE.

2. Website

i. The URL address of official journal website is https://accesson.kr/pnie/.

ii. 'Aims and Scope' statement
It aims to promote, but is not limited to, the achievements of basic ecological research conducted at home and abroad. The prospective audience is researchers conducting global collaborative research as well as ecological studies in the Asia-Pacific region. The scope is not only basic ecological research on terrestrial and aquatic populations, communities, ecosystems and landscapes but also applied issues such as data science and climate change based on ecological research.

iii. Readership
For those who study basic ecological studies of terrestrial and aquatic populations, communities, ecosystems and landscapes, as well as those who study applied ecology such as climate change and data science based on ecological studies. Its readership can be expanded to other positions: • Researchers can obtain the latest topics in domestic and international ecological research; • Professors can access and adopt a variety of data for education; • Students can understand the latest trends in ecological research at home and abroad; • Policy makers can reflect the results of the papers in international ecological research policies.

iv. Duplicate submission and redundant publication
Submitted manuscripts must not have been previously published or be under consideration for publication elsewhere. No part of the accepted manuscript should be duplicated in any other scientific journal without the permission of the Editorial Board. Submitted manuscripts are screened for possible plagiarism or duplicate publication by iThenticate upon arrival. If plagiarism or duplicate publication related to the papers of this journal is detected, the manuscripts may be rejected, the authors will be announced in the journal, and their institutions will be informed. There will also be penalties for the authors. A letter of permission is required for any and all material that has been published previously. It is the responsibility of the author to request permission from the publisher for any material that is being reproduced. This requirement applies to text, figures, and tables.

v. Authorship criteria
Authorship credit should be based on 1) substantial contributions to the conception or design of the work; or the acquisition, analysis, or interpretation of data for the work; 2) drafting the work or reviewing it critically for important intellectual content; 3) final approval of the version to be published; and 4) agreement to be accountable for all aspects of the work in ensuring that questions related to the accuracy or integrity of any part of the work are appropriately investigated and resolved. Every author should meet all of these four conditions. After the initial submission of a manuscript, any changes whatsoever in authorship (adding author(s), deleting author(s), or rearranging the order of authors) must be explained by a letter to the editor from the authors concerned. This letter must be signed by all authors of the paper. Copyright assignment must also be completed by every author.

vi. Corresponding author and first author
PNIE does not allow multiple corresponding authors for one article. Only one author should correspond with the editorial office and readers for one article. PNIE does accept notice of equal contribution for the first author when the study was clearly performed by co-first authors. Correction of authorship after publication: PNIE does not correct authorship after publication unless a mistake has been made by the editorial staff. Authorship may be changed before publication but after submission when an authorship correction is requested by all of the authors involved with the manuscript.

vii. pISSN: 2765-2203, eISSN: 2765-2211

3. Publishing Schedule

PNIE is published quarterly in a year (February 1, May 1, August 1, November 1). Supplement issues may be published.

4. Archiving

It is accessible without barrier from KoreaScience (https://koreascience.or.kr/) or National Library of Korea (https://

nl.go.kr) in the event a journal is no longer published.

5. Copyright

All published papers become the permanent property of the National Institute of Ecology. Copyrights of all published materials are owned by the National Institute of Ecology. Every author should sign the Copyright Transfer Agreement forms.

6. Licensing

This is an open-access journal distributed under the terms of the Creative Commons Attribution Non-commercial license, which permits unrestricted use, distribution, and reproduction in any medium, provided the original work is properly cited for non-commercial purpose (https://creativecommons.org/licenses/by-nc/4.0/).

Deposit policy: According to the deposit policy (self-archiving policy) of Sherpa/Romeo (https://www.sherpa.ac.uk/), authors cannot archive pre-print (i.e. pre-refereeing), but they can archive post-print (i.e. final draft post-refereeing). Authors can archive publisher's version/PDF.

7. Publication Ethics and Related Editorial Policies

i. Journal policies on authorship and contributorship

Authorship credit should be based on 1) substantial contributions to the conception or design of the work; or the acquisition, analysis, or interpretation of data for the work; 2) drafting the work or reviewing it critically for important intellectual content; 3) final approval of the version to be published; and 4) agreement to be accountable for all aspects of the work in ensuring that questions related to the accuracy or integrity of any part of the work are appropriately investigated and resolved. Authors should meet conditions of 1, 2, 3, and 4. After the initial submission of a manuscript, any changes whatsoever in authorship (adding author(s), deleting author(s), or rearranging the order of authors) must be explained by a letter to the editor from the authors concerned. This letter must be signed by all authors of the paper. Copyright assignment must also be completed by every author.

Corresponding author and first author: PNIE does not allow multiple corresponding authors for one article. Only one author should correspond with the editorial office and readers for one article. PNIE does accept notice of equal contribution for the first author when the study was clearly performed by co-first authors.

Correction of authorship after publication: PNIE does not correct authorship after publication unless a mistake has been made by the editorial staff. Authorship may be changed before publication but after submission when an authorship correction is requested by all of the authors involved with the manuscript.

ii. How the journal will handle complaints and appeals

The policy of the journal is primarily aimed at protecting the authors, reviewers, editors, and the publisher of the journal. If not described below, the process of handling complaints and appeals follows the guidelines of the Committee of Publication Ethics available from: https://publicationethics.org/appeals.

iii. How the journal will handle allegations of research misconduct

When the journal faces suspected cases of research and publication misconduct such as redundant (duplicate) publication, plagiarism, fraudulent or fabricated data, changes in authorship, an undisclosed conflict of interest, ethical problems with a submitted manuscript, a reviewer who has appropriated an author's idea or data, complaints against editors, and so on, the resolution process will follow the flowchart provided by the Committee on Publication Ethics (COPE; https://publicationethics.org/resources/flowcharts). The discussion and decision on the suspected cases are carried out by the PNIE Editorial Board and Research Ethics Committee of the National Institute of Ecology (https://www.nie.re.kr/nieEng/main/contents.do?menuNo=400093). If any individuals or institutions want to inform the cases, they can submit a report to the National Institute of Ecology Research Misconduct Report Center (https://www.nie.re.kr/nieEng/main/contents.do?menuNo=400093) and send a letter to the editor. For the complaints or appeals, concrete data with answers to all factual questions (who, when, where, what, how, why) should be provided.

iv. Journal policies on conflicts of interest/competing interests

The corresponding author is required to disclose any potential conflicts of interest that may influence the interpretation of the study's data or results. Examples include, but are not limited to, financial support or affiliations with pharmaceutical companies, and academically related relationships that may affect objectivity.

All sources of funding related to the study must be explicitly declared. If there are no competing interests, the manuscript should include the following statement:

"The authors declare that they have no competing interests."

In addition, any potential conflicts of interest involving editorial board members must also be transparently disclosed within the manuscript.

v. Journal's policies on data sharing and reproducibility

Authors should include a data accessibility statement, including a link to the repository they have used, in order that this statement can be published alongside their paper. This journal follows the data sharing policy described

in "Data Sharing Statements for Clinical Trials: A Requirement of the International Committee of Medical Journal Editors". The ICMJE's policy regarding trial registration is explained at https://www.icmje.org/recommendations/browse/publishing-and-editorial-issues/clinical-trial-registration.html. If the data sharing plan changes after registration this should be reflected in the statement submitted and published with the manuscript, and updated in the registry record.

vi. Journal's policy on ethical oversight

The Editorial Board will continuously work to monitor and safeguard publication ethics: guidelines for retracting articles; maintenance of the integrity of the academic record; preclusion of business needs from compromising intellectual and ethical standards; publishing corrections, clarifications, retractions, and apologies when needed; and excluding plagiarism and fraudulent data. The editors maintain the following responsibilities: responsibility and authority to reject and accept articles; avoiding any conflict of interest with respect to articles they reject or accept; promoting publication of corrections or retractions when errors are found; and preservation of the anonymity of reviewers.

vii. Journal's policy on intellectual property

The authors of the article hereby agree that the National Institute of Ecology holds the copyright on all submitted materials upon acceptance of the manuscript and the right to publish, transmit, sell, and distribute them in the journal or other media.

viii. Journal's policies on corrections and retractions

Cases that require editorial expressions of concern or retraction shall follow the COPE flowcharts available from: https://publicationethics.org/resources/flowcharts. If correction is needed, it will follow the ICMJE Recommendation for Corrections, Retractions, Republications and Version Control available from: https://www.icmje.org/recommendations/browse/publishing-and-editorial-issues/corrections-and-version-control.html.

Honest errors are a part of science and publishing and require publication of a correction when they are detected. Corrections are needed for errors of fact. Minimum standards are as follows: First, it shall publish a correction notice as soon as possible detailing changes from and citing the original publication on both an electronic and numbered print page that is included in an electronic or a print Table of Contents to ensure proper indexing; Second, it shall post a new article version with details of the changes from the original version and the date(s) on which the changes were made through K-Mark; Third, it shall archive all prior versions of the article. This archive shall be directly accessible to readers; and Fourth, previous electronic versions shall prominently note that there are more recent versions of the article via K-Mark.

8. Peer Review Process

PNIE reviews all manuscripts received. A manuscript is first reviewed for its format and adherence to the aims and scope of the journal. PNIE is a peer-reviewed (single-blind peer review) journal and the manuscripts are reviewed by two referees with abundant research experience in the relevant fields of the submitted manuscript, and the final editorial decision is made by the Editorial Committee, based on the referees' evaluations. After reviewing, the manuscript is returned to the corresponding author for revision; the revised manuscript must be re-submitted within one month. If it is not submitted within the designated period without any special reasons, such manuscript is deemed to be withdrawn from evaluation voluntarily.

9. Access

This is an open access journal distributed under the terms of the Creative Commons Attribution Non-Commercial License (https://creativecommons.org/licenses/by-nc/4.0/), which permits unrestricted non-commercial use, distribution, and reproduction in any medium, provided the original work is properly cited.

10. Ownership and Management

i. Information about the ownership: This journal is owned by the publisher, the National Institute of Ecology of the Republic of Korea (https://www.nie.re.kr/).

ii. Management team of a journal (https://accesson.kr/pnie/menu/51/57/)

- Journal management team (2025-2030)
- Journal Manager: Ohseok KWON, Kyungpook National University, Korea
- Manager of the Review Process: Ohseok KWON, Kyungpook National University, Korea
- Manuscript Editor: Yuseong JO, MEDrang Inc., Korea
- Layout Editor: Suok JOH, MEDrang Inc., Korea
- Website and JATS XML File Producers: Gowoon BAE, Inforrang, Korea
- Ethics Manager: Jinyoung PARK, National Institute of Ecology, Korea
- Administrative Manager: Min-Ho CHANG, Younmi RYU, National Institute of Ecology, Korea

11. Governing Body

The governing body is the journal's editorial board.

12. Editorial Team and Contact Information

i. Editorial team: https://accesson.kr/pnie/menu/46/49/

ii. Contact information

Administrative Manager: Min-Ho CHANG, Younmi RYU
1210, Geumgang-ro, Maseo-myeon, Seocheon-gun, Chungcheongnam-do, 33657, Korea. E-mail: pnie@nie.re.kr

13. Author Fees

There are no charges to publish an article in PNIE. There is also no submission fee. PNIE is an academic journal published with the support of the National Institute of Ecology.

14. Other Revenue

There are no submission, review, and publication costs borne by the authors.
Revenue sources of the journal include support from the publisher (National Institute of Ecology) and the Korean Government.

15. Advertising

PNIE accepts advertisements on the following basis:

i. Eligibility of the advertised products or services

All products or services should be safe and reliable, and not cause any harm to the health and welfare of humans. Advertisements may promote information and technologies relevant for authors, editors, reviewers, and readers. Pharmaceutical products may also be considered.

- Advertising is separate from content. Advertisers and sponsors have no advance knowledge of our editorial contents, nor do the editors have advance knowledge of advertisers. Content is never altered, added, or deleted to accommodate advertising. Advertisers and sponsors have no input regarding any of our editorial decisions or advertising policies.
- We reserve the right to decline or cancel any advertisement at any time.
- Advertisements for pharmaceutical products must conform to all regulations and policies of the Ministry of Food and Drug Safety, Republic of Korea in every respect.

ii. Orders

Any individuals or organizations who are interested in advertising their products or services in the print copies of the journal or on its website are encouraged to contact the editorial office. The acceptance of advertisement will be discussed by the editorial board and will be ultimately approved by the publisher.

iii. Advertisement fee

For one print copy issue, the advertisement price for one whole page is USD 500 (or KRW 500,000). If the advertisement is half a page, the price is reduced by half. For a quarter of the page, this price is reduced by one quarter. For banner advertisements on the website, the price is negotiable according to the duration of its exposure on the journal homepage. The price is usually greater than that for print copies.

iv. Disclaimer

Liability: Neither the publisher nor the editors will be legally liable for advertisements presented in the journal. In addition, they cannot guarantee the accuracy, completeness, or usefulness of the information provided.
Endorsement: The publisher and the editors do not endorse any products or services that are advertised.
Disclaimer: Neither the publisher nor the editors will be legally liable for any of the content of advertisements, so readers must keep this in mind when reading or seeing advertisements.

16. Direct Marketing

Journal propagation has been done through the journal web site and distribution of an introduction pamphlet. Invitations to submit a manuscript are usually focused on the presenters at conferences, seminars, or workshops if the topic is related to the journal's aims and scope.

Research Ethics Pledge and Copyright Transfer Agreement

PNIE PROCEEDINGS OF THE NATIONAL INSTITUTE OF ECOLOGY OF THE REPUBLIC OF KOREA

Manuscript Title : _____

Authors : _____

Author(s) must read and sign the statements below about authorship responsibility and copyright transfer. In the case of an article having more than one author, the signature of one of the authors is sufficient, provided that the signing author understands that he or she is signing on behalf of all of the authors and that all the other authors understand that the signing author is acting as their proxy in signing the manuscript submission form.

1. The manuscript has not been previously published and is not currently under consideration for publication elsewhere, nor will the research reported be submitted for publication elsewhere until a final decision has been made as to its acceptability by Proceedings of the National Institute of Ecology of the Republic of Korea.
2. The manuscript represents truthful and original work without fabrication, fraud, or plagiarism.
3. All authors have made an important scientific contribution to the study and are thoroughly familiar with the primary data. All authors have read the complete manuscript, take responsibility for the content and completeness of the manuscript, and understand that they share responsibility if the paper, or part of the paper, were found to be faulty or fraudulent.
4. This manuscript contains no violation of any existing copyright or other third party right, and to the best of the authors' knowledge, this work does not infringe the rights of others.
5. The authors of the article hereby agree that the National Institute of Ecology holds the copyright on all submitted materials upon acceptance of the manuscript and the right to publish, transmit, sell, and distribute them in the journal or other media.

Date:

Corresponding Author : _____ Signature



PROCEEDINGS OF THE

NATIONAL INSTITUTE OF ECOLOGY OF THE REPUBLIC OF KOREA